ABSTRACT

Title of dissertation: LITHIUM AND δ^7Li BEHAVIOR DURING METAMORPHIC DEHYDRATION PROCESSES AND CRUSTAL EVOLUTION

Lin Qiu, Ph.D., 2011

Dissertation directed by: Professor Roberta L. Rudnick, Geology
Professor William F. McDonough, Geology

Li isotopes have been used as a tracer of a wide range of geological processes, because the two stable isotopes of Li have significant relative mass difference and large elemental dispersion in Earth. In order to understand better Li behavior during the processes of sub-greenschist to granulite facies metamorphism and partial melting, fluid transport in subduction zones, weathering of continental crust and the evolution of juvenile continental crust, a large variety of samples have been studied in this thesis. These samples include mudrocks from British Caledonides, schists from Otago, New Zealand, high-grade metapelites and metabasites from Ivrea-Verbano Zone, Italy, Archean shales from the Kaapvaal Craton, South Africa, and Archean granitoids from Scotland, South Africa and Canada.

Investigations of metapelites from several localities show that: 1) sedimentary provenance exerts the greatest control on Li in fine grained sediments, and Li concentrations generally increase while δ^7Li decreases with CIA (Chemical Index of Alteration) in post Archean shales, 2) sub-greenschist facies metamorphism has negligible effect on Li concentrations and isotopic compositions, 3) metamorphic

dehydration from greenschist to granulite facies may cause significant Li depletion, but has had little influence on δ^7Li, and 4) a key factor controlling [Li] in metapelites during metamorphism is the stability of Mg-bearing phyllosilicates. Furthermore, based on the understanding gained of the Li behavior above, the Li signature in Archean shales and granitoids may indicate that: 1) more severe weathering conditions prevailed during the Archean, 2) the Archean upper continental crust had a heavier Li isotopic composition than post Archean upper continental crust, and 3) Archean juvenile granitoids have heavier Li isotopic compositions than post-Archean equivalents. Collectively, the results for Archean samples may indicate that Li isotopes can be used as tracers of paleoclimate change, and also can be used to understand the nature of the source of Archean juvenile magmas.

LITHIUM AND δ^7Li BEHAVIOR DURING METAMORPHIC DEHYDRATION PROCESSES AND CRUSTAL EVOLUTION

By

Lin Qiu

Dissertation submitted to the Faculty of the Graduate School of the
University of Maryland, College Park, in partial fulfillment
of the requirements for the degree of
Doctor of Philosophy
2011

Advisory Committee:
Professor Roberta Rudnick, Chair
Professor William McDonough, Co-Chair
Professor Sarah Penniston-Dorland
Professor Steven Shirey
Professor Dorothy Beckett

Preface

A significant portion of the work reported in this thesis was previously published, submitted or in preparation in the form of peer-reviewed journal articles. All samples analyzed in this thesis are from my co-authors, provided either as powders or rock specimens. Therefore, this thesis reflects not only my own work, but also the contributions of my co-authors and insightful reviewers and editors.

Dedication

This dissertation is dedicated to

my parents Fuqiang Qiu and Guiru Cui.

兹将本论文献给我最亲爱的爸爸妈妈，邱福强， 崔桂茹。

Acknowledgements

I am grateful for my doctoral study at the Department of Geology and I thank my advisors Roberta and Bill for guiding me to use diverse methods to investigate geological phenomena. Roberta and Bill are not only great scientists but also great mentors. Before I entered the doctoral program, I knew little about lithium isotopes; Roberta taught me everything step by step with great patience, from clean lab chemistry to data analysis. When I made mistakes, Roberta never blamed me but told me "this is the way of learning it" with a big smile. Her encouragement and trust really motivated me and kept me working on the project with abiding enthusiasm. Bill's guidance usually comes in his unique way, starting with questions and jokes; I was always instructed by Bill under an amiable atmosphere like friends chatting with each other. Every time I talked about my project with Bill, he can always come up with great ideas to improve it and asked me his famous question "Do you want to be a great graduate student or scientist?" My ambitious was initiated from there and interacting with him made me think actively, work independently, and always try to come up with new ideas. I also thank them for pushing me to improve my English speaking and writing

I thank Dr. Sarah Penniston-Dorland for providing suggestions on my Otago Schist project and serving on my thesis committee.

I thank Dr. Steve Shirey for serving on my committee as well and sharing his sanukitoids samples with me.

I thank Dr. Dorothy Beckett for serving on my committee as the Dean's representative.

I thank Richard Ash and Igor Puchtel who generously offered their help in the clean lab and plasma lab, which keep my research progress in an ideal speed.

As for my colleagues, I thank Jingao Liu, Xiaoming Liu and Yu Huang first, since they provide helps both on science work and sundries of the daily life.

I thank Rick Arevalo for always being the first to proof read my manuscripts. As my officemate, he liked to tease me when I was working. So every time I saw him walking to me, I knew it was the time to take a break.

I thank Jeremy, Nick, Brian and other graduate students for helping me on the lab work and manuscripts.

Finally, I thank my parents and my wife for their mighty love and support.

Table of Contents

List of Tables

Chapter 3

Chapter 4

Chapter 5

Chapter 6

Chapter 7

List of Figures

Chapter 3

Chapter 4

Chapter 5

Chapter 6

Chapter 7

Chapter 1: Introduction[1]

[1] The text in this chapter was created/written by Lin Qiu.

Lithium isotope geochemistry has been a fast developing research field in recent decades and has proven useful for studying a variety of geological phenomena. Lithium is moderately incompatible element with two stable isotopes, ^{6}Li and ^{7}Li, which have a large mass difference (~16% mass difference) and do not fractionate during mantle melting and basalt crystallization (e.g., Tomascak et al., 1999). Lithium is fluid mobile and its high ionization potential makes it stable in aqueous solutions; moreover, its two isotopes have a large mass dependent isotopic fractionation potential during fluid-rock exchange (e.g., Chan and Kastner, 2000; Richter et al., 2003; Pistiner and Henderson, 2003; Huh et al., 2004; Rudnick et al., 2004; Pogge von Strandmann et al., 2006; Penniston-Dorland et al., 2010; Wimpenny et al., 2010b). Since the stronger bonds favor heavier isotopes and tetrahedral coordination yields stronger bonds than octahedral coordination, during fluid rock interactions, such as secondary mineral formation, ^{6}Li is preferentially retained in silicates occurring in octahedral coordination, where it can substitute for Mg^{2+}, and ^{7}Li preferentially enters the aqueous fluid, where Li exists in tetrahedral coordination (e.g., Teng et al., 2004; 2006a; Vigier et al., 2008). This behavior of Li during fluid-rock interaction leads to lower $\delta^{7}Li$ in the upper continental crust (0 ± 2, Teng et al., 2004, $\delta^{7}Li=(^{7}Li/^{6}Li)_{sample}/(^{7}Li/^{6}Li)_{LSVEC}-1] \times 1000$) compared to the mantle (+4 ± 1, Chan et al., 1992; Elliott et al., 2006; Moriguti and Nakamura, 1998; Nishio et al., 2007; Tomascak et al., 2008) and ocean water ($\delta^{7}Li$=31‰, Chan and Edmond, 1988;

You and Chan, 1996); more than 50‰ variation of Li isotopes has been observed on the Earth's surface (e.g., Tomasack et al., 2004; Rudnick et al., 2004).

Lithium isotopes have been investigated particularly to understand crustal recycling processes at subduction zones, though the δ^7Li in arc basalts is not as heavy as what some earlier studies suggested. The oceanic crust is enriched in Li and has heavy Li isotopic composition relative to the fresh basalts because of the uptake of heavy Li into basalts from seawater (e.g., Chan and Edmond, 1988; Chan et al., 1992). During subduction, low-temperature metamorphic dehydration will release fluids from the slab, which will ascend and infiltrate sediments at shallow depths (in accretionary wedges) and the overlying mantle wedge at the greater depth. Early studies suggested that the Li isotopic composition in slab-derived fluids should be even heavier than the slab because ^{7}Li preferentially partitions into fluids during metamorphic dehydration (e.g., Tomasack et al., 2000); as a result, arc basalts should have heavier Li isotopic compositions than the mantle and the dehydrated slab would, consequently, have isotopically light Li (Zack et al., 2003). However, the δ^7Li in arc basalts is now well characterized and they have mantle-like signatures; moreover, later studies (e.g., Teng et al., 2007; Marschall et al., 2007) argue that metamorphic dehydration has little influence on δ^7Li in rocks. In order to address this debate, one goal of this study is to determine the behavior of Li during sub-greenschist to granulite facies metamorphism.

Based on the understanding of Li behavior during metamorphism, we might be able to use the Li signature to evaluate the influence of weathering on the compositional of the continental crust through time. Understanding the origin and evolution of the continental crust has been a major goal for geologists for centuries. A fundamental observation

requiring explanation is that the continental crust has an average andesitic composition that does not match that of its basaltic building blocks. This enigma cannot simply be solved by intracrustal magmatic differentiation, and weathering of basaltic crust is a solution favored by some studies (e.g., Albarede, 1998; Lee et al., 2008) to solve it. Chemical weathering preferentially removes Mg from the crust relative to Si, because Si-rich minerals, such as quartz, is more resistant to weathering than Mg-rich mafic minerals; as a result, chemical weathering leaches and subsequently depletes the soluble elements in the continental crust. Therefore, a study of soluble elements, such as Li, will shed light on the extent to which weathering influences the composition of the continental crust. Liu and Runick (2010) used Li isotopes and a simple mass balance model to quantify how much continental crust is lost due to chemical weathering. There are several parameters in their model that could be better constrained, such as Li concentrations and compositions in juvenile continental crust, delaminated lower crust, bulk continental crust, subducted terrigenous sediments. In order to constrain well some parameters in the model of Liu and Rudnick (2010) and quantify better the time-integrated weathering flux of the continental crust, I also investigate the Li isotopes in Archean shales and Archean granitoids.

The following five chapters of this thesis are presented as five independent papers. The first three chapters discuss the behavior of Li during low to high- grade metamorphic dehydration in metapelites. The sixth chapter discusses the Li concentration and isotopic composition of Archean shales and the influence of weathering on the Li composition of the continental crust through time. The last chapter examines the Li isotopic composition of juvenile magma added to the continental crust in the Archean, as viewed from the Li

signature in Archean TTGs (Tonalite-Trondhjemite-Granodiorite) and sanukitoids (high-Mg granitoids, e.g., monzodiorites, trachyandesites).

Chapter Three examines the influence of sub-greenschist facies metamorphism on Li concentration and isotopic composition of shales from three Paleozoic basins in the British Caledonides. These shales exhibit wide variation of lithium concentration and isotopic composition, ranging from 29 to 139 μg/g and -4.4‰ to +3.7‰ respectively. [Li] and δ^7Li in the mudrocks do not correlate with sub-greenschist facies metamorphic grade determined by the Kübler index, suggesting little impact of low grade metamorphism on these variables. This study shows that Li concentrations and δ^7Li can provide additional information on the degree of weathering of the provenance of mudrocks. This work was published in an article entitled "Li and δ^7Li in mudrocks from the British Caledonides: metamorphism and source influences" in *Geochimica et Cosmochimica Acta*.

Chapter Four examines the behavior of Li during sub-green schist to greenschist facies metamorphism and fluid fluxing in an accretionary prism, Otago Schist, New Zealand. The [Li] and δ^7Li signatures of the Otago Schist indicate that, although prograde metamorphism from sub-greenschist facies to greenschist facies may have depleted the Li concentrations in these rocks, it had no discernible effect on the rocks' Li isotopic compositions. Further depletion of [Li] in greenschist facies composites is caused by mass addition of Li-poor quartz veins. An isotopic equilibrium fluid flow model indicates that the δ^7Li of the precursor sediments of the Otago Schist can be preserved after fluid fluxing if the [Li] in the fluid is relatively low. This work was published in an article entitled "A Li isotopic study of sub-greenschist to greenschist facies metamorphism in an accretionary prism, New Zealand" in *Earth and Planetary Science Letters*.

Chapter Five examines the signature of Li in amphibolite to granulite facies metapelites, leucosomes and metabasites from the Ivrea-Verbano Zone, NW Italy, a classic section of lower continental crust. The [Li] and δ^7Li signatures of the metapelites indicate that, although prograde metamorphism from amphibolite facies to granulite facies has greatly depleted the Li concentrations in these rocks, there is no Li isotopic fractionation at these metamorphic temperatures. Mg-bearing phyllosilicate minerals have a great control on [Li] in the metapelites. A batch melting model indicates some of the Li released during partial melting of metapelites can contribute to S-type granites, with excess Li being partitioned into Li-pegmatites. This work is currently in review in an article entitled "The behavior of lithium in amphibolite- to granulite-facies rocks of the Ivrea-Verbano Zone, NW Italy" in *Chemical Geology*.

Chapter Six examines the Li signature in shales deposited between 2.2 and 3.0 Ga from the Kaapvaal Craton, South Africa. Generally, [Li] of the shales from the Kaapvaal Craton negatively correlates with their δ^7Li, which is similar to that found in Post Archean shales. However, some of the Kaapvaal shales have low [Li] and significantly high δ^7Li that have not yet been observed in post Archean shales, and may reflect severe weathering conditions in the Archean that caused the complete removal of Li-hosting Mg-bearing clays. This work is in preparation for publication as an article entitled "Lithium isotopic study of ancient shales from the Kaapvaal Craton, Southern Africa".

Chapter Seven examines the Li signature of Archean juvenile magma as reflected in TTGs and sanukitoids from Scourie, Scotland, Barberton, South Africa and the Rainy Lake Region of the Superior Province, Canada. TTG magma derived from slab-melting or partial melting of thickened crust at relatively shallow depths may have variable δ^7Li;

by contrast, TTG magma derived directly from mantle or partial melting of thickened crust have mantle-like δ^7Li. Based on the mass balance model of Liu and Rudnick (2010), the [Li] in Archean TTGs and sanukitoids suggest that around 30% crustal mass has been lost due to chemical weathering. This work is in preparation for an article entitled “Lithium concentrations and isotopic compositions of Archean Trondhjemites-Tonalites-Granodiorites and sanukitoids: evaluating the flux of Li to the continents through time”.

Chapter 2: Analytical methods[1, 2]

[1] The text in this chapter was created/written by Lin Qiu.

[2] The chromatographic separation of Li is created by Moriguti and Nakamura (1998) and then developed and reported by Teng et al. (2006b). The MC-ICP-MS analytical method of Li isotopes has been reported by Teng et al. (2004).

Li isotopic compositions are reported in terms of parts per mil deviation from an international reference material, LSVEC: $\delta^7Li=[(^7Li/^6Li)_{sample}/(^7Li/^6Li)_{LSVEC}-1] \times 1000$. In the early literature, the Li isotope notation has also been used as δ^6Li, which now can be generally converted to δ^7Li with a value close to the corresponding δ^7Li ($\delta^7Li=[-\delta^6Li/(1+(\delta^6Li/1000)]$). The international reference material, LSVEC, is the U.S. National Institute of Standards and Technology (NIST) high purity Li_2CO_3 reference, which is fabricated from spodumene and has $^7Li/^6Li = 12.02 \pm 0.03$ (Flesch et al., 1973). After the establishment of the L-SVEC standard, the first precise measurement of Li isotopes was by Chan (1987) using TIMS (Thermal Ionization Mass Spectrometry) with a long term reproducibility < 2‰ in the late 1980's; however, due to the problem that there are only two isotopes of Li, making mass bias corrections difficult on TIMS, and the mass bias changes progressively with the analysis time, most of the recent studies have used MC-ICP-MS (Multi-Collector Inductively Coupled Plasma Mass Spectrometry) rather than TIMS to analyze Li isotopes. In addition, measurements of Li on TIMS are time consuming and have relatively high detection limit and low tolerance of sample impurities. The recent development of MC-ICP-MS technique allows considerably faster measurements of Li isotopes using bracketing standard methods, with reproducibility better than 1‰ (e.g., Tomascak et al., 2004). In addition, both TIMS and MC-ICP-MS

methods require the extraction and purification of Li from the sample matrix by using exchange chemistry. During my doctoral research, an integral portion of my lab work was devoted to employing ion exchange chromatography and multi-collector inductively-coupled mass spectrometry, and these analytical methods are described below, step by step.

1.1. Sample dissolution

Generally, 20−50 mg powdered samples (~0.5− 1μg Li in the sample) were weighed into Savillex screw-top beakers and dissolved in a ~ 4:1 mixture of concentrated HF-HNO_3 on a hot plate (T< 120 °C) until there was only white, powdery material at the bottom of the solution. The solutions were then dried down and followed by the replenishment with concentrated HNO_3 overnight until the solutions were fully clear. The solutions were then dried down again and re-dissolved in 4 M HCl for the preparation of chromatographic separation. In addition, for the samples that contained organic carbon, $HClO_4$ in a 0.2:1 mixture with HF was used for the first step and then dried down in a perchloric acid fume hood.

1.2. Chromatographic separation

Lithium was eluted though four sets of columns, each of which contains 1 mL of cation-exchange resin (BioRad AG50W-×12). The first three sets are following the three column procedures described by Moriguti and Nakamura (1998) and Teng et al. (2006b), and the fourth column is the repeat of the third column in order to additionally separate Na from Li.

1.2.1. First column: the major elements were roughly removed

The sample were dissolved in 1ml of 4 M HCL and then loaded into Bio-rad polypropylene column with internal diameter of 8mm; 9 ml of 2.5 M HCL was then introduced into the column. The total 10 ml elution was collected in a 60 ml-Teflon beaker which was also used for column 2, 3 and 4.

1.2.2. Second column: Li and Na separated from other elements

The second column set is the same as the first column. The dried sample collected from the first column was dissolved in 1.5 ml of 0.15 M HCL and then loaded into the column; the first 1.5ml elution was discarded. Subsequently, 30 ml of 0.15 M HCL was added to the column and collected.

1.2.3. Third and the fourth column: Removal of Li from Na

The dried sample gained from the second column was dissolved in 1 ml of 0.15 M HCL and then loaded into a quartz column with internal diameter of 3.8 mm. Subsequently, 16 ml of 30% vol. ethanol in 0.5 M HCl was added into the column, which was pressured by the Nitrogen air flow with a rate of 2−4 ml/minute. The total 16 ml elution was collected and dried down for the fourth column, which is the same as the third column.

These four steps of column chemistry were calibrated using different types of samples by Teng et al. (2006b) (peridotite, basalt, granite and pure Li solution) and the Li yield (with ~100 ng sample Li load) is > 98% (Teng et al., 2006b; Marks et al., 2007).

1.3. Mass spectrometry

Sample solutions are analyzed using a Nu Muti-Collector-Inductively Coupled Plasma-Mass Spectrometer. Before making Li isotopic analyses on the unknown samples,

the Na/Li voltage ratio of each solution was tested semi-quantitatively using MC-ICP-MS. Solutions with a Na/Li voltage ratio $\geqslant 5$ were reprocessed through the glass columns before measurement. Generally, after the four stages of column chemistry, the Na/Li ratio is <0.1. The final Li solutions that has Na/Li voltage ratio ≤ 5 are introduced into the plasma by an auto-sampler (ASX-100® Cetac Technologies) through a desolvating nebulizer, either Aridus® Cetac Technologies fitted with a PFA spray chamber and micro-nebulizer or Apex-IR with 2 PFA micro-flow nebulizers (Elemental Scientific Inc.). The solutions usually have ~50 ppb Li and the uptake rate of the solution is 30 to 50μl/m, which works out to ~0.005% transmission efficiency.

The ^{7}Li and ^{6}Li are measured simultaneously in two Faraday cups, H6 and L5, respectively. The typical voltage on the measurements of Li in a 50 ppb solution is ~ 2 volts on ^{7}Li (20 pA on 10^{11} ohm resistor), and comparably, the blank of Li is about 10 mV on mass 7. Li concentration and isotopic composition measurements were determined by voltage and ^{7}Li/^{6}Li comparisons, respectively, between sample solutions and 50 ppb L-SVEC bracketing standard. Two other Li standards (in-house Li-UMD-1 and IRMM-016) were routinely analyzed during the course of an analytical session in order to evaluate the stability of the analysis. Precision on pure Li standards analyzed during my PhD is as follows: UMD-1 (50 ppb, n = 120 runs) δ^{7}Li = 54.1 ± 0.6, IRMM-016 (50 ppb, n = 110 runs) δ^{7}Li = 0.1 ± 0.5 and the rock reference material BCR-1 gives δ^{7}Li = 2.0 ± 0.3 (n = 4 runs). As a benchmark, Teng et al. (2006b) reported BCR-1 δ^{7}Li = 2.0 ± 0.7 in 10 runs and Rudnick et al. (2004) reported a single BCR-1 analysis of δ^{7}Li = 2.7 ± 1. The rock reference material BCR-1 gives [Li] = 12.6 ± 0.6 μg/g (n = 2 runs) and GEOREM preferred value is [Li] = 13 ± 1 μg/g. The two measurements of the rock

reference material BHVO-1 gives δ^7Li = 4.8 ± 0.2 and [Li] = 4.8 ± 0.6 μg/g; in comparison, Magna et al. (2004), Rudnick et al. (2004) and Aulbach and Rudnick (2009), reported the δ^7Li of BHVO-1 to be 5.3 ± 0.2, δ^7Li = 4.3 ± 1 and δ^7Li = 4.5 ± 1, respectively, and the GEOREM (Jochum and Nohl, 2008) preferred BHVO-1 [Li] =4.6 ± 0.2 μg/g. The total procedural blank measured during the course of this study is Li = 0.11 ± 0.12 ng/g (n >200 runs) and δ^7Li = 30.3 ± 40 (8 runs). The long-term external precision of Li isotopic and concentration analyses, over the past ten years, is ≤ 1.0‰ and ±10%, (2σ) respectively, based on the repeat analyses on Li standard (Teng et al., 2006b, Qiu et al., 2009; 2011a)

Chapter 3: Li and δ^7Li in mudrocks from the British Caledonides: metamorphism and source influences[1, 2]

[1] L. Qiu, R.L. Rudnick, W.F. McDonough and R.J. Merriman contributed to the interpretation of the data. The text, tables and figures (except where noted) were created/written by L. Qiu.

[2] This chapter has been published as:
Qiu, L., Rudnick, R.L., McDonough, W.F., Merriman, R.J., 2009. Li and δ^7Li in mudrocks from the British Caledonides: Metamorphism and source influences. *Geochimica Cosmochimca Acta* 73, 7325-7340, doi:10.1016/j.gca.2009.08.017.

Abstract:

Mudrocks from three lower Paleozoic basins in the British Caledonides (southern Lake District, northern Lake District and Southern Uplands) were investigated to determine the influence of sub-greenschist facies metamorphism on Li and the factors that control Li in fine-grained terrigenous sedimentary rocks. Metamorphic grade, as determined by KI (Kübler index) does not correlate with Li content ([Li]) and δ^7Li, indicating that subgreenschist facies metamorphism has negligible effect on Li in these rocks. Collectively, the data for all three basins show a negative correlation between [Li] and δ^7Li and a positive correlation between [Li] and the chemical index of alteration (CIA), suggesting that provenance exerts the greatest control on Li in mudrocks. Samples from the northern Lake District, which were deposited in an extensional basin, have homogeneous REE patterns, similar to shale composites (PAAS), the highest CIA, Th/U and [Li] and the lowest δ^7Li and ε_{Nd}, consistent with their derivation from a highly weathered, ancient continental source. By contrast, mudrocks from the Southern Uplands

range to the lowest CIA, Th/U and [Li] and have the highest δ^7Li and ε_{Nd}. These samples were deposited in a forearc basin on the southern margin of the Laurentian craton and contain volcanic detritus. Their REE patterns are the most variable, ranging from average shale-like patterns to less LREE-enriched patterns. The compositional heterogeneity within the Southern Uplands mudrocks is consistent with a mixed provenance that includes juvenile crustal materials (lower [Li], ε_{Nd} and Th/U, higher δ^7Li), likely derived from the arc, as well as more highly weathered continental detritus. Mudrocks from the southern Lake District were deposited in a foreland basin, and exhibit geochemical characteristics intermediate between the northern Lake District and the Southern Uplands mudrocks, indicating their derivation from a mixed source. Our study shows that Li concentrations and δ^7Li can provide additional information on the degree of weathering of the provenance of mudrocks.

1. Introduction

Lithium, a light alkali metal with its two stable isotopes, ^{6}Li and ^{7}Li, has received significant attention during the last decade due to the large isotopic fractionation that has been documented in near-surface environments (δ^7Li = ~-20‰ to ~ +40‰) (Rudnick et al., 2004; Pogge von Strandmann et al., 2006), and its potential to trace crustal recycling into the mantle. Recent studies have demonstrated large Li isotopic fractionation during arrested diffusion (Richter et al., 2003; Lundstrom et al., 2005; Teng et al., 2006aa; Parkinson et al., 2007; Jeffcoate et al., 2007; Marks et al., 2007; Beck et al., 2005), terrestrial weathering (Pistiner and Henderson, 2003; Huh et al., 2004; Rudnick et al., 2004; Kisakurek et al., 2004), and seafloor alteration (Chan et al., 1993; 1992; 1994; Seyfried et al., 1998; Chan and Kastner, 2000; James et al., 2003; Bouman et al., 2004).

By contrast, very limited Li isotopic fractionation occurs during igneous differentiation (Tomascak et al., 1999; Bryant et al., 2004; Teng et al., 2004; 2006b; Halama et al., 2007). Consequently, this system has been suggested to be a potentially useful tracer of crustal recycling in subduction zones (e.g., Elliott et al., 2004; 2006).

Marine sediments are a major source of Li in subducting slabs and may therefore control the Li budget of recycled materials (Chan et al., 2006). However, the behavior of Li during metamorphic devolatilization of sedimentary rocks has only been partially explored (e.g., Teng et al., 2007), as have the factors that control the Li isotopic composition of terrigneous sediments (Teng et al., 2004; Chan et al., 2006). In particular, the effects of sub-greenschist facies metamorphism on [Li] and δ^7Li, during which significant volatiles may be lost (Merriman and Roberts, 2001), is unknown.

The degree of Li isotope fractionation caused by metamorphic devolatilization is a matter of current debate. In a study of alpine eclogites, which are considered analogs for subducted oceanic crust, Zack et al. (2003) suggested that sub-greenschist to greenschist facies metamorphic dehydration of altered basalts produced the light δ^7Li values (as low as -12‰) seen in some of these samples. By contrast, Marschall et al. (2007), using the spodumene-fluid isotopic fractionation factors of Wunder et al. (2007), suggested that dehydration cannot produce such low δ^7Li. These authors concluded that the very light δ^7Li value seen in some massif eclogites are likely the result of kinetic fractionation during diffusive influx of Li from the country rocks into the eclogite body. Similarly, in a study of the effects of contact metamorphic dehydration of chlorite to sillimanite zone metapelites, Teng et al. (2007) suggested that metamorphic dehydration had little discernible effect on the δ^7Li of the rocks, despite the fact that up to half of the Li was

lost during metamorphism. They showed that the limited isotopic fractionation of up to 3‰ is consistent with published fluid-mineral isotopic partitioning studies (Wunder et al., 2006). However, to date, no comprehensive study of the factors that control Li and its isotopic composition in very low temperature metasediments, i.e., sub-greenschist facies metasediments has been carried out. Such conditions should be representative of metamorphism in the forearc of subduction zones when initial dewatering process occurs.

In a recent review, Chan et al. (2006) document the major influences on the Li abundance and δ^7Li of marine sediments. While a number of factors influence Li in marine sediments, provenance plays a major role in determining the bulk Li isotopic composition and concentration of global marine sediments, with clay-rich sediments generally having higher Li abundance and lower δ^7Li than other oceanic sediments (calcareous oozes, carbonates, sand, and hydrothermally altered sediments). Sediments derived from mature continental crust are especially light and may reflect enhanced or prolonged weathering, whereas volcanogenic sediments derived from unweathered sources have relatively heavier δ^7Li values. It has yet to be established how well these provenance differences are preserved during subduction and metamorphic dehydration and to what degree Li in terrigenous sediments may act as a proxy for weathering in the source region.

We present here the Li concentration [Li], isotopic composition, major-element and trace-element abundances and Nd and Sr isotopic composition for three suites of mudrocks from Lower Paleozoic basins within the British Caledonides. These samples have experienced metamorphic conditions ranging from deep diagenetic to epizonal (lower greenschist facies) metamorphism over a range of dP/dT gradients. These rocks

are used to explore the factors that control lithium concentration and its isotopic composition in subgreenschist facies metapelites and determine whether lithium is lost during dehydration reactions that occur during subgreenschist facies metamorphism, and if so, whether isotopic fractionation occurs.

2. Geological background and samples

The Caledonian mudrocks examined here come from Ordovician to Silurian sedimentary basins that are juxtaposed across the Iapetus Suture, the structural trace within the British Caledonides of the early Paleozoic Iapetus Ocean (Fig. 3-1, Merriman et al., 2009). In the northern Lake District, the Skiddaw Group formed in a sedimentary basin that developed in an extensional setting on the southern margin of the Iapetus Ocean during the early to mid-Ordovician. Thus, these sediments were metamorphosed under relatively high heat flow conditions (35-50°C km^{-1}, Stone and Merriman, 2004). By contrast, the other two sedimentary basins formed in relatively low heat flow regimes (<25°C km^{-1} in the Southern Uplands and <20°C km^{-1} in the southern Lake District, Merriman and Roberts, 2001; Soper and Woodcock, 2003). The Southern Uplands terrane formed as an accretionary thrust complex at the Laurentian continental margin and the southern Lake District evolved largely in response to flexural subsidence of the crust, in convergent plate settings. These latter two basins formed as the Iapetus Ocean closed during the late Ordovician and early Silurian (Leggett et al., 1979; Stone et al., 1987; Kneller, 1991).

In response to sedimentary burial and enhanced heat flow, minerals in sediments undergo diagenetic to very low-grade metamorphic reactions as soft clays and muds are

systematically converted to lithified mudrocks (Merriman and Peacor, 1999). The Caledonian samples from the three basins consist of clays, mostly <2μm in grain size, as

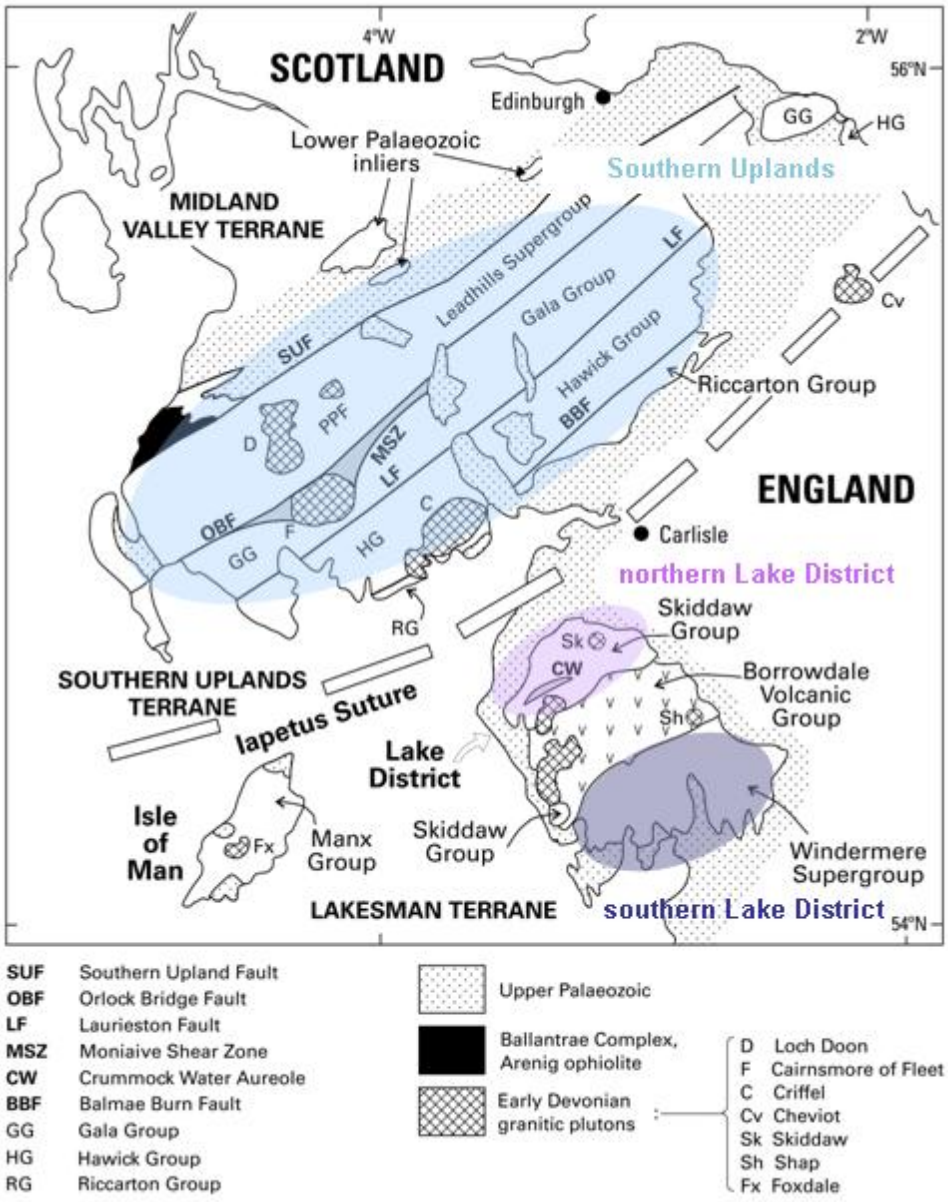

Figure 3-1. Sketch map showing the location of Caledonian terranes and the sedimentary basins sampled for this study (after Merriman et al., 2009).

well as non-clay minerals. The latter include quartz (<40%), albite (<15%) minor amounts (<5%) of calcite, dolomite, K-feldspar, hematite, pyrite, and trace amounts (1<%) of rutile or anatase (Merriman, 2006). In the northern Lake District, clay mineral assemblages include K- and Na-rich white micas, chlorite, minor pyrophyllite, rectorite $(Na,Ca)Al_4(Si,Al)_8O_{20}(OH)_4 \cdot 2(H_2O))$ and corrensite $(Ca,Na,K)(Mg,Fe,Al)_9(Si,Al)_8O_{20}(OH)_{10} \cdot n(H_2O)$. The Na-rich clays indicate relatively high heat flow conditions in the mudrocks (Merriman, 2006). By contrast, Na-micas and pyrophyllite are much less abundant or absent in clay minerals from the Southern Uplands and the southern Lake District (Merriman et al., 2009) due to relatively low heat flow (Fortey, 1989; Cooper et al., 2004). Southern Uplands mudrocks also contain volcanic detritus, including unaltered pyroxene, probably derived from a nearby eroded volcanic arc. The clay minerals in the Southern Uplands samples are rich in chlorite and other Fe, Mg-clays, likely derived from weathering of mafic volcanic detritus.

The metamorphic grade of the samples was determined using the Kübler index (KI), which is a measure of small changes in the width at half-height of the illite-muscovite ~10 Å XRD peak. These changes occur when illite reacts to form muscovite in response to deep diagenesis and low-grade metamorphism in sedimentary basins. With increasing metamorphic grade, the half-height of the illite-muscovite ~10 Å XRD peak value is reduced and the Kübler index decreases (Peacor, 1992). With increasing grade, the KI value is: deep (or late) diagenetic zone KI > 0.42, anchizone KI = 0.42-0.25, and epizone/lower greenschist facies KI < 0.25 (Merriman and Frey, 1999). Typical uncertainty of the KI value determined in this way is less than <10% (2σ, Merriman and Peacor, 1999). Samples from all three basins show a range of KI values of 0.20-0.66, thus

metamorphic grade of the mudrocks varies from diagenesis to lower greenschist facies in each basin.

3. Analytical methods

Samples for chemical analysis were selected to span a range of KI values, which were previously determined by X-ray diffraction (XRD) in order to define the metamorphic grade (Merriman and Peacor, 1999). Whole rock major-elements compositions were determined by X-Ray Fluorescence (XRF) on fused glass disks at Franklin and Marshall College. Accuracy of the XRF data from this lab can be evaluated from results obtained for the BHVO-1 and QLO-1 standards, which are published on the lab website (http://www.fandm.edu/x7992.xml). The accuracy is better than 4% for most major elements except Na_2O for BHVO-1 ($2\sigma = 6.6\%$) and TiO_2 and MnO for QLO-1 ($2\sigma = 4.8\%$ and 11.1%, respectively).

Lithium concentrations and isotopic compositions were determined at the Geochemistry Laboratory of the University of Maryland, College Park. Most of the whole rock powders measured for Li isotopes were the same as those previously analyzed by one of us (Merriman) for selected major and trace elements, as well as KI. However, some original sample powders were fully consumed in that study, necessitating re-sampling and creation of a second batch of whole rock powders for a subset of samples. The new samples were collected at the same outcrop within a few meters from the original site and, thus, should have the same metamorphic grade (KI value) as the original samples. These samples are marked by an "r" in Tables 3-1 and 3-2.

Procedures for sample dissolution, column chemistry and instrumental analysis are the same as those reported in Teng et al. (2006b). The sample dissolution procedure does not

include the high-P teflon bomb process, however, for the samples that contained organic carbon (labeled "o" in Tables 3-1 and 3-2), we used $HClO_4$ in a 1:1 mixture with HF in the first step of sample dissolution. The presence of organic carbon in the samples does not correlate with lithium concentration or isotopic composition, suggesting that there is no organic matter influence on lithium behavior our samples. The long-term external precision of Li isotopic analyses, based on repeat analyses of pure Li standards in this laboratory over the past eight years is $\leq 1.0‰$ (2σ) (Teng et al., 2006b). Precision on pure Li standards analyzed during the course of our analyses is as follows: UMD-1 (50 ppb, n = 40 runs) $\delta^7Li = 54.2 \pm 0.6$, IRMM-016 (100 ppb, n = 38 runs) $\delta^7Li = -0.2 \pm 0.5$ and the rock reference material BCR-1 gives $\delta^7Li=2.0 \pm 0.3$ (n = 2 runs). As a benchmark, Teng et al (2006b) reported BCR-1 $\delta^7Li=2.0 \pm 0.7$ in 10 runs and Rudnick et al (2004) reported BCR-1 $\delta^7Li=2.7 \pm 1‰$. The total procedural blank measured during the course of this study is Li= 0.11 ± 0.12 ng and $\delta^7Li = -25.3\pm 40$. Given the amount of Li processed in any one sample (minimum Li = 30 ng), this blank has negligible effect on both concentration and isotopic composition and thus no blank correction was applied.

Li concentration measurements were determined by voltage comparisons between sample solutions and measurements for a 50 ppb L-SVEC bracketing standard solution and then adjusting for sample weight. The rock reference material BCR-1 gives [Li] $=12.6 \pm 0.6$ μg/g (n = 2 runs) and GEOREM preferred value is [Li] $=13 \pm 1$ μg/g. Typical uncertainty of concentration determined in this way was previously established to be ±10% (1σ, Teng et al., 2006b).

Trace-element abundances were measured using an Element 2 ICP-MS in the Geochemistry Lab, University of Maryland. The digestion procedures were the same as

for Li measurements. Final sample solutions were diluted 2000 times in 2% HNO_3. An indium spike (3 ppb) was introduced to the solutions in order to monitor and correct for signal drift. BHVO-1 served as our calibration standard after applying a blank correction. BHVO-1 analyzed as unknowns during our analyses return concentration within 10% uncertainty of preferred values (Table 3-1).

Strontium and Nd were separated from sample solutions prepared for Li chemistry. Cation exchange column separation was performed in three steps. Strontium and REE cuts were collected by eluting with 2.5N HCl and 6.0N HCl through the column filled with AG 50 W-X12 (200-400) mesh resin. Separation of Nd from other REE was done in another column filled with the same resins. The column was eluted with 0.15N HCl and 0.25N HCl first, followed by 0.34N HCl for Nd cuts. The Sr cut purification was performed using Eichrom Sr-Spec resin in order to remove any remaining Rb (Rb in Sr cut $\leq$ 0.2 %, Aulbach et al., 2008). Strontium was measured at the University of Maryland by VG Sector 54 TIMS in dynamic collection mode after loading cuts onto Re filaments, and using $^{87}Sr/^{86}Sr$ of 0.1194 for mass fractionation correction. The average value of multiple analyses of SRM987 determined during the course of this study is 0.710258±32 (2σ, n=4) relative to the recommended value 0.71025. Neodymium isotopes were measured using a Nu plasma MC-ICP-MS with an Apex nebulizer in the Geochemistry Laboratory, University of Maryland, following the method described by Aulbach et al. (2008). Multiple $^{143}Nd/^{144}Nd$ analyses of AMES Nd standard averaged 0.512175±18 (2σ, n=5); rock standards and samples were normalized to a $^{143}Nd/^{144}Nd$ for AMES of 0.512138 (Aulbach et al., 2008). Using this method, a single analysis of BHVO-1 yielded 0.513048±28 (2σ).

Table 3-1 Geographical, major (%) and trace (μg/g) element data for mudrock samples from the three basins. (continued on next page)

Sample	Grid Reference[M]	SiO_2	TiO_2	Al_2O_3	Fe_2O_3	MnO	MgO	CaO	Na_2O	K_2O	P_2O_5	Total	LOI	LOI*	CIA	Li	Sc	V	Cr	Co
southern Lake District																				
SH19	SD 4085 9840	60.35	0.90	18.4	8.4	0.10	4.94	0.83	1.15	4.27	0.18	99.52	5.3	5.3	71	52	24	160	194	28
SH22	SD 4320 9921	60.86	0.91	18.0	8.3	0.13	4.89	0.57	1.43	4.19	0.21	99.46	4.8	4.8	71	50	19	137	188	22
SH24[o]	NY 4145 0115	59.65	0.88	19.1	8.4	0.08	5.18	0.31	1.30	4.47	0.17	99.58	4.7	4.7	73	40	21	153	183	24
SH59	SD 6219 9093	60.47	0.84	17.4	8.0	0.34	4.53	2.73	1.39	3.83	0.18	99.69	6.2	5.0	67	51	18	126	174	24
LC940	SD 4060 8437	64.88	0.83	14.8	6.7	0.17	3.90	3.14	1.81	3.07	0.23	99.52	5.2	4.0	61	41	14	105	158	16
LC1617[o]	SD 6924 9318	60.73	0.79	15.2	7.0	0.10	4.98	5.99	0.95	3.48	0.14	99.43	8.9	4.9	69	51	14	112	132	19
LC1606[r, o]	SD 5528 8712	62.28	0.90	17.6	8.0	0.08	4.72	0.24	1.66	3.90	0.18	99.52	4.5	4.5	72	53	19	130	215	22
LC1570[r, o]	SD 6860 8770	46.37	0.62	14.1	7.1	0.55	1.89	26.5	0.72	2.24	0.18	100.14	19.3	N/A	75	55	12	102	106	16
LC1618[r, o]	SD 7051 9580	60.15	0.93	18.8	8.8	0.17	2.14	4.46	0.95	3.09	0.13	99.65	8.0	5.2	74	93	19	54	149	10
northern Lake District																				
LC142	NY 1560 1825	65.60	1.06	17.8	9.1	0.10	2.20	0.27	0.75	2.86	0.14	99.92	3.6	3.6	80	80	23	149	209	20
LC199[o]	NY 1649 2111	58.28	1.21	24.0	8.5	0.07	1.98	0.29	0.81	4.14	0.19	99.44	9.6	9.6	80	137	22	144	108	5
LC348	SD 1476 8617	56.83	1.15	25.0	8.8	0.21	1.79	0.35	0.33	5.12	0.26	99.79	4.2	4.2	79	56	22	130	121	9
LC434	NY 3827 2586	57.05	1.24	23.3	11.0	0.29	2.10	0.24	0.97	3.28	0.13	99.63	6.4	6.4	82	108	23	140	134	26
LC507	NY 2956 2520	66.05	1.02	18.8	8.5	0.10	1.87	0.26	0.71	2.36	0.17	99.86	4.6	4.6	83	90	17	118	124	25
LC521[r]	NY 2565 2634	57.88	1.25	24.2	9.4	0.14	1.92	0.34	0.99	3.48	0.13	99.70	4.9	4.9	81	139	23	155	171	15
LC495[r]	NY 4732 2201	56.17	1.09	25.9	9.5	0.18	1.49	0.28	1.00	3.93	0.16	99.70	8.0	8.0	81	69	21	158	149	26
LC482[r]	NY 5506 1311	52.36	1.12	28.9	10.2	0.24	2.05	0.12	0.58	3.85	0.11	99.53	6.3	6.3	85	139	23	154	148	22
Southern Uplands																				
BRS882	NX 830 884	56.07	1.07	20.1	9.0	0.09	5.32	0.45	1.65	5.51	0.25	99.50	4.7	4.7	69	54	22	143	167	32
BRS1028	NX 859 728	58.45	1.02	19.8	7.3	0.06	3.93	3.52	0.41	4.98	0.21	99.67	9.0	6.6	75	68	23	176	167	21
BRS 822[r]	NX 733 754	55.90	0.93	20.9	9.5	0.07	4.89	0.26	1.13	5.74	0.20	99.48	4.2	4.2	72	74	22	147	146	24
BRS 781[r]	NX 7115 8385	58.08	1.04	19.8	8.1	0.07	5.92	0.30	1.11	5.21	0.20	99.88	5.0	5.0	72	55	20	159	206	20
BRS 879[r]	NX 824 908	55.25	1.09	22.0	7.7	0.06	5.47	0.78	1.00	6.12	0.23	99.69	5.2	5.2	71	47	24	162	184	9
BRS753[r]	NX 6358 8363	65.67	0.81	16.4	7.5	0.06	3.64	0.26	1.39	3.51	0.17	99.44	4.2	4.2	73	49	17	123	369	18
BRS742[r, o]	NX 657 823	58.08	1.01	22.9	7.4	0.06	3.30	0.23	1.67	5.34	0.23	100.20	5.3	5.3	73	46	26	170	183	25
BRS710[r, o]	NX 717 488	69.58	0.67	11.9	5.7	0.15	4.09	3.49	2.07	2.07	0.17	99.86	6.9	5.7	57	29	12	94	310	14
BRS807[r]	NX6590 7895	56.98	1.02	19.6	8.8	0.09	5.48	0.65	1.72	4.96	0.21	99.49	4.1	4.1	69	55	23	162	317	20
BRS824[r]	NX 6945 7616	60.34	0.86	19.4	8.2	0.07	4.44	0.42	1.33	4.39	0.26	99.71	4.3	4.3	73	56	18	117	170	17
BRS829[r, o]	NX 688 857	61.40	0.97	21.1	6.0	0.09	3.37	0.12	1.12	5.39	0.17	99.74	5.1	5.1	73	31	22	147	183	17
BRS790[r]	NX 7051 8024	59.90	0.82	16.9	6.9	0.11	4.74	3.85	1.67	3.92	0.78	99.58	5.8	4.1	63	40	18	127	218	15
BHVO-1																	34	337	301	45
BHVO-1[p]																	31	318	287	45

[M]: Merriman et al., 2009

*: corrected by removing CO_2 content, see text for details

[r]: re-sample from the original sample of Merriman et al. (2009)

[o]: sample with organic carbon

[P]: Preferred values from GEOREM; URL:http://georem.mpch-mainz.gwdg.de/

$_n$: chondrite normalized (Sun and McDonough, 1989).

Table 3-1 (continued)

Ni	Cu	Y	Zr	La	Ce	Pr	Nd	Sm	Eu	Gd	Tb	Dy	Ho	Er	Tm	Yb	Lu	Pb	Th	U	Th/U	Th/La	Th/Sc	$(La/Yb)_n$
southern Lake District																								
101	38	25	159	49	101	12	44	8.1	1.7	7.2	1.1	5.0	1.0	3.0	0.42	2.9	0.42	49	14	3.2	4.5	0.29	0.61	11.7
80	31	27	157	42	83	10	38	7.1	1.5	6.2	1.0	5.0	1.0	3.0	0.41	2.7	0.38	12	11	2.7	4.2	0.28	0.61	10.6
96	50	17	142	12	25	4	14	3.1	0.8	3.1	0.5	3.2	0.7	2.2	0.36	2.5	0.38	23	12	2.9	4.2	1.0	0.58	3.2
77	37	26	157	37	77	9	34	6.5	1.4	6.3	0.9	4.8	0.9	2.9	0.41	2.7	0.38	21	11	2.5	4.3	0.29	0.59	9.4
62	30	30	173	42	87	10	39	7.4	1.6	6.8	1.0	5.5	1.1	3.1	0.43	2.8	0.40	23	11	2.6	4.4	0.27	0.77	10.2
56	44	24	133	35	75	9	33	6.2	1.3	5.8	0.9	4.5	0.9	2.7	0.38	2.5	0.36	50	10	2.9	3.4	0.29	0.71	9.5
90	48	24	158	40	86	10	35	6.3	1.2	5.9	0.8	4.6	0.9	2.7	0.42	2.7	0.40	11	13	3.4	3.7	0.31	0.68	10.2
82	14	25	73	39	73	9	34	6.7	1.3	6.6	0.9	4.7	0.9	2.6	0.34	2.2	0.31	19	9	1.7	5.4	0.23	0.74	11.8
64	74	26	129	43	84	10	38	6.4	1.2	6.0	0.9	4.3	0.9	2.7	0.37	2.5	0.36	89	13	2.2	5.8	0.30	0.67	11.7
northern Lake District																								
48	55	26	88	47	102	12	44	8.7	1.9	9.5	1.1	5.7	1.1	3.2	0.47	3.2	0.48	157	15	2.8	5.2	0.31	0.64	9.9
21	11	26	142	49	100	12	44	8.3	1.7	6.8	1.1	5.4	1.0	3.0	0.41	2.7	0.40	57	16	2.8	5.7	0.33	0.73	12.2
40	6	33	134	57	108	13	47	8.9	1.9	9.0	1.3	6.3	1.2	3.6	0.48	3.1	0.44	5	18	2.8	6.4	0.31	0.80	12.2
51	38	27	154	49	97	11	39	6.9	1.5	5.7	0.9	4.9	1.0	3.1	0.44	2.9	0.42	14	14	2.4	5.9	0.29	0.63	11.5
48	28	22	165	43	88	10	35	6.2	1.4	5.7	0.8	4.2	0.8	2.5	0.35	2.4	0.35	14	14	2.3	5.9	0.32	0.80	12.2
40	21	26	134	46	97	11	41	7.8	1.7	7.4	1.1	5.1	1.0	3.0	0.41	2.7	0.40	27	15	2.5	6.2	0.33	0.66	11.5
50	4	33	133	67	136	15	53	9.8	2.1	9.1	1.2	6.3	1.2	3.6	0.50	3.2	0.45	9	20	2.8	7.0	0.29	0.92	14.3
51	22	29	117	67	132	14	51	8.7	1.8	7.3	1.1	5.6	1.1	3.2	0.45	2.9	0.41	23	20	3.0	6.7	0.29	0.86	15.9
Southern Uplands																								
83	9	43	223	44	94	11	40	7.6	1.9	7.6	1.2	7.4	1.5	4.3	0.62	3.9	0.57	11	15	3.1	4.9	0.34	0.67	7.6
77	54	29	165	40	83	10	35	6.6	1.4	6.1	1.0	5.3	1.1	3.2	0.47	3.1	0.45	17	14	3.1	4.3	0.34	0.58	9.0
100	35	40	216	92	153	18	64	11.4	2.6	11.3	1.6	7.8	1.5	4.3	0.59	3.7	0.53	29	14	3.1	4.7	0.16	0.64	16.8
92	33	33	287	53	105	13	46	7.5	1.7	6.8	1.1	5.7	1.2	3.8	0.56	3.8	0.56	6	11	3.5	3.3	0.22	0.58	9.6
50	27	29	201	5	16	2	11	3.7	1.1	4.0	0.7	5.1	1.1	3.1	0.50	3.2	0.48	11	14	3.5	3.9	2.7	0.55	1.1
124	36	23	146	36	76	9	32	5.9	1.3	6.0	0.8	4.4	0.9	2.5	0.35	2.3	0.34	29	10	2.9	3.4	0.28	0.57	10.5
96	91	25	193	43	87	10	36	6.5	1.6	5.9	0.9	4.6	0.9	2.9	0.41	2.7	0.40	20	12	3.2	3.9	0.29	0.48	10.8
107	11	20	53	32	62	7	27	5.2	1.2	5.2	0.7	3.8	0.7	2.2	0.30	1.9	0.28	11	7	1.7	4.3	0.22	0.62	11.4
120	241	18	159	18	40	5	19	3.7	1.0	3.7	0.6	3.2	0.7	2.2	0.35	2.4	0.36	11	12	3.1	3.9	0.65	0.53	5.1
77	4	28	164	49	104	12	47	9.2	1.8	7.9	1.1	5.5	1.0	3.0	0.41	2.7	0.40	6	12	2.7	4.5	0.25	0.68	12.3
66	130	32	166	47	88	11	41	7.6	1.7	7.7	1.1	5.7	1.1	3.2	0.45	2.9	0.41	5	12	2.4	5.1	0.26	0.55	11.1
125	46	28	165	48	80	11	41	7.3	1.7	7.3	1.0	5.0	1.0	3.1	0.44	2.9	0.43	723	10	2.5	4.1	0.21	0.56	11.2
126	152	27	184	16	39	5.6	26	6.4	2.2	6.8	1.0	5.6	1.0	2.7	0.3	2.1	0.29	2.6	1.1	0.4				
118	137	26	174	16	38	5.4	25	6.1	2.1	6.3	1.0	5.3	1.0	2.6	0.3	2.0	0.27	2.4	1.2	0.4				

Table 3-2. Lithium concentrations and Li, Sr and Nd isotopic compositions for whole rock samples from the three basins.

Sample	KI[M]	Li	Li[M]	δ^7Li	Sr	Rb	$^{87}Rb/^{86}Sr$	$^{87}Sr/^{86}Sr$	$^{87}Sr/^{86}Sr_{(i)}$	Sm	Nd	$^{147}Sm/^{144}Nd$	$^{143}Nd/^{144}Nd$	$\varepsilon Nd_{(i)}$
southern Lake District														
SH19	0.29	52	46	-1.4										
SH22	0.29	50	45	-0.5	47	162	10.1	0.77792	0.71311	7.13	38.3	0.114	0.51195	-8.6
SH24[o]	0.27	40	41	0.0	41	177	12.6	0.79914	0.71830	3.15	13.6	0.141	0.51203	-8.6
SH59	0.33	51	48	-0.6										
LC940	0.26	41	38	-0.4	135	104	2.2	0.72899	0.71468	7.44	39.1	0.116	0.51201	-7.6
LC1617[o]	0.45	51	46	-0.6										
LC1606[r, o]	0.34	53	56	-0.4										
LC1570[r, o]	0.40	55	43	-1.4	1179	85	0.2	0.70914	0.70780	6.87	34.0	0.124	0.51202	-8.0
LC1618[r, o]	0.66	93	65	-3.4	565	131	0.7	0.71225	0.70795	6.58	38.6	0.104	0.51199	-7.4
northern Lake District														
LC142	0.32	80	67	-3.5										
LC199[o]	0.22	137	129	-1.8	136	189	4.0	0.74046	0.71459	8.26	43.8	0.114	0.51193	-9.2
LC348	0.20	56	50	-3.2	55	237	12.5	0.79018	0.71037	9.11	48.2	0.116	0.51195	-8.8
LC434	0.51	108	116	-3.8										
LC507	0.46	90	86	-3.7	81	114	4.1	0.73956	0.71355	6.28	34.3	0.112	0.51196	-8.3
LC521[r]	0.39	139	118	-4.0	134	161	3.5	0.73553	0.71318	7.89	42.5	0.117	0.51194	-9.1
LC495[r]	0.63	69	138	-3.7										
LC482[r]	0.40	139	130	-2.2										
Southern Uplands														
BRS882	0.28	54	46	1.0	135	165	3.5	0.73675	0.71413	7.64	39.8	0.121	0.51207	-6.6
BRS1028	0.44	68	70	-2.4	101	175	5.0	0.74419	0.71212	6.61	34.9	0.116	0.51207	-6.5
BRS 822[r]	0.37	74	60	-4.4	66	213	9.3	0.76776	0.70811	11.43	63.7	0.109	0.51199	-7.6
BRS 781[r]	0.20	55	42	1.6										
BRS 879[r]	0.29	47	37	2.1	55	227	12.0	0.78527	0.70831	3.75	10.7	0.213	0.51235	-6.7
BRS753[r]	0.32	49	45	2.2										
BRS742[r, o]	0.45	46	45	0.3	100	121	3.5	0.74172	0.71918	6.76	36.2	0.116	0.51204	-7.0
BRS710[r, o]	0.50	29	43	0.7	74	80	4.9	0.72714	0.69570	5.32	26.8	0.121	0.51211	-6.0
BRS807[r]	0.22	55	52	-1.3	148	109	3.4	0.72812	0.70628	3.86	19.1	0.126	0.51201	-8.2
BRS824[r]	0.23	56	50	0.6										
BRS829[r, o]	0.48	31	43	3.7	41	184	13.1	0.79284	0.70875	7.61	40.2	0.116	0.51198	-8.2
BRS790[r]	0.20	40	43	1.3	224	133	1.7	0.72085	0.70983	7.52	40.9	0.112	0.51203	-7.0
BHVO-1													0.51305	
BHVO-1[p]													0.51298	
BCR-1		12.6±0.6		2.0±0.3										
BCR-1[p]		13		1.8										

KI:Kübler index
[M]: Merriman et al., 2009
[r]: re-sample from the original sample of Merriman et al. (2009)
[o]: sample with organic carbon
[P]: Preferred values from GEOREM; URL:http://georem.mpch-mainz.gwdg.de/
i: initial value, assuming depositional age of sediments are 450ma; $^{143}Nd/^{144}Nd_{chur(0)}$=0.512638

4. Results

Major- and trace-element concentrations of all samples are reported in Table 3-1. Lithium concentrations and isotopic compositions are reported in Table 3-2, along with the KI values and Nd and Sr isotopic compositions.

4.1. Lithium concentration and its isotopic composition

The concentrations of Li determined in this study are generally within 2 sigma analytical uncertainties of those determined by Merriman et al. (2009) via solution ICP-MS (Table 3-2). The exceptions are the samples for which new powders were prepared (sixteen, in total). For three of these samples, LC1618, BRS822 and BRS879, our Li concentrations are about 20-40% higher (i.e., just beyond 2 sigma uncertainty) than those determined by Merriman et al. (2009). By contrast, for three other samples, LC495, BRS710 and BRS829, our Li concentrations are about 20-50% lower than those determined by Merriman et al. (2009). For the remaining 10 new powders, [Li] determined here is within error of that previously determined by Merriman et al. (2009) on the original powders. Because these discrepancies exist only for separate powders of re-sampled outcrops, they likely reflect heterogeneity of Li concentration at the outcrop scale. Although KI was not determined on the new samples, we assume that metamorphic grade will not vary significantly on the outcrop scale, and therefore the KI for the original rock samples also applies to the new powders prepared for samples from the same outcrop.

Lithium concentrations of the mudrocks vary widely, from 29 to 139 μg/g, with samples from the northern Lake District generally having higher concentrations (56-139 μg/g), average 102 μg/g) than those from the Southern Uplands (28-74 μg/g, average 50

μg/g) or southern Lake District (40-93 μg/g, average 52 μg/g) basins. There is no correlation between [Li] and metamorphic grade within a given basin, as indicated by KI (Fig. 3-2a). The only possible exception to this is for the mudrocks from the southern Lake District basin (Fig. 3-2a), but the trend in these data is defined by a single sample with a high [Li].

Lithium isotopic compositions (Fig. 3-2b) of mudrocks from the northern Lake District (average δ^7L= -3.2± 1.1, 1σ) are relatively constant and low compared to those of the mudrocks from the southern Lake District (-3.4 to 0, average = -1 ± 1, 1σ) and the Southern Uplands (-4.4 to +3.7, average = +0.5 ± 2.2, 1σ), the latter of which contain the volcanic arc detritus and show the greatest variation in δ^7Li of all basins. There is no correlation between δ^7Li and metamorphic grade (Fig.3- 2b).

4.2. Chemical index of Alteration (CIA) and Loss on ignition (LOI)

The Chemical Index of Alteration (CIA) is a useful means by which to quantify the intensity of weathering (Nesbitt and Young, 1982). The index is calculated using molar proportions of major oxides: $CIA=Al_2O_3 / (Al_2O_3+CaO^*+Na_2O+K_2O)$, where CaO* is the amount of Ca incorporated in the silicate fraction of the rock. Correction for Ca in apatite is done on the basis of the P_2O_5 concentration. Correction for Ca in carbonate is generally done on the basis of CO_2 concentrations. Due to the lack of CO_2 concentration data for our samples, only Ca in apatite corrections were carried out for samples that have $CaO/ Na_2O < 1$. If $CaO/Na_2O >1$, it was assumed that the concentration of silicate CaO equals that of Na_2O and that the other CaO is from $CaCO_3$ (Bock et al., 1998). In general, the higher the CIA, the more intense the weathering; a value of 40-60 is defined

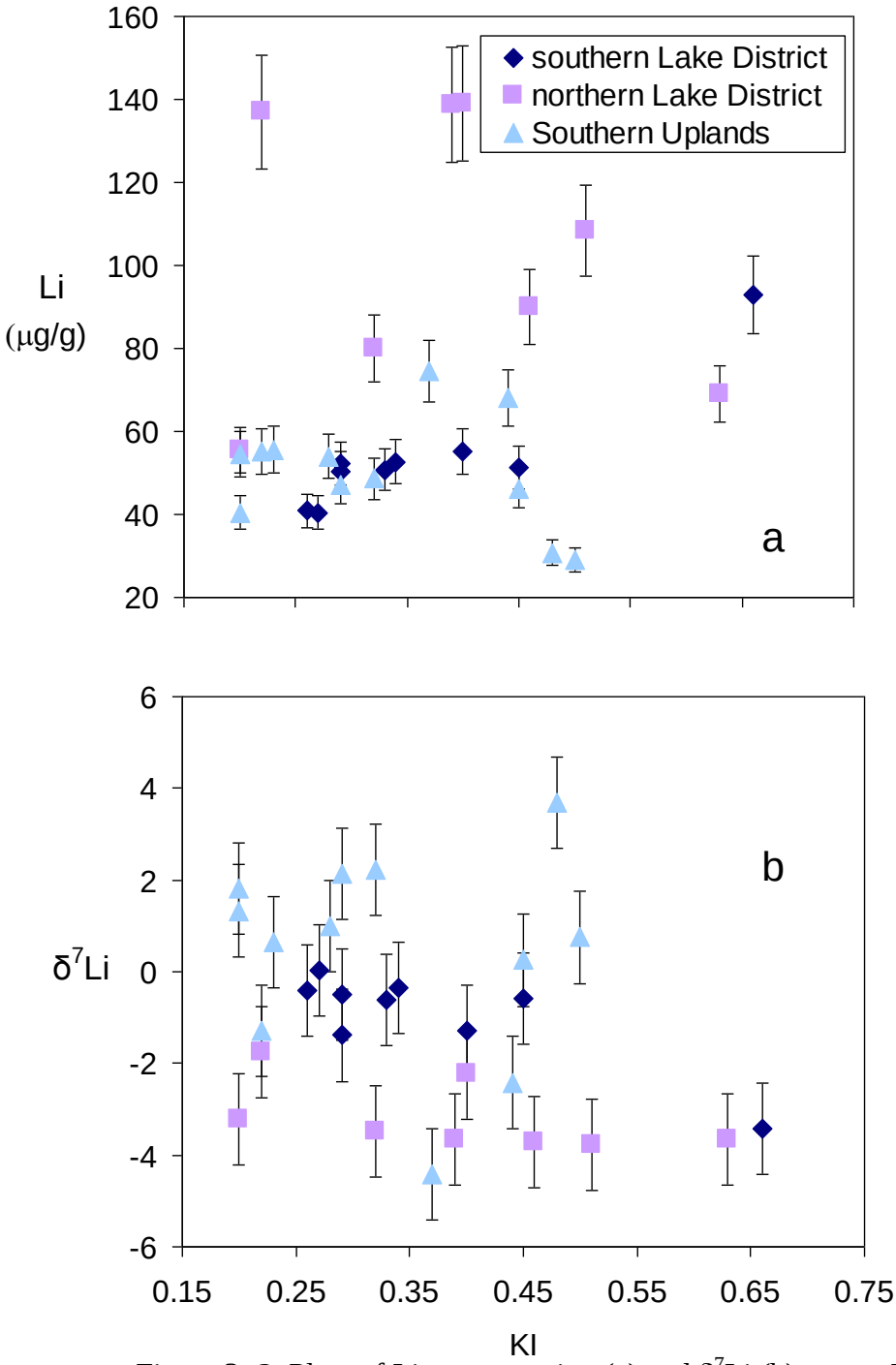

Figure 3- 2. Plots of Li concentration (a) and δ^7Li (b) versus KI value (Kübler index) for mudrocks from the three Caledonian basins.

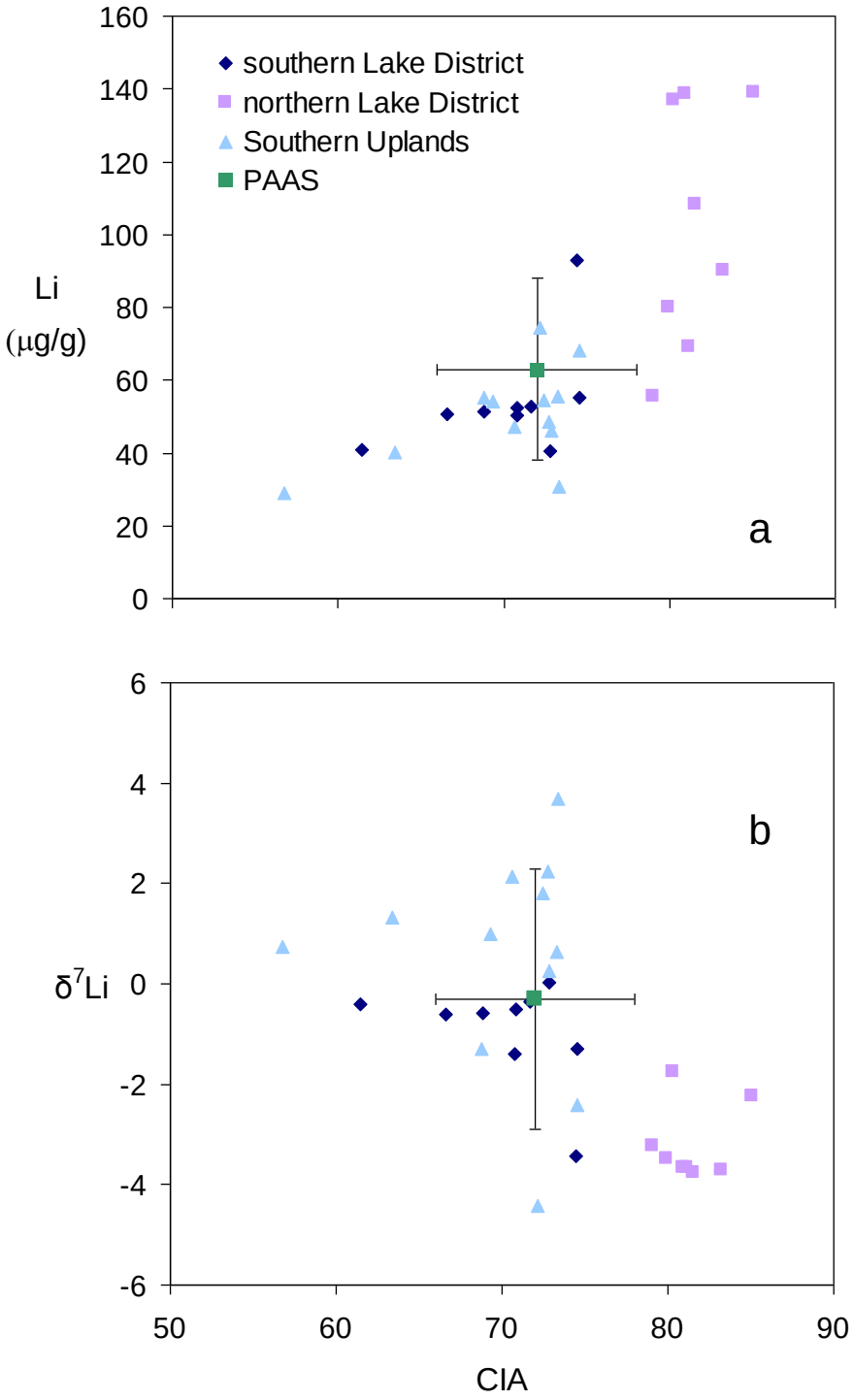

Figure 3-3. Plots of Li concentration [Li] (a) and δ^7Li (b) versus CIA (Chemical Index of alteration) for mudrocks from the three Caledonian basins. PAAS: Post Archean Australian Shales. Average [Li] and δ^7Li of PAAS is from Teng et al. (2004), showing 1σ of the average.

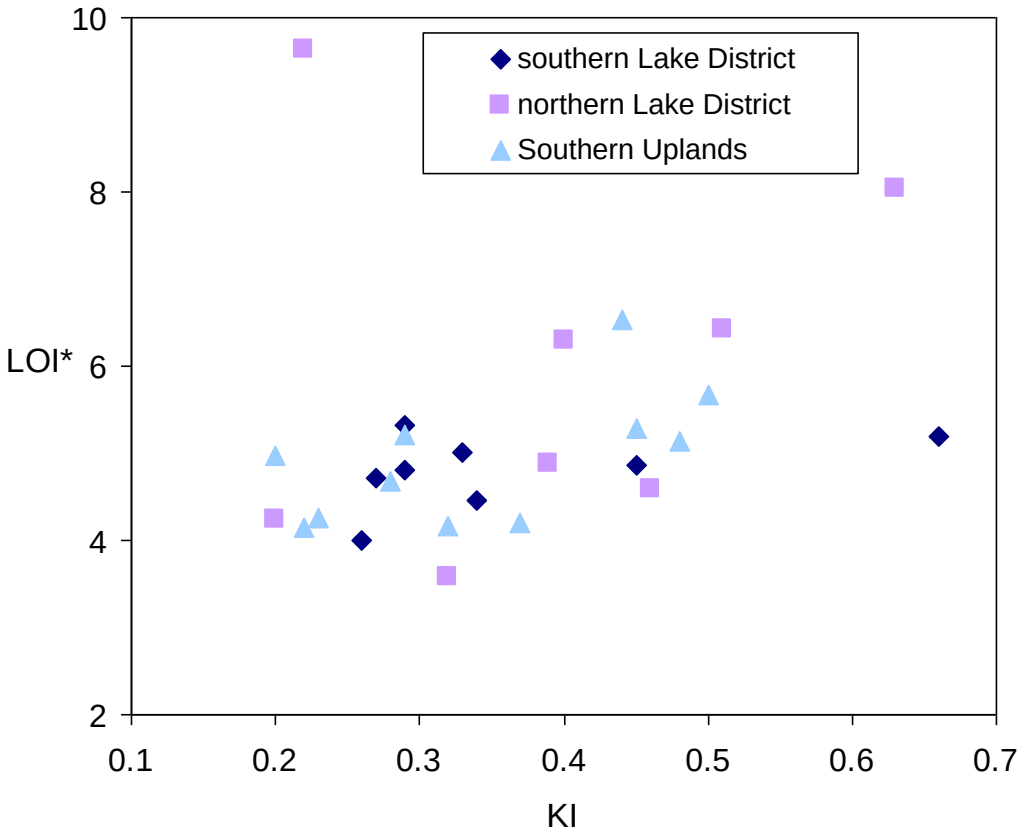

Figure 3-4. Plot of LOI* (loss on ignition) and KI value (Kübler index) for three Caledonian basins. LOI* reflects water content only after removing CO_2 content, see text for details. Correlation coefficients for the data from the three basins are as follows: 0.45 for southern Lake District, 0.82 for northern Lake District (excluding the sample with the highest LOI that clearly deviates from the trend) and 0.61 for Southern Uplands.

as “low weathering”; 60-80 as “intermediate weathering”, and 80-100 as “heavy weathering” (Nesbitt and Young, 1982).

The CIA of most samples from the Southern Uplands and southern Lake District is between 61~75 (Fig. 3-3), indicating an intermediate degree of weathering in the source region. A single sample from the Southern Uplands has a low CIA (57), indicating a low degree of weathering. Northern Lake District mudrocks have the highest CIA values of 79-85, indicating a high degree of weathering of their source rocks. Lithium concentrations generally increase with CIA value (Fig. 3-3a). The correlation between δ^7Li and CIA is not strong, though mudrocks with the highest CIA values generally have the lowest δ^7Li (Fig. 3-3b).

Relative H_2O loss by metamorphic dehydration can be estimated by comparing LOI (loss on ignition, which approximates rock volatile content, mainly $H_2O + CO_2$) contents in the samples (Teng et al., 2007). In order to estimate the H_2O component of the LOI, CO_2 values are subtracted using the same method applied to the CIA correction by calculating $CaCO_3$ based on CaO/NaO. One exception is sample LC1570, which has the highest volatile content, abnormally low SiO_2 and high CaO (Table 3-1). Because these compositional characteristics indicate that this sample has a large carbonate content, it was not included in the LOI study. Generally speaking, LOI* (Table 3-1) shows a positive trend with KI value (Fig. 3-4, except for the sample with the highest LOI*); LOI* changes by a factor of ~3 in northern Lake District samples and by a factor of 1.3~1.6 in samples from the other two basins. Thus, with increasing metamorphic grade, the H_2O content in the samples decreases.

4.3. Trace elements

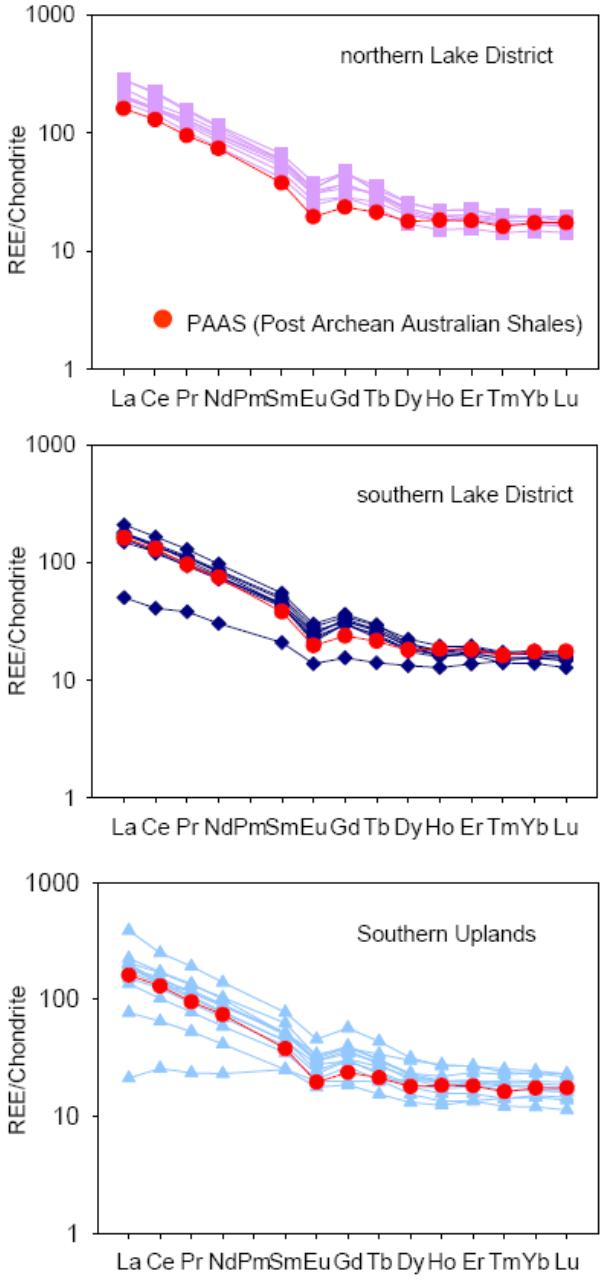

Figure 3-5. Chondrite normalized rare earth element plot for mudrock samples from the three Caledonian basins. Chondrite normalization values are from Sun and McDonough (1989). PAAS value (Post Archean Australian Shales) is from Taylor and McLennan (1985).

REE, Th, Sc are useful elements for determining the proportion of mafic to felsic igneous rocks in the provenance of clastic sedimentary rocks (McLennan et al., 1993a; Asiedu et al., 2000), since they include both incompatible elements (LREE, Th) and compatible elements (Sc), whose concentrations are not significantly affected by weathering, transport and diagenesis. Concentrations of these elements in clastic sedimentary rocks are, thus, also useful for determining the average composition of the upper continental crust (Taylor and McLennan, 1985; Rudnick and Gao, 2003).

On chondrite-normalized REE diagrams (Fig.3-5), all of the samples from the northern Lake District and most of the samples from the southern Lake District exhibit LREE enrichment and a relatively narrow range of $(La/Yb)_n$: 9.9~15.9, which is similar to post-Archean Australian shale (9.3 for PAAS; Taylor and McLennan, 1985). One sample from the southern Lake District (SH24) has a low $(La/Yb)_n$ of 3.2. In contrast, the REE patterns of Southern Uplands mudrocks are more variable ($(La/Yb)_n$ =1.1~16.8), including one sample that has a LREE depleted pattern.

Mudrocks from the northern Lake District have consistent Th/La of 0.29~0.33 relative to the other two basins, and an average value of 0.31± 0.01 (1σ) that is slightly lower than that of PAAS (Th/La = 0.35). Southern Lake District mudrocks have Th/La mostly between 0.23 and 0.31, with one sample (the same one that had a different REE pattern, SH24) having a distinctly higher Th/La of 1.0. As with their REE patterns, the Southern Uplands mudrocks have highly variable Th/La of 0.16~2.7.

The Th/Sc ratios of all mudrocks studied here are, in general, lower than that of PAAS. Amongst the different basins, the northern Lake District mudrocks have the highest average Th/Sc (Th/Sc=0.76± 0.11, 1σ), which is closer to the value of PAAS

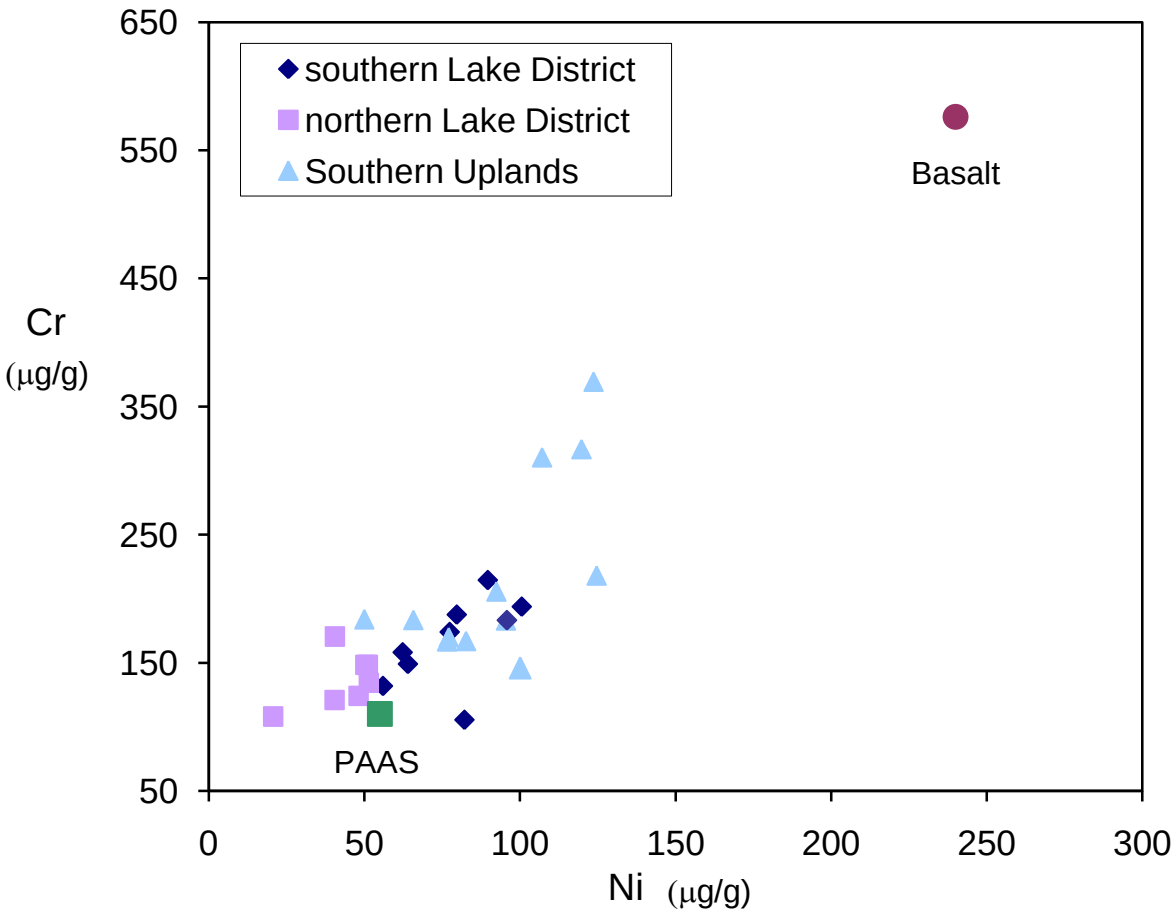

Figure 3-6. Plot of Ni versus Cr concentration for mudrocks from three Caledonian basins. The Ni and Cr contents of PAAS and basalts are from Taylor and McLennan (1985), standard deviations for these estimates are not available. The mudrock data have a correlation coefficient of 0.70.

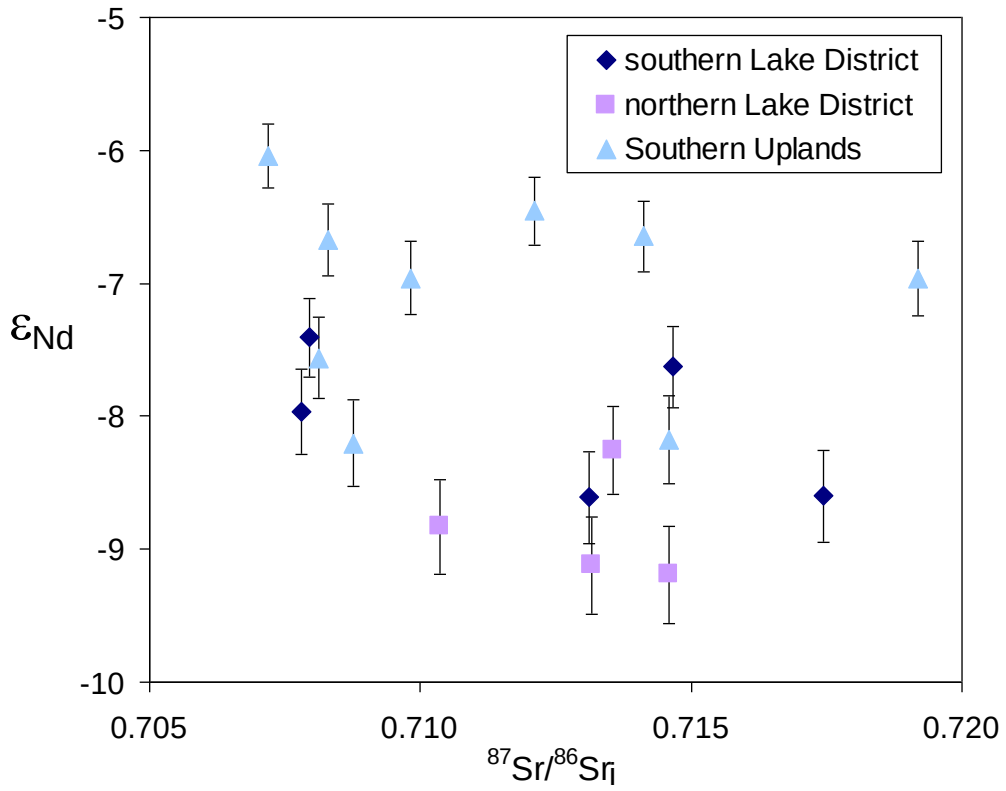

Figure 3-7. Plot of initial $^{87}Sr/^{86}Sr$ and initial ε_{Nd}, assuming that the depositional age of the sediments is 450 Ma and $^{143}Nd/^{144}Nd_{chur(0)}$=0.512638.

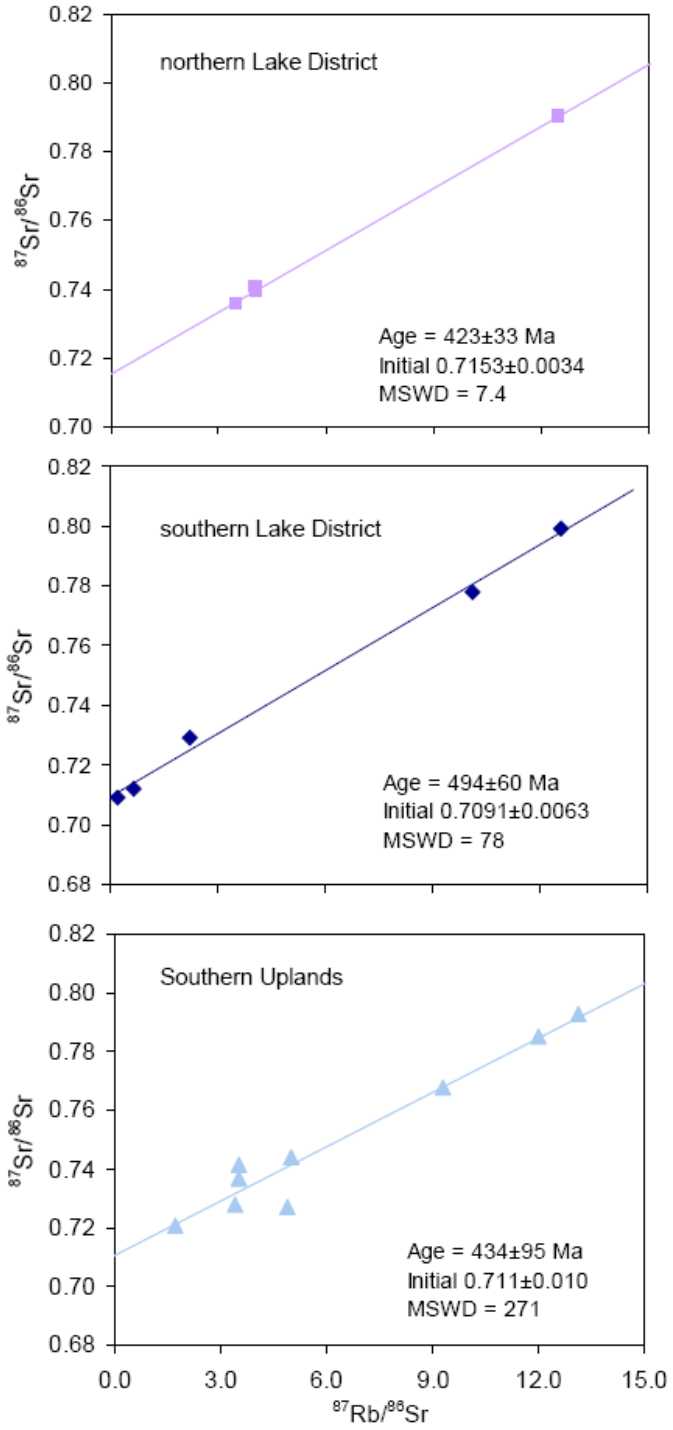

Figure 3-8. Plots of Rb-Sr pseudo-isochron regression lines for mudrocks from three Caledonian basins. Note the MSWD value increases from the northern Lake District to the southern Lake District and to Southern Uplands. See text for details.

(Th/Sc=0.9) than the average Th/Sc of mudrocks from the other two basins (southern Lake District: Th/Sc=0.66 ± 0.07, 1σ; Southern Uplands: Th/Sc=0.58 ± 0.06, 1σ).

Th/U ratio can also be an indicator of weathering intensity of the sediment source (McLennan et al., 1993a). Mudrocks from the northern Lake District have higher average Th/U

ratio (6.1 ± 0.6, 1σ) than those from the southern Lake District (4.4 ± 0.7, 1σ) and Southern Uplands (4.2 ± 0.5, 1σ).

The ferromagnesian trace elements, Ni and Cr, are generally abundant in mafic and ultramafic rocks relative to felsic rocks, so their abundance in sedimentary rocks may be indicative of the provenance of the sediments (McLennan et al., 1993b). In the British Caledonides mudrocks, Ni and Cr are positively correlated (Fig. 3-6), with the northern Lake District samples having the lowest average concentrations (average = 44 and 145 μg/g,

respectively) and the Southern Uplands samples having the highest average concentrations (93 and 218 μg/g, respectively), with the samples from the southern Lake District falling in between (79 and 166 μg/g, respectively).

4.4. Sr and Nd isotopes

Samples chosen for Nd and Sr isotope analyses are representative of the three basins and include samples with suspected mantle-derived signatures based on their trace-element abundances as well as the presence of volcanic arc detritus; the average [Li] and δ^7Li of the selected rocks are similar to the average value of all the samples within the basin. The Nd and Sr isotopic compositions of sediments reflects the average provenance

age (McCulloch et al., 1987; McLennan et al., 1993b). These mudrocks are marine sediments deposited during the Ordovician to Silurian. Initial Sr and Nd isotope ratios are therefore calculated assuming an average depositional age of 450 Ma (Fig. 3-7). Although the Rb-Sr regression lines (Fig. 3-8) have a large variation in MSWD, the ages corresponding to the regression lines range from 423 ± 33 Ma to 494 ± 60 Ma and therefore the ~450 Ma age is consistent with the interpreted depositional age. Initial ε_{Nd} values for the three basins (Table 3-2) show a general increase from the northern Lake District (average = -8.8±0.4, 1 σ) to southern Lake District (average = -8.0±0.4, 1 σ) to Southern Uplands (average = -7.0 ± 0.8, 1 σ).

5. Discussion

5.1. Effects of metamorphism on Li

Lithium is a fluid-mobile element whose partitioning behavior between fluid and rock ($^{fluid/rock}K_{Li}$) varies as a function of temperature; $^{fluid/rock}K_{Li}$ is always greater than 1, and increases with increasing temperature (Seyfried et al., 1998). This means that Li concentrations in mudrocks are expected to decrease with increasing metamorphic grade, since dehydration reactions dominate in metapelites from sub-greenschist through granulite-facies metamorphism. On the basis of petrologic and thermobarometric studies, Marschall et al. (2007) suggested that, depending on the initial H_2O content, between 5 and 40% of the original Li can be lost from rocks during metamorphic dehydration. Teng et al. (2007) showed that about 50% of Li was lost from regional chlorite-zone metapelites during contact metamorphism up to sillimanite-zone. The correlation between LOI and KI of our samples (Fig. 3-4) indicates that up to 50% of the original

H_2O has been lost during sub-greenschist-facies metamorphism ranging from diagenesis to epizone (90°C~ 300 °C, Frey and Robinson, 1999; Hower, 1976; Kisch, 1983). However, [Li] in the mudrocks (Fig. 3-2a) does not change systematically over this interval, indicating that Li is not progressively lost under conditions of sub-greenschist facies metamorphism. Lithium isotopic compositions also do not show a correlation with metamorphic grade in the sub-greenschist facies (Fig. 3-2b). This relatively stable lithium signature during prograde metamorphism probably reflects Li sorption onto clay minerals, which are relatively abundant in all of the mudrocks investigated here (Merriman, 2006).

5.2. Factors controlling lithium signature in mudrocks: Provenance of sediments

The above observations suggest that variations in [Li] and δ^7Li are not directly influenced by sub-greenschist facies metamorphism. In fact, the relationship between concentration and isotopic composition shows the opposite trend to what would be expected if metamorphism had caused Li loss and lighter isotopic composition via metamorphic dehydration. More specifically, increasing [Li] is correlated with lighter isotopic compositions (Fig. 3-9). The correlation shows a much larger range than the PAAS composite, which has average δ^7Li = -0.3 ± 2.6‰ (1 σ), and [Li] = 63 ± 25 μg/g (1 σ) (Teng et al., 2004). We propose that the correlation in Fig. 3-9 may reflect differences in the provenance of the mudrocks.

A variety of compatible and incompatible elements and their ratios, as well as Nd isotope compositions, have proven useful for deducing the nature of the provenance for fine-grained sedimentary rocks (Taylor and McLennan, 1985; McLennan et al., 1993a, and references therein). Here we use the REE patterns, Th/Sc, La/Th, Th/U, Cr and Ni

Table 3-3. Compositional characteristics used to infer provenance for the mudrocks.

Indicators	Felsic	Mafic	N. Lake District	S. Lake District	Southern Uplands
La/Yb	high	low	high	variable	variable
Th/Sc	high	low	high	intermediate	low
Th/La	high	low	high	variable	variable
Ni, Cr (ppm)	low	high	low	intermediate	high
ε_{Nd}	low	high	low	intermediate	high

Felsic source indicates the provenance includes a PAAS-like component; mafic source indicates an arc volcanic rock component.

concentrations and Nd isotopes to unravel the proportion of felsic to mafic crust in the source region of the mudrocks. The results are summarized in Table 3-3 and discussed below.

In general, mafic rocks contain low LREE/HREE ratios, whereas felsic rocks usually contain higher LREE/HREE ratios (Taylor and McLennan, 1985). One sample from the southern Lake District and three samples from the Southern Uplands have low $(La/Yb)_n$ relative to PAAS (Fig. 3-5), suggesting a higher proportion of mafic rocks in their source region. REE patterns of the other samples assessed here resemble that of PAAS, indicative of an average upper continental crustal source.

The source difference is also reflected by Th, Sc, Ni, Cr signatures. During igneous differentiation, Th is incompatible and, therefore, is expected to be abundant in felsic crust, whereas Sc, which is compatible, is expected to be abundant in mafic crust (Taylor and McLennan, 1985). The increasing average ratio of Th/Sc from Southern Uplands (0.58) to southern Lake District (0.66) and northern Lake District (0.78) indicates that the provenances of these sediments change from relatively mafic to relatively felsic crust that approaches the PAAS value (0.9).

Another ratio that may discriminate mafic from felsic sources is Th/La ratio, which is high in the upper continental crust (0.25 to 0.35, Rudnick and Gao, 2003 and references therein), low in intraplate and mid-ocean ridge basalts (< 0.1, Sun and McDonough, 1989) and highly variable in arc basalts (0.06 to 0.6), reflecting the variable amount of subducted sediments in their sources (Plank, 2005). Mudrocks from the northern Lake District have fairly constant Th/La at about (0.29 to 0.33), which is close to the value for PAAS (0.35, Taylor and McLennan, 1985) and overlaps that of the upper continental

crust. This consistency in Th/La of the northern Lake District mudrocks suggests their derivation from well-homogenized upper continental crust, possibly pre-existing mudrocks. By contrast, the large variation in Th/La of Southern Uplands (0.15 to 2.5) and southern Lake District mudrocks (0.23 to 1) indicates a heterogeneous source of sediments, which likely includes arc volcanic rocks.

The compatible elements Cr and Ni are especially sensitive to the proportion of mafic to ultramafic rocks in a sedimentary source region. The northern Lake District has lower Cr and Ni contents (Fig. 3-6) than the other two basins, and average concentrations (Cr=145, Ni=44) close to those of PAAS (Cr=110, Ni=55, Taylor and McLennan, 1985). The Southern Uplands and southern Lake District mudrocks have a larger range of Cr and Ni contents, and the concentrations are much higher than northern Lake District (up to Cr=369 and Ni=124), which is close to the concentrations in island arc volcanic rocks (Cr=330, Ni=185, Taylor and McLennan, 1985). The Ni and Cr signature also indicates that the Southern Uplands and southern Lake District have a significant proportion of mafic rocks in their provenance, but the northern Lake District has a provenance similar to that of PAAS. The Southern Uplands samples contain volcanic detritus, including unaltered pyroxene, attributed to an eroded volcanic arc (Merriman et al., 2009), which is consistent with a greater proportion of mafic rocks in their source region. Recycling of this volcanic detritus into the southern Lake District basin may have occurred during the uplift and erosion of the Southern Uplands terrane (Stone et al., 1987).

Mantle versus older crustal sources can also be distinguished by their distinctive Nd isotopic ratios (Figs. 3-7 and 3-8). Old continental crust is typically characterized by ε_{Nd}<-6 (McCulloch and Wasserburg, 1978), and juvenile crust has ε_{Nd}>+5 (DePaolo et

al., 1991, Kelemen et al., 2003). From the Southern Uplands, to the southern Lake District to the northern Lake District, the average value of initial ε_{Nd} decreases slightly from ~ -7 to ~ -9, reflecting increasingly older components in their provenances.

5.3. Mixing model for Lithium

As discussed above, the provenance of these three basin sediments include mafic juvenile sources, and older, more felsic, upper continental crust sources. Southern Uplands and southern Lake District samples contain both of these components, whereas the northern Lake District appears to have a more homogeneous provenance similar to upper continental crust material, like PAAS, but with higher [Li] and lower δ^7Li. Basaltic arc lavas have [Li] = 6.5 ± 2.9 μg/g (1 σ) and δ^7Li = 4.7 ± 1.8‰ (1 σ) (based on 65 samples, Moriguti and Nakamura, 1998; Magna et al., 2006a; Moriguti et al., 2004; Tomascak et al., 2002, 2004; Chan et al., 2002), whereas PAAS has [Li] = 63 ± 25 μg/g (1 σ) and δ^7Li= -0.3 ± 2.6‰ (1 σ) (Teng et al., 2004). Mixing between average basaltic arc lava and PAAS reproduces most of the range seen in the majority of Southern Uplands and southern Lake District samples, albeit with slightly different mixing proportions (the Southern Uplands samples have a greater proportion of the arc component, Fig. 3-9). By contrast, the three samples in these two basins with high [Li] maybe a mixture between an arc lava component and the average northern Lake District mudrocks (Fig. 3-9). However, the majority of the Southern Uplands and southern Lake District samples do not fall on the mixing array between arc basalt and the northern Lake District average composition. This indicates there are likely different mixing end members applying to different samples in the southern Lake District and Southern Uplands basins.

5.4. Lithium: a useful indicator of weathering

Weathering of continental crust produces light lithium isotopic compositions (Chan and Edmond, 1988; Huh et al., 2004; Rudnick et al., 2004.). Based on the observation that the upper continental crust is characterized by lower δ^7Li values of 0 ± 2‰ (1σ, Teng et al., 2004) than upper mantle derived MORB (4 ± 2‰, 1σ, Chan et al., 1992; Elliott et al., 2006; Moriguti and Nakamura, 1998; Nishio et al., 2007; Tomascak et al., 2008), Teng et al. (2004) suggested that the isotopically light signature of the upper continental crust is due to weathering processes, which preferentially remove heavy lithium to water. River water and ocean water have heavy lithium isotopic compositions (ocean water: δ^7Li=31‰, Chan and Edmond, 1988; You and Chan, 1996), and residues of intense crustal weathering, such as saprolites, have very light isotopic composition (δ^7Li down to -20‰, Rudnick et al., 2004).

Besides the Chemical Index of Alteration (section 4.2), the Th/U ratio also reflects the different weathering intensity of the provenances. In an oxidized environment, U is more fluid-mobile than Th, and will be preferentially removed from rocks by weathering, resulting in elevated Th/U in highly weathered domains (McLennan et al., 1993b). Estimates of the average Th/U ratio of the upper continental crust range from 3.8 to 4.3 (Taylor and McLennan, 1985; Rudnick and Gao, 2003), whereas the ratio for mantle rocks varies from 2.6 to 3.8 (Paul et al., 2003). McLennan et al. (1993) suggested sedimentary rocks characterized by Th/U greater than that of PAAS (Th/U = 4.7) have been influenced by weathering processes. All of the northern Lake District samples have Th/U > 5.2, whereas only two samples from the southern Lake District and two samples from the Southern Uplands have Th/U greater than 4.7. Th/U of the mudrocks from the

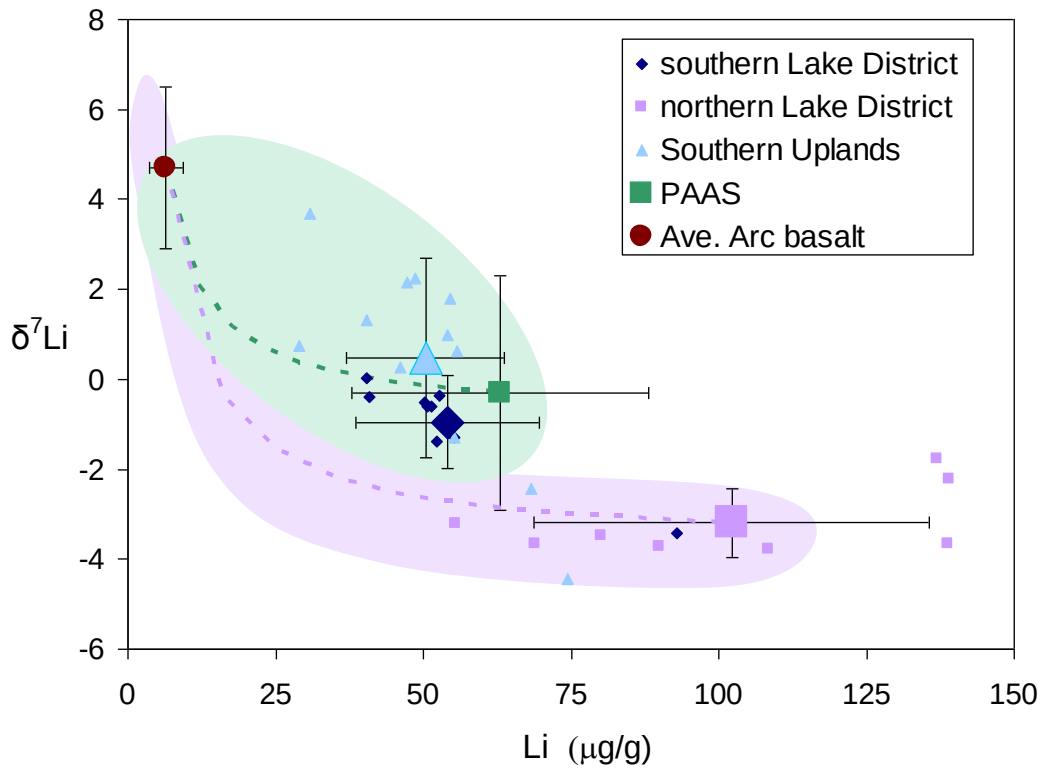

Figure 3-9. Two end-member mixing trends between average basaltic arc lava and either PAAS (light green) or average northern Lake District mudrock (light purple). Basaltic arc lavas have [Li] = 6.5 ± 2.9 (1 σ) μg/g and δ^7Li = 4.7 ± 1.8‰ (1σ), whereas PAAS has 63 ± 25 (1σ) ppm Li and δ^7Li= -0.3 ± 2.6‰ (1σ) and northern Lake District has 102 ± 33 (1σ) μg/g Li and δ^7Li= -3 ± 1‰ (1σ). Large solid symbol for each of the three basins show the average and 1 s for the samples from each basin. The dashed lines are mixing trends between the two end-members, whereas the fields incorporate 1σ uncertainties in the averages. See text for further details.

three basins show a positive correlation with CIA (Fig. 3-10), and therefore like CIA, Th/U also shows a positive correlation with [Li] and negative correlation with δ^7Li (Fig. 3-11). According to these signatures, the northern Lake District samples are clearly derived from a more highly weathered provenance compared to samples from the other basins.

Lithium concentrations generally increase and δ^7Li values decrease with higher CIA (Fig. 3-3). Although the northern Lake District mudrocks exhibit consistently low δ^7Li (down to -3.8), consistent with significant weathering, the Li abundances of these samples are actually enriched relative to PAAS, counter to what is expected from a weathered provenance. The high [Li] in these samples is likely due to an abundance and wide variety of clay minerals, including Na-bearing species in these samples (Merriman, 2006). Thus, although the northern Lake District mudrocks derived from a highly weathered source that has preferentially lost ^{7}Li during weathering process, the concentration of Li is elevated by the abundance of clay minerals.

During clay mineral formation process, Li likely substitutes for Mg^{2+} in the octahedral sites in the crystal lattice (Vigier et al., 2008; Williams and Hervig, 2005). This process may be responsible for higher lithium concentration in the mudrocks of the northern Lake District. A way of evaluating the relative clay mineral proportion is through an A-CN-K ternary plot (Al_2O_3-CaO+Na_2O-K_2O); the closer to the Al_2O_3 apex, the higher the clay mineral proportions in the samples (Nesbitt and Young, 1984) (Fig. 3-12). The first stage of weathering on this type of diagram is represented by the lower arrow in Fig. 3-12, radiating away from the CaO+Na_2O apex, resulting in the depletion of CaO and Na_2O in primary minerals such as feldspars or pyroxenes. Later stages of

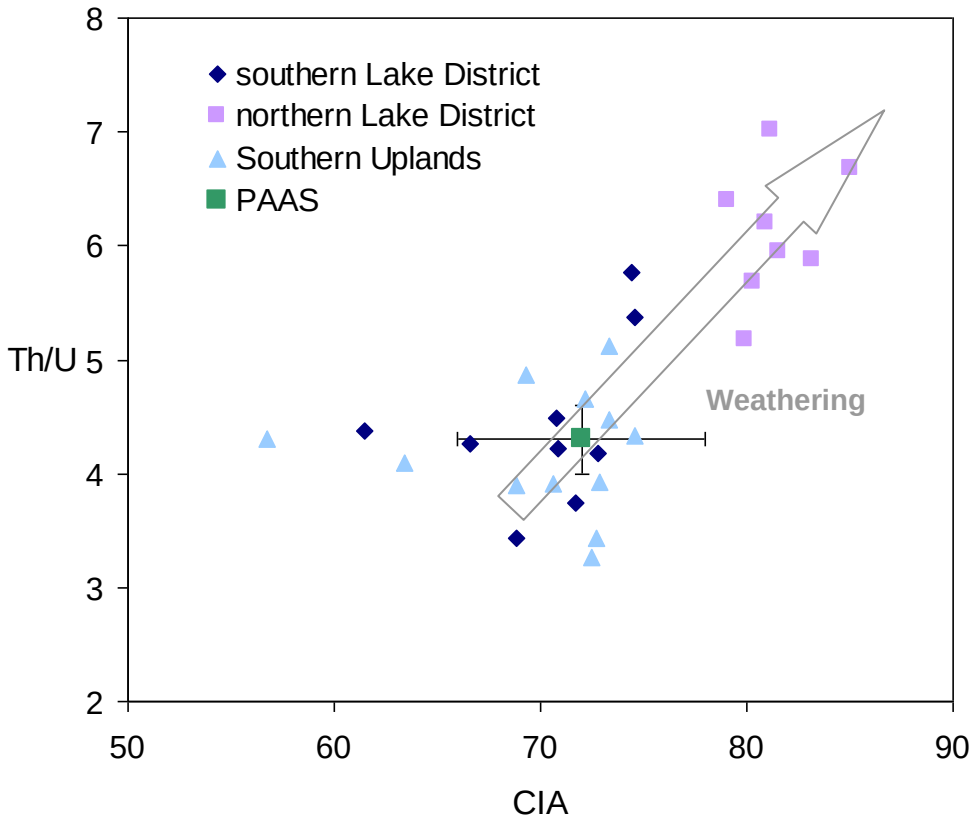

Figure 3-10. Plot of Th/U versus CIA value (Chemical Index of Alteration). Open arrow indicates the direction of increased weathering. Th/U of PAAS is from Taylor and McLennan (1985). CIA of PAAS is from Teng et al. (2004). See text for discussion.

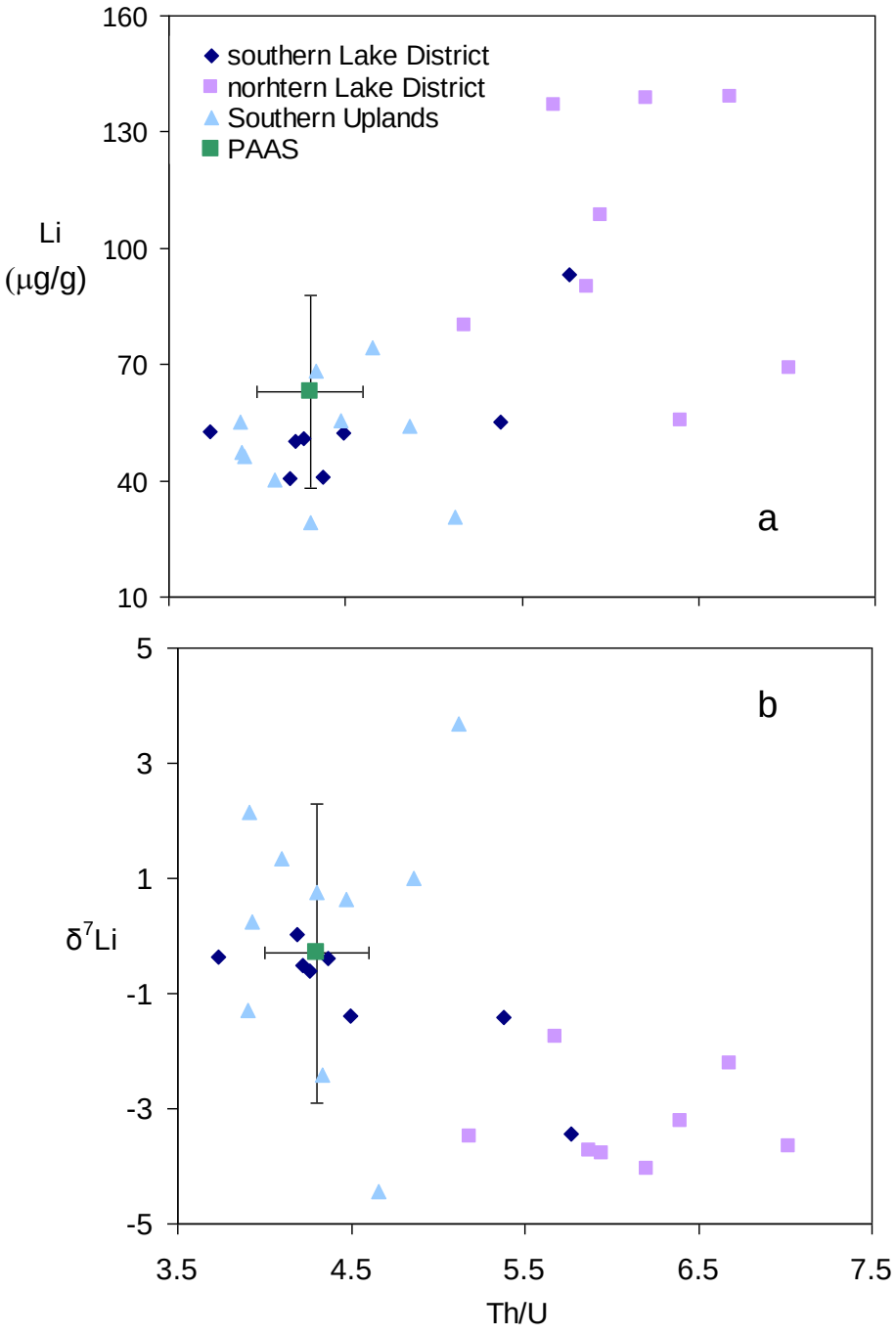

Figure 3-11. Plots of [Li] (a) and δ^7Li (b) versus Th/U, respectively. CIA, [Li] and [δ^7Li] of PAAS is from Teng et al. (2004). Th/U of PAAS is from Taylor and McLennan (1985)

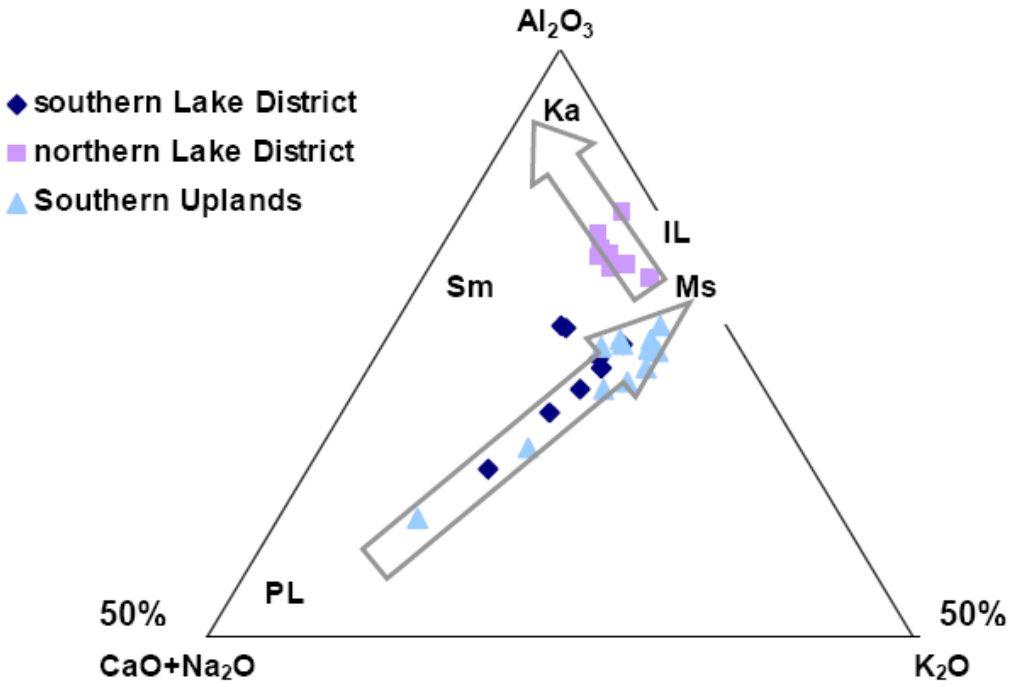

Figure 3-12. The Al_2O_3-(CaO*+Na_2O)-K_2O (A-CN-K) ternary diagram for mudrocks from the three basins (after Nesbitt and Young, 1984). Open arrows are plotted according to Wollast and Chou (1992). See section 4.2 and 5.4 for details. Abbreviations mark position on plot for the following minerals: Pl – plagioclase feldspar; Sm – Smectite; Ms – Muscovite; IL – Illite; Ka – Kaolinite.

weathering produce clays that are enriched in Al_2O_3 by removing K_2O and forming Al-rich clay minerals such as kaolinite and halloysite (upper arrow, Wollast and Chou, 1992). Southern Lake District and Southern Uplands mudrocks fall on the first stage of this weathering trend, whereas northern Lake District mudrocks fall on the second stage of the weathering trend, which indicates higher degrees of weathering, significant clay mineral formation and possibly multiple cycles of sedimentation in the northern Lake District samples. Therefore, the high lithium concentration in the northern Lake District basin likely reflects the high modal proportions of clay minerals.

In conclusion, Li isotopic compositions, when combined with concentration data, is an indicator of weathering intensity for pelitic sediments; mudrocks with high Li concentrations (over 63 μg/g, average of PAAS, Teng et al., 2004) but light isotopic compositions (<-3‰) likely derive from a highly weathered provenance.

6. Conclusions

Three suites of mudrocks from three Lower Paleozoic basins within the British Caledonides exhibit wide variation of lithium concentration and isotopic composition, ranging from 29 to 139 μg/g and -4.4‰ to +3.7‰ respectively. [Li] and δ^7Li in the mudrocks do not correlate with sub-greenschist facies metamorphic grade determined by the Kübler index, suggesting little impact of low grade metamorphism on these variables. CIA values, trace elements, and Nd and Sr isotope data indicate that the provenances of the sediments control the signature of lithium in these three basins. Mudrocks from the Southern Uplands and the southern Lake District reflect a mixed provenance of arc lavas and PAAS-like upper continental crust, whereas mudrocks from the northern Lake District are clay-rich, derived from a highly weathered, older upper continental crust

source. The higher [Li] in the mudrocks of the northern Lake District reflects the higher proportions and greater variety of clay minerals in the rocks. Thus, lithium in mudrocks can be used as an indicator of weathering intensity of their source regions.

Chapter 4: A lithium isotopic study of sub-greenschist to greenschist facies metamorphism in an accretionary prism, New Zealand[1, 2]

[1] L. Qiu, R.L. Rudnick, J.J. Ague and W.F. McDonough contributed to the interpretation of the data. The Matlab code was created by J. Ague. Major and trace elements of the composites are from Breeding and Ague (2002). The text, tables and figures (except where noted) were created/written by L. Qiu.

[2] This chapter has been published as:

Qiu, L., Rudnick, R.L., Ague, J.J., McDonough, W.F., 2011a. A lithium isotopic study of sub-greenschist to greenschist facies metamorphism in an accretionary prism, New Zealand. *Earth Planetary Science Letters* 301, 213-221, doi:10.1016/j.epsl.2010.11.001.

Abstract:

To investigate the behavior of Li during low-grade metamorphism and fluid flux in an accretionary prism we measured the Li concentrations ([Li]) and isotopic compositions (δ^7Li) of sub-greenschist and greenschist-facies Otago Schist composites, as well as cross-cutting quartz veins, which are interpreted to have precipitated from slab-derived fluids. The average [Li] of sub-greenschist facies composites (41 ± 13 μg/g, 2σ) is statistically distinct (97% confidence level, student t test) to that of greenschist facies composites (34 ± 9 μg/g, 2σ), which have experienced mass addition of silica in the form of quartz veins having [Li] between 0.4 − 2.3 μg/g. A linear regression of the correlation between [Li] and calculated mass additions suggests that the depletion of [Li] in greenschist facies composites is due to both dilution from the addition of the quartz veins,

as well as metamorphic dehydration. The [Li] of both groups of composites correlates with their CIA (Chemical Index of Alteration) values (50 − 58), which are low, consistent with the inferred graywacke protolith of the Otago Schist. The δ^7Li of sub-greenschist and greenschist facies composites are remarkably constant, with an average δ^7Li of 0.2 ± 1.7 (2σ) and -0.5 ± 1.9 (2σ), respectively, and comparable to that of the average upper continental crust. Thus, metamorphism has had no discernable effect on δ^7Li in these samples. The Li isotopic signature of the schists is similar to that seen in pelitic sedimentary rocks and likely reflects the δ^7Li of the protoliths. The surprisingly light δ^7Li of the quartz veins (-2.8 to -1.4) likely records kinetic fractionation associated with Li ingress into the veins from surrounding wallrock.

An isotopic equilibrium fluid flow model indicates that: 1) if the [Li] of slab-derived fluids is less than a few μg/g, the δ^7Li of the overlying lithologies (i.e., the schists) is not significantly influenced by the fluid flux, regardless of the δ^7Li of the fluids, 2) the slab-derived fluids will have heavy δ^7Li of > +10 after reacting with the prism sediments during their ascent, and 3) the [Li] of the slab-derived fluids is likely in the range of 0 <[Li] ≤ 41(μg/g). Thus, isotopically heavy slab-derived fluids that traverse sediments in accretionary prisms may leave little trace in the rocks and their surface compositional characteristics will reflect the net result of their interaction with the sediments of the prism.

1. Introduction

The fluid-mobile element lithium increasingly receives attention because of the large isotopic fractionation in δ^7Li that can occur at the Earth's surface and its possible

usefulness as a tracer of crustal recycling in subduction zones (e.g., Elliott et al., 2004, 2006 and references therein). Nevertheless, Li isotopic fractionation during low-grade metamorphism, particularly during subduction-zone metamorphism, remains a matter of debate (e.g., Zack et al., 2003; Marschall et al., 2007).

Recent findings reveal that metamorphic dehydration has had little discernible effect on δ^7Li, even in the presence of lithium depletion (Marschall et al., 2007; Teng et al., 2007; Qiu et al., 2009). For example, the Li isotopic compositions of mudrocks from basins in the British Caledonides are unaffected by sub-greenschist facies metamorphism and reflect the Li isotopic signature of the protoliths (Qiu et al., 2009). However, metamorphism in the British mudrocks occurred at shallow depths, where initial dewatering occurs and pore water in the sediments dominates the fluid flux. Fluid flux and metamorphism occurring at deeper levels within accretionary prisms may be more complex. For example, greenschist facies metamorphism in an accretionary prism can be accompanied by ingress of large volumes of fluids derived from metamorphic dehydration of the subducting slab. These fluids may interact with the overlying metamorphic rocks to form quartz veins (Kerrich, 1999; Smith and Yardley, 1999, Breeding and Ague, 2002).

To date, the signature of Li in greenschist facies metamorphic rocks from accretionary prisms and associated fluid fluxing have not been investigated. Here, we report the Li concentrations and isotopic compositions of the Otago Schist, New Zealand, which constitutes a typical sequence of sub-greenschist to highly veined greenschist facies meta-graywackes and metapelites that formed in an accretionary prism (Bishop, 1972; Mortimer, 1993). The results from this study offer insights into the behavior of Li

during low-grade metamorphism, the factors controlling the Li isotopic composition of accretionary prism sedimentary rocks and, for the first time, provide information about the behavior of Li during fluid fluxing in an accretionary prism.

2. Geological background and samples

The Otago Schist is one of the three geographically discrete units of the Mesozoic Haast Schist belt, New Zealand; the other two are the Marlborough and Alpine Schist. The Otago Schist, comprising the Permian-Cretaceous Torlesse and Caples terranes (Fig. 4-1), forms an approximately 150-km-wide structural arch, with prehnite-pumpyllyite facies on the two outer flanks and greenschist facies in the center. The protoliths of the schist, principally graywacke-mudstone turbidites, were deposited and metamorphosed during subduction (Mortimer, 2000, 2003) and the burial and exhumation processes in the accretionary prism are recorded in these regional metamorphic rocks (e.g., Batt et al., 2001).

The composite samples of the Otago Schist (Fig. 4-1, 17 composites from Torlesse terrane and four composites from the Caples terrane) were collected using a traverse sampling technique in order to measure bulk compositions of whole outcrops as a function of metamorphism (Breeding and Ague, 2002). In this method, representative samples (~3–16 kg) were collected at regular intervals along a measuring tape laid out at a high angle to lithologic layering or foliation. The average traverse was ~50-meters long and comprised 26 samples. After pulverizing, two grams of each of the 26 samples were mixed to form the outcrop composite (Breeding and Ague, 2002). The sub-greenschist and greenschist facies samples are characterized by meta-graywacke and metapelitic assemblages, mainly composed of quartz, albite, chlorite and muscovite, with small

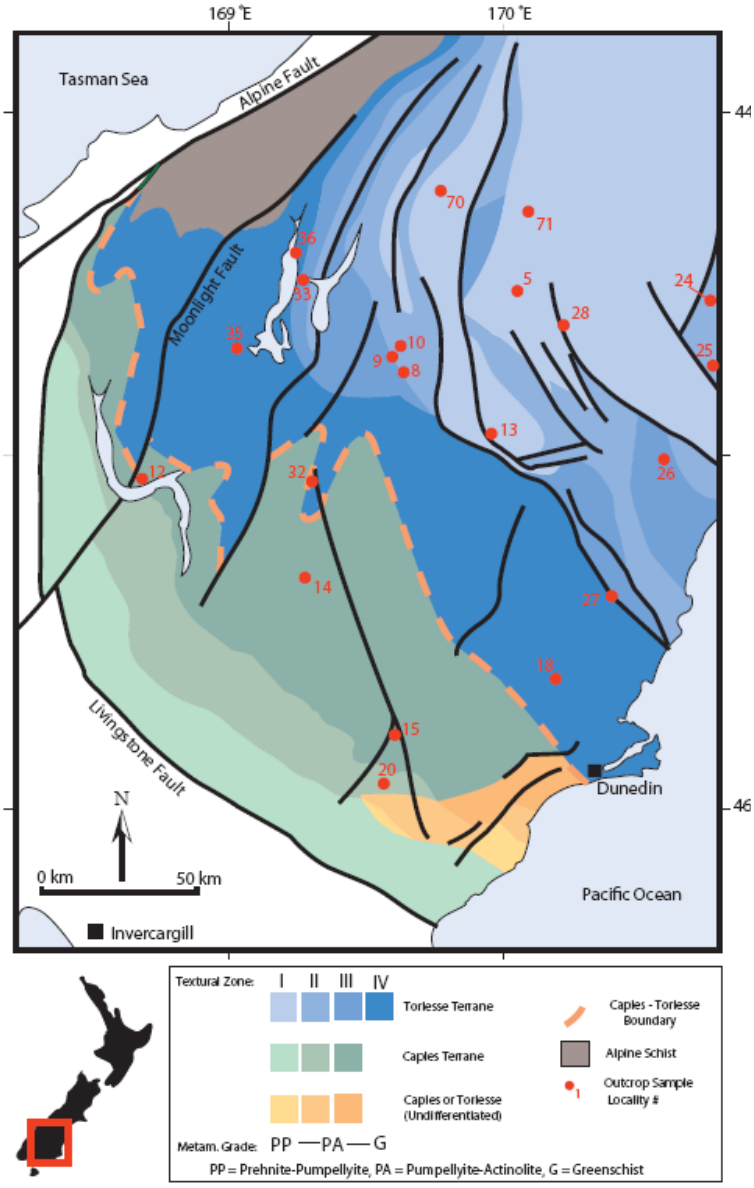

Figure 4-1. Sketch map showing the sample location of Otago Schist, New Zealand (from Breeding, 2004). "Texture zones" indicate the degree of macroscopic deformation textures of the minerals, with zone I being least deformed and zone IV being most deformed (Breeding, 2004).

amounts of calcite, epidote, and stilpnomelane; the sub-greenschist facies samples also contain ~15 vol% of prehnite and pumpellyite. The disappearance of prehnite and pumpellyite and the appearance of clinozoisite marks the change from sub-greenschist to greenschist facies metamorphism (Bishop, 1972).

Relatively undeformed sub-greenschist facies samples are nearly vein-free and are traditionally considered as the precursor lithologies of the greenschist facies metamorphic rocks, which are highly deformed and contain significant amounts of veins (up to 30 vol%) composed primarily of quartz, with lesser amounts of albite, calcite and clinozoisite. According to Breeding and Ague (2002), the greenschist facies outcrops can be divided into three groups. Seven of 10 sampled outcrops (referred to herein as Group A) have experienced mass addition of externally derived silica, interpreted to be deposited from slab-derived fluids originating from the deep prism; one outcrop, in the Macraes Flat area Au-W deposit (referred to herein as Group B), was probably flushed with retrograde metamorphic fluids from relatively shallow depths (De Ronde et al., 2000) or disturbed by later short-lived thermal events (Mortensen et al., 2010). The remaining two outcrops (referred to herein as Group C) contain veins of locally derived silica and may have experienced mass loss. While we present data for all groups, we primarily focus on Group A, as this group likely provides more detailed information about Li behavior during fluid fluxing. Several quartz veins in Group A outcrops, which are coarse enough to be separated completely, were manually cut from the wallrocks and analyzed in order to investigate the Li signature of the fluids (see Appendix 4-A for photos of the veins and thin sections).

3. Methods

Lithium concentration and isotopic compositions of the composites and selected quartz veins were determined at the Geochemistry Laboratory of the University of Maryland, College Park. Sample dissolution procedures, column chemistry and instrumental analysis are reported in Teng et al. (2006b) and Qiu et al. (2009). Briefly, samples were dissolved in a screw-top teflon beaker with a combination of HF–HNO_3–HCl. Lithium was purified on a cation exchange resin (Bio-Rad AG50w-X12, 200–400mesh) first in an HCl medium, followed by an HCl-ethanol medium. Lithium concentrations and isotopic compositions were analyzed using the standard-sample-bracketing method on a Nu Plasma MC-ICPMS. One measurement of the rock reference material BCR-1 gives δ^7Li = 2.2 and [Li] = 12.7 μg/g; as a benchmark, Teng et al. (2006), Rudnick et al. (2004) and Magna et al. (2004) reported the δ^7Li of BCR-1 to be 2.0 ± 0.7 (10 runs), δ^7Li = 2.7 ± 1 (3 runs) and δ^7Li = 2.4 ± 0.5 (4 runs), respectively, and GEOREM (Jochum and Nohl, 2008) preferred BCR-1 [Li] = 13 ± 1 μg/g. The long-term external precision of the Li isotopic composition and concentration analyses are ≤ 1.0‰ (2σ) and ±10% (2σ), respectively, based on repeat analyses of pure Li standards and standard reference materials, respectively, over the past nine years (Teng et al., 2006).

4. Results

Lithium concentrations and isotopic compositions are reported in Table 4-1, along with the major and trace elements of the composites from Breeding and Ague (2002). The [Li] in the sub-greenschist facies composites vary from 26 to 48 μg/g (Fig. 4-2), with an average of 41 ± 13 μg/g (2σ). The [Li] in the Group A greenschist facies composites

Table 4-1. Lithium concentrations (μg/g), isotopic compositions, and major (wt.%) and trace elements (μg/g) data for Otago Schist composites.

		Sample	NZ grid	Li (μg/g)	δ^7Li	Mass.	SiO_2	TiO_2	Al_2O_3	Fe_2O_3	MnO	MgO	CaO	Na_2O	K_2O	P_2O_5	LOI	LOI*	Total	CIA	Rb	Sr	Zr	Ba	W
sub-greenschist facies		JANZ-5	H39 699340	47	0.1	N/A	63.3	0.73	16.2	5.71	0.09	2.16	2.78	3.25	2.0	0.17	3.40	3.40	99.8	57	88	240	164	442	0.58
		JANZ-8	G40 335023	41	0.0	N/A	66.0	0.62	15.3	4.20	0.06	1.60	2.42	3.39		0.16	2.15	2.15	98.6	55	10	308	222	585	/
		JANZ-9	G40 315068	48	0.4	N/A	67.0	0.57	15.4	4.12	0.07	1.44	2.30	3.78	2.8	0.13	2.10	2.10	99.8	54	10	317	212	667	/
		JANZ-10	G40 316067	43	-0.6	N/A	66.9	0.59	15.0	4.15	0.07	1.58	2.13	3.85	2.6	0.11	1.90	1.90	98.9	54	98	287	203	688	0.15
		JANZ-13	H41 653881	47	2.6	N/A	64.3	0.64	16.1	4.75	0.07	1.97	2.40	3.44	2.9	0.17	2.20	2.20	98.9	56	10	386	177	629	0.49
		JANZ-20	G44 373719	47	-0.3	N/A	66.3	0.63	15.8	4.07	0.06	1.42	1.62	3.52	3.3	0.15	2.20	2.20	99.2	57	12	191	205	608	0.28
		JANZ-24	I39 280295	34	0.4	N/A	65.3	0.64	15.7	4.62	0.08	1.89	2.75	3.44	2.5	0.17	2.70	2.70	99.8	55	10	238	188	594	0.43
		JANZ-25	J39 323104	26	-0.5	N/A	66.0	0.60	15.8	3.82	0.07	1.50	2.33	3.83	3.0	0.16	1.90	1.90	99.1	54	98	338	198	662	0.64
		JANZ-28	H39 867235	36	-0.5	N/A	62.4	0.76	16.6	6.11	0.08	1.93	2.41	2.97	2.7	0.16	3.00	3.00	99.1	58	99	285	155	476	0.64
		JANZ-70	H38 528595	42	0.0	N/A	65.6	0.60	15.8	4.38	0.07	1.74	2.50	3.32	2.8	0.17	2.65	2.65	99.7	55	10	496	185	708	0.59
		JANZ-71	H38 759517	41	0.0	N/A	64.4	0.71	15.5	5.09	0.07	2.22	2.99	3.16	2.4	0.19	2.35	2.35	99.1	54	92	365	178	523	0.47
greenschist facies	A	JANZ-12	E41 650637	40	-2.4	5%	63.8	0.66	15.1	5.53	0.09	2.07	3.93	3.57	1.7	0.17	2.35	1.98	99.1	52	63	344	145	477	0.16
		JANZ-15	G44 400820	25	-0.1	11%	70.5	0.48	13.4	3.15	0.06	1.11	2.13	4.31	2.2	0.09	1.65	1.65	99.1	50	84	130	197	470	0.37
		JANZ-18	H43 840096	35	-1.0	5%	68.1	0.51	14.4	3.68	0.06	1.31	1.96	3.77	2.2	0.12	2.25	2.25	98.4	55	91	261	201	502	0.10
		JANZ-26	I41 182821	37	-0.2	4%	65.0	0.63	15.6	4.87	0.07	1.99	2.45	3.29	2.4	0.15	2.90	2.90	99.4	56	10	232	166	539	0.19
		JANZ-32	G41 118657	32	0.4	6%	68.2	0.52	14.2	3.74	0.05	1.51	2.58	3.62	2.4	0.13	2.20	2.20	99.2	52	90	406	188	627	0.16
		JANZ-33	F39 073337	37	-0.6	8%	67.2	0.57	15.2	4.34	0.07	1.53	2.49	3.57	2.3	0.12	2.25	2.25	99.7	55	91	300	169	662	0.14
		JANZ-36	F39 063395	35	0.1	4%	65.2	0.69	14.7	5.59	0.10	2.33	3.58	3.88	1.7	0.17	1.70	1.70	99.7	50	58	352	164	484	0.14
	B	JANZ-27	I42 105336	55	-0.2	3%	64.1	0.75	15.3	5.81	0.08	2.30	1.97	3.28	2.3	0.18	3.20	3.20	99.3	58	81	200	160	558	0.43
	C	JANZ-14	G43 190301	26	-0.8	-2%	60.1	0.81	16.2	6.46	0.10	2.69	5.06	3.67	1.8	0.18	1.90	0.72	99.0	54	56	453	150	517	0.11
		JANZ-35	F40 913095	48	0.0	-2%	63.9	0.67	15.3	5.35	0.11	1.75	2.13	3.12	2.1	0.15	4.60	4.60	99.2	58	97	179	184	551	0.07
	Qtz veins	JANZ12Q	E41 650637	0.4	-2.8																				
		JANZ32Q	G41 118657	2.3	-1.7																				
		JANZ33Q	F39 073337	1.7	-1.4																				

A, B and C indicates different groups in greenschist facies composite.

Mass A.: Mass Addition.

Grid reference, mass addition value, major (%) and trace elements (ppm) data are from Breeding and Ague (2002).

CIA = $Al_2O_3/(Al_2O_3 + CaO^* + Na_2O + K_2O) \times 100$ (molar contents, with CaO* being CaO content in silicate fraction of the sample)

At least two aliquots (~25 mg each) of each composite sample were digested and put through the column chemistry procedures.

One aliquot (~50 mg) of each quartz vein sample was digested and put through column chemistry.

The Li data reported in this study represent the averages of ≥3 measurements of each composite sample, and ≥2 measurements of each quartz vein sample.

The uncertainties for [Li] (mg/g) and d^{7}Li are ±10 (2s) and ±1 (2s), respectively.

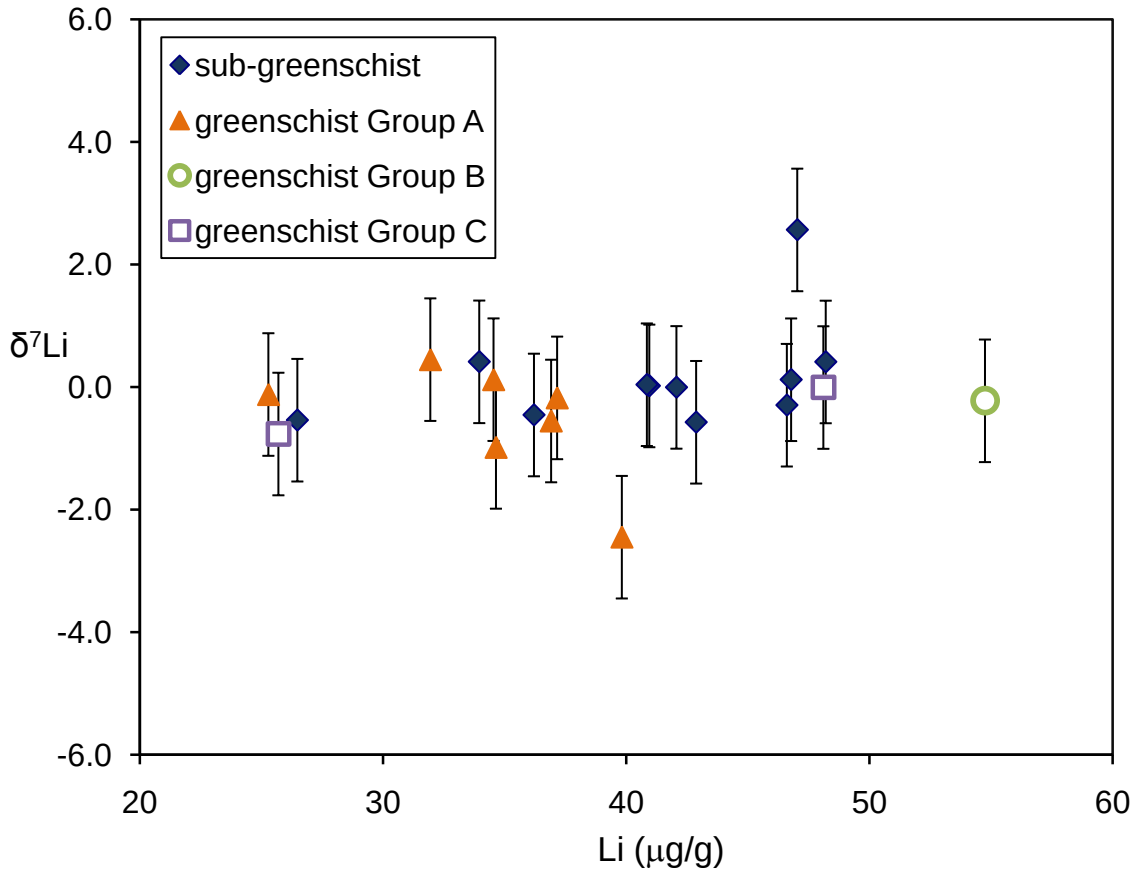

Figure 4-2. Li isotopic composition (δ^7Li) versus Li concentration ([Li]) for the Otago Schist composites. Error bars represent 2σ uncertainty in the y-axis only. Uncertainties (2σ) in the x-axis are 10% of the concentration.

show a lower and narrower range (25 to 40μg/g), with an average of 34 ± 9 μg/g (2σ), which is statistically distinct from sub-greenschist facies composite at the 97.7% confidence level, as indicated by the univariant Student's t-test. Both data populations have a normal distribution, with negligible differences in their respective values of average, median and log-normal average. The Au-W deposit composite of Group B has the highest [Li] measured in any of the sub-greenschist and greenschist facies samples of 55 μg/g, whereas the two composites in Group C have a relatively large variation in [Li] of 26 and 48 μg/g. In contrast to the variable Li concentration observed between sub-greenschist and greenschist facies composites, the δ^7Li of both sample suites are statistically indistinguishable (Student's t-test); the average δ^7Li of the sub-greenschist and greenschist facies composites is 0.2 ± 1.7 (2σ) and -0.5 ± 1.6 (2σ), respectively (Fig. 4-2). The selected quartz veins from the Group A outcrops show [Li] and δ^7Li in the range of 0.4 to 2.3 (μg/g) and -2.8 to -1.4, respectively.

5. Discussion

5.1. Factors controlling [Li] in the greenschist facies composites

The Chemical Index of Alteration (CIA, see Table 4-1 for definition) is a useful way of quantifying the degree weathering in the source regions of sedimentary rocks (Nesbitt and Young, 1982) and generally shows a positive correlation with [Li] (Qiu et al., 2009). The [Li] in all groups of composites correlates with their CIA (values between 50 and 58, Fig. 4-3). The Otago Schists plot at the lower end of the trend defined by pelites from the British Caledonides (Qiu et al., 2009), consistent with their inferred graywacke protolith and indicating that the [Li] in the protolith has a great control on the [Li] of the Otago

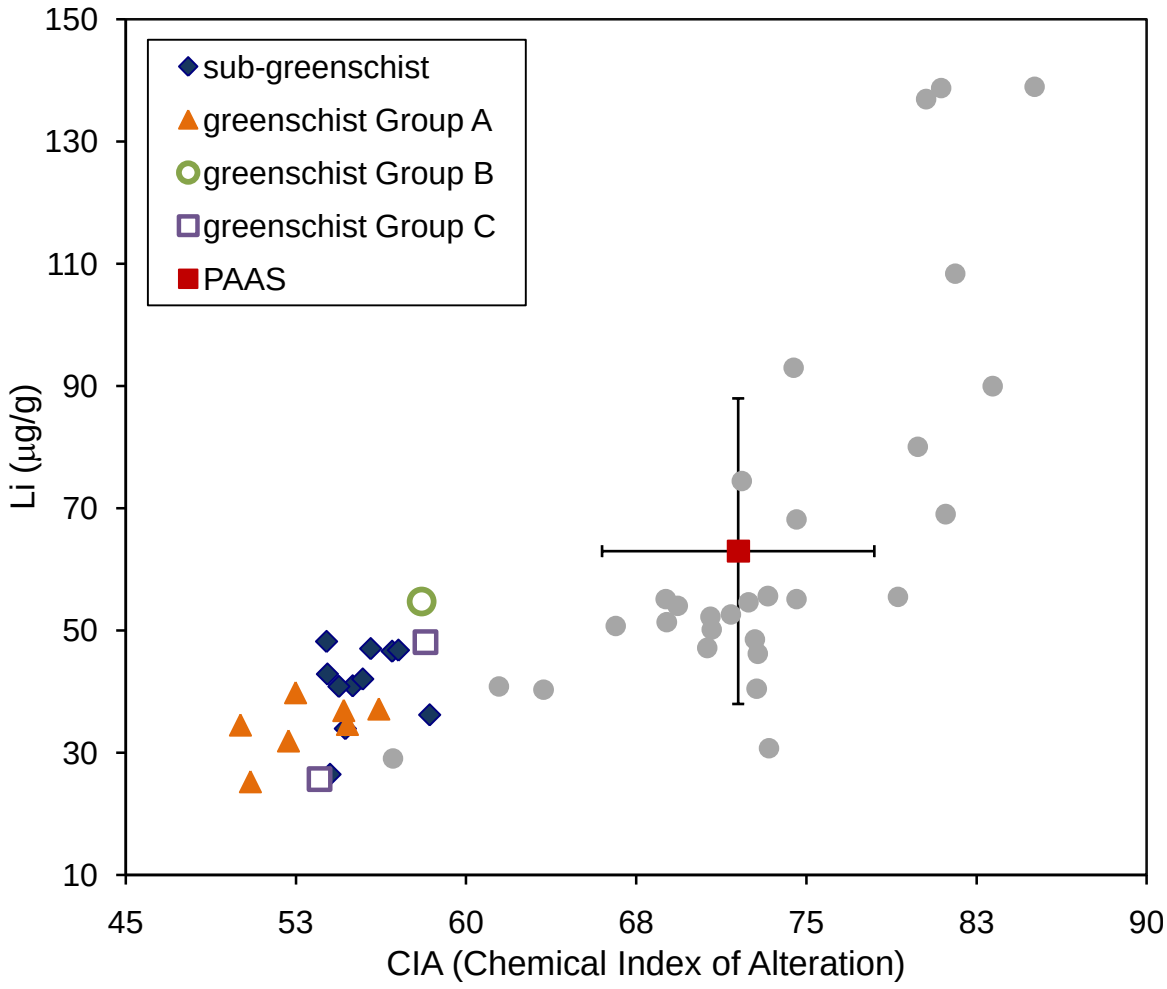

Figure 4-3. Li concentration versus CIA (Chemical Index of Alteration) value for the Otago Schist composites. The gray dots are the British mudrocks from Qiu et al. (2009). PAAS: Post Archean Australian Shales. Average [Li] and CIA value of PAAS (with 1 σ uncertainty of the average) are according to Teng et al. (2004).

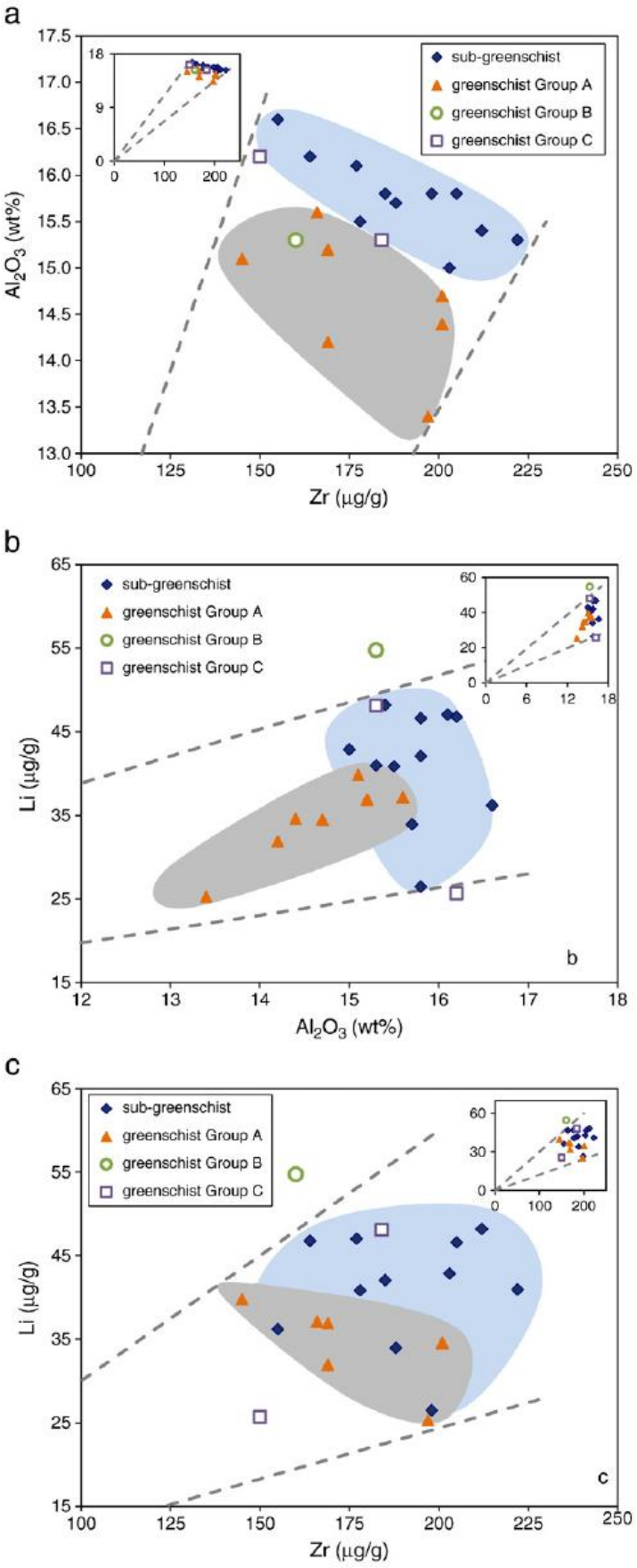

Figure 4-4. Wedge diagrams of (a) Al_2O_3 versus Zr, (b) Li versus Al_2O_3 and (c) Li versus Zr for the Otago Schist composites. The wedge region (dashed lines) is projected from the origin, and elongated in order to include all the plots of precursor rocks (sub-greenschist facies composites in the blue cloud). The small plots in a, b and c are the full wedge diagrams showing axes extending to the origin. Note all altered rocks (greenschist facies Group A in the gray cloud) plot inside the wedge, and the trend from precursor rocks to altered rocks projects towards the origin, indicating a residual dilution effect (Ague, 1994; Philpotts and Ague, 2009). See text for details.

Schist. Other factors that may influence [Li] in these rocks, such as metamorphism and dilution due to quartz vein precipitation are considered next.

The fluids from which the quartz veins precipitated in the greenschist facies Group A composites are inferred to be Na-rich, K-poor and silica-saturated (Breeding and Ague, 2002); consequently, insoluble elements, like Zr, are diluted by the mass addition of quartz veins (Breeding and Ague, 2002). The dilution effect for any element can be investigated by correlations with an immobile reference element in a wedge diagram (Ague, 1994; Philpotts and Ague, 2009), a graphical way to assess the mass change (i.e., addition or dilution) in altered rocks relative to the precursor rocks. In these diagrams, a wedge-shaped region is defined between the origin and the precursor rock compositions (traditionally, the immobile reference element and studied element are plotted on the x- and y-axis, respectively). Altered rocks experienced dilution if they plot in the wedge-shaped region between the origin and the precursor rocks (Ague, 1994; Philpotts and Ague, 2009).

Figure 4-4 demonstrates that Group A composites (gray cloud) plot between the origin and sub-greenschist facies composites (blue cloud) for Al and Zr, two fluid-immobile elements. Further, using the two-dimensional Kolmogorov-Smirnov (2DKS) test (Press et al., 1992), the difference between these two groups is statistically significant at the 98.5% confidence level. Therefore, in Group A samples, Al, like Zr, has been diluted and can be used as a reference immobile element in a wedge diagram.

In order to constrain the dilution effect for Li, both Al and Zr are employed as immobile reference elements in two wedge diagrams. The plots of Li vs. Al (Fig. 4-4b) and Li vs. Zr (Fig. 4-4c) show that Group A composites plot between the origin and the

sub-greenschist facies composites in the two wedges. Furthermore, the two groups in the two plots differ at the 99.8 and 97.1 confidence levels (2DKS test), respectively. These results indicate that, in the Group A composites, Li has also been diluted by mass addition of externally derived silica, consistent with the low [Li] of the quartz veins ([Li] $\leq$ 2.3 μg/g). By contrast, the Group B composite, which has the highest [Li] of any of the samples at 55 μg/g, plots above the wedge, indicating that it experienced enrichment in [Li]. Li may have been added from retrograde metamorphic fluids or hydrothermal fluids that contributed to the mineralization in this region. The two Group C composites show a large variation in [Li] and plot on the upper and lower bounds of the wedge within the field of sub-greenschist facies composites. There is no obvious change in [Li] associated with dilution within this group.

Whether or not dilution was the only process producing the lower [Li] in the greenschist facies composites can be evaluated from the linear correlation between the [Li] of Group A composites (34 ± 9 μg/g, 2σ) and the percentage of mass addition, previously calculated by Breeding and Ague (2002) based on a statistical (bootstrap) mass balance calculation (Fig. 4-5). This plot indicates that [Li] in the precursor rocks (prior to any mass addition) is on the order of 45 μg/g, similar to the average [Li] in the sub-greenschist facies composites (41 ± 13 μg/g, 2σ) and in the range typical of shales and graywackes (Teng et al., 2004; Qiu et al., 2009). Nevertheless, the mass addition of Li-depleted quartz veins cannot account for the total depletion of [Li] observed in the Group A composites, since the percentage of [Li] depletion does not match the percentage of calculated mass addition. For example, assuming ~45 μg/g Li in the Group A protolith, the abundance of Li in composite JANZ15 (25 μg/g) requires ~40 wt% mass

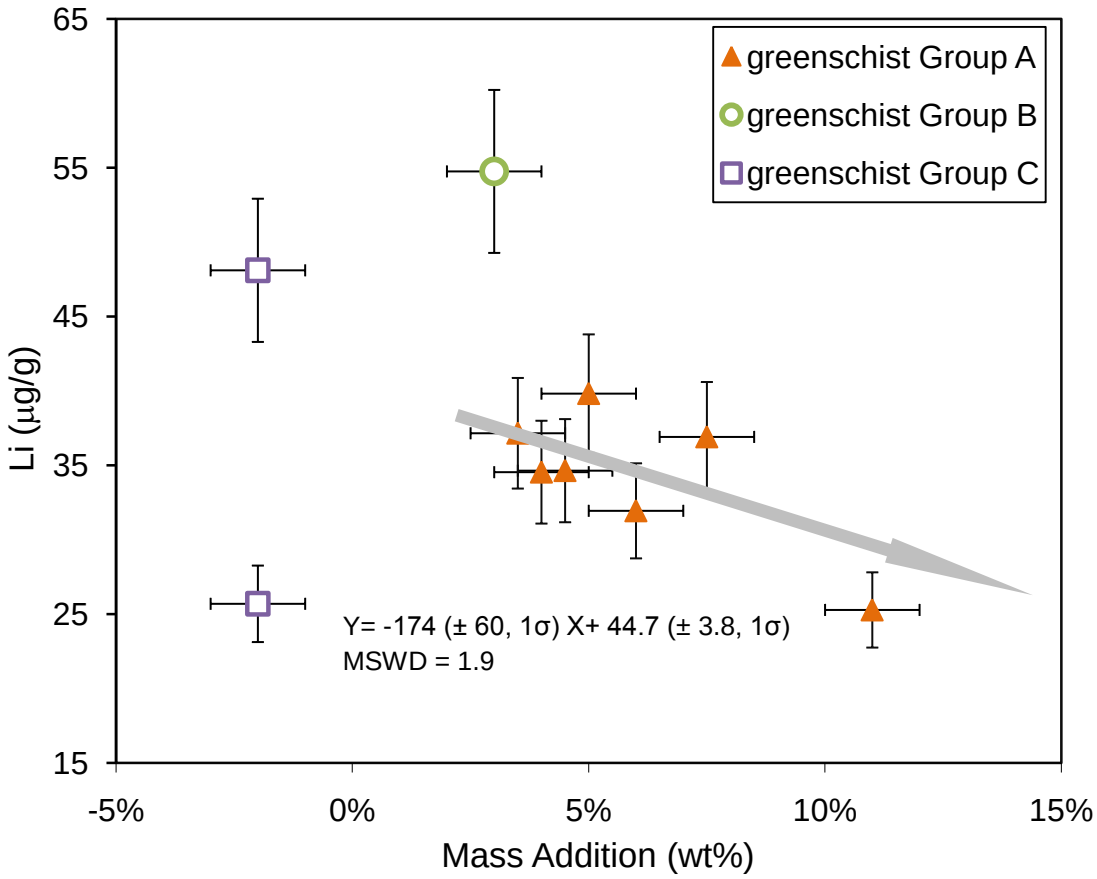

Figure 4-5. Li concentration versus percent mass addition. The calculated mass addition and the horizontal error bars, which represent analytical variability in replicate composites, are from Fig.1B of Breeding and Ague (2002). The gray trend line and equation show the linear regression (calculated by Isoplot) between [Li] and mass addition.

addition, whereas the calculated mass addition is only ~10 wt%; therefore, another process must also have caused depletion of Li in the Group A samples.

Metamorphic dehydration has been implicated as a process that can cause Li depletion (e.g., Zack et al., 2003; Marschall et al., 2007; Teng et al., 2007). Although Qiu et al. (2009) established that [Li] in sub-greenschist facies mudrocks do not change systematically as a function of H_2O loss, sub-greenschist facies metamorphism may represent the lower boundary for Li depletion during metamorphism. Accordingly, higher grade metamorphism of metapelites may deplete Li during dehydration, as inferred from the results of Teng et al. (2007) and Bea and Montero (1999), which indicate that [Li] was depleted by ~ 50% during amphibolite facies metamorphism and 98% during granulite facies metamorphism, respectively. Therefore, dehydration accompanying greenschist facies metamorphism may also be capable of causing Li depletion. Consequently, greenschist facies metamorphism, together with mass addition, likely leads to the lower [Li] seen in Group A composites.

5.2. δ^7Li signatures

In contrast to [Li], the δ^7Li of sub-greenschist and greenschist facies composites are remarkably constant, averaging -0.1 ± 1.8 (2σ), which is indistinguishable from the value suggested for upper continental crust of 0.3 ± 2 (2σ; Teng et al., 2004) and overlapping with values observed in terrigenous turbidites and oceanic pelitic sedimentary rocks (δ^7Li = -1.6 to 5; Chan et al., 2006). Thus, there is no evidence for lithium isotopic fractionation during greenschist facies metamorphism, and the isotopic signatures of these metasediments likely reflect the δ^7Li of their protoliths.

The Li isotopic compositions of the quartz veins are surprisingly light (ranging from -2.8 to -1.4), given that quartz takes up ^{7}Li preferentially from fluids (Sartbaeva et al., 2004; Teng et al., 2006b) and slab-derived fluids in the accretionary prism are suggested to have heavy δ^{7}Li signatures, up to ~+10 (Tomascak, 2004; Elliott et al., 2004 and references therein). If slab-derived fluids interacted with the wallrocks before the precipitation of the quartz veins, the fluids should be even heavier, because ^{7}Li preferentially partitions into fluids, similar to the effects of weathering (Chan and Edmond, 1988; Huh et al., 2004; Rudnick et al., 2004). Therefore, assuming that there are no other fluid sources contributing to quartz vein formation, the light δ^{7}Li of the quartz veins may record Li diffusion from Li-rich minerals in the wallrocks (e.g., chlorite, muscovite) into minerals in the veins. Such diffusion may occur in response to a chemical potential gradient between wall rock and vein, and may have been assisted by the presence of grain-boundary fluids, which have high partition coefficients for Li relative to rocks (e.g., Brenan et al., 1998). Since ^{6}Li diffuses faster than ^{7}Li (Richter et al., 2003; 2006; Dohmen et al., 2010), Li isotopes are fractionated during diffusion. Assuming that diffusion is arrested (i.e., the rocks do not fully equilibrate), this would produce quartz veins with low δ^{7}Li. Because the wall rocks have up to two orders of magnitude more [Li] than the quartz veins, small-scale diffusion may not influence the signature of Li in the wallrocks but may significantly change the δ^{7}Li of the quartz veins (Widmer and Thompson, 2001; Beinlich et al., 2010). As a result, the quartz veins likely do not reflect the isotopic signature of Li in the vein-forming fluids.

5.3. Isotopic equilibrium fluid flow model

The results above indicate that the slab-derived fluids have had no discernible effects on the δ^7Li of the schist composites. However, the dynamics of how the slab-derived fluid flux influences the δ^7Li of the overlying accretionary prism is still an open question. In order to investigate the extent to which slab-derived fluid flux might have affected the δ^7Li of the overlying greenschist-facies sediments, a one-dimensional local isotopic equilibrium model, following Dipple and Ferry (1992), has been applied. The MatLab code for the model is supplied in Appendix 4-B and the equations used in the model are simply expressed as:

$$\delta^7Li_{rock}(z, t) = \delta^7Li_{fluid}(z - QN_f/V_r, 0) + \delta^7Li_{rock}(z, 0) - \delta^7Li_{fluid}(z, 0)$$

$$\delta^7Li_{rock}(z, t) - \delta^7Li_{fluid}(z, t) = \Delta_{rock\text{-}fluid}(T)$$

$$T = T_i + dT/dz * z$$

in which z is the distance along the flow path (cm), t is the time (s), Q is the time integrated flux (mol fluid/cm^2 rock), N_f (mol Li/mol fluid) and V_r (mol Li/ cm^3 rock) are the initial Li concentrations in the fluids and rocks, respectively, $\Delta_{rock\text{-}fluid}$ (T) is the temperature-dependent fractionation factor, T (K) is the temperature and T_i is the initial temperature at the crustal base, dT/dz (K/cm) is the temperature gradient along the flow path. The model also assumes that transport is by advection, and that diffusion and mechanical dispersion are negligible. Diffusion will operate locally (e.g., Penniston-Dorland et al., 2010), but mechanical dispersion can be important at regional length scales. If there was a significant component of mechanical dispersion, the geochemical fronts would be broader than shown, but the positions of the front mid-points would be unchanged.

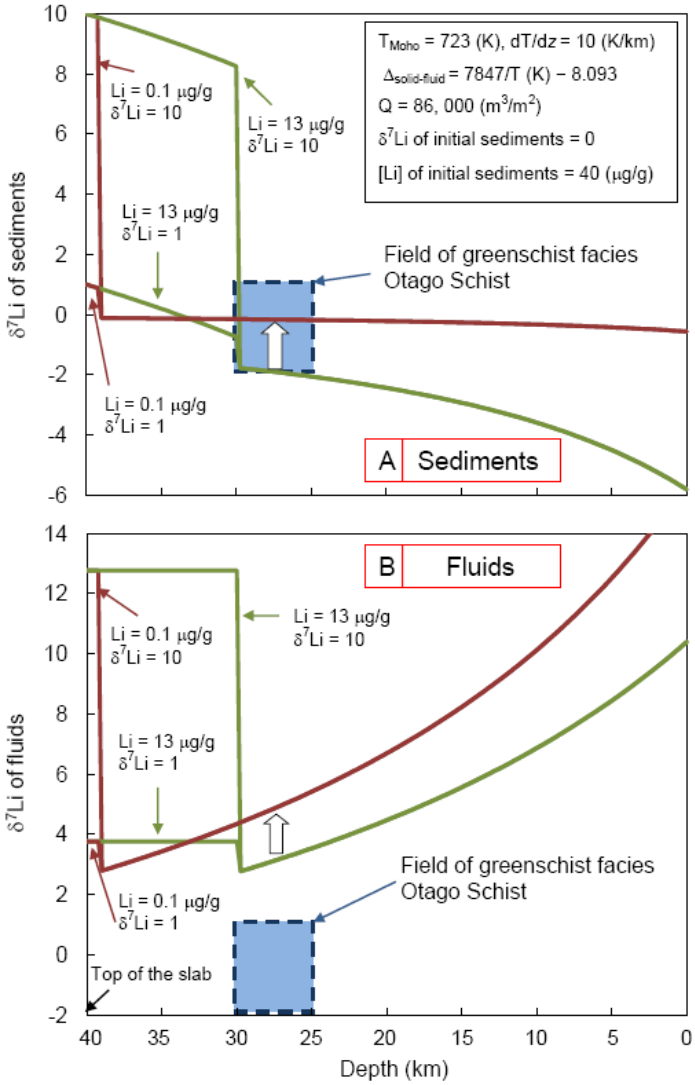

Figure 4-6. Results of isotopic equilibrium fluid flow model (after Dipple and Ferry, 1992; calculated using a MatLab script, which is provided in Appendix B) showing (a) δ^7Li of the rocks and (b) fluids versus depth. Both red and green lines are calculated based on the assumptions that the temperature at the base of the crust is 450°C, the fluid-rock isotopic fractionation is from Millot et al. (2010), the time integrated fluid flux is the mean of the values calculated by Breeding and Ague (2002) (86,000 m^3/m^2), and the initial [Li] and δ^7Li of the rocks are 40 μg/g and 0, respectively. The blue dashed box shows the field of the greenschist facies Otago Schist (25-30 km depth, δ^7Li = -0.5 ± 1.6, 2σ). The [Li] and δ^7Li of the model fluids are plotted next to the green and red lines, which indicate the results of modeling with high and low [Li] of the fluids, respectively. The white arrows indicate the direction that the curve moves as [Li] of the fluids decreases. Note that the isotope reaction front (i.e., the region at the base of the section where sediment compositions are overprinted with the isotopic composition of the fluids), generally propagates several kilometers upward from the slab into the overlying sediments. In this region the δ^7Li of the sediment closely follows the δ^7Li of the fluid, as indicated by the leftmost red and green curves on the upper panel.

The high grade Otago Schist records equilibration pressures equivalent to 25-30 km depth (Mortimer, 2003), which is relatively close to the higher end-member of the range of present day crustal thickness in this region (15-30 km, e.g., Davey et al., 2007; Stern et al., 2007); therefore, the crust could have been thicker at the time of fluid flow and we assume that the flow path region above the slab is 40 km thick. The results of our model indicate that the thickness of the crust does not significantly impact our model; for instance, by increasing the crustal thickness to 50 km, the maximum value of the [Li] in the fluids decreases slightly by ~2 μg/g, and decreasing the crustal thickness will not influence the [Li] of the fluids. The remaining variables include the temperature at 40 km depth (the base of the crust), the initial δ^7Li and [Li] of the rocks and fluids, the temperature-dependent fractionation factor $\Delta_{solid\text{-}fluid}$, and the time-integrated fluid flux. Of these parameters, the temperature at the base of the crust and the temperature-dependent fractionation factor ($\Delta_{solid\text{-}fluid}$) have negligible influence on the δ^7Li of the sediments at 25-30 km depth (the derivation depth of the Otago Schist, Breeding and Ague, 2002). Changing temperature from 450 °C to 850 °C and adopting either the $\Delta_{solid\text{-}fluid}$ -equation from Wunder et al. (2006, determined for low temperature basalt- seawater interactions), or the $\Delta_{solid\text{-}fluid}$ –equation from Millot et al. (2010, determined for high temperature clinopyroxene-fluid interaction), results in < 1‰ variation (i.e., within analytical uncertainties) in δ^7Li of the sediments. Therefore, we set the temperature at the base of the crust to 450 °C and use the isotopic fractionation equation ($\Delta_{solid\text{-}fluid}$) of Millot et al. (2010), since this equation is more suitable for our case, which is for whole rock – fluid systems.

The main contributors to the total Li flux in the model are the [Li] of the fluids and the time-integrated flux function. The time integrated flux is suggested to change over a narrow range (about one order of magnitude, from 27,000 to 144,000 m^3_{fluid}/m^2_{rocks}, as cited in Breeding and Ague, 2002), as compared to the range of the [Li] of the fluids from the prism (which may vary by two orders of magnitude, 0.1− 10 μg/g, e.g., Chan and Kastner, 2000; Millot et al., 2010); thus, the variation of [Li] in the fluids has a greater impact on the model than does the time integrated fluid flux. We therefore set the integrated flux at 86,000 m^3_{fluid}/m^2_{rocks} (mean value of Breeding and Ague, 2002), in order to evaluate the impact of [Li] in the fluids. In contrast to the uncertainty of some of the input parameters above, the [Li] and δ^7Li of the sedimentary precursors are relatively well-established at 40 μg/g and 0, respectively, which is the Li signature of the sub-greenschist facies rocks of the Otago Schist, as well as typical graywackes (Teng et al., 2004). As a result, there are only two parameters that can be varied in the model to arrive at a range of acceptable solutions: the [Li] and the δ^7Li of the fluids.

The Li isotopic compositions observed in the greenschist facies Otago Schist (δ^7Li = -0.5 ± 1.6, 2σ) and the depth of the precursor sediments are shown as a field in Fig. 4-6 (blue box). The curves in Fig. 4-6a show the evolution of the δ^7Li of the rocks throughout the accretionary prism for four different model fluid compositions. The two green lines represent two isotopic equilibrium models with a Li-enriched fluid (13 μg/g Li), one having δ^7Li = 10, and the other having δ^7Li = 1. The two red lines represent the same models, but with a Li-depleted fluid (0.1 μg/g Li), one end-member with δ^7Li = 10, and the other one with δ^7Li = 1; the white arrow indicates the direction of the change of the curve in the box due to lowering [Li] of the fluids. When the fluid [Li] > 13 μg/g, the

model curve plots outside of the field defined by the greenschist facies Otago Schist, regardless of the δ^7Li of the model fluid. The more Li-depleted fluid models, however, intersect the Otago Schist field, even when the δ^7Li of the model fluid varies from 0 to > +30, suggesting that such fluids are potentially representative of the fluids that reacted with the Otago Schist protolith. The green lines in Fig. 4-6a predict that shallower rocks should have noticeably lighter δ^7Li, which is not seen in the sub-greenschist facies Otago Schist. The constant δ^7Li of sub-greenschist to greenschist facies schist indicates the whole metamorphic sequence may not represent a connected flow system, or, the fluid flux becomes more channelized toward the surface and leaves the low-grade schist essentially unaltered. The discontinuities in both red and green lines in Fig. 4-6a mark the position of the advective isotopic front; the sections above the discontinuity indicate that the sediments have not tapped the heavy isotopic front of the fluids, taking into account the temperature-dependent isotopic fractionation. Critically, however, there is no discontinuity in time-integrated fluid flux across the geochemical front. After reacting with the 40 km-thickness of sediments, the fluids ascending to the surface of the prism, regardless of their initial [Li] and δ^7Li, end up with heavy δ^7Li (>10, Fig. 4-6b) due to their interaction with the sediments. As expected, the Li-poor fluids (red lines) have heavier δ^7Li and less influence on the δ^7Li of the sediments than the Li-rich fluids.

The modeling results above were derived using a constant time integrated flux of 86,000 m^3_{fluid}/m^2_{rocks}; however, the time-integrated flux may vary between 27,000 to 144,000 m^3_{fluid}/m^2_{rocks} (Breeding and Ague, 2002). Using a time integrated flux lower than 86,000 m^3_{fluid}/m^2_{rocks}, allows the [Li] of the fluids to be higher than13 μg/g without changing the δ^7Li of the schists. For instance, if the time-integrated flux is set to the

minimum value of 27,000 m^3_{fluid}/m^2_{rocks}, then the [Li] of the initial fluids will be 86,000(m^3_{fluid}/m^2_{rocks})/27,000(m^3_{fluid}/m^2_{rocks}) ×13 (μg/g) ≈ 41 (μg/g). This is the maximum value that can fit the δ^7Li of the Otago Schist data. The lower limit for [Li] in the fluids in our model is above ~ 0, i.e., the point where the δ^7Li of the sediments will be unchanged by fluids with low [Li]. The range of [Li] in the slab-derived fluids from our model, $0 < [Li] \leq 41$ (μg/g), is slightly lower than the modeling result of Marschall et al. (2007) for slab-derived fluid [Li] (~58 μg/g), which was calculated based on dehydration of average altered oceanic crust at 450 °C. Our range overlaps with the modeling results of Simons et al. (2010), $16 < [Li] < 43$ (μg/g), which were estimated based on the dehydration of 90% altered oceanic crust with 10% sediments at 450 °C.

In summary, although there are potentially a significant number of variables that can influence the equilibrium fractionation of Li between the fluid flux and the Otago Schist protolith, two variables, [Li] and δ^7Li of the fluids, are primarily responsible for the Li signatures observed in the Otago Schist, whose constant δ^7Li is best explained by interaction with a fluid depleted in Li (less than few μg/g), regardless of its isotopic composition. The total range of permissible [Li] in the fluids, $0 < [Li] \leq 41$(μg/g), overlaps with previous estimates of the composition of slab-derived fluids. Such fluids will have little influence on the δ^7Li of the sediments in the accretionary prism and will, in turn, be strongly influenced by their reaction with the sediments, such that their isotopic composition at the surface will be strongly altered from their original composition.

6. Conclusion

The [Li] and δ^7Li signatures of the Otago Schist indicate that, although prograde metamorphism from sub-greenschist facies to greenschist facies may have depleted the Li concentrations in these rocks, it had no discernible effect on the rocks' Li isotopic compositions. Further depletion of [Li] in greenschist facies composites is caused by mass addition of Li-poor quartz veins. The unusually low δ^7Li of the veins likely reflects preferential addition of ^{6}Li during Li diffusion into the veins from surrounding wall rocks. An isotopic equilibrium fluid flow model indicates that:

1) the δ^7Li of the precursor sediments of the greenschist-facies Otago Schist can be preserved after fluid fluxing if the [Li] in the fluid is relatively low;

2) the fluids have δ^7Li > +10 when they approach the surface after reacting with the sediments;

3) the [Li] of the slab-derived fluids is in the range of $0 < [Li] \leq 41(\mu g/g)$; and

4) forearc fluids emerging at the surface may carry with them the compositional characteristics established during their interaction with prism sediments.

Appendix 4-A.

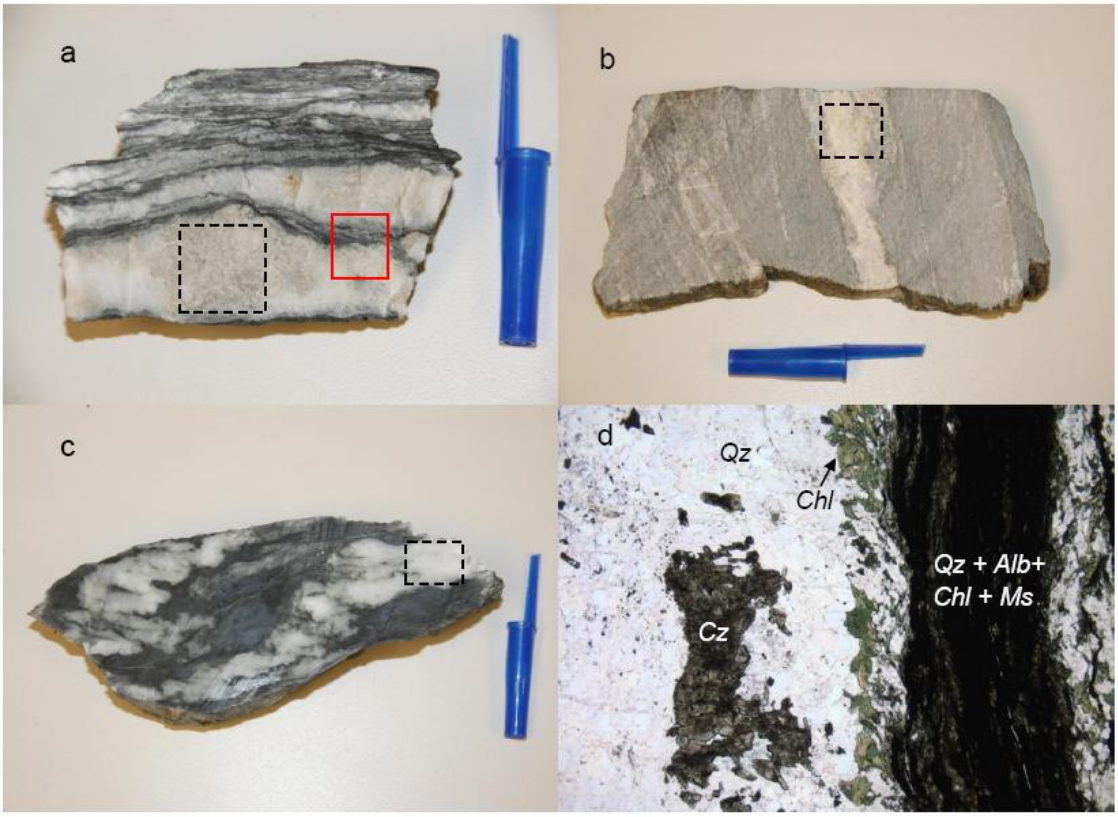

Photographs of sample specimens from Group A composite, (a) JANZ 12, (b) JANZ32 and (c) JANZ33 and (d) representative thin section. The pen cap in (a), (b) and (c) is 5cm long and the black dashed rectangles indicate from where the analyzed quartz vein was cut. The thin section image (d) is plane-polarized and taken from the red square on (a); it shows a layered structure between quartz veins and wall rocks (white and black stripes), which is composed of quartz (Qz), albite (Alb), chlorite (Chl) and muscovite (Ms). Some quartz veins include clusters of clinozoisite (Cz). The field of view in (d) is 0.9 cm wide.

Appendix 4-B Matlab code

```
% r = rock; f = fluid.
%
clear;
close all;
DR=0; % initial isotopic composition of rock.
VR=input; % mol Li/cm3 rock;
RNF=input; % mol Li/mol fluid;
DTDZ=-1.0e-4; % -10 deg. C/km.
Z=0.25e5; % km.
DZ=0.25e5;
a=8.093; % fractionation coefficient
b=0.0; % fractionation coefficient
c=-7.847; % fractionation coefficient
DISEQ = 10; % Rock at z=0 has d7Li = DR+DISEQ for all time
ZZ(1) = 0.0;
RR(1) = DR+DISEQ;
DELTA(1) = 0.0 + DISEQ;
%
Q = 8.6e6; %time integrated flux
TI =450; %temperature at the crust base
TT(1) = TI;
TI=TI+273.0;
Q = Q/18.0; % convert to mol/cm2 assuming H2O is 1g/cm3.
%
% Compute initial fluid composition at z=0 (FI1) and z (FI2).
%
for i=1:160
if(i==1)
DELT = (c*1000)/TI + b/TI + a;
FI1 = DR - DELT + DISEQ;
FF(1) = FI1;
fprintf(1,'FI1 %d\n',FI1);
end
T = TI + DTDZ*Z;
DELT = (c*1000)/T + b/T + a;
FI2 = DR - DELT;
%
% Compute z-Bt (D). When D=0, fluid and rock are fully equilibrated.
%
D = Z - Q*RNF/VR;
%
% Compute T and fluid composition (aa) at D and t=0.
%
if(D > 0.0)
T = TI + D*DTDZ;
DELT = (c*1000)/T + b/T + a;
AA = DR - DELT;
else
T = TI + D*DTDZ;
AA = FI1;
end
%
% Compute rock composition (ROCKNEW) and final fluid composition
(FFINAL)
```

```
% at z.

%
ROCKNEW = AA - FI2 + DR;
FFINAL = (c*1000)/(TI + DTDZ*Z) + b/(TI + DTDZ*Z) + a...
- ROCKNEW;
%
if(D < 0.0)
fprintf(1,'*ROCK IS EQUILIBRATED*\n');
end
fprintf(1,' INITIAL FLUID: %d\n',FI1);
fprintf(1,' FLUID AT Z= %d km: %d\n',Z/1e5,FFINAL*-1.0);
fprintf(1,' T AT Z (DEG. C)= %d\n',(TI + DTDZ*Z)-273.);
fprintf(1,' FLUX; FLUX; DIST; T (DIST); ROCK; NEW ROCK; Delt\n');
fprintf(1,' %d %d %d %d %d %d %d\n\n',Q*18,Q,D/1E5,T-273.,DR,...
ROCKNEW,ROCKNEW-DR);
ZZ(i+1) = Z/1e5;
DELTA(i+1) = ROCKNEW - DR;
TT(i+1) = (TI + DTDZ*Z)-273.;
RR(i+1) = ROCKNEW;
FF(i+1) = FFINAL*-1.0;
Z = Z + DZ;
end
```

Chapter 5: The behavior of lithium in amphibolite- to granulite-facies rocks of the Ivrea-Verbano Zone, NW Italy[1, 2]

[1] L. Qiu, R.L. Rudnick, W.F. McDonough and F. Bea contributed to the interpretation of the data. The modal mineralogy and major and trace element concentrations are from Bea and Montero (1999). The text, tables and figures (except where noted) were created/written by L. Qiu.

[2] This chapter has been submitted as:

Qiu, L., Rudnick, R.L., McDonough, W.F., and Bea, F. 2011. The behavior of Li in amphibolite- to granulite-facies rocks of the Ivrea-Verbano Zone, NW Italy. *Chemical Geology*, in review.

Abstract:

To investigate the behavior of Li during high-grade metamorphism and the Li composition of the lower continental crust, the Li concentrations ([Li]) and isotopic compositions (δ^7Li) of amphibolite- to granulite-facies metapelites, leucosomes and metabasites from the Ivrea-Verbano Zone, NW, Italy were determined. The average [Li] of amphibolite facies kinzigites (79 ± 69 μg/g, 2σ) is higher than that of granulite facies stronalites (8 ± 6 μg/g, 2σ) that experienced partial melting via biotite dehydration reactions. Biotite abundance and the [Li] in metapelites correlate positively, reflecting the importance of Mg-bearing phyllosilicates in controlling the Li budget of the metapelites. Despite the loss of Li following biotite breakdown, there is no significant change in δ^7Li, which averages -1.4 ± 2.0 (2σ, excluding an anomalously light sample) in the kinzigites (amphibolite facies) and +0.9 ± 2.9 (2σ) in the stronalites (granulite facies). Both δ^7Li values are comparable with other pelitic sediments and likely reflect the δ^7Li of their protoliths. An anomalous kinzigitic sample, with the lowest δ^7Li (-8.4) and the highest [Li] (120 μg/g), has extremely low Ba and Sr concentrations and the highest CIA

value, all indicators of a highly weathered protolith, which was likely isotopically light prior to significant metamorphism. This sample may also have experienced Li addition via diffusion, increasing [Li] and lowering δ^7Li. The leucosomes in the kinzigites and stronalites are interpreted to have formed in different ways; the former precipitated from hydrothermal fluids, have an average [Li] = 13 ± 2.6 μg/g (2σ) and are isotopically similar to the kinzigites (δ^7Li = -1.0 ± 0.2, 2σ); the latter formed by dehydration melting and have lower [Li] (3 ± 2.6 μg/g, 2σ) that is heavier (δ^7Li = +6.0 ± 6.3, 2σ) than the stronalites or kinzigites. The mineralogical and compositional characteristics of the stronalites are consistent with substantial Li loss during partial melting. A melting model indicates that Li removed from the stonalites may contribute to the formation of S-type granites or Li-enriched pegmatites.

Three granulite-facies metabasites have relatively constant [Li] of 3.0 – 4.2 μg/g (average 3.6 ± 1.2, 2σ) and variable δ^7Li of -3.2 to +3.3 (average 0 ± 6.5, 2σ). While these concentrations are typical of those of possible basaltic protoliths, the highly variable δ^7Li suggests Li mobility during metamorphism. Collectively, the Li signature in granulite facies stronalites and metabsites indicate the [Li] of this section of lower continental crust is close to 8 μg/g or less, and the concentration weighted δ^7Li of this section of the lower continental crust is +1.0, which is similar to a previous estimate (8 μg/g, +2.5).

1. Introduction

Since the original work of Zack et al. (2003) on Li fractionation in eclogites, several studies have focused on the behavior of Li during metamorphic dehydration (e.g., Teng et

al., 2007; Marschall et al., 2007) because it is necessary for understanding the distribution of Li concentrations ([Li]) and isotopic compositions (δ^7Li) during crustal recycling at subduction zones (e.g., Elliott et al., 2004; 2006; Tomascak, 2004). The consensus of these latter studies is that metamorphic dehydration has had only a subtle influence on δ^7Li in rocks metamorphosed at amphibolite or eclogite facies. Likewise, our recent studies have shown that, although Li depletion may occur during sub-greenschist to greenschist facies metamorphic dehydration, Li isotopic fractionation is indiscernible (Qiu et al., 2009; 2011a). Rather, the [Li] and δ^7Li of low grade metapelites correlates with the weathering intensity experienced in the sedimentary provenance, as reflected by indicators such as the Chemical Index of Alteration (CIA); [Li] generally increases and δ^7Li values typically decrease with increasing weathering intensity (Qiu et al., 2009; 2011a). Despite recent progress in understanding the geochemical behavior of Li during low- to intermediate-grade metamorphism, the behavior of Li during high-grade (amphibolite to granulite facies) metamorphic devolatilization, which is accompanied by partial melting and migmatization processes, remains unresolved.

Regional granulite facies metamorphism in water-bearing rocks, such as pelites, is generally envisaged as causing the dehydration of the protolith, and the release of fluids can subsequently affect element distributions in crustal rocks. Previous geochemical studies of the metapelites from the Ivrea-Verbano Zone, NW Italy (e.g., Sighinolfi and Gorgoni, 1978; Schnetger, 1994; Bea and Montero, 1999), have suggested that granulite facies metamorphism, initiated by the intrusion of mantle-derived magma, resulted in significant depletion of fluid-mobile elements in the metapelites. The depletion of Li and other fluid-mobile elements (e.g., K, Rb, Sr, and Cs) has been used to mark the transition

from amphibolite to granulite facies metamorphism (Sighinolfi and Gorgoni, 1978; Schnetger, 1994). Among these elements, Li is depleted by the greatest amount, with 80% to 98% being lost in the granulite facies rocks (Sighinolfi and Gorgoni, 1978; Schnetger, 1994; Bea and Montero, 1999). These results indicate strong partitioning of Li into the fluids liberated by granulite facies metamorphic dehydration and partial melting reactions. Thus, the Li signatures in granulite-facies metapelites from the Ivrea-Verbano Zone can provide important information about the behavior of Li during high-grade metamorphism.

These granulite-facies samples also supply a means to investigate the Li composition of the lower continental crust, since granulite-facies metamorphic terranes are one of the two types of samples (the other is granulite-facies xenoliths) that have been used to study the composition of lower continental crust (e.g., Rudnick and Presper, 1990; Rudnick and Fountain, 1995). Estimates of the Li concentration in the lower continental crust (6 to 14 μg/g) have been made based on studies of high grade metamorphic terranes and granulite xenoliths (Taylor and McLennan, 1985; Shaw et al., 1994; Wedepohl, 1995; Rudnick and Fountain, 1995; Rudnick and Gao, 2003; Teng et al., 2008); however, the Li isotopic composition of lower continental crust is still poorly constrained. By studying three suites of granulite-facies xenoliths from China and Australia, Teng et al., (2008) found the lower crust to be strongly heterogeneous in δ^7Li, with δ^7Li of individual samples ranging from −14 to +14.3, with a concentration weighted average of +2.5.

In order to understand the behavior of Li during high-grade metamorphic devolatilization and partial melting, and place further constraints on the Li concentration

and Li isotopic composition of lower continental crust, previously well-characterized samples from the Ivrea-Verbano Zone are investigated here.

2. Geological setting and samples

The Ivrea-Verbano Zone is a SW-NE-striking section of Paleozoic basement exposed in the Southern Alps in northern Italy, which is ~15 km in width and 120 km in length, bordered by the Insubric Line to the NW and by the Strona-Ceneri Zone to the SE (Fig.5-1). The Ivrea-Verbano Zone includes three major lithologic divisions: 1) supracrustal rocks (traditionally called the Kinzigite Formation), 2) mantle peridotites, and, 3) a mafic complex. The Mafic Complex is commonly considered as the heat source for the regional metamorphism observed in the Kinzigite Formation, ca. 270-290 Ma (Voshage et al., 1990; Barboza and Bergantz, 2000 and references therein); it comprises the base of the Ivrea-Verbano Zone and consists of a variety of gabbros and diorites metamorphosed up to the granulite facies. The Kinzigite Formation comprises middle amphibolite- to granulite-facies, migmatized metapelites and metapsammite with minor intercalations of metabasites and quartzites (Zingg, 1984). The lowest grade metapelites of the Kinzigite Formation are mica schists. With increasing metamorphic grade, these lithologies evolve into garnet- and sillimanite-bearing schists called kinzigites. The biotite in this prograde sequence is progressively replaced by garnet, until biotite is completely replaced by garnet in granulite-facies metapelites, which are locally called stronalites (Bertolani and Garuti, 1970). In addition, one of the kinzigite samples, P1, contains > 5 cm-thick quartz veins and it is the only kinzigite that does have quartz veins; the quartz veins of P1 were

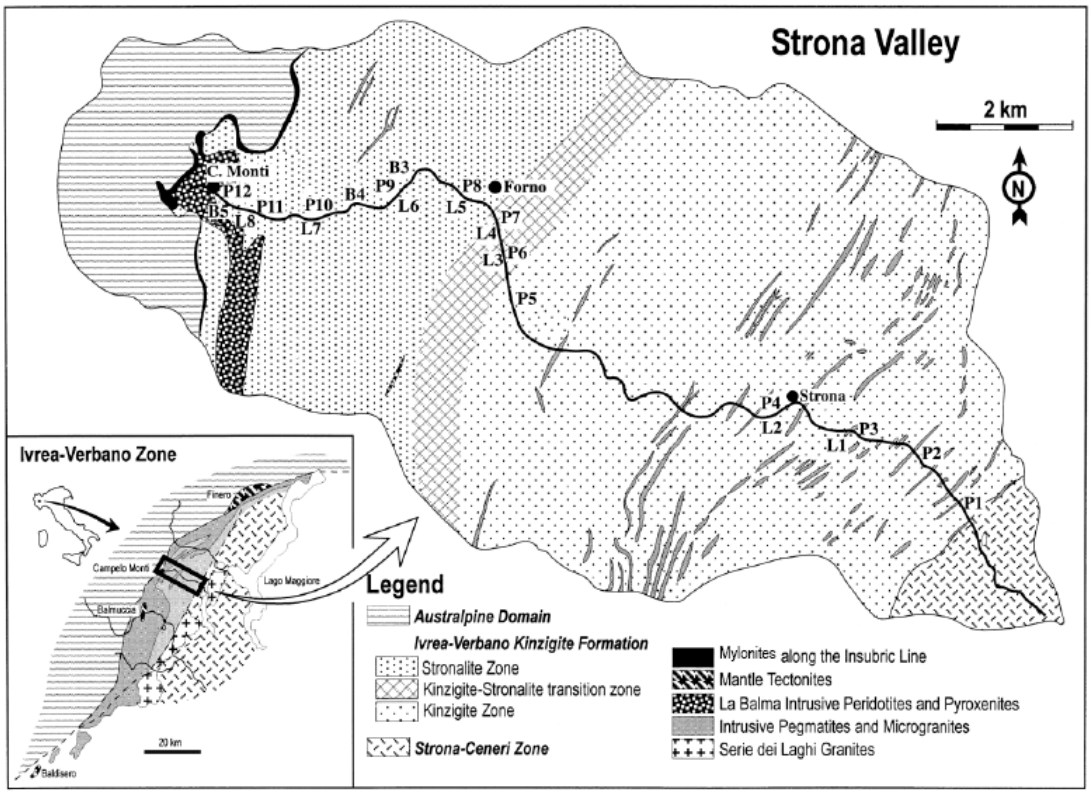

Figure 5-1. Sketch map showing the location of Ivrea-Verbano zone, NW, Italy (from Bea and Montero, 1999).

separated out completely during the sample preparation. The granulite-facies metabasites, which are intercalated with the stronalites, are migmatized and composed of brown hornblende, clinopyroxene, orthopyroxene and plagioclase, with accessory opaques and apatite (Mazzucchelli and Siena, 1986).

In this study, following Bea and Montero (1999), the prograde metapelitic sequence along the Strona Valley (Fig. 5-1) is divided into three zones: the kinzigite, transition and stronalite zones, having modal biotite/garnet > 2, between 0.5 and 2, and < 0.5, respectively, and peak metamorphic pressures of roughly 0.4–0.5 GPa, 0.5–0.6 GPa, and 0.6–0.8 GPa, respectively. Leucosomes, the formation of which are related to the dehydration melting of biotite, are widespread in the stronalite zone and occur as different sizes of dikes or lenses, all with compositions similar to that of a garnet-bearing leucogranite or leucogranodiorite. By contrast, leucosomes are less abundant in the transition zone and upper kinzigite zone, where they are interpreted to derive from partial melting associated with muscovite breakdown (Bea and Montero, 1999, and references therein). Generally, the leucosomes are composed of quartz + plagioclase + K-feldspar ± garnet.

The modal mineralogy, based on point counting, and estimated P-T of the 12 metapelites investigated here are reported in Table 5-1 (Bea and Montero, 1999). Additionally, seven leucosome samples were collected from the kinzigite zone, transition zone and stronalite zone along the Strona Valley, and three granulite-facies metabasites were collected from the stronalite zone; their compositions are reported in Tables 5-3 and 5-2, respectively.

Most of the whole rock powders analyzed in this study have previously been analyzed for major and trace elements by Bea and Montero (1999). Two powders (P7 and P12) analyzed in our study were obtained by re-crushing the hand specimens because the original powders were exhausted. Additionally, the [Li] of two samples (P6 and L7) are taken from Bea and Montero (1999) since the original powders and specimens are both exhausted, and therefore the Li isotopic compositions of these samples are not reported.

3. Analytical methods

Lithium concentrations and isotopic compositions of the metapelites, leucosomes and metabasites collected for this study were determined at the Geochemistry Laboratory of the University of Maryland, College Park.

Sample dissolution procedures, column chemistry, instrumental analysis and external precision are reported in Teng et al. (2006b) and Qiu et al. (2009). Briefly, samples were dissolved in a screw-top teflon beaker with a combination of HF–HNO_3–HCl. Lithium was purified on a cation exchange resin (Bio-Rad AG50w-X12, 200–400 mesh) first in an HCl medium, followed by an HCl-ethanol medium. Lithium concentrations and isotopic compositions were analyzed using the standard-sample-bracketing method on a Nu Plasma MC-ICPMS. The long-term external precision of the Li isotopic composition and concentration analyses are $\leq$ 1.0‰ (2σ) and ±10% (2σ), respectively, based on repeat analyses of pure Li standards and standard reference materials, respectively, over the past nine years (Rudnick et al., 2004; Teng et al., 2006b; Qiu et al., 2011a). Qiu et al. (2009; 2011a) reported results for three separate analyses of BCR-1 [δ^7Li = +2.1 ± 0.3 and [Li] = 12.7 ± 0.7 μg/g], which were analyzed during the course of this study; in comparison, Magna et al. (2004), Rudnick et al. (2004) and Teng et al. (2006b), reported the δ^7Li of

BCR-1 to be +2.0 ± 0.7 (10 runs), δ^7Li = +2.7 ± 1 (3 runs) and δ^7Li = +2.4 ± 0.5 (4 runs), respectively, and the GEOREM (Jochum and Nohl, 2008) preferred BCR-1 [Li] =13 ± 1 μg/g.

4. Results of Lithium concentrations and isotopic compositions

Lithium concentrations and isotopic compositions of the metapelites, metabasites and leucosomes analyzed here are reported in Tables 5-2 and 5-3, respectively, along with the previously published major and trace element concentrations from Bea and Montero (1999).

The [Li] determined in this study are generally within 2σ analytical uncertainties of those determined by Bea and Montero (1999) via PE SCIEX ELAN-5000 spectrometer (Tables 5-2 and 5-3 and appendix 5-A). Exceptions are samples with [Li] < 20 μg/g (P9, P10, P12, L1, L2, L5,L11, B4 and B5); the [Li] of these samples determined by Bea and Montero (1999) are generally 10-50% higher than the value determined in this study. However, since the [Li] between low- and high-grade metapelites differ by about two orders of magnitude (a few μg/g to hundreds of μg/g), the discrepancy in [Li] of the metapelites between the two studies (less than one order of magnitude) will not influence the discussion and conclusions related to the metamorphic effects. Additionally, the average [Li] of granulite-facies samples (stronalites and metabasites) between the two studies generally overlap, considering the 2σ uncertainties; therefore, the discrepancy has only a minor influence on the estimates of [Li] in the lower continental crust. We also report both the arithmetic and log-normal mean of [Li] in kinzigite, transition, stronalite, leucosomes and metabasite samples in Table 5-4. The arithmetic and log-normal mean

Table 5-1. Modal composition and geothermobarometric estimations of metapelites from the Strona Valley section, taken nearly perpendicular to metamorphic gradient. Values are from Bea and Montero (1999).

	Kinzigites					Transition		Stronalites				
Sample No.	P1	P2	P3	P4	P5	P6	P7	P8	P9	P10	P11	P12
	Estimated PT conditions											
P^{Gasp} (Kb)	4	4.2	4.3	4.5	5.0	5.5	6.0	6.3	7	7.3	7.8	8.0
$T^{bi\text{-}gar}$ (°C)	500	560	560	600	630	670	700	750	750	≈800	≈800	≈800
	Modal composition (wt%)											
Orthopyroxene	—	—	—	—	—	—	—	7.2	—	—	—	—
Cordierite	2.6	—	—	—	—	—	—	—	—	—	—	—
Biotite	25.6	21.9	20.2	44.1	22.2	15.4	14.8	2.8	5.1	4.1	0	0.3
Garnet	0.0	1.5	1.7	1.3	5.1	16.1	19.3	15.3	28.8	35.1	48.6	53.6
Sillimanite	10.8	3.8	5.0	10.2	1.0	6.8	5.6	10.3	19.3	14.3	29.0	31.4
Quartz	49.5	51.6	46.3	28.9	33.0	34.6	28.6	34.7	26.8	17.7	13.4	8.9
K-feldspar	1.3	2.7	2.9	1.6	0.7	12.8	10.7	11.9	14.8	15	6.4	1.9
Plagioclase	9.0	17.3	23.0	11.0	37.5	13.4	20.3	16.8	3.9	12.1	1.1	3.4
Apatite	0.31	0.3	0.37	0.31	0.35	0.22	0.07	0.1	0.05	0.09	0.03	0.008
Monazite	0.037	0.018	0.026	0.03	0.03	0.021	0.029	0.024	0.024	0.053	0.041	0.036
Xenotime	0.003	0.002	0.001	0.00	0.001	0.0005	—	—	—	—	—	—
Zircon	0.051	0.022	0.038	0.04	0.038	0.049	0.048	0.048	0.044	0.038	0.054	0.062
Others*	0.80	0.85	0.50	2.50	0.20	0.60	0.65	0.90	1.20	1.60	1.40	0.50

* ilmenite + rutile + graphite + sulphides; —: the modal composition is 0.

Table 5-2. Lithium concentrations (μg/g), Li isotopic compositions (δ^7Li), major (wt%) and trace element concentrations (μg/g) of metapelites from the Strona Valley. Values of major and other trace elements are from Bea and Montero (1999).
continued on next page

	Kinzigites					Transitional		Stronalites					Metabasites		
Sample No.	P1	P2	P3	P4	P5	P6	P7*	P8	P9	P10	P11	P12*	B3	B4	B5
δ^7Li	-8.5	-1.8	-0.1	-1.5	-2.4	N/A	0.4	2.1	-0.2	-1.1	1.8	1.8	3.3	0.0	-3.2
Li	120	58	60	113	46	N/A	42	10.8	5.2	6.3	11.1	4.6	4.2	3.6	3.0
Li[a]	122	55	63	107	49	39	42	12	9	9	12	8	4	7	7
SiO_2	70.4	73.9	72.9	56.8	63.9	64.9	63.9	59.2	58.1	56.7	41.8	45.0	45.8	48.6	50.8
TiO_2	0.71	0.78	0.73	1.28	0.85	0.77	0.88	1.45	1.42	1.54	2.09	1.95	2.21	1.71	1.76
Al_2O_3	15.8	12.7	13.0	21.5	16.3	16.1	16.8	22.1	22.6	22.3	30.0	30.1	12.2	20.0	14.5
FeO^{Total}	3.70	4.95	4.47	8.68	5.83	7.65	7.35	10.11	10.22	9.83	15.25	13.67	12.73	10.48	10.28
MgO	4.89	1.86	2.62	3.33	3.04	2.74	3.79	3.34	3.43	3.4	5.57	5.06	13.53	4.7	7.46
MnO	0.03	0.09	0.06	0.13	0.10	0.12	0.10	0.11	0.10	0.10	0.28	0.12	0.20	0.20	0.18
CaO	0.29	0.82	1.15	0.77	4.43	1.53	1.58	0.45	0.33	0.75	1.36	0.69	10.92	9.67	11.5
Na_2O	0.28	1.14	2.45	1.02	1.87	0.95	1.72	0.53	0.43	1.38	0.79	0.75	0.9	2.79	0.52
K^2O	2.62	2.3	1.94	4.4	2.12	3.47	3.32	2.09	2.98	3.01	1.18	1.81	0.07	0.28	0.05
P_2O_5	0.15	0.16	0.18	0.15	0.18	0.14	0.03	0.06	0.06	0.08	0.06	0.02	0.02	0.33	0.22
L.O.I	1.05	0.71	0.87	1.4	0.92	1.03	0.57	0.48	0.09	0.68	0.79	0.38	0.44	0.82	1.79
Total	99.8	99.4	100.3	99.5	99.6	99.5	100.0	99.9	99.7	99.7	99.1	99.5	99.1	99.6	99.0
CIA	82	70	62	74	56	N/A	N/A	N/A	N/A	N/A	N/A	N/A	N/A	N/A	N/A
Rb	64	112	80	203	87	75	81	16	35	44	21	12	1.2	1.6	1.7
Cs	1.8	5.5	1.5	11	4.1	0.2	0.3	0.3	0.2	0.3	0.3	0.2	0.1	0.3	0.1
Be	1.7	1.9	1.3	3.9	2.9	1.6	1.7	0.3	0.3	0.3	0.6	0.9	0.3	1.3	2.5
Sr	15	125	134	103	177	189	172	81	95	160	129	61	157	422	180
Ba	183	509	554	626	608	621	589	356	427	717	411	387	24	116	72
Sc	10	10	12	21	15	20	18	19	21	26	44	35	44	43	39
V	81	65	87	151	106	127	104	177	171	183	280	220	389	239	273
Cr	66	57	76	159	67	133	109	193	186	118	222	240	686	5.5	576
Ni	37	30	32	62	40	56	43	99	59	85	78	65	268	15	162
Cu	5	8	27	33	138	5	7	14	13	52	24	7	71	18	18
Zn	36	63	36	147	81	38	47	128	108	120	183	131	135	109	151

Ga	22	17	15	33	22	21	23	30	30	30	42	42	17	24	20
Y	22	11	13	14	33	30	27	22	31	34	60	66	27	40	40
Nb	18	15	10	22	13	19	22	18	17	18	37	43	1.7	8.8	12
Ta	1.5	1.2	0.8	1.7	1.2	1.7	1.9	0.9	0.9	1.0	2.0	2.2	0.1	0.5	1.1
Zr	339	136	211	255	204	293	280	275	264	220	327	394	56	120	107
Tl	0.4	0.6	0.4	1.2	0.6	0.4	0.4	0.3	0.5	0.4	0.2	0.1	0.0	0.0	0.0
Pb	2.5	20	4.3	18	15	17	21	12	13	9	6	5	1	3	4
U	2.6	1.4	1.6	2.8	3.0	2.0	2.0	0.6	0.8	1.5	1.0	1.0	0.0	0.0	0.2
Th	14	8.2	10	16	16	11	12	8.8	13	21	15	15	0.1	0.0	0.8
La	46	30	33	53	50	40	42	26	34	63	52	45	1.4	11	15
Ce	94	65	69	114	98	84	89	58	74	126	101	93	6.4	28	38
Pr	11	7.3	7.8	13	11	10	10	6.8	9.2	14	12	10	1.4	4.5	5.6
Nd	39	27	29	48	42	27	33	25	35	55	45	41	9.2	22	25
Sm	6.9	5.5	6.0	9.6	7.9	5.7	6.2	5.3	7.4	9.6	8.7	8.6	3.5	6.6	7.0
Eu	1.1	1.4	1.5	1.8	1.6	1.3	1.3	1.2	1.7	1.8	1.3	1.2	1.1	2.5	2.1
Gd	6.2	5.5	5.6	9.0	6.8	5.6	6.3	5.3	6.9	7.5	10.1	7.6	4.3	6.5	6.7
Tb	0.9	0.6	0.7	0.9	1.0	0.8	0.9	0.7	1.0	1.1	1.7	1.5	0.8	1.1	1.1
Dy	4.7	2.4	2.9	3.5	5.7	5.1	5.0	4.1	5.7	6.3	10.8	10.6	4.7	6.8	6.8
Ho	0.9	0.4	0.5	0.5	1.2	1.1	1.0	0.9	1.2	1.4	2.4	2.5	1.0	1.5	1.4
Er	2.1	1.0	1.3	1.3	3.2	3.1	2.8	2.5	3.4	3.6	6.4	7.3	2.8	4.0	3.9
Tm	0.3	0.2	0.2	0.2	0.5	0.5	0.5	0.4	0.5	0.6	1.0	1.2	0.4	0.6	0.6
Yb	1.8	1.0	1.1	1.1	3.1	3.1	3.3	2.7	3.6	3.7	6.5	7.5	2.5	3.6	3.7
Lu	0.24	0.14	0.16	0.15	0.44	0.48	0.47	0.40	0.53	0.53	0.94	1.19	0.34	0.53	0.55
Nb/Ta	12.0	12.5	13.1	12.9	10.8	11.1	11.5	18.9	17.3	18.0	18.5	19.5	7.4	17.7	11.3
Nd/Th	2.7	3.3	2.8	3.0	2.7	2.5	2.7	2.9	2.7	2.6	2.9	2.7	92	555	33
Th/U	5.5	6.0	6.3	5.6	5.3	5.3	6.1	14.6	15.5	13.9	14.8	14.5	4.5	4.0	3.2

a: Li concentrations from Bea and Montero (1999), analyzed by PE SCIEX ELAN-5000 spectrometer.

*: powders for these samples are from re-crushing the same handsamples used in Bea and Montero (1999).

At least two aliquots (~25 mg each) of each sample were digested and put through the column chemistry procedures.

The Li data reported in this study represent the averages of ≥ 4measurements of each sample.

The uncertainties for [Li] (μg/g) and δ^7Li are ±10 (2σ) and ±1 (2σ), respectively.

Table 5-3. Lithium concentrations (μg/g), Li isotopic compositions, major (wt%) and other trace elements (μg/g) of leucosomes from the Strona Valley. Major and trace element data are from Bea and Montero (1999). *Continued on next page*

	Kinzigites		Transition		Stronalites		
Sample No.	L1	L2	L3	L4	L5	L7	L8
δ^7Li	-1.0	-0.9	7.5	3.3	3.7	N/A	8.2
Li	14.7	12.1	7.7	5.6	4.6	N/A	2.6
Li[a]	18	18	8.1	6.2	8.4	3.2	2.4
SiO_2	78.4	79.7	76.4	73.1	72.4	71.5	74.7
TiO_2	0.15	0.05	0.02	0.04	0.39	0.38	0.18
Al_2O_3	12.6	12.1	13.2	14.9	14.5	15.1	13.7
FeO^{Total}	0.97	0.28	0.55	0.79	2.77	2.51	1.71
MgO	0.38	0.2	0.12	0.21	0.91	0.81	0.36
MnO	0.02	0.01	0.04	0.04	0.06	0.04	0.04
CaO	1.81	1.90	1.50	0.82	1.52	1.39	1.06
Na_2O	3.13	4.58	2.14	2.16	2.27	2.41	3.10
K^2O	1.53	0.20	5.78	7.42	5.18	5.41	4.52
P_2O_5	0.15	0.24	0.05	0.02	0.11	0.12	0.13
L.O.I	0.7	0.33	0.12	0.35	0.09	0.24	0.1
Total	99.8	99.5	99.9	99.9	100.1	99.9	99.7
Rb	45	3.7	120	167	95	110	153
Cs	0.9	0.04	0.97	1.9	0.06	0.25	0.1
Be	2.8	1.4	1.4	1.5	0.26	0.62	0.53
Sr	323	221	225	207	161	165	67
Ba	993	104	496	1010	723	659	344
Sc	2.4	1.1	1.4	1.9	7.1	7.6	3.5
V	16	2.8	0.9	1.6	34	19	12
Cr	0	2.8	5.4	1.4	0.5	1	7.7
Ni	1.7	4.7	4.2	0.5	0.0	13	3.3
Cu	4.8	4.1	1.9	1.2	2.2	3.7	2.4
Zn	26	6	8	23	20	42	21
Ga	9.6	7.1	10	11	15	14	17
Y	9.9	7.6	6.5	2.7	55	9.6	21
Nb	2.2	0.88	0.19	0.26	4.1	4.1	5.3
Ta	0.49	0.26	0.03	0.08	0.3	0.89	0.52
Zr	24	6	66	46	166	83	92
Tl	0.19	0.02	0.63	0.91	0.49	0.60	0.80
Pb	50	8.8	65	60	29	45	21
U	0.44	0.26	0.31	0.42	0.42	0.33	0.44
Th	1.9	0.27	0.23	0.90	9.0	5.3	4.2
La	9.2	1.3	2.1	1.9	25.6	17.3	10.9
Ce	18	3.0	4.3	3.9	64	42	26
Pr	2.1	0.4	0.4	0.4	6.3	4.5	2.9
Nd	7.8	1.9	1.3	1.6	23	15	11
Sm	1.7	0.66	0.26	0.32	5.5	3.8	2.6

Eu	2.7	0.67	0.71	0.58	0.95	0.77	0.44
Gd	1.8	0.87	0.31	0.30	6.0	3.7	2.9
Tb	0.28	0.17	0.10	0.07	1.0	0.45	0.55
Dy	1.7	1.1	1.0	0.62	7.5	2.1	3.7
Ho	0.35	0.24	0.30	0.16	1.9	0.38	0.75
Er	0.97	0.67	0.98	0.49	6.2	0.94	1.9
Tm	0.15	0.11	0.16	0.08	1.1	0.14	0.28
Yb	0.87	0.66	0.89	0.47	6.7	0.86	1.72
Lu	0.12	0.09	0.13	0.07	0.94	0.13	0.23
Nb/Ta	4.4	3.3	5.4	3.3	13.8	4.6	10.1
Nd/Th	4.0	7.0	5.4	1.8	2.6	2.8	2.5
Th/U	4.4	1.0	0.7	2.1	21	16	9.6

a: Li concentrations from Bea and Montero (1999)

At least two aliquots (~25 mg each) of each sample were digested and put through the column The Li data reported in this study represent the averages of ≥4measurements of each sample.

The uncertainties for [Li] (μg/g) and δ^7Li are ±10 (2σ) and ±1 (2σ), respectively.

Table 5-4. Comparison of Li concentration (μg/g) of metapelites and leucosomes between different studies. a is from this study, b is from Schnetger (1994), and c is from Sighinolfi and Gorgoni (1977).

	kinzigites			transition	stronalites			leucosomes	metabasites
From	a	b	c	a	a	b	c	a	a
N.	5	14	38	2	5	46	33	7	3
Max.	120	81	N/A	42	11	70	N/A	15	4.2
Min.	46	16	N/A	39	5	2	N/A	3	3.0
Mean	79	57	103	41	8	14	15	7	3.6
Mean (LN.)	74			41	7			6	3.7

N.: the numbler of total samples

LN.: lognormal

are similar, reflecting the normal distribution of the data; we use the arithmetic mean for comparisons of the data.

Lithium concentrations in the metapelites vary widely (Tables 5-2 and 5-4 and Figs. 5-2 and 5-3a), from a low of 5, up to 120 μg/g; kinzigites have significantly higher concentrations (46-120 μg/g, average 79 ± 69 μg/g, 2σ) than samples from the transition zone (39-42 μg/g, average 41 ± 8.4 μg/g, 2σ) and the stronalite zone (5-11 μg/g, average 8 ± 6 μg/g, 2σ). Previous studies have reported average [Li] for kinzigite zone metapelites between 103 μg/g (Sighinolfi and Gorgoni, 1978) and 57 μg/g (Schnetger, 1994). Previously reported average [Li] of stronalite zone samples are 15 μg/g (Sighinolfi and Gorgoni, 1978) and 14 μg/g (Schnetger, 1994); these values are within 2 σ uncertainty of the average [Li] determined in our study. The [Li] of three granulite-facies metabasites is systematically lower than that of stronalites (3.0 – 4.2 μg/g versus 4.6 −11 μg/g, respectively).

The leucosomes analyzed here exhibit a relatively limited range in Li concentrations (3-15 μg/g, Tables 5-2 and 5-4 and Fig. 5-3a), with samples from the kinzigite zone (12 − 15 μg/g) characterized by higher concentrations than samples from the transition zone (6 − 8 μg/g) and stronalite zone (3 − 5 μg/g).

Lithium isotopic compositions of metapelites from the kinzigite zone (Figs. 5-2 and 5-3b) show a large range (-8.5 to -0.1) relative to samples from higher metamorphic grade; the δ^7Li of one anomalously light sample (P1, δ^7Li = -8.5) is not included in the average δ^7Li of kinzigites, since it is a statistical outlier (plotting outside of the "outer fence", defined by 3× the interquartile range). This sample's unusual composition is

discussed in section 5.2. The average δ^7Li of kinzigites, δ^7Li= -1.4 ± 2.0 (2σ), is indistinguishable from that of the transition (δ^7Li = +0.4) and stronalite (average = +0.9 ± 2.9, 2σ) zones. The δ^7Li values of the leucosomes get progressively heavier from the kinzigite (-0.9 to -1, average δ^7Li = -1.0 ± 0.2, 2σ) to transition (+3.3 to +7.5, average δ^7Li = +5.4 ± 6.0, 2σ) to stronalite (δ^7Li = +6.0 ± 3.2, 1σ) zones (Fig. 5-3b). The granulite metabasites have δ^7Li of -3.2 to +3.3 (average 0 ± 6.5, 2σ), which overlaps that of the stronalites.

5. Discussion

5.1. Factors controlling the [Li] of metapelites

Recent studies have concluded that Li in metamorphic rocks can be depleted by 20-50% during greenschist to lower amphibolites facies (250 to 650°C) metamorphic dehydration (e.g., Zack et al., 2003; Marschall et al., 2007; Teng et al., 2007; Qiu et al., 2011a). These results are consistent with Li being a fluid-mobile element having a fluid rock partition coefficient ($^{fluid/rock}K_{Li}$) that positively correlates with temperature (Seyfried et al., 1998). From amphibolite to granulite facies (i.e., kinzigites to stronalties), the [Li] of Ivrea-Verbano Zone metapelites are depleted by up to ~90% (Figs. 5-2 and 5-3a), suggesting that dehydration-related partial melting significantly contributes to the depletion of Li in metapelitic granulites.

The positive correlation between [Li] and biotite abundance (Fig. 5-4), which is not found for any other mineral, suggests that biotite is the main host for [Li] in kinzigite and stronalite rocks. The breakdown of biotite during partial melting occurs through the reaction (Schnetger, 1994):

Biotite + Sillimanite + Plagioclase+ Quartz → K-feldspar + Garnet + Rutile + melt

Consumption of biotite releases Li and, if this Li is not significantly partitioned into any other mineral in the rock, then large amounts of Li are lost with the melt; as a result, the stronalites are significantly depleted in Li relative to the kinzigites. The protolith of the metapelites experienced other dehydration reactions prior to biotite breakdown in the Ivrea-Verbano Zone. One such major reaction is muscovite breakdown (Sighinolfi and Gorgoni, 1977):

$$\text{Muscovite} + \text{Quartz} \rightarrow \text{Sillimanite} + \text{K-feldspar} + H_2O$$

during the formation of kinzigites.

Thus, we wish to test whether [Li] in the kinzigites reflects the net result of a series of dehydration reactions from diagenesis to amphibolite facies metamorphism; if Li is released during dehydration, the [Li] in kinzigites should be lower than that of their pelitic protolith. We note, however, that the average [Li] of the kinzigites (79 ± 69 μg/g, 2σ) is within the range of PAAS (Post Archean Australian Shales, average 63 ± 50 μg/g, 2σ, Teng et al., 2004) and other pelitic sediments (Chan et al., 2006) and sedimentary rocks (Qiu et al., 2009), which are considered representative of typical pelitic sediments. Notably, the [Li] of two kinzigites is as high as the most Li-enriched pelitic sediments found in British shales (Fig. 5-2, [Li] >100 μg/g, Qiu et al., 2009) and all kinzigites plot on the correlation between [Li] and weathering intensities (Chemical Index of Alteration, CIA) (Fig. 5-5) defined by previous studies (Qiu et al., 2009; 2011a). These observations suggest that the protoliths of the kinzigites, and not metamorphic dehydration reactions (i.e., muscovite breakdown), exerted the greatest control on [Li] in these rocks.

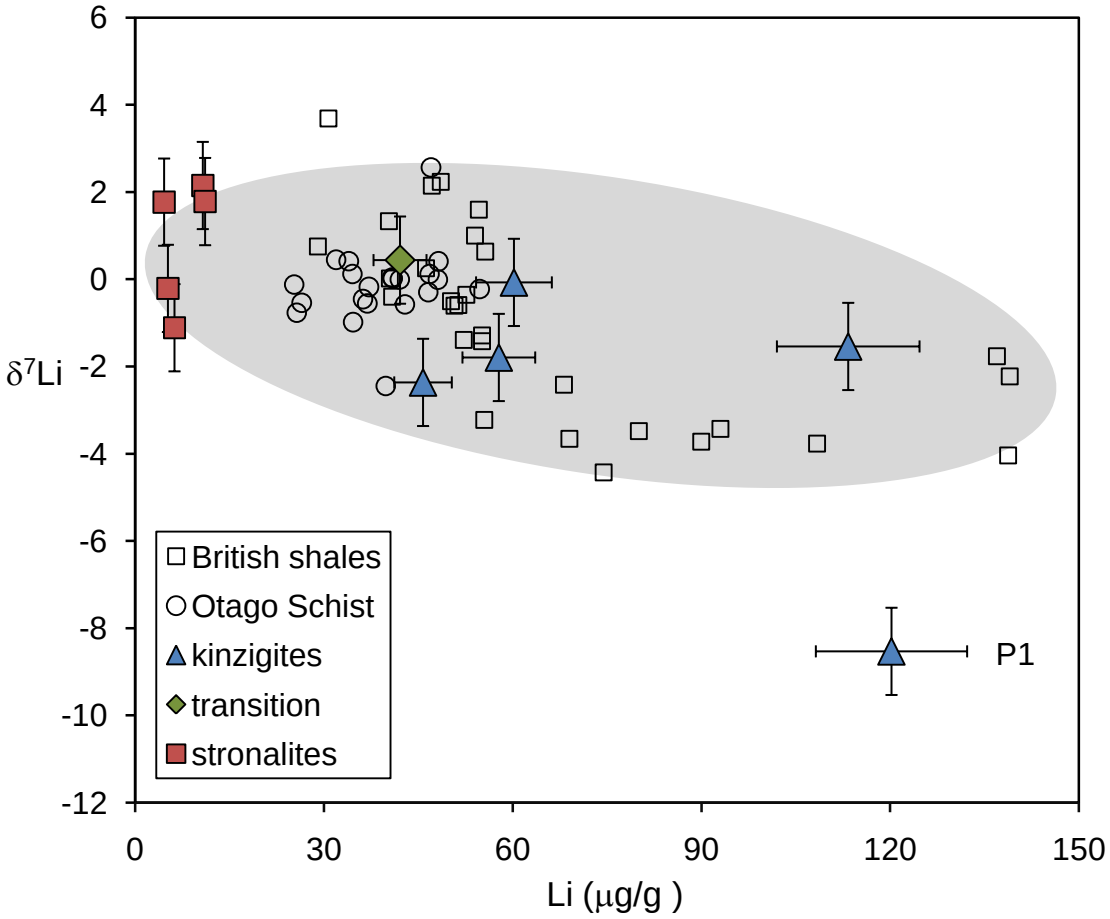

Figure 5-2. Plot of δ^7Li versus [Li] for metapelites from the three zones. Error bars indicate the 2σ uncertainty of Li isotopic compositions (± 1‰) and 2σ uncertainties of Li concentrations (± 10%). British shales and Otago Schist data are from Qiu et al. (2009) and Qiu et al. (2011aa), respectively. Sample P1 has different Li signature from the other metapelites, which is indicated by the gray cloud.

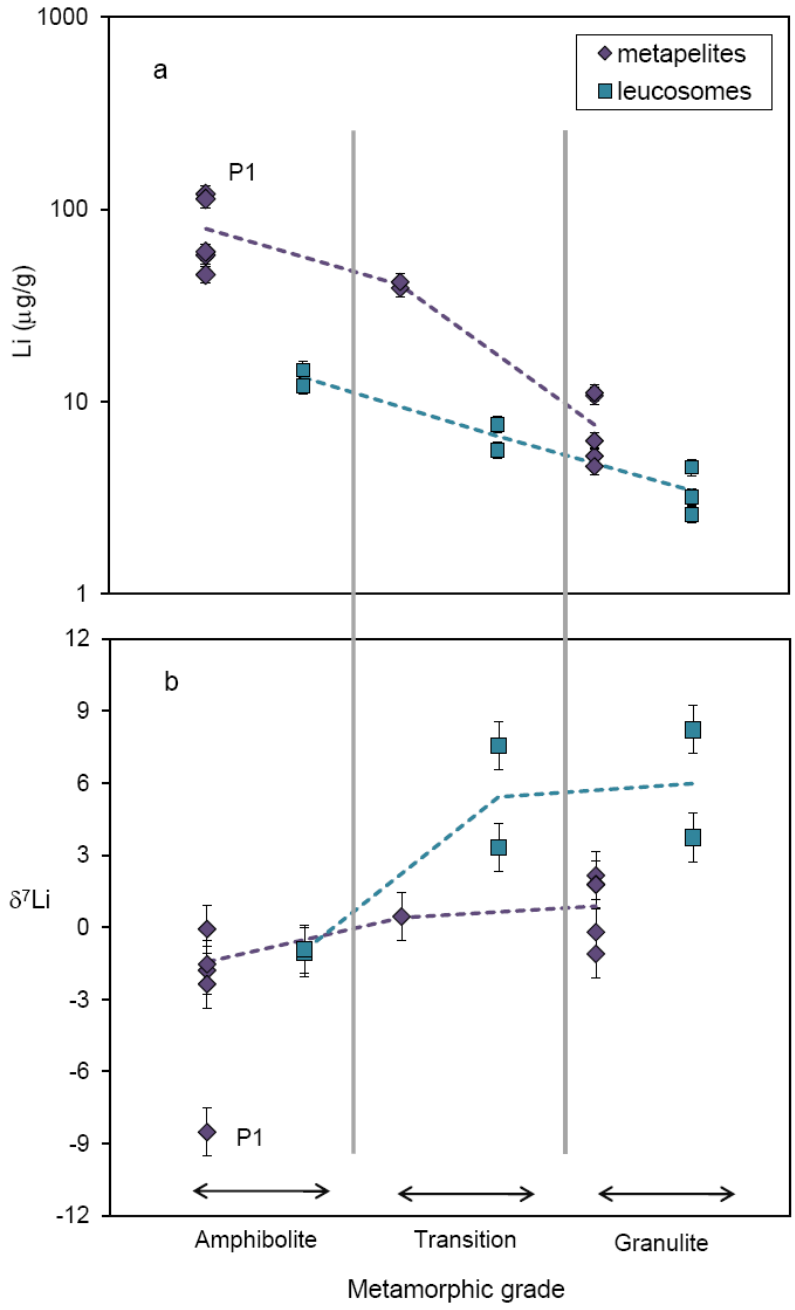

Figure 5-3. Plot of Li concentrations (a) and Li isotopic compositions (b) versus metamorphic grade for the metapelites and leucosomes from the three zones. Note y-axis of (a) is logarithmic. The dashed purple and green lines are connected by the average value of [Li] and δ^7Li in metapelites and leucosomes of three zones, respectively. Error bars indicate 2σ uncertainty. The long gray bars are indicative of the transition of metamorphic grade.

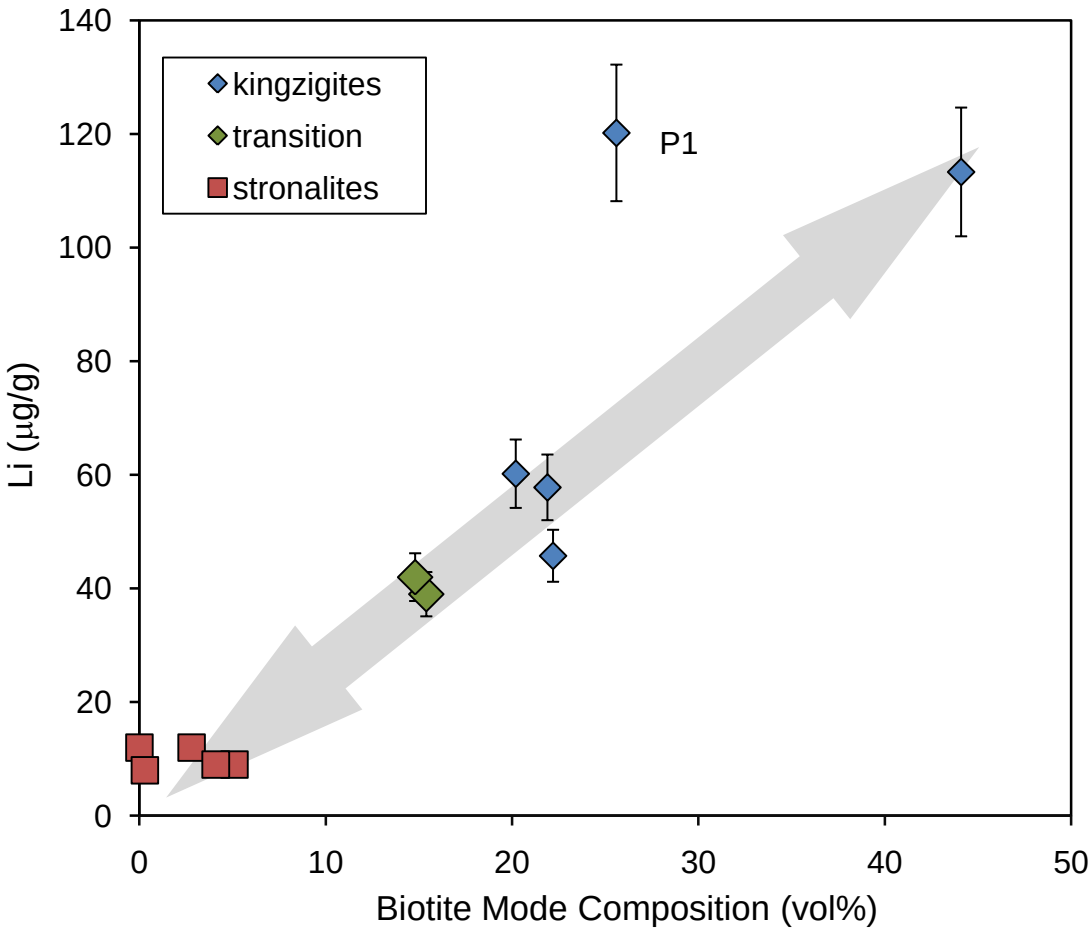

Figure 5-4. Plot of Li concentrations versus biotite mode for the metapelites from the three zones. Error bars indicate 2σ uncertain of Li concentrations (±10%).The gray trend line shows the positive correlation between [Li] and biotite modal compositions in the metapelites except sample P1.

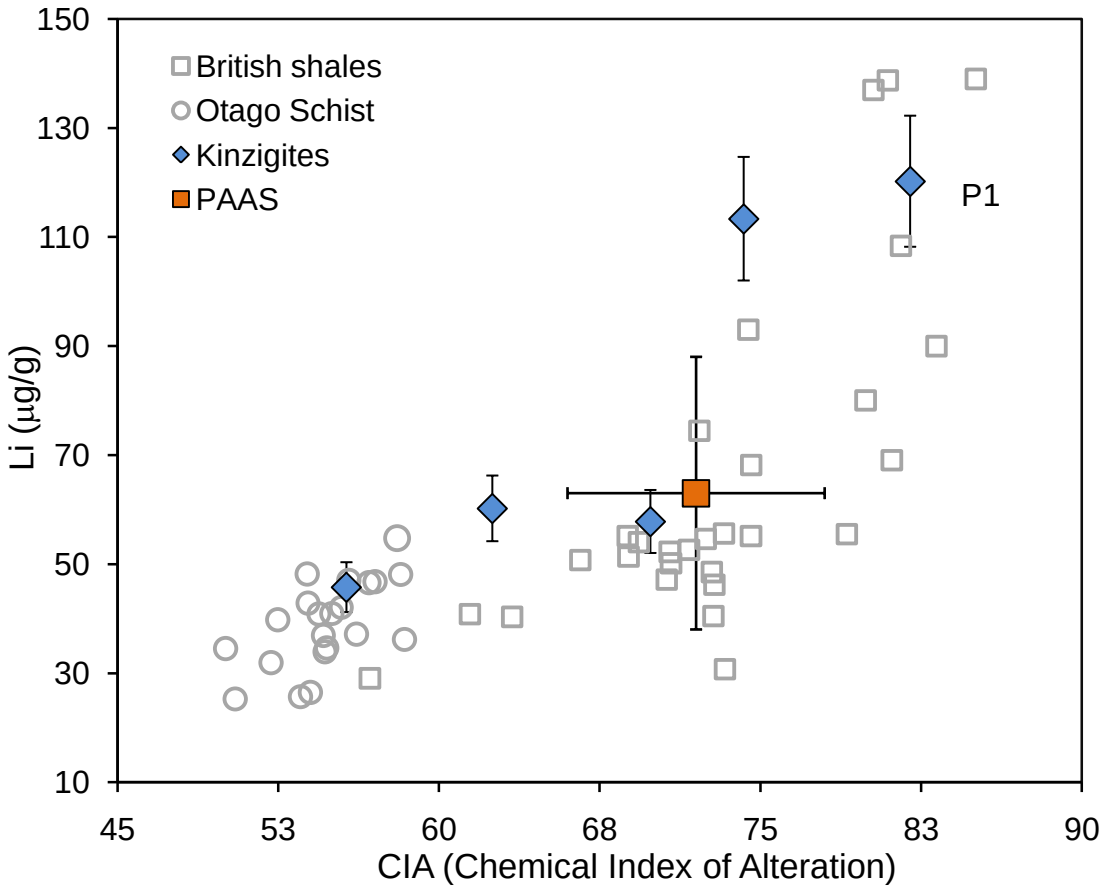

Figure 5-5. Plot of Li concentrations versus CIA (Chemical Index of alteration) for the metapelites from the kinzigite zone. PAAS: Post Archean Australian Shales. Average [Li] and CIA value of PAAS is from Teng et al. (2004).

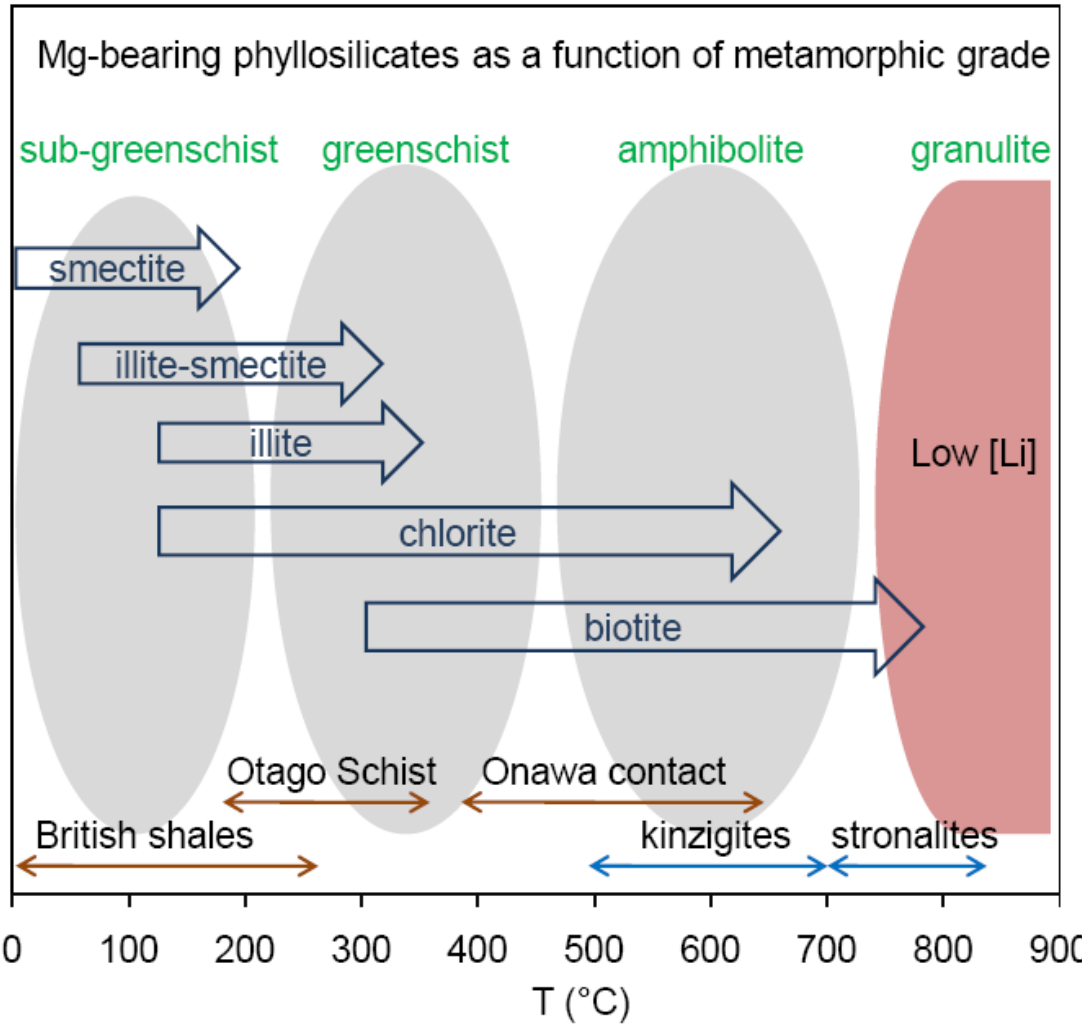

Figure 5-6. Evolution of Mg-bearing phyllosilicates as a function of metamorphic grade in pelitic sediments. The ellipses indicate the sequence of metamorphism from sub-greenschist to granulite facies. The Mg-bearing phyllosilicates listed on the figure may contain most of Li in the metapelites. During granulite facies metamorphism, most of the phyllosilicates break down, resulting in low [Li] in the rocks. The relationship between minerals and temperature is according to Eberl (1984) and Winter (2010). The temperature range of British shales, Otago Schist and Onawa contact aureole are from Qiu et al. (2009), Qiu et al. (2011) and Teng et al. (2007), respectively. See text for details.

Enrichments of Li in the pelitic sediments are linked to the abundance of Mg-bearing clay minerals, such as chlorites and smectites, which play an important role in the Li geochemical cycle (Stoffynegli and Mackenzie, 1984). Because of its similar ionic radius, Li^+ substitutes for Mg^{2+} in the octahedral sites of the clay's crystal lattice, with additional Li^+ going into the interlayer position for charge compensation (Vigier et al., 2008; Williams and Hervig, 2005). Fig. 5-6 illustrates the possible Li-enriched phyllosilicates present during prograde metamorphism of pelitic sediments (based on Eberl, 1984). During sedimentation and low-grade metamorphism (up to greenschist facies), the original smectite is gradually converted into mixed-layer illite-smectite and chlorite, which retain Li, since smectite, illite and chlorite are all Mg-bearing. Illitization and chloritization is the likely reason for the lack of Li depletion during sub-greenschist facies metamorphic dehydration observed in the British shales (Qiu et al., 2009). During higher grade metamorphism (up to amphibolite facies) chlorite breaks down, but Li released from chlorites may be quantitatively incorporated into newly formed biotite (Chlorite + K-feldspar → Biotite + Muscovite; Spear and Cheney, 1989), and, thus, the rocks maintain the original Li signature of the protolith, as seen in the kinzigite samples. However, if the metamorphic reaction causes the breakdown of Mg-bearing phyllosilicates without forming new ones, then the Li will be lost during dehydration, as observed in the granulite facies stronalites, as well as the greenschist facies Otago schist (Qiu et al., 2011a) and amphibolite facies Onawa contact aureole (Teng et al., 2007). Thus, a key factor in determining the [Li] of metapelites during metamorphism is the stability of Mg-bearing phyllosilicates.

5.2. Factors controlling the δ^7Li of metapelites

In contrast to [Li], no significant difference is observed in the average δ^7Li values of kinzigites, transition, and stronalite zone rocks (Fig. 5-2), demonstrating that metamorphic dehydration in stronalites has no appreciable effect on the whole rock δ^7Li, and the δ^7Li values of the metapelites likely reflect the signature of their protoliths.

One unusual kinzigite sample (P1) has the lightest δ^7Li (-8.4), most abundant [Li] (120 μg/g) (Fig. 5-2) and highest CIA (82) value of the suite (Fig. 5-5). The highly weathered protolith signature of this sample is also reflected in its markedly low concentrations of Sr and Ba (Table 5-2), which are characteristics of chemical weathering of feldspar and loss of these soluble elements. Therefore, the Li composition of sample P1 may reflect the influence of severe weathering in the provenance of the sediment, which concentrates ^{6}Li relative to ^{7}Li in the regolith (Kisakurek et al., 2004; Rudnick et al., 2004; Qiu et al., 2009). Moreover, the abnormally low δ^7Li of P1 may also reflect Li addition through diffusion. Since ^{6}Li diffuses faster than ^{7}Li, significant isotopic fractionation occurs during diffusion (e.g., Richter et al., 2003; Lundstrom et al., 2005; Teng et al., 2006a; Jeffcoate et al., 2007; Penniston-Dorland et al., 2010; Halama et al., 2011). Therefore, if Li diffused into this sample, it would create low δ^7Li and elevated [Li]; the field evidence that P1 sample includes numerous quartz veins may indicate an event of hydrothermal fluids percolation, though based on the study of the Otago Schists (Qiu et al., 2011a) one would predict that hydrothermal fluids may have little leverage on Li in such a Li-rich lithology. The fact that this sample plots above the trend in the modal biotite vs. [Li] plot (Fig.5-4) and below the trend in the [Li] vs. δ^7Li plot (Fig. 5-2) supports the possibility of Li diffusion. Thus, either of these two processes, or both, may have played a role in producing the distinctive composition of this sample.

The reason for the lack of significant Li isotopic fractionation during metamorphism is apparent from studies of Li isotopic fractionation factors, α, or $\Delta_{fluid\text{-}rock}$. Most such factors are inferred from the interaction between seawater and basalts (Chan and Edmond, 1988; Chan et al., 1994; James et al., 1999; Millot et al., 2010) or determined from equilibration experiments between fluids and minerals (Wunder et al., 2006; 2007; Vigier et al., 2009). The isotopic fractionation factors inferred from these studies give $\Delta_{solution–rock(mineral)}$ values of 1 to 3‰ at 500 - 900°C, 1- 5‰ at 250 °C, ~10 ‰ at 150 °C and ~19‰ at 2 °C. These experimental results show that Li isotopic fractionation is limited or analytically unresolvable at temperatures above 250 °C, which is generally the temperature for sub-greenschist facies metamorphism. Consequently, Li loss during higher-grade metamorphism may not result in discernable Li isotopic fractionation.

5.3. Li signature of leucosomes

The average [Li] of the leucosomes is significantly lower than that of the metapelites from the same metamorphic zone (Fig. 5-3), consistent with the mineralogy of the leucosomes (mainly quartz and minor feldspar, which typically have low Li concentrations), which lack a Li-rich phase such as biotite. Leucosomes from the stronalite zone, interpreted as partial melts, have, on average, higher δ^7Li than those of the metapelites from the same zones (Fig. 5-3). This difference is consistent with equilibrium Li isotopic fractionation accompanying crystallization of the leucosomes from a melt having an isotopic composition similar to the stronalites, as quartz preferentially takes ^{7}Li into its two- and four-fold-coordinated interstitial sites during crystallization (Sartbaeva et al., 2004; Teng et al., 2006b).

Compared with the leucosomes from the stronalite zone, the leucosomes in the kinzigite zone are quartz- and Na-rich and K-poor and were interpreted to have precipitated from hydrothermal fluids (Bea and Montero, 1999). Consequently, these leucosomes should have lower [Li] and higher δ^7Li relative to the leucosomes from the stronalite zone. However, the opposite is true. Qiu et al (2011a) reported surprisingly light Li isotopic composition for fluid-precipitated quartz veins in the Otago Schists, which have δ^7Li similar to that of their enclosing wall rocks (δ^7Li = -1.4 to -2.8). These isotopic values were interpreted to reflect the influence of Li ingress from surrounding wallrock. A similar explanation may hold for the fluid-precipitated leucosomes in the kinzingite zone. The somewhat higher [Li] in these leucosomes (12-15 μg/g) compared to that of the quartz veins in the Otago Schists ([Li] = 0.4 to 2.3 μg/g, Qiu et al., 2011a) may reflect the generally higher [Li] in the Ivrea kinzigites compared to the Otago Schists (Fig. 5-2) and the presence of feldspar and garnet, in addition to quartz in the Ivrea leucosomes.

5.4. Li depletion and partial melting

The depleted [Li] of the leucosomes in the stronalite zone suggests that they are not the repository for the significant amounts of Li removed from the metapelites during granulite-facies partial melting/dehydration. Large amounts of Li must have been removed from the system. One possible scenario is that a granitic melt ascended into the upper crust, leaving a restite depleted in incompatible elements (Schnetger, 1994; Quick et al., 2009).

In order to model the change in [Li] during partial melting, we employ a batch melting model that uses the composition of the kinzigites and stronalites to represent the

composition of the parent rocks and the restites, respectively. The partial melting model of Schnetger (1994) suggested that granulite facies partial melting produced about 40% melt with a composition similar to average S-type granite. However, [Li] in the model melt (> 100 μg/g) is higher than [Li] in average S-type granite (<100 μg/g). Schnetger (1994) suggested that this discrepancy may be due to insufficient Li data for S-type granites or that the Li from the granite is lost during pegmatite formation. Recent studies (Bryant et al., 2004; Teng et al., 2006b; Magna et al., 2010) have reported more Li data for S-type granites, both for [Li] and δ^7Li, thus, providing the opportunity to evaluate these possibilities.

Following Schnetger (1994), we employ a batch melting model, $C_1 = [C_0 - (1 - F) C_s] / F$, in which C_1 is the calculated composition of the melt, C_o is the composition of the parent rocks (kinzigites), F is the melt fraction and C_s is the composition of the restite (stronalites). In order to investigate the possible range of melt compositions, each kinzigite and stronalite sample measured in this study (excluding P1) is considered as the individual composition of parent rock and restite, respectively, and the volume of melt is allowed to vary between 20 to 50% (possible melt volume generated from partial melting of kinzigites; Schnetger, 1994). Figure 5-7 shows the modeling results for [Li] and δ^7Li in the melt compared with data for S-type granites. Model C_l compositions that plot within the range of S-type granites (gray field, Fig. 5-7) are derived from kinzigites having low [Li] (in the range of 46 to 60 μg/g); partial melting of parent rocks with high [Li] (60 – 113μg/g) results in melts that have higher [Li] than any granite analyzed, to date.

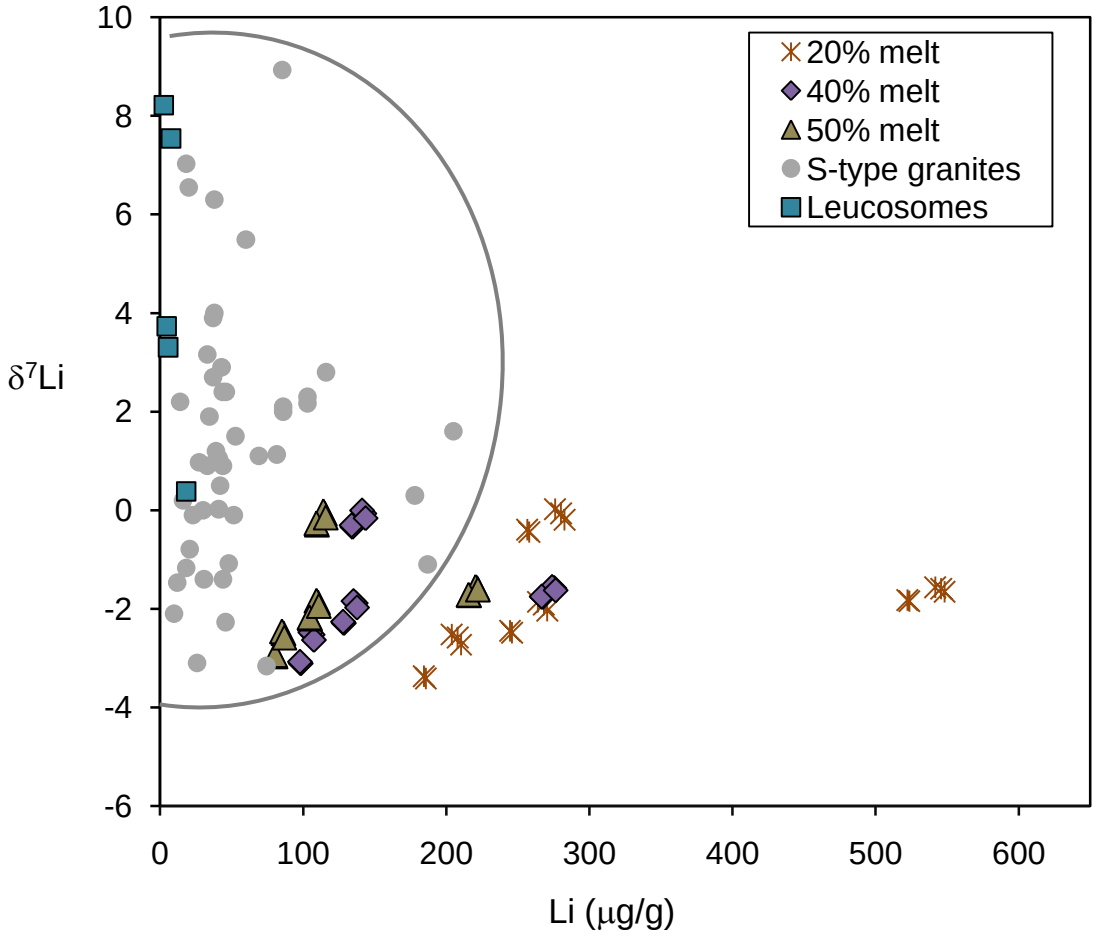

Figure 5-7. Plot of [Li] and δ^7Li of calculated partial melts. Data for S-type granites (gray field) are from Teng et al. (2006b), Bryant et al. (2004) and Magna et al. (2010). The fraction of the melt in the model is 20%, 40% and 50% (see text for details).

Pegmatites are generally much more enriched in Li than S-type granites (Cerny et al., 1985; Teng et al., 2006b; Liu et al., 2010); therefore, such Li-enriched melts from the partial melting model may give rise to pegmatites. The δ^7Li of minerals from pegmatites (e.g., quartz, plagioclase, mica, spodumene) has a large range, but is generally heavier (+1.5 to +21.3, Teng et al., 2006b; Liu et al., 2010) than that of the melt calculated in this study (δ^7Li of −0.3 to −3.1). Consequently, if the modeled melts contribute to the formation of pegmatites, isotopic fractionation must occur during the crystallization of those minerals. These results indicate that partial melting of metapelites with [Li] ~50 μg/g and δ^7Li of ~-1, regardless of the fraction of the melt (20 – 50%) produced, may generate the Li compositions seen in S-type granites.

5.5. Li concentration and isotopic composition of lower continental crust

The stronalites, along with other granulite facies mafic-ultramafic rocks in Ivrea-Verbano Zone, are considered as a representative section of lower continental crust (e.g., Berckhem, 1969; Fountain, 1976; Voshage et al., 1990). Moreover, the average composition of the stronalties in this study is similar to the average composition of lower continental crust in terms of SiO_2 and Na_2O+K_2O (e.g., 52.1% and 3.0%, respectively, for the stronalites, cf. 53.4% and 3.26%, respectively, for the lower crust of Rudnick and Gao, 2003). Therefore, the Li composition of the stronalites may provide insight into the Li signature of the lower continental crust.

The stronalites have [Li] of 5-11 μg/g (average 8 ± 6 μg/g, 2σ) and δ^7Li of -1.1 to 2.1, (average = 0.9 ± 2.9, 2σ), with a concentration weighted average δ^7Li of +1.1. This [Li] falls within the range of [Li] in different models for the lower crust (between 6 and 14 μg/g, Taylor and McLennan, 1985; Shaw et al., 1994; Wedepohl, 1995; Rudnick and

Fountain, 1995; Rudnick and Gao, 2003; Teng et al., 2008), and is identical to the value determined by Teng et al. (2008) for the lower crust based on several xenolith suites as well as granulite terrane composites.

By contrast, the δ^7Li of stronalites are lower but more constant compared to the results of Teng et al. (2008). Teng et al. (2008) suggested that the variable δ^7Li seen in the xenoliths is the result of a combination of effects, including isotopic fractionation during prograde metamorphism, kinetic fractionation caused by basaltic intrusions and variable protolith compositions. Our results suggest that prograde metamorphism (up to granulite facies) does not likely cause Li isotopic fractionation. Furthermore, the three granulite facies metabasites have lower [Li] (average 3.6 ± 1.2 μg/g, 2σ) but comparable average δ^7Li (-3.2 to 3.3, average 0 ± 6.5, 2σ) as the stronalites, indicating that heterogeneous protoliths may contribute little to the variable δ^7Li. Therefore, kinetic isotopic fractionation is the most likely cause of the strongly heterogeneous δ^7Li in the xenoliths. It is noteworthy that one granulite metabasite (B5) has negative δ^7Li (δ^7Li = -3.2). Such low values have not found in any mantle-derive melts and the depleted mantle is suggested to have δ^7Li +3.4 ± 1.4 (2σ) (Tomascak et al., 2008, and references therein); therefore, the low δ^7Li in this sample may represent a kinetically disturbed signature.

Based upon the Li signature in stronalites and metabsites, the [Li] of lower continental crust, as sampled in the Ivrea-Verbano Zone, is around 8 μg/g or less, and the concentration weighted δ^7Li is +1.0.

6. Conclusions

The [Li] and δ^7Li in amphibolite facies kinzigites likely reflect the Li signature of their protolith, which, in turn, reflects the composition of the provenance of the

sediments; [Li] in the metapelites positively correlates with the abundance of biotite, reflecting the influence of Mg-bearing phyllosilicates on [Li] in these rocks. Pre-granulite facies metamorphic dehydration reactions may have had minor influence on Li in the kinzigite samples; however, dehydration melting associated with biotite breakdown during granulite facies metamorphism caused extreme [Li] depletion in stronalites. The δ^7Li in both amphibolite- and granulite-facies metapelites is statistically indistinguishable, indicating no Li isotopic fractionation at these metamorphic temperatures (500-800^{o}C). Leucosomes in the kinzigite zone were precipitated from hydrothermal fluids, but those in the stonalite zone formed by partial melting. The low [Li] and relatively high δ^7Li of leucosomes in the stronalite zone are consistent with their origin as quartz-rich precipitates from a partial melt, since the crystallization of quartz may cause significant Li isotopic fractionation. The lower δ^7Li of leucosomes in the kinzigite zone may reflect Li diffusion into the quartz-rich veins from surrounding Li-rich metapelite. A batch melting model indicates some of the Li released during partial melting of metapelites can contribute to S-type granites, with excess Li being partitioned into Li-pegmatites. The Li compositions in stronalites and metabsites indicates that the lower continental crust, as represented by the Ivrea-Verbano Zone, has [Li] of 8 μg/g or less, and a concentration weighted δ^7Li of +1.0.

Appendix 5-A

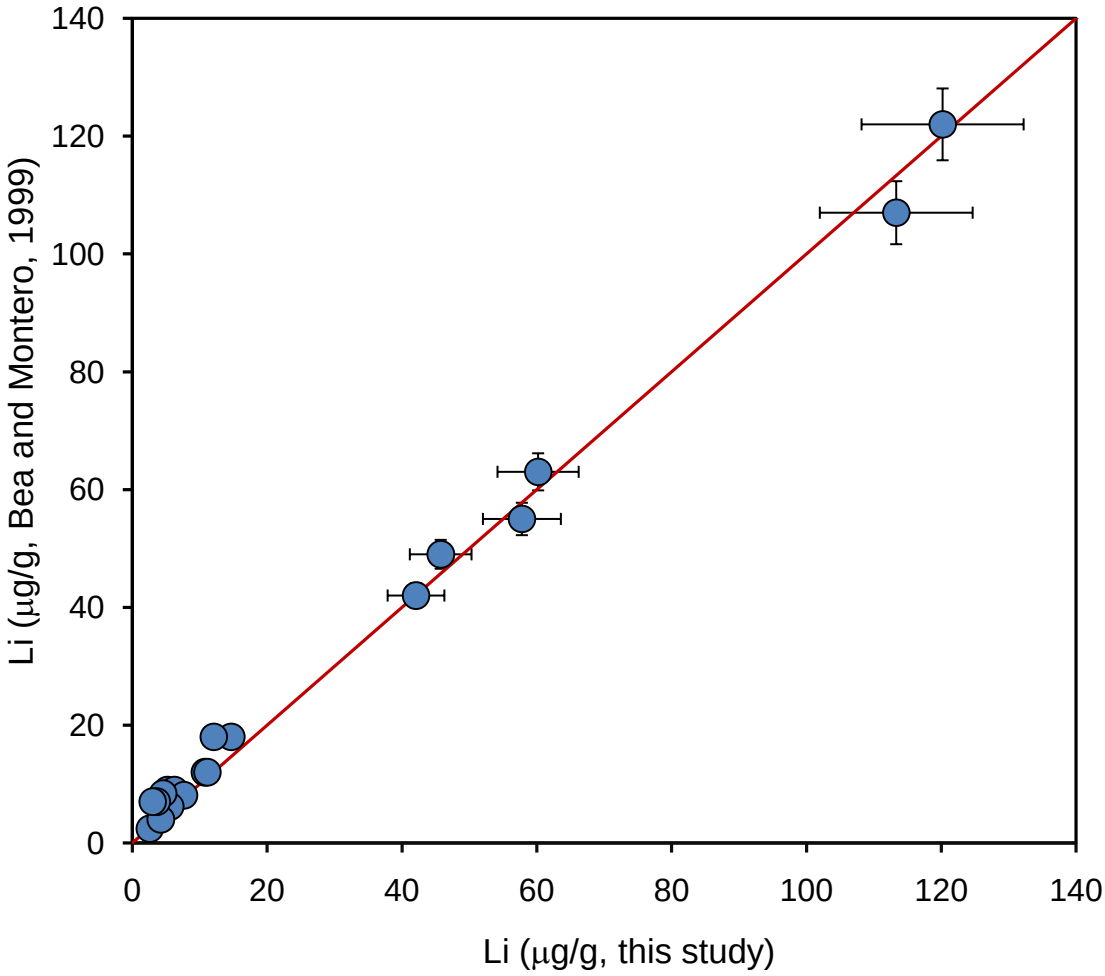

Appendix 5-A. Comparison of [Li] between the measurements from this study and Bea and Montero (1999). Vertical and horizontal error bars indicate 2σ uncertain of Li concentrations is ± 5% (Bea and Montero, 1999) and 10% (this study), respectively. Red line is indicative of 1:1. See text for details.

Chapter 6: Lithium isotopic study of ancient shales from the Kaapvaal Craton, Southern Africa[1]

[1] L. Qiu, R.L. Rudnick and W.F. McDonough contributed to the interpretation of the data. Major and trace elements are from Wronkiewicz and Condie (1987; 1989; 1990). The text, tables and figures (except where noted) were created/written by L. Qiu.

Abstract:

To investigate the compositional evolution of continental crust and weathering conditions during the Neoarchean, 25 shales from three Supergroups in the Kaapvaal Craton, South Africa having depositional ages from 3.0 Ga to 2.2 Ga, were analyzed for Li isotopes. Within a given formation, Li concentrations ([Li]) and Li isotopic compositions (δ^7Li) of the shales are relatively constant, but [Li] and δ^7Li may vary significantly from one formation to another, even within the same Supergroup. The Li signatures in shales do not correlate with their depositional age, indicating the provenance of shales is not significantly changed during the transition from late Archean to early Proterozoic. The [Li] in all shales varies by a factor of twenty-two, with the following ranges: 8 to 78 μg/g in the Witwatersrand Supergroup, 9 to 16 μg/g in the Ventersdop Supergroup and of 36 to 178 μg/g in the Transvaal Supergroup. The three Supergroups are also isotopically variable, with δ^7Li spanning the range of -2.2 to +12.7. Generally, [Li] of the shales from the Kaapvaal Craton negatively correlate with their δ^7Li, which is similar to the correlation found in Post Archean shales. The [Li] of Archean shales increases and then decreases with increasing weathering intensity, as marked by the Chemical Index of Alteration (CIA), but Post Archean shales only show

the positive correlation with CIA. Moreover, several Archean shales (e.g., K8, Orange Grove Formation, Witwatersrand Supergroup) have low [Li] (<16 μg/g), high δ^7Li (>3.0) and very high CIA (81-95), characteristics not seen in Post Archean shales. The differences between these Archean shales and post Archean shales are likely the result of severe weathering conditions (e.g., heavy rainfall and high surface temperature) in the provenance region of the shales; therefore, Li isotopes may have the potential to be used as an indicator of weathering intensity and paleo-climate conditions, in addition to CIA. The Li signatures in all the shales from the Kaapvaal Craton indicate [Li] in the upper continental crust may have increased from the Archean to the post Archean, and the Archean upper continental crust may have had heavier Li isotopic compositions than modern upper continental crust.

1. Introduction

Understanding the origin and evolution of the continental crust has been a major goal of geologists for centuries. A fundamental observation requiring explanation is that the continental crust has an average andesitic composition that does not match that of its basaltic building blocks. This enigma, which has been referred as the "Crust Composition Paradox," (Rollinson, 2008) cannot simply be solved by intracrustal magmatic differentiation; other processes are needed to preferentially remove Mg and enrich Si during continental crust evolution (Rudnick, 1995). Weathering of basaltic crust is favored by some studies as a process that can potentially solve this paradox (e.g., Albarede, 1998; Lee et al., 2008). During chemical weathering of upper continental crust, Mg is preferentially removed from the crust relative to Si, because Si-rich minerals (e.g., quartz) are more resistant to weathering than Mg-rich silicate minerals; as a result,

chemical weathering leaches and subsequently depletes the soluble elements in the continental crust. Therefore, a study of soluble elements and their secular attributes in sediments may shed light on the extent to which weathering influences the composition of the continental crust.

Lithium and its isotopes has the potential of tracing weathering processes due to the large mass differences between its isotopes (^{6}Li and ^{7}Li), which leads to significant fractionation at the Earth's surface during low temperature continental weathering (e.g., Tomascak, 2004; Elliott et al., 2004). During primary mineral dissolution, heavy ^{7}Li is preferentially removed from the regolith into aqueous fluids (e.g., Chan and Edmond, 1988; Huh et al., 2004), and during secondary mineral formation, ^{6}Li is preferentially retained in silicates, such as smectite, via substitution for Mg^{2+} (e.g., Vigier et al., 2008; Wimpenny et al., 2010a); consequently, weathering process produce continental crust with a lighter Li isotopic composition (δ^{7}Li = 0 ± 2‰, 1σ, e.g., Rudnick et al., 2004. Teng et al., 2004) than the upper mantle, as sampled by fresh MORB (δ^{7}Li = 4 ± 2‰, 1σ, e.g., Chan et al., 1992; Elliott et al., 2006; Moriguti and Nakamura, 1998;Nishio et al., 2007; Tomascak et al., 2008). Therefore, the Li isotopic composition of terrigenous sediments may provide useful information about the influence of weathering on the continental crust composition, as well as potentially illuminating weathering conditions. Importantly, metamorphic dehydration, from greenschist to granulite facies, may cause Li depletion, but has been shown to have little influence on the δ^{7}Li in metasedimentary rocks (e.g., Teng et al., 2007; Qiu et al., 2009; 2011a; 2011b); further more, sub-greenschist facies metamorphism has negligible effect on [Li] in sediments (Qiu et al., 2009).

Fine-grained sediments, like shales, generally derive from a wide variety of provenances, are thoroughly homogenized prior to deposition and occur in stratigraphic sections that cover most of geologic time. Therefore, shales, which reflect the composition of contemporary upper continental crust for immobile elements, provide a perspective on the temporal evolution of the composition of the upper continental crust (Taylor and McLennan, 1985; Gibbs et al., 1986; McLennan and Taylor, 1991; Condie, 1993, Lahtinen, 2000; Rudnick and Gao, 2003), and the Li signatures in shales may further help constrain to what extent the weathering processes influence the composition of continental crust.

The Li signature of typical Post-Archean shales, PAAS (Post Archean Australian shales), has been documented by Teng et al. (2004). These shales have an average [Li] of ~ 63 μg/g and δ^7Li of ~0 (Teng et al., 2004). In contrast to the Li signature in PAAS, the Li concentrations and isotopic compositions of Archean shales may be different due to more intense weathering conditions in the Archean. Several studies have postulated that the early Archean Earth experienced heavier rainfall, higher Pco_2 and surface temperature than in the post Archean (e.g., Kasting, 1993; Knauth and Lowe, 2003; Lowe and Tice, 2004; Rasmussen and Buick, 1999); however, whether these severe weathering conditions existed throughout the Archean and to what degree Li signatures in Archean shales are influenced by Archean weathering are not clear.

In order to investigate possible correlations between the Li signature and Archean weathering conditions, we analyzed the Li concentration and isotopic compositions in Archean shales. These shales were deposited in a series of rifts and basins in the Kaapvaal Craton, South Africa, between 2.9 Ga to 2.2 Ga and have been previously used

to monitor the changes in the chemical composition of upper continental crust over that time interval from (e.g., Wronkiewicz and Condie, 1987; 1989; 1990; Jahn and Condie, 1995).

2. Geologic setting

It is generally accepted that the Kaapvaal Craton, the ancient segment of continental crust in southern Africa, formed between ~3.7 to 2.6 Ga. Much of this continental nucleus was formed between ~3.2 and 3.1 Ga through the tectonic imbrication of slabs of oceanic lithosphere, which are represented by mafic/ultramafic volcanic rocks and associated sediments (e.g., De Wit et al., 1992). The continental nucleus was then modified and enlarged by further continental magamatic activity related to Cordilleran-type subduction-accretion processes between ~3.1 and 2.6 Ga (e.g., De Wit et al., 1992). The first major sedimentary basin formed on the craton was the Witwatersrand Basin, which is now a 300 km × 200 km northeast-trending elliptical structural remnant, consisting of four major unconformity-bounded supracrustal sequences, the Dominion Group and the Witwatersrand, Ventersdorp, and Transvaal Supergroups. This study focuses on the shales from the formations that belong to the later three Supergroups; the general stratigraphic sequence is shown in Fig. 6-1 and each supergroup is described below.

2.1. Witwatersrand Supergroup

The Witwatersrand Supergroup comprises an epicontinental siliclastic sequence up to 7 km thick, and is divided into the lower West Rand and the upper Central Rand Groups, with the former conformably overlying the volcanic rocks of the Dominion Group and lying unconformably upon Archean basement rocks of Kaapvaal Craton. The West Rand

Group is dominated by shallow marine to subtidal argillaceous-arenaceous sedimentary rocks, with equal proportions of shales and quartzite (Tankard et al., 1982). The gold-bearing Central Rand Group comprises more coarse-grained fluviatile to subtidal arenaceous-rudaceous sedimentary rocks, chiefly subgraywacke, quartzite and conglomerate, with minor shales (Pretorius, 1976). The rocks experienced regional greenschist facies metamorphism (350 ± 50 °C, 1-2 kbar) (Pretorius, 1981). Deposition of the Witwatersrand section occurred over 360 Ma, as constrained by U-Pb zircon ages of volcanic rocks from the underlying Dominion Group and the overlying Ventersdorp Supergroup (Armstrong et al., 1991). Deposition commenced at ~3.07 Ga and was terminated at 2.71 Ga by Ventersdorp magmatism, which is manifest by mafic dykes and sills intruded into the Witwatersrand Supergroup strata (Armstrong et al., 1991).

2.2. Vendersdorp and Transvaal Supergroups

The Ventersdorp and Transvaal Supergroups occur in northeast-southwest trending belts, covering areas greater than 200,000 and 500,000 km^2, respectively (Wronkiewicz and Condie, 1990). The Ventersdorp Supergroup is composed dominantly of volcanic rocks, including up to three km of tholeiitic flood basalts, which are overlain by up to two km of more localized rift sedimentary rocks (Crow and Condie, 1988). The Pniel Group of the Ventersdrop Supergroup, studied here, was deposited in an alluvial plain (Tankard et al., 1982) and is characterized by cyclic units of conglomerate, quartzite, pelite and carbonate (Button, 1981).

Following an erosional interval after the deposition of the Ventersdorp Supergroup (2.71− 2.69 Ga, Armstrong et al., 1991), much of the Kaapvaal Craton was inundated at ~2.6 Ga by a shallow sea to from the Transvaal Supergroup (Gibson and Jones, 2002).

An evolution from local rifts to a large cratonic basin is recorded by the Transvaal Supergroup succession, which is divided into three groups, the lower Wolkberg Group (2.7-2.6Ga), the middle Chuniespoort Group (2.6-2.4Ga) and the upper Pretoria Group (2.4-2.1Ga) (Jahn et al., 1990; Barton et al., 1994; Walraven and Martini, 1995). The Chuniespoort Group is not examined in this study. The Wolkberg Group is composed of fluvial to shallow marine feldspathic to subgraywacke, arkose, siltstone, pelite, conglomerate and some basalt flows, and Pretoria Group is composed of marine tidal quartzite, pelite and lesser carbonate and volcanic rocks; these sedimentary rocks have experienced sub-greenschist to a maximum of greenschist-facies metamorphism (Wronkiewicz and Condie, 1987).The deposition of the Transvaal Supergroup was terminated by the massive infusion of mafic-ultramafic and silicic magamas at 2.06 Ga to produce the Bushveld Complex (Walraven, 1997).

3. Sample Selection and Analytical Methods

All of the samples analyzed here are shales from drill hole cuttings, and the major and trace element compositions of the shales were previously reported in Wronkiewicz and Condie (1987; 1989; 1990). Because the samples are cuttings from recent drill holes, the influence of modern weathering is minimal.

Lithium concentrations and isotopic compositions of the shales were determined in the Geochemistry Laboratory at the University of Maryland, College Park. Sample dissolution procedures, column chemistry, instrumental analysis, and external precision are reported in Rudnick et al. (2004) and Teng et al. (2006a). Briefly, samples were dissolved in a combination of HF–HNO_3–HCl. However, for the samples that contained organic carbon (labeled “o” in Tables 6-1 and 6-2), perchloric was used with HF and

Age (Ga)	Formation (n.)	Group	Supergroup
2.2-2.4	Silverton (2) Strubenkop(3) Timballhill(1)	Pretoria	Transvaal
A/P Boundary			
2.5-2.6	Black Reef(2) Selati(2)	Wolkberge	
2.7	Bothavill(2)	Pniel	Ventersdorp
2.8-3.0	K8(5) Booysens(2)	Central Rand	Witwatersrand
	Roodepoort(4) Parktown(1) Orange Grove(1)	West Rand	

Figure 6-1. The sequence of stratigraphic units in the Witwatersrand basin of the Kaapvaal Craton, South Africa (after Condie and Wronkiewicz, 1990). A/P boundary indicates the transition from Archean to Proterozoic.

HNO_3 for the first step of sample dissolution. The presence of organic carbon in the samples does not correlate with lithium concentration or isotopic composition, indicating the negligible influence of organic matter on lithium behavior. Lithium was purified on a cation exchange resin (Bio-Rad AG50w-X12, 200–400mesh) first in a HCl medium, followed by a HCl-ethanol medium. Lithium concentrations and isotopic compositions were analyzed using the standard- bracketing method on a Nu Plasma MC-ICPMS. The long-term external precision of the Li isotopic composition and concentration analyses are ≤ 1.0‰ (2σ) and ±10% (2σ), respectively, based on repeat analyses of pure Li standards and standard reference materials, respectively, over the past nine years (Rudnick et al., 2004; Teng et al., 2006b; Qiu et al., 2011a). Qiu et al. (2009; 2011a) reported results for three measurements of BCR-1 [δ^7Li = 2.1 ± 0.3 and [Li] = 12.7 ± 0.7 μg/g]; in comparison, Magna et al. (2004), Rudnick et al. (2004) and Teng et al. (2006b), reported the δ^7Li of BCR-1 to be 2.0 ± 0.7 (10 runs), δ^7Li = 2.7 ± 1 (3 runs) and δ^7Li = 2.4 ± 0.5 (4 runs), respectively, and the GEOREM (Jochum and Nohl, 2008) preferred BCR-1 [Li] =13 ± 1 μg/g.

4. Results

Lithium concentrations and isotopic compositions are reported in Table 6-1, along with the major and trace elements from Wronkiewicz and Condie (1987; 1989; 1990).

Generally, the shales within a given formation have relatively similar [Li] and δ^7Li, but Li signatures vary significantly from one formation to another (Fig. 6-2 and 6-3); the [Li] in all shales span a range from 7 to 177 μg/g and δ^7Li from -1.7 to +12.3. The [Li] and δ^7Li of the shales do not show a simple correlation with their depositional ages. The most Li-poor formations are Orange Grove and K8 from the Witwatersrand Supergroup,

Table 6-1. Li concentration (μg/g) and isotopic composition, major (wt.%) and trace elements (μg/g) for the shales from Kaapvaal Craton. *Continued on next pages*

Supergroup	Transvaal										Ventersdop	
Group	Pretoria						Wolkberg				Pniel	
Formation	Silverton		Strubenkop			Timeball Hill	Black Reef		Selati		Bothavill	
Sample	D-79	D-84	CDV-1-	CDV-1-4	CDV-1-5	D-31	CDV-1-28	MEE-20	D56	D111	JWS-8-	JWS-8-12
Age (Ga)	2.20	2.20	2.30	2.30	2.30	2.40	2.55	2.55	2.60	2.60	2.70	2.70
Li	39	83	40	40	52	99	36	67	112	177	16	9
δ^7Li	-0.6	-2.2	2.3	1.8	1.2	-1.7	5.8	1.3	8.6	12.3	-0.1	2.0
SiO_2	69.4	57.8	56.8	66.7	54.5	71.8	61.8	48.5	50.4	42.4	63.4	75.6
TiO_2	0.62	0.77	0.51	0.80	1.00	0.53	0.82	0.87	2.42	0.66	0.45	0.19
Al_2O_3	13.45	21.5	24.04	19.81	24.33	10.56	16.99	17.96	16.54	14.91	16.63	8.32
Fe_2O_3T	5.48	7.55	8.97	7.63	10.36	11.32	4.51	5.5	10.74	30.35	5.72	3.14
MgO	2.92	1.75	1.14	1.12	1.67	1.57	3.86	5.26	7.14	2.96	5.94	3.23
CaO	0.60	0.25	0.24	0.09	0.25	0.23	0.49	5.78	2.90	0.13	0.21	3.52
Na_2O	2.10	0.72	0.83	0.31	0.69	0.34	0.21	0.03	0.49	0.20	0.23	0.22
K_2O	2.53	3.26	2.09	0.66	1.82	0.89	6.32	4.88	6.83	0.02	3.48	1.60
MnO	0.07	0.05	0.05	0.05	0.08	0.06	0.01	0.40	0.04	0.05	0.00	0.01
P_2O_5	0.15	0.05	0.14	0.08	0.18	0.14	0.27	0.13	0.55	0.13	0.13	0.07
Total	97.36	93.7	95.32	97.27	94.84	97.42	95.30	89.27	98.09	91.76	96.20	95.89
CIA	66	80	88	94	89	79	70	76	67	98	62	50
Rb	151	193	94	32	97	48	198	145	107	5.5	136	59
Sr	104	63	100	62	95	29	18	53	31	9	24	166
Ba	482	416	525	197	395	160	209	292	607	54	548	272
Th	12	17	21	15	24	23	5.4	6.1	5.7	6.4	5.9	2.2
U	3.3	4.2	5.3	4.8	8.1	3.5	1.9	1.8	1.7	1.7	1.7	0.66
Pb	25	30	23	16	21	11	9.8	26	10	9.8	25	11
Zr	200	113	280	322	197	449	151	151	377	88	131	44
Hf	6.3	3	8.3	10	6.2	14	4.7	5	9.3	2.4	3.3	1.3
Ta	0.5	1.4	1.7	1.3	1.5	1.3	0.7	0.7	1.5	0.8	0.6	0.2
Nb	10	13	20	18	19	11	5.7	7.9	23	10	6	0.5

La	26	48	58	39	54	14	22	35	28	29	68	5.6
Ce	119	32	122	84	120	31	46	68	65	50	131	11
Sm	4.5	7.3	8.5	5.9	8.9	2.8	4.4	6.2	7.1	4.9	6.1	0.91
Eu	1.0	1.3	1.7	1.3	1.8	1.0	0.9	1.4	1.6	1.8	0.9	0.2
Gd	4.0	6.0	6.9	5.5	8.3	3.4	3.6	5.4	8.5	3.1	3.8	0.8
Tb	0.61	0.87	1.00	0.85	1.30	0.61	0.53	0.81	1.50	0.39	0.49	0.13
Yb	1.9	2.7	3.3	3.4	3.9	2.7	2	3.4	4.9	2.3	1.5	0.72
Lu	0.3	0.4	0.6	0.5	0.6	0.5	0.3	0.5	0.8	0.4	0.2	0.1
Y	23	32	33	36	45	25	36	32	47	21	24	10
V	87	170	154	140	249	139	149	203	391	246	123	64
Sc	13	27	23	19	34	8.6	20	31	35	23	18	9.3
Cr	119	156	177	132	234	85	402	464	82	1723	659	337
Co	6.3	8.2	28	27	36	8.2	13	40	43	19	43	17
Ni	27	61	71	114	120	30	99	362	65	502	330	130

continued

Supergroup	Witwatersrand												
Group	Central Rand							West Rand					
Formation	K8					Booysens		Roodepoort				Parktown	Orange Grove
Sample	MED-8	MEE-21	MEE-39	MEE-34	MED9	730-5	SJ-3-5	AA0099	AA0096	AA0097	C-75	C-72	D14
Age (Ga)	2.80	2.80	2.80	2.80	2.80	2.80	2.80	2.90	2.90	2.90	2.90	2.95	3.00
Li	16	8	7	12	9	78	58	51	53	45	41	40	14
δ^7Li	4.4	9.3	5.4	2.6	12.3	3.7	-1.0	-0.9	0.1	-1.1	-1.6	-0.4	7.8
SiO_2	64.85	58.5	62.41	59.36	63	51.09	53.65	58.88	56.83	64.65	59.33	54.62	53.52
TiO_2	0.90	0.92	0.99	0.97	0.93	0.75	0.64	0.94	1.01	0.78	0.78	0.49	1.19
Al_2O_3	24.89	24.48	29.44	26.1	24.01	18.94	19.38	20.51	21.75	16.84	17.51	12.04	27.68
Fe_2O_3T	2.46	6.54	1.02	6.58	4.21	10.87	7.63	6.68	7.03	6.14	11.04	23.96	4.84
MgO	0.44	1.02	0.34	1.55	0.95	7.75	8.41	4.69	4.80	4.44	3.99	2.33	0.20
CaO	0.70	0.05	0.07	0.03	0.10	0.12	1.02	0.24	0.19	0.23	0.14	0.02	0.01
Na_2O	0.71	0.50	0.39	0.18	1.84	0.14	1.41	1.29	1.47	1.18	0.22	0.19	0.55
K_2O	1.34	4.32	0.90	0.94	1.96	1.70	2.73	2.35	2.48	1.76	3.09	0.42	5.07
MnO	0.00	0.30	0.00	0.03	0.04	0.08	0.04	0.06	0.07	0.06	0.05	0.11	N/A
P_2O_5	0.05	0.06	0.07	0.6	0.05	0.08	0.11	0.08	0.06	0.04	0.12	0.043	0.14
Total	96.34	96.69	95.63	96.34	97.09	91.52	95.02	95.72	95.69	96.12	96.27	94.22	99.21
CIA	91	82	95	95	82	90	78	81	80	80	82	95	81
Rb	55	141	35	36	74	64	121	98	102	74	121	29	240
Sr	82	105	80	51	220	26	105	117	110	87	15	8.2	92
Ba	237	261	245	156	405	286	643	443	422	327	349	172	313
Th	17	10	10	11	8.5	5.1	4.9	6	6	5.3	4.3	3.5	14
U	7.6	3.9	2.6	3.8	4.2	1.6	1.7	2.1	2.2	2.2	1.2	1.1	3.7
Pb	21	20	27	17	34	N/A	9.8	16	15	15	9.8	9.8	12
Zr	334	193	173	181	188	121	125	171	168	144	141	114	239
Hf	13	6.3	4.2	5.6	4.5	3.6	3.8	4.9	5.1	3.9	4.2	3.1	8.8
Ta	1.8	1.2	1.1	1.1	1.0	0.7	0.6	0.8	0.9	0.7	0.7	0.6	1.5
Nb	18	16	12	12	11	9.2	8	12	12	11	9.2	7.2	13
La	68	56	47	53	40	16	25	30	31	31	27	19	84
Ce	141	111	86	110	75	34	56	65	66	66	57	30	159

Sm	8.1	9.7	8	9.2	8.1	3.6	5.4	5.7	5.4	5.6	5.3	2.8	13
Eu	1.5	2.0	1.5	2.0	1.3	0.9	1.4	1.3	1.2	1.4	1.2	0.7	3.1
Gd	6.5	9.4	6.0	9.2	8.5	4.3	5.0	4.9	5.2	7.8	5.5	1.9	N/A
Tb	0.94	1.50	0.83	1.50	1.40	0.76	0.77	0.73	0.83	1.50	0.90	0.26	1.70
Yb	3.2	6.5	2.8	4.8	4.9	2.7	2.5	2.3	2.4	4.5	3	1.4	5.2
Lu	0.6	1.1	0.5	0.7	0.7	0.4	0.4	0.4	0.4	0.5	0.4	0.2	0.8
Y	28	63	31	52	55	23	34	23	24	66	42	17	61
V	181	222	252	235	229	193	190	199	230	164	210	115	278
Sc	29	31	25	27	23	30	26	25	27	19	28	14	N/A
Cr	884	816	581	765	543	1202	1017	776	867	6.44	1112	538	572
Co	60	46	36	52	61	43	51	30	46	38	48	26	7.6
Ni	277	347	99	419	384	563	370	281	319	286	365	252	77

Major (%) and trace elements (μg/g) data are from Wronkiewicz and Condie (1987; 1989; 1990).
The Li data reported in this study represent the averages of $\geqslant$2 measurements of each sample.
The uncertainties for [Li] (μg/g) and δ^7Li are ±10% (2σ) and ±1 (2σ), respectively.

which have [Li] from 7 to 16 μg/g; the δ^7Li of these formations spread over a large range, from ~+3 to +12.3. The two shales from the Selati Formation from Transvaal Supergroup have a strikingly different Li signature than that of all the other shales, with significantly higher [Li] (112 and 177 μg/g) and δ^7Li (+8.6 and +12.3). In terms of Supergroups, both the Witwatersrand and Transvaal Supergroups show a large variation in [Li], with an average [Li] of 33± 47 μg/g (2σ) and 75 ± 90 μg/g (2σ), respectively; the δ^7Li of these two Supergroups both have average δ^7Li of +3 ± 9(2σ).

The Chemical Index of Alteration (CIA) is a useful way of quantifying the intensity of weathering experienced by the source regions of sedimentary rocks (Nesbitt and Young, 1982). The index is calculated using molar proportions of major oxides: CIA = $Al_2O_3/(Al_2O_3 + CaO^* + Na_2O+K_2O)$, where CaO* is the amount of Ca incorporated in the silicate fraction of the rock (Bock et al., 1998). Except for the two shales from the Bothavill Formation, which have CIA = 50 and 62 (Fig. 6-4), all other shales in this study have intermediate to high weathering intensity with CIA of 66 – 94 and most (about 80%), plot in the range of heavy weathering intensity (CIA: 80 – 100, Nesbitt and Young, 1982).

5. Discussion

The [Li] and δ^7Li of the Archean shales (2.55 to 3.0 Ga) and Early Proterozoic shales (2.2 to 2.4 Ga) in this study (Fig. 6-2) do not show a clear difference, suggesting Li signatures are not directly correlated with the Archean/Proterozoic (A/P) transition. The correlation between [Li] and δ^7Li shown by most of the Kaapvaal shales are comparable to those of world-wide Post Archean shales (Fig. 6-3), and [Li] generally increases with decreasing δ^7Li (data for post Archean shales are from Teng et al., 2004; Qiu et al., 2009;

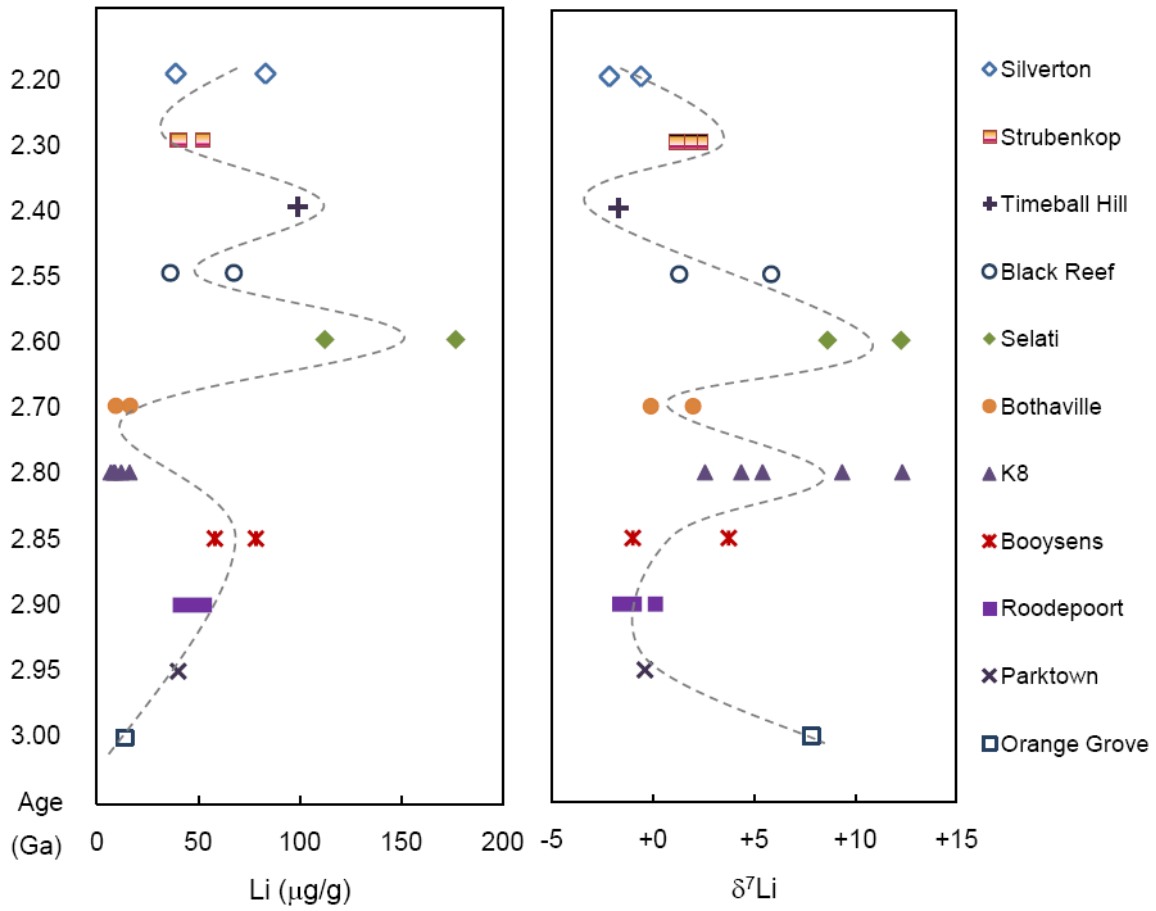

Figure 6-2. Plot of Li concentration (μg/g) and isotopic compositions (δ^7Li) versus the stratigraphic formations and the depositional ages (in Ga) of the shales from Kaapvaal Craton. The name of the formations on the right column and the depositional ages on the left column are sorted according to the stratigraphic sequence which is inferred from Jahn and Condie (1995). The gray dashed line roughly indicates the trend of the change of Li concentration and isotopic compositions.

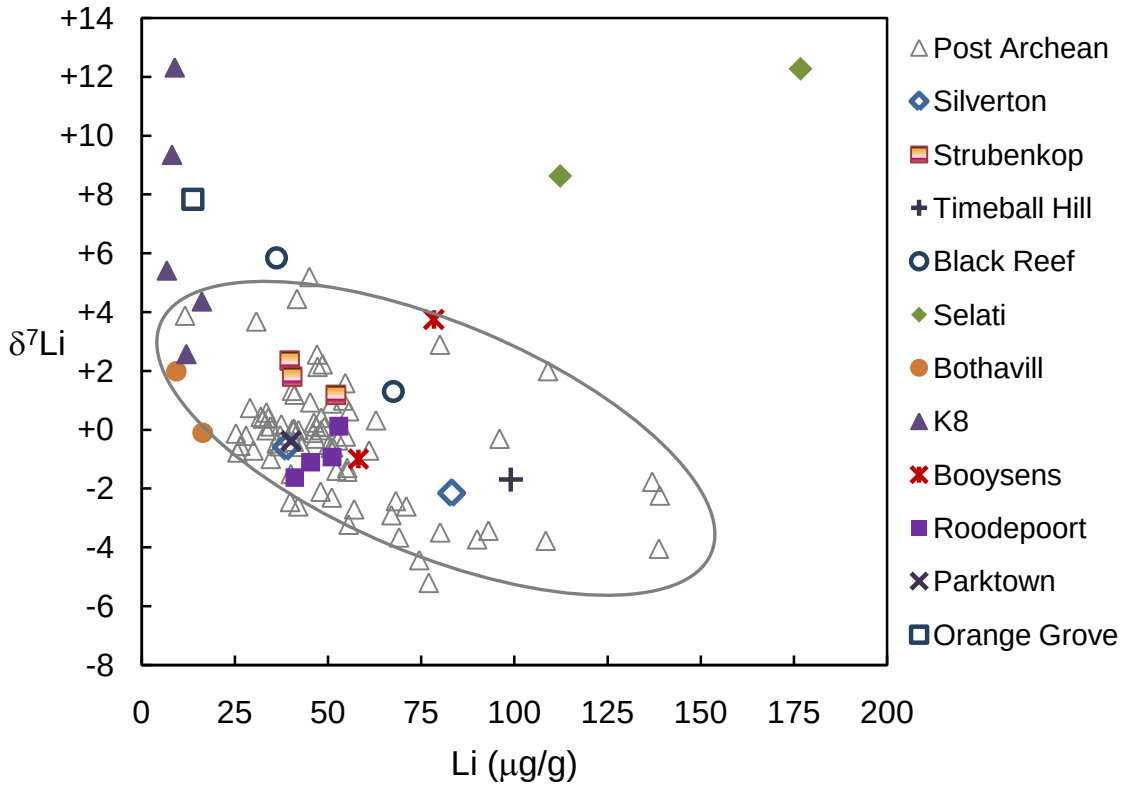

Figure 6-3. Plot of Li concentration versus δ^7Li for the shales from Kaapvaal. The data for Post-Archean shales are from the literatures (Teng et al., 2004; Qiu et al., 2009; 2010).Gray line encompasses post Archean shales.

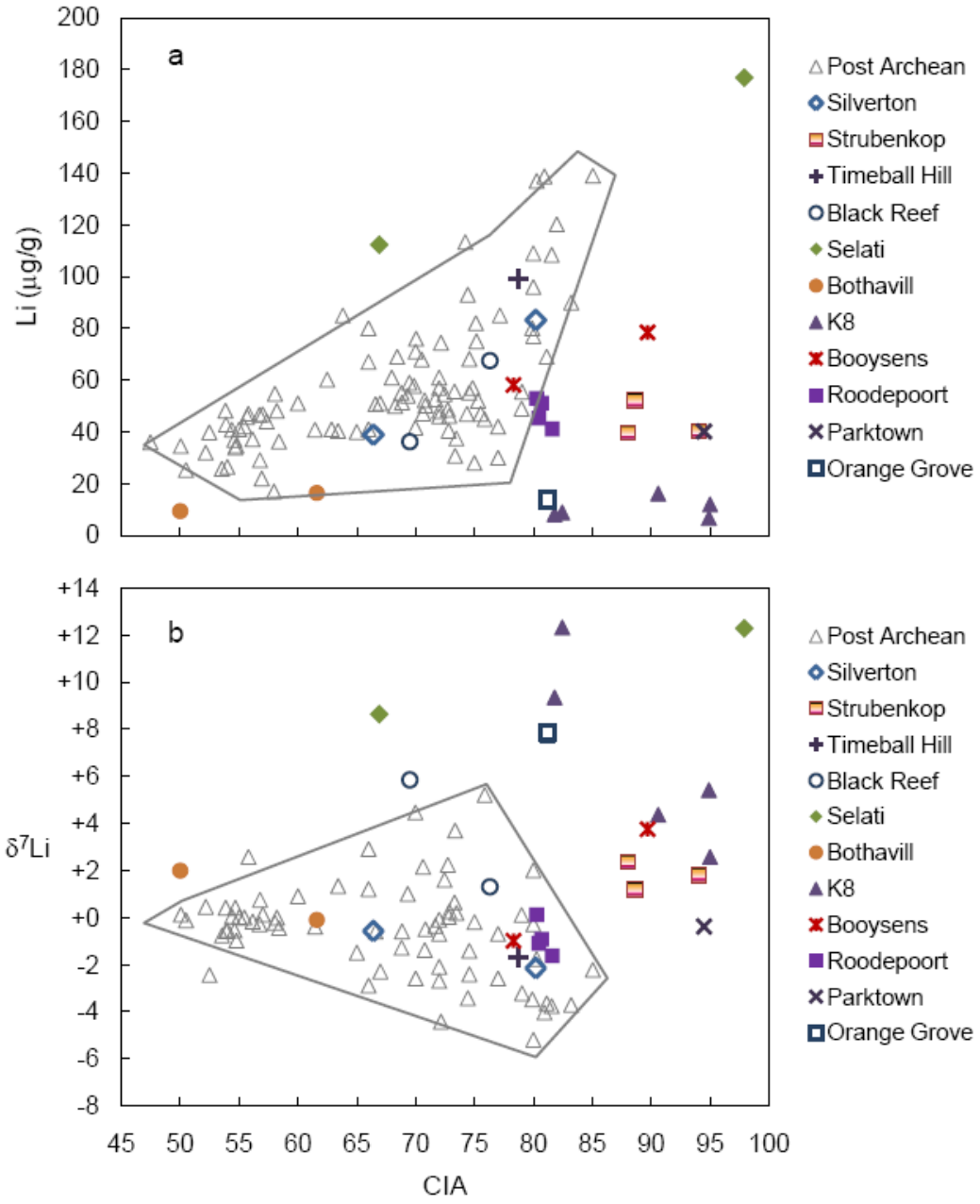

Figure 6-4. Plot of Li concentrations (a) and isotopic compositions (b) versus CIA (Chemical Index of alteration) for the shales from Kaapvaal Craton. The data for Post-Archean shales are from the literature (Teng et al., 2004; Manikyamba and Kerrich, 2006; Qiu et al., 2009; 2010; Cameron and Garrels, 1980). Gray lines indicate the general range of post Archean shales on the plot.

2011a). This global correlation has been interpreted to reflect mixing in the provenance between a juvenile, less-weathered component having low [Li] and mantle-like δ^7Li and a more highly weathered continental crustal component having higher [Li] (due to sorption of Li onto clays) and lower δ^7Li (due to stripping of ^{7}Li during weathering) (Qiu et al., 2009). Nevertheless, some Kaapvaal shales from the Selati, K8 and Orange Grove Formations, have significantly different Li signatures relative to the Post Archean shales and either fall off of (Selati) or extend (K8, Orange Grove) the global correlation (Fig. 6-3).

5.1. The provenance of shales from Selati, K8 and Orange Grove Formations

The two samples from the Selati Formation analyzed here have similar Li signatures, which are strikingly different from those of any other shales, as they have both high δ^7Li (>+12) and [Li] (> 112 μg/g) (Figs. 6-3 and 6-4). Given the similarity in their Li characteristics, it is surprising that these two samples have widely varying compositions. For example, Ni and Cr concentration and CIA values spread over nearly the entire range observed for the Kaapvaal shales (Figs. 6-4 and 6-5). Wronkiewwicz and Condie (1990) suggested that the variable compositions of the Selati shales may reflect variable climatic conditions, sediment heterogeneity and element mobility during diagenesis or secondary processes. The two samples analyzed here represent the two end members of the whole spectrum of Ni and Cr and CIA values within the formation (Wronkiewwicz and Condie, 1990). One sample (D111) is enriched in Ni and Cr and has the highest CIA value, suggesting its provenance is largely derived from highly weathered mafic-komatiitic sources. The other sample (D56), is suggested to derive from a source that experienced moderate weathering intensity and its source is mainly composed of tonalite (~65%) and

basalt (~25%) with small amounts of granite (~5%) and komatiite (~5%) (Wronkiewicz and Condie, 1990). However, the significantly different provenances of these two shales and the different weathering intensities that their provenance experienced did not result in distinct Li concentration and isotopic compositions, suggesting that the Li signature of these two shales may have been overprinted by a secondary process. While the nature of this secondary process is not obvious, given their highly unusual compositions, they will not be considered further in the following discussions.

The K8 and Orange Grove shales also have high δ^7Li (>+8), but very low [Li] (< 14 μg/g) (Fig. 6-3). Such heavy Li isotopic compositions have not been observed in younger shales, to date, and the low [Li] is also quite distinct for shales. Wronkiewicz and Condie (1987) suggested that the K8 and Orange Grove shales, constituting the stratigraphically highest and lowest shales of the Witwatersrand Supergroup, are different relative to the other shales in the following two aspects: 1) the K8 and Orange Grove are significantly enriched in Al_2O_3 relative to the intervening shales within the Supergroup, indicating high contents of clay minerals; this is reflected in their high CIA values, and 2) unlike other shales within the Witwatersrand Supergroup, the REE and HFSE (Zr, Ti, Nb, Hf, Ta) patterns and concentrations of K8 and Orange Grove shales are similar to those of Post-Archean shales, reflecting the recycling of older continental crust component in their source regions (Wronkiewicz and Condie, 1987). Based on a mixing model of six immobile elements (Th, Hf, Yb, La, Sc, Co), Wronkiewicz and Condie (1987) suggested that the provenance of K8 and Orange Grove shales require greater amounts of granite component (40%) than all the other shales , and the remainder of the source region is composed of basalt (30%), komatiite (20%), and tonalite (10%). As granites generally

have elevated [Li] relative to mafic igneous rocks, with [Li] in granites up to hundreds of μg/g and the [Li] in fresh basalts around 4 μg/g (e.g., Teng et al., 2008), the depletion of

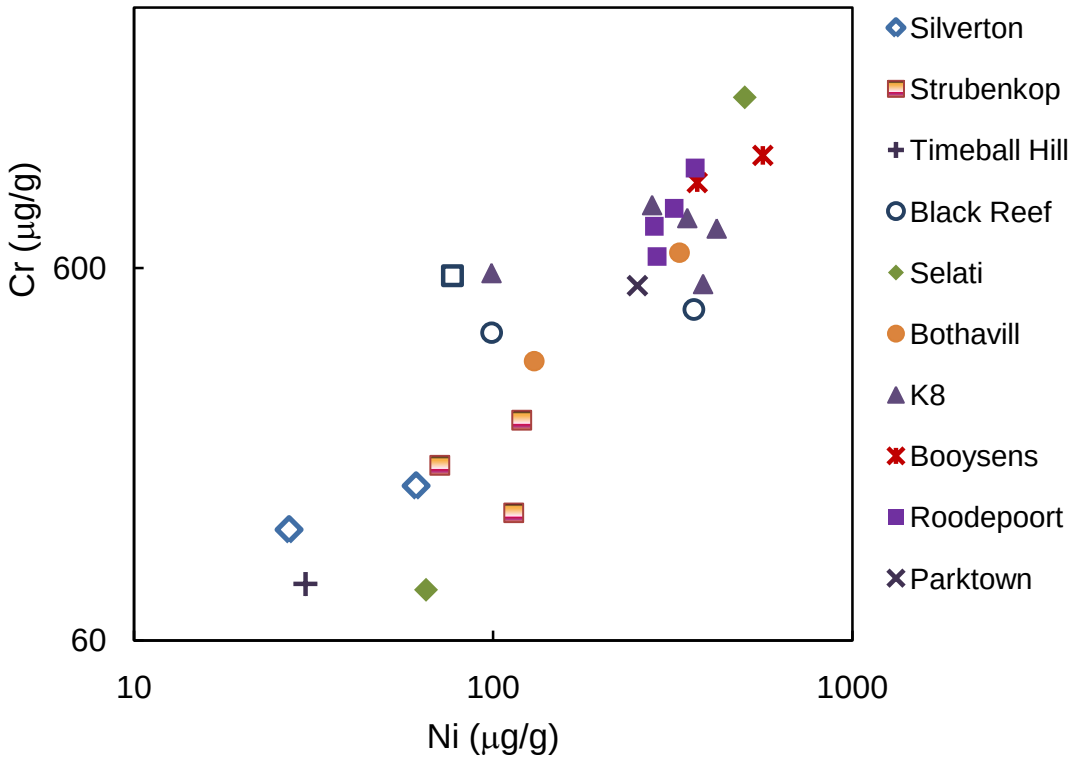

Figure 6-5. Plot of Ni versus Cr concentration of the shales from Kaapvaal Craton (log scale). Ni and Cr value are from Wronkiewicz and Condie (1987; 1989; 1990).

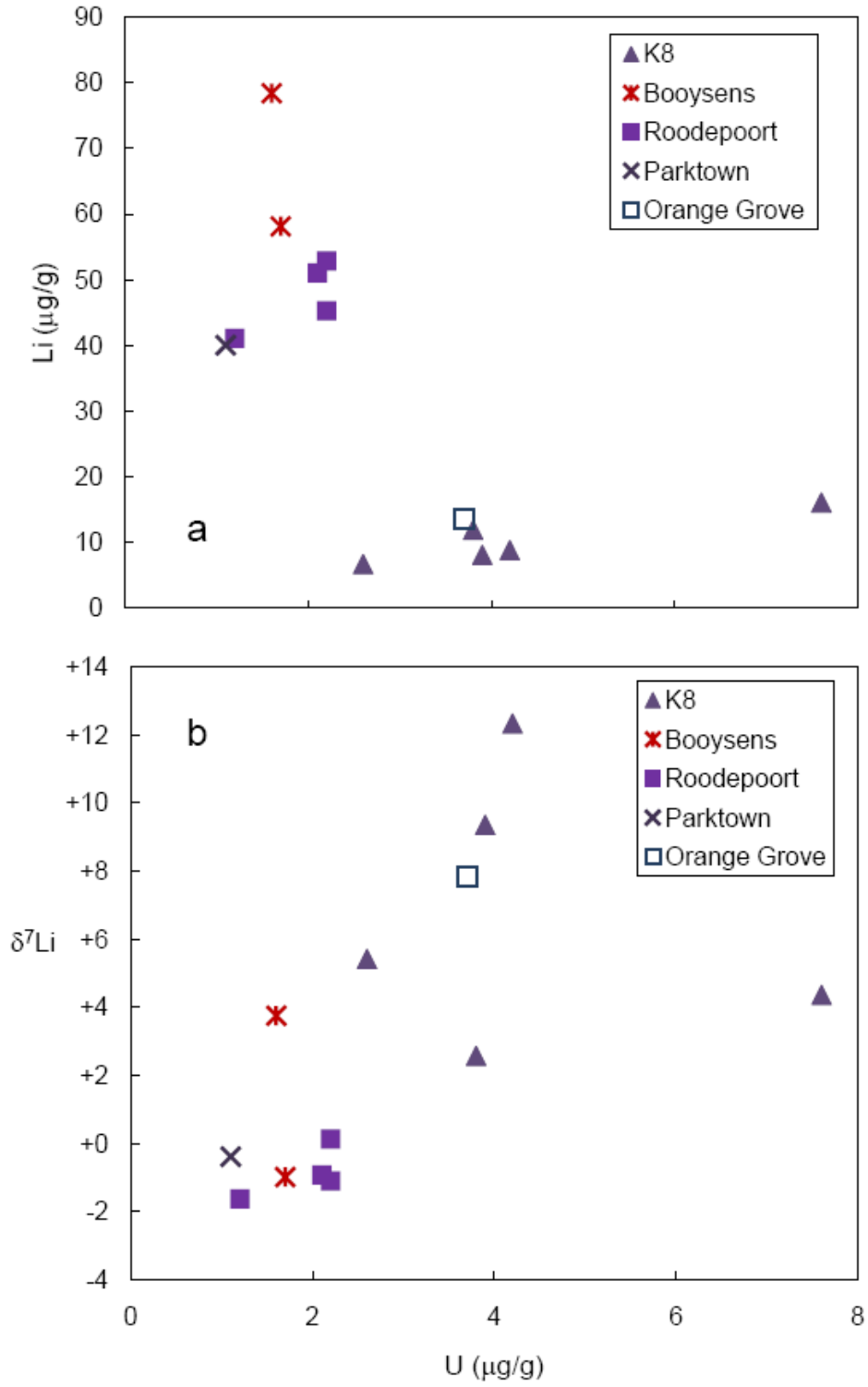

Figure 6-6. Plot of Li concentrations (a) and isotopic compositions (b) versus U contents for the shales from different formations in Witwatersrand Supergroup. U contents are from Wronkiewicz and Condie (1987; 1989; 1990).

Li in K8 and Orange Grove shales suggests typical granite is not a major component in their provenances. Furthermore, several studies have suggested that the granites that contribute to the K8 shales are hydrothermally altered, causing elevation of their U concentrations, which correlate positively with the intensity of alteration (e.g., Robb and Meyer, 1990; Kamo et al., 1995; Klemd, 1999). Fig. 6-6 shows that the U contents of K8 and OG shales are distinctly higher than those of other shales in the Witwatersrand Supergroup; however, there is no clear correlation between [Li] and δ^7Li with U concentration within the K8 and OG shales (Fig. 6-6). Therefore, it is unlikely that hydrothermal alteration of the granites in the provenance of the shales gave rise to the low [Li] and high δ^7Li signature in these shales, and their Li signature might be controlled by another process, such as weathering in their source region.

5.2. Influence of severe weathering on the Li signature

Weathering conditions on the early Earth are not well constrained by direct geologic evidence beyond modeling and speculations. Some models have suggested intense weathering conditions prevailed on the early Earth, with Pco_2 being 100-1000 times higher than modern levels and the corresponding surface temperature as high as ~ 85°C (Walker, 1986; Kasting and Ackerman, 1986; Kasting, 1987; 1993; Knauth and Lowe, 2003; Hessler and Lowe, 2006). Such conditions might have a significant influence on [Li] and δ^7Li in sediments and detrital minerals derived from such crust (e.g., Ushikubo et al., 2009). A compilation of all published [Li] and CIA values in shales (Fig. 6-4, data from this study and Cameron and Garrels, 1980; Teng et al., 2004; Manikyamba and Kerrich, 2006; Qiu et al., 2009; 2011a;) shows: 1) [Li] of Post-Archean shales correlates positively with CIA in the range of ~ 50< CIA < ~85, 2) a few of the Archean shales plot

on the trend defined by the Post Archean shales, and 3) most of the Archean shales have higher CIA (85-100) and much lower [Li] than post-Archean shales. As suggested by previous studies, the concentration of Li in shales is linked to the abundance of Mg-bearing clay minerals, such as smectites and illites, which play an important role in the Li geochemical cycle (e.g., Williams and Hervig, 2005; Stoffynegli and Mackenzie, 1984; Vigier et al., 2008; Qiu et al., 2011b). Figure 6-7 shows that most of the Li-enriched shales (average [Li] >60 μg/g, Teng et al., 2004) plot in the area that is close to the CIA of smectites, illite or muscovite; by contrast, [Li] depleted shales ([Li] < 20 μg/g), either plot in the high CIA region (> 80), including K8 and Orange Grove shales, towards the kaolinite and gibbsite apex, or plot below the general trend, with CIA values below 70. In general, the clay mineral assemblage of Archean shales lacks smectite (Weaver, 1989), presumably because the intense leaching and weathering that occurred in their source region produced kaolinite as the dominant clay mineral, as well as gibbsite (Tosca et al., 2010). Therefore, the relationship between [Li] and CIA suggests that Li is incooporated into Mg-bearing clays during the early stages of weathering, but, with greater weathering intensity it is lost during the breakdown of Mg-bearing clays.

Like [Li], the δ^7Li of Archean shales do not correlate with their CIA value (Fig. 6-4b). Nevertheless, most Kaapvaal shales have relatively heavy Li isotopic compositions compared to their younger counterparts (Fig. 6-4b); this signature could also be the result of Archean weathering conditions. An experimental study of seawater/basalt interactions showed that the leaching of Li from basalts into seawater correlates positively with temperature, with about twice the amount of Li removed at 75°C than removed at 25°C (Millot et al., 2010). Furthermore, δ^7Li in the altered basalts at 75°C is higher than that at

25°C, due to the temperature influence on the isotopic fractionation factor (less fractionation at higher temperatures) (Millot et al., 2010). These experimental results indicate that it becomes more difficult for ^{6}Li to partition into the secondary minerals at higher temperatures, leaving the secondary minerals with lower [Li] and higher $\delta^{7}Li$ relative to the ones formed at lower temperatures. Furthermore, in addition to surface temperature, intense rainfall could also lead to less ^{6}Li to being incorporated into secondary minerals. Becuase labile minerals are more easily dissolved during heavy rainfall, the CIA values will increase in the resulting sediments (Basu, 1981; James et al., 1981; Dutta and Suttner, 1986; White and Blum, 1995). If heavy rainfall continuously leaches sediments with under saturated fluids, ion exchange between the fluids and rocks is less dramatic (Hessler and Lowe, 2006), and, as a result, ^{6}Li has less opportunity to partition into the structure of clay minerals. Collectively, high surface temperature and heavy rainfall, both of which have been postulated to occur in the Archean, are two factors that could produce Archean shales with lower [Li] and heavier $\delta^{7}Li$ relative to Post Archean shales. If so, [Li] and $\delta^{7}Li$ in shales may reflect paleo-climate conditions, in addition to CIA.

5.3. Li concentration and isotopic composition of Archean upper continental crust

The [Li] in the upper continental crust can be established using a weighted averages of [Li] in the rocks exposed at the surface or by using correlation between insoluble elements and [Li] in shales and loess to infer the [Li] of upper continental crust (Teng et al., 2004). Currently, there is not enough Li data for exposed Archean rocks to allow an estimate of the Li characteristics of the Archean upper continental crust, and the insoluble

elements (e.g., Al_2O_3, TiO_2, Th and Nb, Fig 6-8) of Kaapvaal shales in this study do not correlate with [Li], perhaps because of the more intense weathering conditions in the

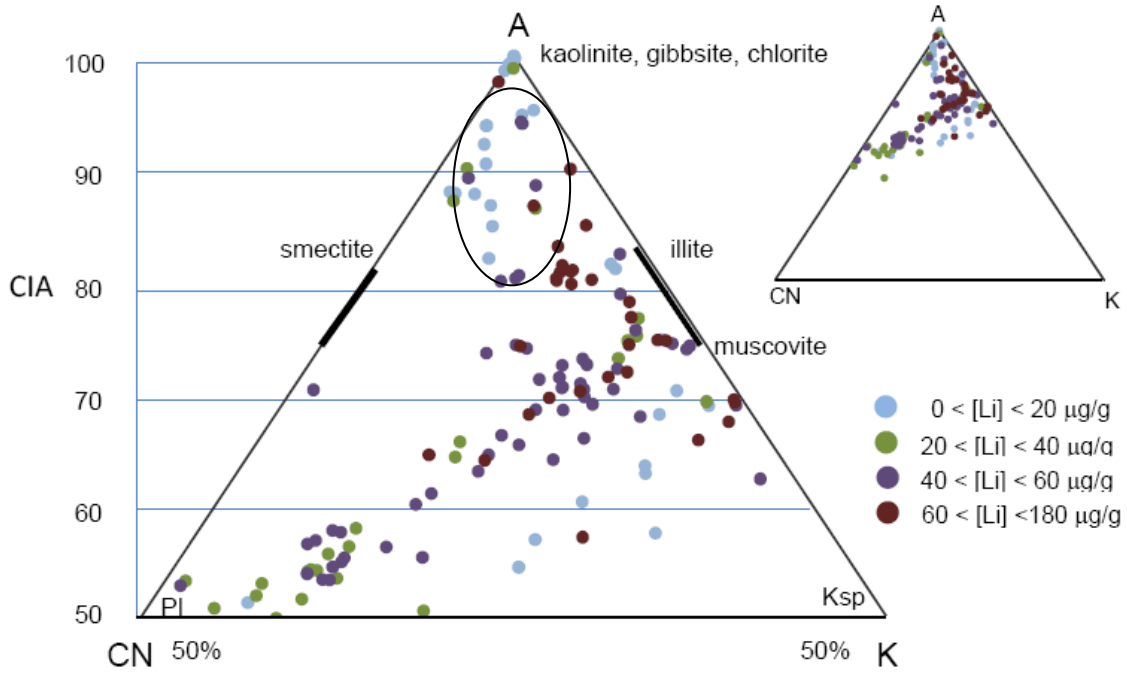

Figure 6-7. The Al_2O_3–(CaO*+Na_2O)–K_2O (A–CN–K) ternary diagram for shales from this study and the literatures used in Fig.6-4. The light blue dots in the black circle indicate the low-[Li] and high-CIA Archean shales from this study. See text for details. Abbreviations mark the position on plot is for the following minerals: Pl – plagioclase feldspar; Ks – potassium feldspar.

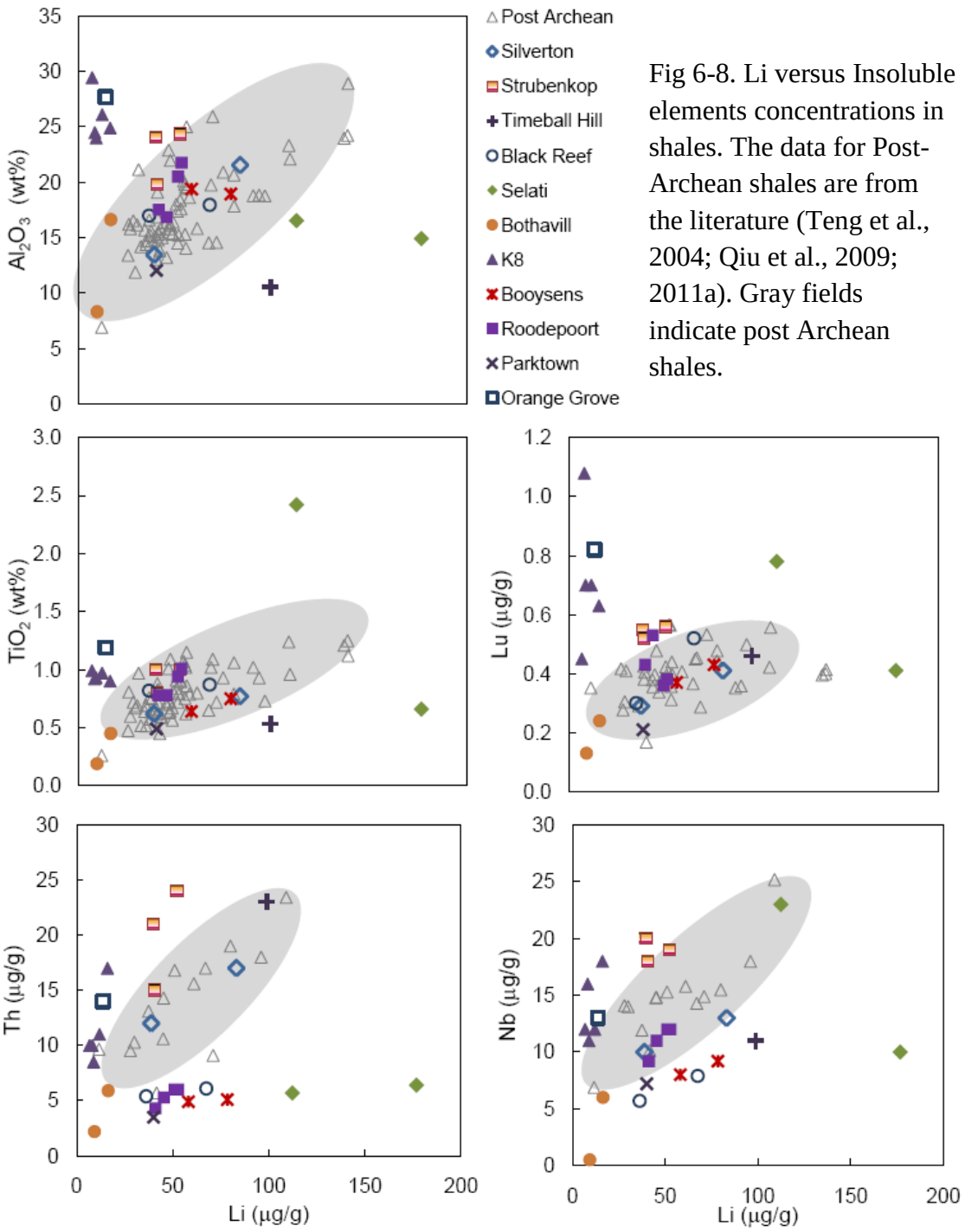

Fig 6-8. Li versus Insoluble elements concentrations in shales. The data for Post-Archean shales are from the literature (Teng et al., 2004; Qiu et al., 2009; 2011a). Gray fields indicate post Archean shales.

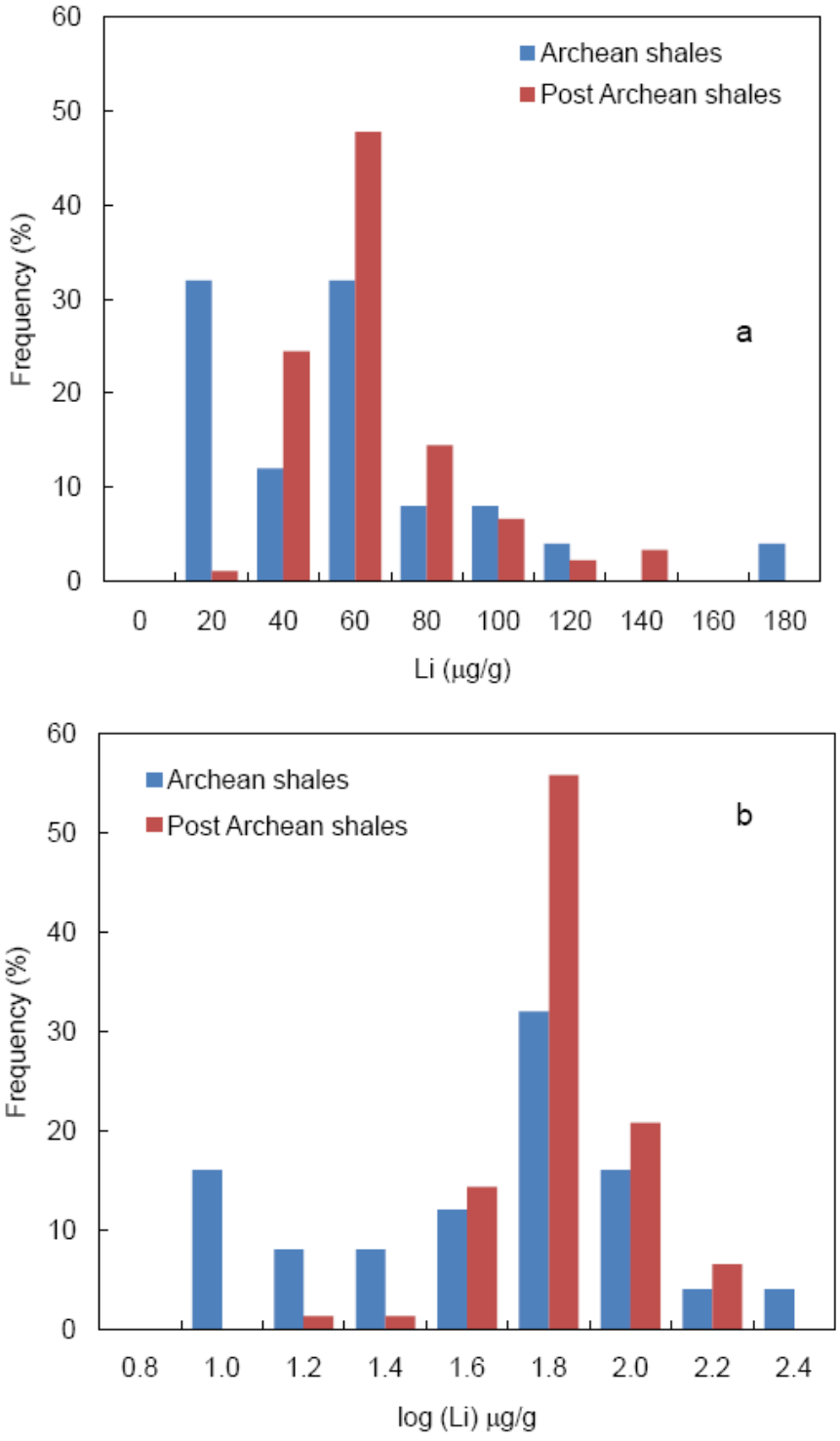

Figure 6-9. Histogram of Li concentrations (a) and log(Li) concentrations in Archean shales and post Archean shales. The [Li] in post Archean shales are from Teng et al. (2004), Manikyamba and Kerrich (2006); Qiu et al. (2009; 2011) and Cameron and Garrels (1980).

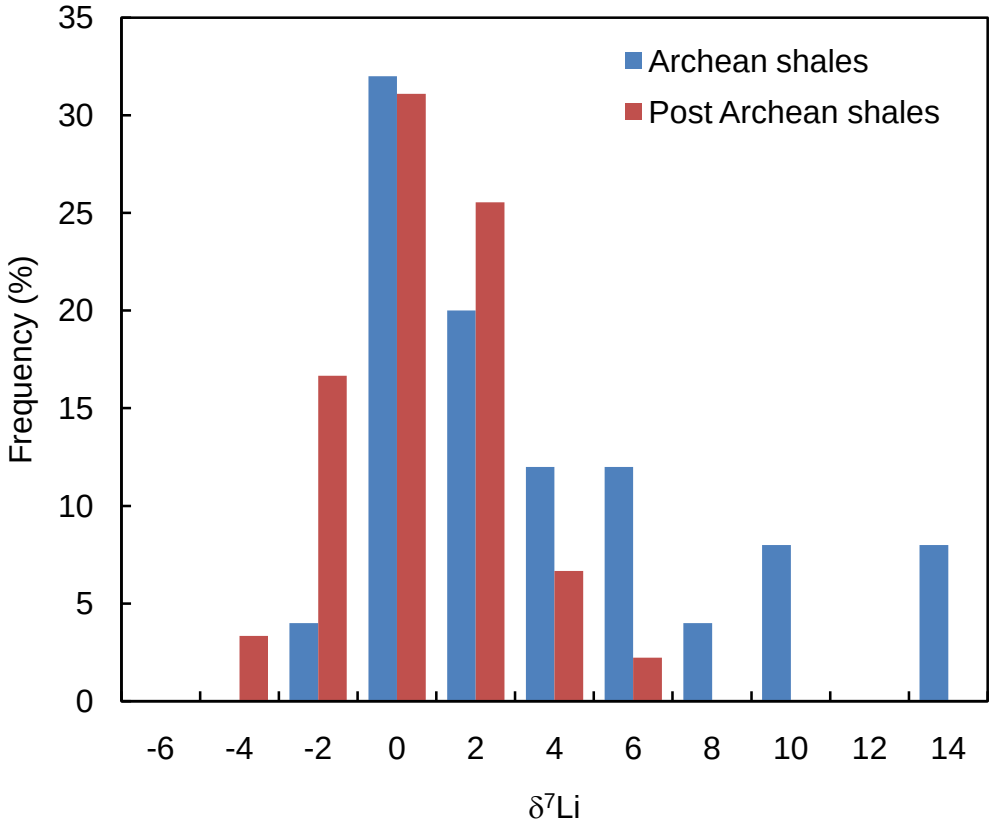

Figure 6-10 Histogram of Li isotopic compositions in Archean shales and post Archean shales. The Li isotopic compositions in post Archean shales are from Teng et al. (2004) and Qiu et al. (2009; 2011a).

Archean. Accordingly, we offer some observations on the general relationship between Li concentration and isotopic compositions in the Archean and post Archean upper continental crust.

The distribution of [Li] in Archean shales from this study is neither normal nor log-normal (Figs 6-9a and 6-9b), but rather bimodal, with one mode at higher [Li] comparable to that of post Archean shales (average [Li] ≈ 60 μg/g) and the other mode at lower [Li] (< 20μg/g) much lower than that of post Archean shales. Nevertheless, the mean of [Li] in Kaapvaal shales (~33μg/g, excluding the two unusual samples from Selati Formation) is lower than the average [Li] in post Archean shales (54 μg/g), indicating that the Archean upper continental crust may have, on average, lower [Li] relative to the post Archean upper continental crust. This may be because of the severe weathering conditions, or may reflect a less differentiated upper crust during the Archean. In contrast to the distribution of [Li], the distribution of δ^7Li in Archean shales is significantly skewed to higher values compared to the post Archean shales (Fig.6-10), with a concentration weighted average δ^7Li of +3.2, whereas post Archean shales have concentration weighted average δ^7Li of -0.8. The difference in δ^7Li may indicate that the Archean upper continental crust had heavier Li isotopic compositions than post Archean upper crust, which may have also been produced by the more intense weathering conditions during the Archean, as discussed above.

6. Conclusions

Most of the Kaapvaal shales analyzed here follow the trend defined by the Post Archean shales, which show a rough negative correlation between [Li] and δ^7Li. Shales

from the K8 and Orange Grove Formations, which have higher δ^7Li and lower [Li] relative to the other Kaapvaal shales, may derive from a provenance that has experienced severe weathering, due tothe high surface temperatures and heavy rainfall. Li concentration first increases and then decreases with increasing CIA value in Archean shales, and most have lower [Li] but higher CIA than Post Archean shales; this likely reflectes the result of the absence of Mg-bearing clay minerals in Archean shales due to the greater weathering intensity in their provenances. Severe weathering conditions favor the formation of gibbsite and kaolinite should might be Li-poor and become the dominant minerals in Archean shales. The findings of low [Li], high δ^7Li and high CIA for Archean shales appears to be recording a different weathering conditions prevalent then. Finally, [Li] in the upper continental crust may have increased from the Archean (~3.0 Ga) to the post Archean, but the Archean upper continental crust may have had heavier average Li isotopic composition than post Archean due to more inense weathering.

Chapter 7: Lithium concentrations and isotopic compositions of Archean Trondhjemites-Tonalites-Granodiorites and sanukitoids: evaluating the flux of Li to the continents through time[1]

[1] L. Qiu, R.L. Rudnick and W.F. McDonough contributed to the interpretation of the data. Major and trace elements of TTGs and sanukitoids are from Clemens et al. (2006), Rollinson and Windley (1980), Burton et al. (2000) and Shirey and Hanson (1984; 1986). The text, tables and figures were created/written by L. Qiu.

Abstract:

The Li abundance in the juvenile magmatic flux to the continental crust plays an important role in determining the weathering flux from the continents (Lee et al., 2008; Liu and Rudnick, 2011); moreover, [Li] in juvenile continental crust is mainly controlled by the [Li] in Archean juvenile additions because most of the crust likely formed in the Archean. In order to constrain better the Li signature in Archean juvenile additions, the Li concentration ([Li]) and Li isotopic compositions (δ^7Li) were determined in Archean Tonalite–trondhjemite–granodiorite (TTGs) from Scourie, Scotland, and Barberton, South Africa, and Archean sanukitoids (diorites, monzodiorites, and trachyandesites) from the Rainy Lake Region of the Superior Province, Canada. These TTGs and sanukitoids have been interpreted to be generated by three types of magma petrogenesis during the Archean. The Scourian TTGs are interpreted to be slab melts; Barberton TTGs are interpreted to have formed by partial melting of thickened basaltic crust; the sanukitoids are suggested to have derived from melting of mantle peridotite hybridized by slab melts/fluids. These different heterogeneous petrogeneses resulted in distinct Li signatures in the rocks.

The older Barberton TTGs (3.45-3.55 Ga) have more variable, and, on average, higher lithium concentrations ([Li] = 10-96 μg/g, average [Li] = 42 ± 54, 2σ) and more variable Li isotopic compositions (δ^7Li = +0.8 ~ +7.0, average δ^7Li = 4.5 ± 3.6 (2σ) than those of the younger Barberton TTGs (3.24 Ga), which have [Li] = 13 to 33 μg/g with average [Li] = 24 ± 16, 2σ and δ^7Li = +3.8 ~ +5.0 with average δ^7Li = 4.4 ± 0.9 (2σ). Since the older Barberton TTGs are interpreted to derive from partial melting of basaltic crust at shallower depth than the younger Barberton TTGs, the more variable [Li] and δ^7Li in the older TTGs is likely the result of incorporation of an evolved crust component in their source region; by contrast, the Li signature in the younger Barberton TTGs indicates a primitive basaltic source that experienced little crustal interaction. The sanukitoids have relatively consistent [Li] and δ^7Li, with average [Li] = 27 ± 20 (2σ) and mantle-like δ^7Li = 4.6 ± 0.8 (2σ), further indicating their source is dominated by a mantle source region. The depletion of [Li] in the Scourian TTGs (3.0 to 12.5 μg/g, average [Li] = 8.1 ± 5.5 μg/g, 2σ) could be caused by the initial dehydration during slab-subduction, but is more likely caused by later granulite-facies metamorphism. The [Li] in Scourian TTGs lends further support to the hypothesis that granulite-facies lower crust has average [Li] of ~8 μg/g. The highly variable δ^7Li in Scourian TTGs (+0.2 to +11.7) may reflect a variety of components in their source region, such as hydrous oceanic crust, detrital sediments and mantle.

Collectively, the Archean mantle-related juvenile additions to the continental crust have average [Li] (~ 25 μg/g) similar to that of post Archean I-type granites, but significantly higher than the [Li] in modern arc basalts (~6.9 μg/g), which represent juvenille additions to the modern continental crust. By contrast, the δ^7Li in juvenile

additions to the crust (+4.5) is higher than that of post Archean I-type granites (+2.6), but similar to that of the δ^7Li in modern arc basalts (~+4). According to the mass balance model of Liu and Rudnick (2010), the average [Li] in the Archean TTGs investigated here (~ 25 μg/g) suggests, consequently, around 30% crustal mass has been lost due to chemical weathering.

1. Introduction

It is generally accepted that the average composition of present-day continental crust is andesitic (SiO_2 = 57~ 64 wt. %, Rudnick and Gao, 2003 and references therein); however, the building blocks of continental crust is basaltic. This enigma indicates that certain processes have preferentially removed Mg and enriched Si during continental crust evolution. Weathering of basaltic crust is favored by some studies as a hypothesis that can potentially solve this enigma (e.g., Albarede, 1998; Lee et al., 2008; Liu and Rudnick, 2010). During weathering of continental crust, soluble elements, such as Mg and Li, are transported from crust to the ocean, leaving behind insoluble elements such as Al and Si in the weathered regolith. Several studies have tried to quantify the influence of weathering on the composition of continental crust (e.g., Albarede, 1998; Lee et al., 2010; Liu and Rudnick 2010); for instance, Liu and Rudnick (2010), using a simple mass balance model of Li inputs and outputs of the continental crust, suggested that 50% mass of the original continental crust have been lost due to chemical weathering. Furthermore, Liu and Rudnick (2010) indicate that the Li signatures in the juvenile continental crust (JCC) is an very sensitive parameter in their mass balance model; importantly, if [Li] in Archean juvenile additions, which make up ~38% of JCC in the model, is significantly different from what Liu and Rudnick (2010) assumed in the model (~6.9 μg/g, based on

the [Li] of global arc basalts), the modeling result will be significantly impacted (Liu and Rudnick, 2010). Therefore, the Li signature in Archean juvenile additions needs to be constrained in order to interpret better the influence of chemical weathering on the composition of continental crust.

Juvenille additions to the continental crust in the Archean are dominated by two major contrasting lithological associations, mafic volcanic rocks and TTG suites, both of which are typically found together in greenstone belts. Although magmas of the TTG type formed today are not common, they were the dominant felsic magmatic suite in the Archean, and are estimated to make up more than 2/3 of Archean cratons (De Wit and Ashwal, 1997). Compositionally, the vast majority of TTG suites are silica and alumina-rich, with SiO_2~70%, Al_2O_3>15%, Na_2O/K_2O>1 (Barker et al., 1976), and with average $Mg^{\#}$ of ~41 (Drummond et al., 1996). However, the petrogenesis of TTG magma is the subject of debate, and the focus of the debate is mainly between the melting of basaltic rocks in either the subducting slab or in thickened lower continental crust. For example, based on a compilation of 1100 chemical analyses of Archean TTGs, Martin and Moyen (2002) suggested that Archean TTGs are derived from partial melting of subducting slabs; moreover, the melting conditions significantly changed from 4.0 to 2.5 Ga, with interactions between felsic melts (generated by metabasalt melting) and mantle peridotite increasing through the Archean era as slab dip steepened significantly (Martin and Moyen, 2002). By contrast, some studies argue that the experimental results of partial melting of basaltic slabs shows a mismatch with the compositions of Archean TTGs in terms of the Al_2O_3, TiO_2 and Na_2O abundances (Rudnick, 1995; Rapp, 1997) and, thus, other processes are needed for explaining the mismatch.

An alternative model for the petrogenesis of TTG magma is partial melting of basaltic lower crust (e.g., Berger and Rollinson, 1997; Clemens et al., 2006). Furthermore, several studies indicate that since the TTGs are H_2O-undersaturated, they are derived through fluid-absent partial melting of pre-existing crustal rocks in the deep crust instead of subducting slab (e.g., Rapp et al., 2003; Clemens et al., 2006).

In addition to TTGs, there is another group of Archean magmas that are less siliceous and more magnesian than average TTGs and share chemical features with the so-called sanukitoids (consisting of diorites, monzodiorites, and trachyandesites). Their parental magma is considered to form by melting mantle peridotite (e.g., Shirey and Hanson, 1984). Shirey and Hanson (1984) first described sanukitoids from Late Archean formations in the Rainy Lake region of the Superior Province, Canada. Important chemical characteristics of these rocks include: 1) the initial Pb, Sr, and Nd isotopic compositions are close to that of the mantle, 2) they generally have $Mg^{\#}$ >60, high Ni (up to 188 μg/g) and Cr contents (up to 469 μg/g), and 3) REE abundances are 6-12 times higher than that of chondrites, with strong enrichments in LREE and depletions in the HREE. These signatures led Shirey and Hanson (1984) to conclude that these rocks were produced by melting of an enriched mantle source. Moyen et al. (2001) suggested that the degree of slab melting at the end of the Archean decreased due to lower geothermal gradients; as a result, slab melts were consumed by reaction with the mantle, imparting a strongly fractionated REE (Rare Earth Elements) pattern, indicative of residual garnet. Subsequent melting of this hybridized mantle may have generated the sanukitoid magmas.

Archean magmas derived from such different sources may have distinct δ^7Li, because of the variation of the Li signature among lower continental crust, oceanic crust, marine sediments and mantle, which have all been implicated in the generation of of TTGs and sanukitoids. Modern lower continental crust has average [Li] ≈ 8 μg/g and $1< \delta^7\text{Li} < 2.5$ (Teng et al., 2008; Qiu et al., 2011b); modern seawater-altered basaltic crust has higher [Li] (up to 30 μg/g) and higher δ^7Li (up to +20) than that of the fresh basalts ([Li] ≈ 6 μg/g, $\delta^7\text{Li} \approx 3.8$) and mantle ([Li] ≈ 1.5 μg/g, $\delta^7\text{Li} \approx 3.8$) because of the uptake of Li from seawater ($\delta^7\text{Li} = 32$) into the altered basalts (e.g., Chan and Edmond, 1988; Chan et al., 2002; Magna et al., 2008); modern marine sediments that are derived from weathered continental crust have high [Li] (up to 70-80 μg/g) and low δ^7Li (down to -4.3, Chan et al., 2006). Therefore, TTG magmas derived through partial melting of subducting slabs, which may include different proportions of oceanic crust, marine sediments and mantle component, could have higher [Li] and exhibit a larger variation of δ^7Li than magmas generated from lower crust and hybridized mantle.

To date, few studies on the Li signature of Archean juvenile crustal rocks have been carried out. Teng et al. (2008) showed that thirteen Archean TTG composites from the North China Craton, which are believed to be derived from melting of thickened crust at shallow depth (e.g., Liu et al., 2004), have higher average [Li] (14.6 ± 5.6 μg/g, 1σ, Teng et al., 2008) than arc basalts but similar average δ^7Li (4 ± 1.4, 1σ) (cf. $\delta^7\text{Li} \approx 4$ in most arc basalts, Teng et al., 2008; Moriguti and Nakamura, 1998; Magna et al., 2006a; Moriguti et al., 2004; Tomascak et al., 2002, 2004; Chan et al., 2002). Because the TTGs studied by Teng et al. (2008) experienced upper amphibolite facies metamorphism, it is

possible that their [Li] has been depleted during metamorphic dehydration. It is also unclear to what degree their Li signature is representative of all Archean juvenile crust.

This study examines the Li systematics of TTGs from Scourie, Scotland, and Barberton, South Africa, as well as Archean sanukitoids from the Superior Province, Canada in order to provide information about the Li signature in Archean juvenile continental crust and to see what constraints Li may place on the origin of these rocks that have been interpreted to derive from slab-melting, thickened crust, and the mantle, respectively. Moreover, [Li] in Archean TTGs and sanukitoids will help constrain the juvenile flux of Li into continental crust, which impacts the calculated weathering flux on the crustal composition.

2. Geological settings

2.1. TTGs from the Barberton Mountain Land, South Africa

The Barberton TTGs analyzed in this study (Table 7-1) were previously studied by Clemens et al. (2006) and are derived from seven different granitoid plutons in Barberton Mountain Land, South Africa, which intruded into a well preserved early Archean greenstone belt. These plutons are relatively small (<100 to ~500 km^2) and intruded in three magmatic pulses based on their zircon U-Pb dates (Kamo and Davis, 1994; De Ronde et al., 2000; Armstrong et al., 1990; Kroner et al., 1996): ~3.55 Ga Steynsdorp (STY) Pluton, ~3.45 Ga Eerstehoek (EHK), Stolzburg (STZ), Theespruit (THE) and Doornhoek (DNK) Plutons, and ~3.24 Ga Nelshoogte (NLG) and Badplaas (BDP) Plutons. The plutons consist of tonalite and trondhjemites, which are dominated by plagioclase and quartz with biotite as the major mafic mineral and minor hornblende, in addition to biotite, occurring in the tonalites. The TTG bodies experienced amphibolite-

facies metamorphism (Clemens et al., 2006); however, since the igneous mineral assemblages in the TTGs are similar to those stable in the upper amphibolite facies, Clemens et al. (2006) suggest that metamorphism caused neither by dehydration nor partial melting and therefore had little influence on the chemistry of the rocks. Based on the concentrations and the patterns of the major and trace elements in these TTGs, Clemens et al. (2006) suggest that the Barberton TTGs are derived from melting of thickened Archean crust where the older TTGs, such as STY, EHK and DNK Plutons were derived from shallower depth than the younger TTGs, which were derived from a depth of at least 50 km.

2.1. TTGs from Scourie, NW Scotland

The Scourian TTGs studied here are from the central region (Scourie-Badcall) of the Lewisian Complex of northwest Scotland, which is predominantly composed of tonalities and trondhjemites that are metamorphosed to granulite facies (e.g., Rollinson and Fowler, 1987; Rollinson and Windley, 1980; Rollinson, 1996; Weaver and Tarney, 1980). Most studies agree that the TTGs in the central region formed at about 2900-2950 Ma (Rollinson, 1987; 1994; Rollinson and Fowler, 1987; Rollinson and Windley, 1980), but were metamorphosed to granulite-facies at 2680 Ma (e.g., Chapman and Moorbath, 1977). Early studies have attributed the depletion of K, U, Rb, Th in Scourian TTGs to the granulite facies metamorphism (e.g., Rollinson and Windley, 1980; Weaver and Tarney, 1980); by contrast, later studies interpreted the TTG magmas to be the products of a two-stage process of crust formation (e.g., Rollinson, 1996) and suggested that granulite facies metamorphism is not the cause of the deletion of fluid mobile elements. The first stage was triggered by relatively deep slab subduction, during which the mafic

oceanic crust and metasediments experienced dehydration (causing depletion of K, U, Rb, Th), and, during the second stage, the slab experienced partial melting to produce the TTG magma (Rollinson, 1996). Most of the Scourian samples in this study are from resampling the same localities that have been previously studied by Rollinson and Windley (1980) and Burton et al. (2000), whereas other Scourian samples are reported for the first time in this study (see Table 7-2 for details).

2.3. Sanukitoids from Rainy Lake, Canada

The sanukitoids (diorites, monzodiorites, and trachyandesites) selected for this study (Table 7-3) have been previously studied by Shirey and Hanson (1984; 1986) and are from the Rainy Lake area, Superior Province, Canada and Vermilion district in Minnesota, which consist of a series of alternating, linear greenstone and gneiss terrains (e.g., Stockwell, 1982). The sanukitoids of are 2680-2750 Ma old and occur as volcanic units in the Keewatin Series and Rock Islet Bay complex (e.g., Goldich and Fischer, 1986). The four sanukitoid samples from the Rainy Lake region are monzodiorite (135-81, 5-80, 68-80) and trachyandesite (53-80); one hornblendite sample (21-80) in the same region is also included since it has similar major and trace element compositions to the monzodiorite and trachyandesite (Shirey and Hanson, 1984; 1986); one sample from the Vermilion district is a trachyandesite (B-18), which has been previously studied by Arth and Hanson (1975) and Shirey and Hanson (1984). These samples have experienced metamorphism up to upper amphibolite facies, but they do not show depletion of large ion lithophile elements (Shirey and Hanson, 1986). Shirey and Hanson (1984) suggest that these samples are derived by melting of peridotitic mantle at depths of < 50 km that has been enriched in incompatible trace elements.

3. Analytical methods

Lithium concentrations and isotopic compositions of the TTGs and sanukitoids collected for this study were determined at the Geochemistry Laboratory of the University of Maryland College Park. Sample dissolution procedures, column chemistry, instrumental analysis and external precision are reported in Teng et al. (2006b) and Qiu et al. (2009). Briefly, samples were dissolved in a screw-top teflon beaker with a combination of HF–HNO_3–HCl. Lithium was purified on a cation exchange resin (Bio-Rad AG50w-X12, 200–400 mesh) first in an HCl medium, followed by an HCl-ethanol medium. Lithium concentrations and isotopic compositions were analyzed using the standard-sample-bracketing method on a Nu Plasma MC-ICPMS. The long-term external precision of the Li isotopic composition and concentration analyses are ≤ 1.0‰ (2σ) and ±10% (2σ), respectively, based on repeat analyses of pure Li standards and standard reference materials over the past nine years (Rudnick et al., 2004; Teng et al., 2006b; Qiu et al., 2011a). Two measurements on two separate column separations of the rock reference material BHVO-1that were analyzed along with the TTG samples, give δ^7Li = 4.8 ± 0.2 (2σ) and [Li] = 4.8 ± 0.6 μg/g (2σ); in comparison, Magna et al. (2004), Rudnick et al. (2004) and Aulbach and Rudnick (2009), reported the δ^7Li of BHVO-1 to be 5.3 ± 0.2, δ^7Li = 4.3 ± 1 and δ^7Li = 4.5 ± 1, respectively, and the GEOREM (Jochum and Nohl, 2008) preferred BHVO-1 [Li] =4.6 ± 0.2 μg/g.

4. Results

Lithium concentrations and isotopic compositions are reported in Tables 7-1, 7-2 and 7-3, along with the major and trace elements from Clemens et al. (2006) (Barberton TTGs), Rollinson and Windley (1980) and Burton et al. (2000) (Scourian TTGs), and

Table 7-1. Lithium concentrations (μg/g), Li isotopic compositions (δ^7Li), along with major (wt%) and other trace element concentrations (μg/g) in TTGs from Barberton, South Africa.

Sample	STY1	STY3A	STY4A	STY4B	DNK1	EHK1	EHK2A	THE4A	THE5	STZ1	STZ16	STZ17	STZ19	BDP5A	BDP5C	BDP7	BDP8A	NLG1	NLG14A	NLG15	NLG25A
Li μg/g	96	72	54	21	41	78	29	52	23	11	36	26	10	22	16	19	13	31	35	22	33
δ^7Li	5.0	4.6	3.5	1.5	5.8	7.0	5.2	0.8	5.3	5.5	6.6	3.4	4.4	4.7	4.7	4.2	4.3	4.6	3.8	3.8	5.0
Age (Ga)	3.55	3.55	3.55	3.55	3.45	3.45	3.45	3.45	3.45	3.45	3.45	3.45	3.45	3.24	3.24	3.24	3.24	3.24	3.24	3.24	3.24
SiO_2	65.7	72.9	73.7	75.1	74.0	72.4	72.8	70.3	71.4	70.7	71.2	71.6	72.0	70.5	72.8	73.8	74.0	70.1	72.2	63.1	71.1
TiO_2	0.46	0.23	0.2	0.14	0.18	0.29	0.19	0.25	0.23	0.26	0.21	0.23	0.22	0.21	0.23	0.15	0.1	0.34	0.22	0.62	0.23
Al_2O_3	17.7	15.65	14.97	14.04	14.65	15.37	15.44	16.04	15.74	15.68	15.47	15.03	15.14	16.83	15.84	15.62	15.42	15.73	15.67	17.33	16.09
FeOT	3.75	1.52	1.93	1.26	1.91	2.3	1.57	2.01	1.94	1.82	1.48	1.62	1.42	1.95	1.56	1.34	1.27	2.56	2.12	4.04	2.05
MnO	0.06	0.03	0.03	0.02	0.04	0.04	0.03	0.03	0.02	0.04	0.05	0.06	0.04	0.03	0.01	0.02	0.02	0.06	0.03	0.04	0.03
MgO	1.82	0.43	0.44	0.18	0.48	0.81	0.6	1.1	1.05	0.64	0.51	0.79	0.52	0.61	0.41	0.48	0.27	1.3	0.83	2.63	0.62
CaO	3.89	1.78	1.93	1.13	2.04	3.33	2.24	2.85	2.66	2.27	1.88	1.79	1.4	3.35	2.62	1.5	1.87	2.31	2.16	5.18	2.75
Na_2O	4.43	4.81	4.6	3.56	4.21	4.28	5.43	5.74	5.19	6.94	7.08	7.01	7.2	5.28	5.5	5.43	5.74	6.45	4.91	5.56	5.34
K_2O	1.99	2.6	2.17	4.54	2.44	1.12	1.61	1.56	1.69	1.59	2.1	1.78	2.02	1.15	0.95	1.55	1.24	0.99	1.8	1.31	1.68
P_2O_5	0.24	0.08	0.06	0.04	0.07	0.09	0.06	0.08	0.07	0.07	0.06	0.07	0.06	0.09	0.08	0.06	0.05	0.12	0.08	0.17	0.08
Total	99.6	100	99.7	99.7	99.7	99.6	99.7	99.6	100.2	100.44	100.13	99.07	100.56	98.8	99.5	99.2	99.6	100.49	100.7	99.05	100.5
Ba	316	604	438	575	240	145	496	312	376	476	526	388	489	128	153	240	151	134	260	253	223
Rb	100.5	103.7	52.8	111.7	117.3	71.4	34.4	51.3	48.1	27.0	48.0	44.0	46.0	39.8	29.3	38.6	32.2	46.0	57.9	39.4	43.1
Sr	587	388	380	166	162	266	707	624	583	736	649	590	611	606	705	510	473	486	391	823	493
Y	13.3	19.2	5.7	5.5	17.5	22.6	3.4	7.0	5.7	4.0	4.0	5.0	4.0	6.4	2.6	2.9	2.5	3.0	6.5	7.2	9.1
Zr	205.6	178.2	131.1	128.4	136.4	144.4	111.3	127.1	118.0	110.0	91.0	104.0	87.0	116.2	165.4	118.0	103.4	128.0	88.7	177.6	96.9
Nb	11.1	8.3	6.6	7.3	10.2	11.8	4.0	4.6	4.9	n/a	n/a	n/a	n/a	2.5	1.4	1.5	2.0	n/a	3.3	1.7	4.0
Zn	97.2	37.0	39.9	34.0	37.4	46.1	43.4	47.6	48.2	43.0	35.0	42.0	37.0	39.7	37.8	32.8	33.2	46.0	36.6	50.2	36.9
Cu	6.9	n/a	9.0	n/a	9.4	n/a	n/a	n/a	n/a	2.0	2.0	2.0	2.0	n/a	4.7	n/a	n/a	2.0	3.1	27.8	7.7
V	48.3	10.9	14.6	6.9	16.6	23.1	10.6	22.1	24.8	15.0	15.0	15.0	15.0	21.6	11.0	12.9	7.9	25.0	29.6	88.6	21.2
La	16.0	54.7	22.8	21.9	18.0	16.8	15.2	11.7	18.1	9.6	15.4	18.5	12.1	8.6	15.5	13.8	12.2	11.5	8.5	6.4	8.5
Ce	27.8	56.4	39.4	45.7	31.3	31.2	23.5	19.8	30.5	15.0	25.1	26.1	21.4	14.1	24.2	23.0	19.9	21.4	16.5	13.3	13.3
Nd	12.1	15.0	13.8	15.7	13.1	13.1	9.2	10.0	11.5	6.1	9.9	10.9	8.8	6.1	8.4	8.0	7.2	8.4	8.0	7.4	6.7
Sm	2.47	1.88	2.22	2.88	2.3	3.15	1.48	1.6	1.71	1.27	1.62	1.51	1.47	1.2	1.01	1.2	1.58	1.09	1.53	1.48	1.3
Eu	0.84	0.63	0.58	0.5	0.55	0.82	0.52	0.54	0.49	0.34	0.5	0.49	0.36	0.43	0.38	0.35	0.42	0.4	0.38	0.51	0.4
Gd	2.78	2.38	1.85	2.21	2.35	3.15	1.17	1.36	1.54	0.82	1.13	1.13	0.87	1.07	0.8	0.98	1	1.02	1.2	1.48	1.43
Tb	0.38	0.39	0.2	0.33	0.42	0.57	0.13	0.18	0.22	0.11	0.14	0.19	0.11	0.17	0.11	0.09	0.16	0.09	0.19	0.24	0.23
Yb	1.31	1.39	0.49	0.46	1.56	2.01	0.14	0.48	0.32	0.24	0.3	0.33	0.2	0.36	0.21	0.21	0.3	0.17	0.55	0.33	0.4
Lu	0.18	0.24	0.09	0.09	0.25	0.38	0.05	0.06	0.07	0.03	0.04	0.06	0.03	0.08	0.05	0.05	0.05	0.03	0.11	0.05	0.06

Major (%) and trace elements (μg/g) data are from Clemens et al. (2006).
The Li data reported in this study represent the averages of ≥2 measurements of each sample.

The uncertainties for [Li] (μg/g) and δ^7Li are ±10 (2s) and ±1 (2s), respectively.

Table 7-2. Lithium concentrations (μg/g), Li isotopic compositions (δ^7Li), along with major (wt%) element concentrations in TTGs (tonalites) from Scourie, Scotland. *Continued on next page.*

	1	2	3	4	5	6
Sample	09-01	09-02	09-03	09-04	09-05	09-06*2
UK ordnance survey grid	NC 1494744871	NC 1494044893	NC 1426144193	NC 1427644196	NC 1415944264	NC1414644248
Li μg/g	12.3	6.4	8.9	6.9	3.0	8.7
δ^7Li	3.7	4.7	6.6	8.6	2.9	3.6
Age	2.95	2.95	2.95	2.95	2.95	2.95
SiO_2	N/A	N/A	66.4	66.4	57.27	57.27
TiO_2	N/A	N/A	0.46	0.46	0.68	0.68
Al_2O_3	N/A	N/A	16.2	16.2	16.69	16.69
FeOT	N/A	N/A	N/A	N/A	6.67	6.67
MnO	N/A	N/A	0.06	0.06	N/A	N/A
MgO	N/A	N/A	2.14	2.14	4.55	4.55
CaO	N/A	N/A	4.68	4.68	8.28	8.28
Na_2O	N/A	N/A	5.6	5.6	4.64	4.64
K_2O	N/A	N/A	0.62	0.62	0.7	0.7
P_2O_5	N/A	N/A	N/A	N/A	0.15	0.15
Total	N/A	N/A	100.84	100.84	100.4	100.4

The uncertainties for [Li] (μg/g) and δ^7Li are ±10 (2s) and ±1 (2s), respectively.

The Li data reported in this study represent the averages of ≥2 measurements of each sample.

Major (%) and trace elements (ppm) data are from Burton et al. (2000) and Rollinson and Windley (1980).
Sample 09-03 and 09-04 is equivalent to the tonalite sample 043 in Burton et al. (2000)
Sample 09-05 and 09-06*2 are equivalent to the tonalite sample 266 in Rollinson and Windley (1980).
Sample 09-09 and 0910 are equivalent to the tonalite sample 189 in Rollinson and Windley (1980).

Table 7-2 continued

	7	8	9	10	11	12
Sample	09-09	09-10	09-11	09-12	09-13	09-14
UK ordnance survey grid	NC1466041713	NC1462841707	NC1461341713	NC1460241725	NC1486341489	NC1532141704
Li μg/g	10.0	12.5	5.0	8.6	8.4	6.4
δ^7Li	11.7	9.6	4.6	7.9	0.2	5.0
Age	2.95	2.95	2.95	2.95	2.95	2.95
SiO_2	66.07	66.07	N/A	N/A	N/A	N/A
TiO_2	0.48	0.48	N/A	N/A	N/A	N/A
Al_2O_3	16.9	16.9	N/A	N/A	N/A	N/A
FeOT	3.57	3.57	N/A	N/A	N/A	N/A
MnO	0.05	0.05	N/A	N/A	N/A	N/A
MgO	1.01	1.01	N/A	N/A	N/A	N/A
CaO	5.45	5.45	N/A	N/A	N/A	N/A
Na_2O	4.81	4.81	N/A	N/A	N/A	N/A
K_2O	0.35	0.35	N/A	N/A	N/A	N/A
P_2O_5	0.1	0.1	N/A	N/A	N/A	N/A
Total	98.79	98.79	N/A	N/A	N/A	N/A

Table 7-3. Lithium concentrations (μg/g), Li isotopic compositions (δ^7Li), along with major (wt%) and other trace element concentrations (μg/g) in sanukitoids from Rainy Lake region, Canada and Vermilion district in Minnesota.

	1	2	3	4	5	6
	trachyandesite	monzodiorite	trachyandesite	hornblendite	monzodiorite	monzodiorite
Sample	B-18	SS-5-80	SS-21-80	SS-53-80	SS-68-80	SS-135-81
Li (μg/g)	36	17	16	40	27	28
δ^7Li	4.0	5.1	4.6	4.3	4.9	4.7
Age	2.7	2.7	2.7	2.7	2.7	2.7
SiO_2	54.6	54.6	51.4	55.9	N/A	54.2
TiO_2	0.73	0.72	0.54	0.81	N/A	1.55
Al_2O_3	15.1	14.4	8.8	14.8	N/A	15.0
Fe_2O_3	3.04	8.56	8.38	8.73	N/A	10.35
MnO	0.14	0.12	0.12	0.14	N/A	0.15
MgO	6.4	7.98	17.13	6.72	N/A	3.93
CaO	7.42	8.71	10.25	7.57	N/A	7.51
Na_2O	4.27	2.87	1.09	3.38	N/A	4.05
K_2O	2.22	1.34	1.01	1.73	N/A	1.59
P_2O_5	0.34	0.36	0.16	0.3	N/A	0.45
Total	99.6	99.6	98.87	100.09	N/A	98.81
Mg#	0.62	0.69	0.83	0.64	N/A	0.47
V	N/A	131	92.6	116	N/A	130
Cr	N/A	469	2059	429	N/A	123
Ni	N/A	188	698	163	N/A	68.6
Zn	N/A	95	79	122	N/A	141
Sr	1237	627	361	650	N/A	1193
Zr	N/A	138	64.4	167	N/A	171
Nb	N/A	7	4.1	9.2	N/A	12
La	N/A	28.4	17	N/A	N/A	N/A
Ce	94.6	64.7	45.3	72.7	N/A	132
Nd	44	33.4	26.4	34.7	N/A	63.1
Sm	8.15	6.39	4.76	6.2	N/A	11
Eu	2.12	1.64	1.21	1.67	N/A	2.82
Gd	6.37	5.1	3.38	4.49	N/A	7.42
Dy	4.04	4.44	2.59	3.51	N/A	4.97
Er	1.97	2.5	1.34	1.8	N/A	2.17
Yb	1.92	2.31	1.27	1.61	N/A	1.71

The uncertainties for [Li] (μg/g) and δ^7Li are ±10 (2s) and ±1 (2s), respectively.

The Li data reported in this study represent the averages of ≥2 measurements of each sample.

Major (%) and trace elements (μg/g) data are from Shirey and Hanson (1984, 1986).

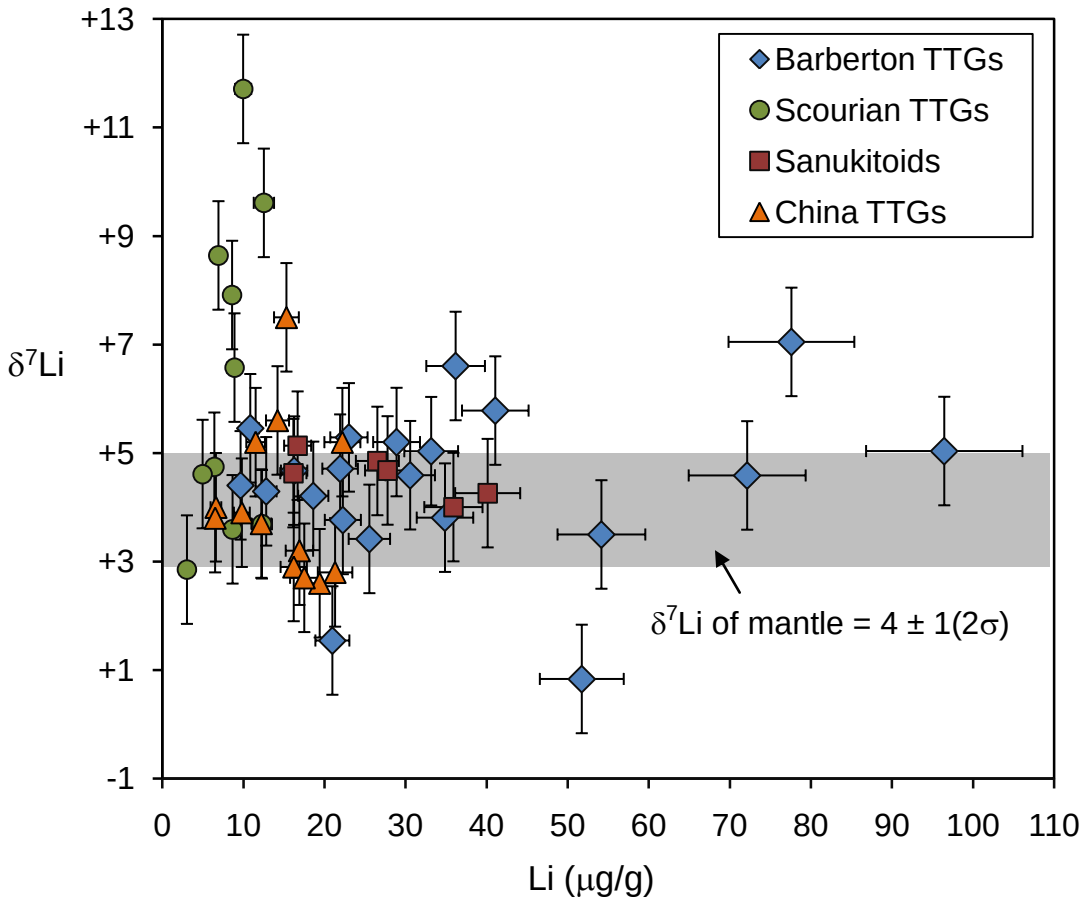

Figure 7-1. [Li] versus δ^7Li for Archean TTGs from Barberton, South Africa and Scourie, North Scotland and sanukitioids from the Rainy Lake Region, Canada. Error bars indicate the long-term 2σ uncertainty of Li isotopic compositions (± 1‰) and 2σ uncertainties of Li concentrations (± 10%). δ^7Li of the mantle is from Magna et al. (2006). The δ^7Li and [Li] of China TTGs are from Teng et al. (2008).

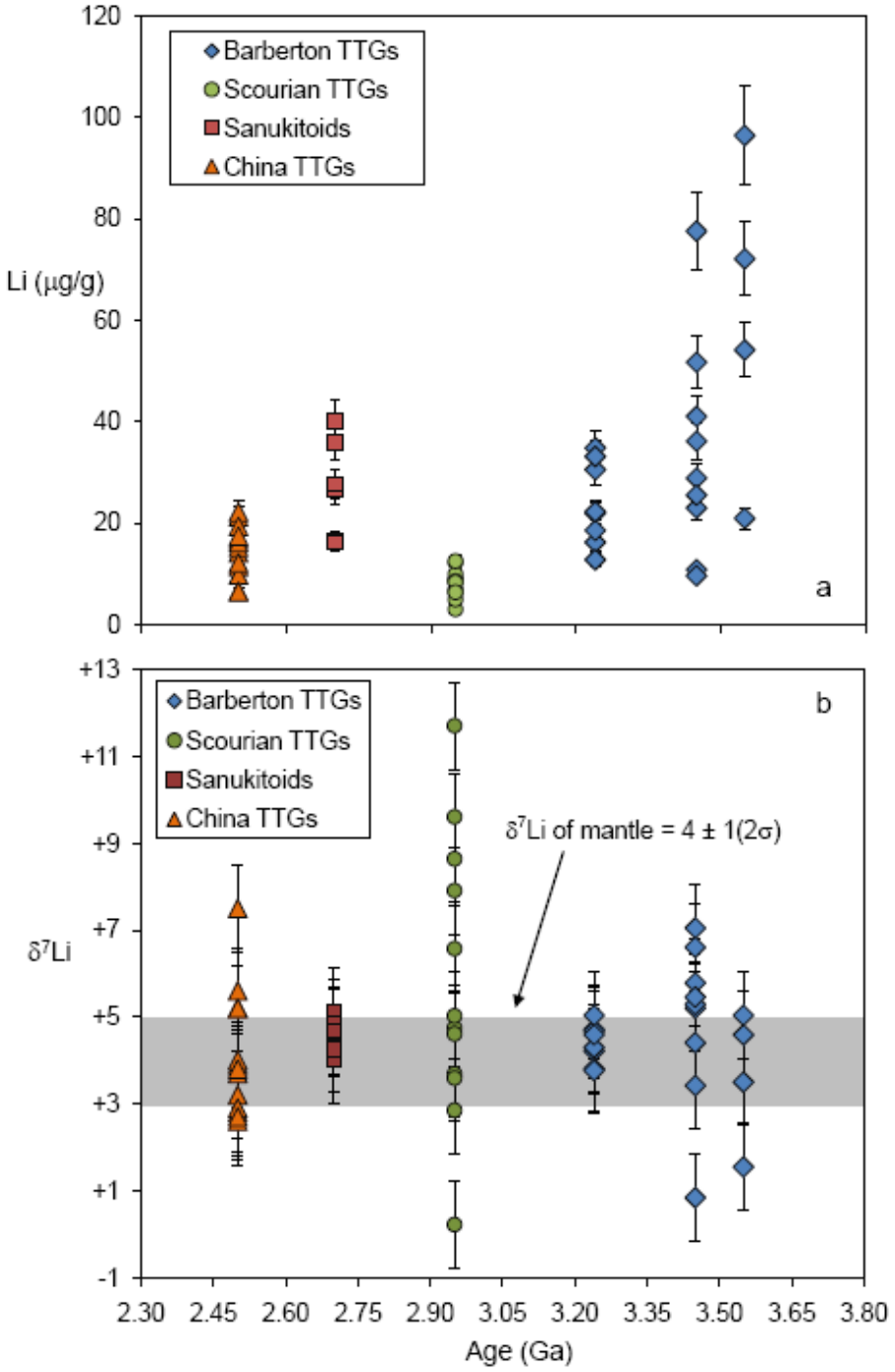

Figure 7-2. Plot of Li concentrations (a) and Li isotopic compositions (b) versus the magmatic ages of the TTGs and sanukitoids. The δ^7Li and [Li] of China TTGs are from Teng et al. (2008). Error bars indicate 2σ uncertainty. δ^7Li of the mantle is from Magna et al. (2006).

Shirey and Hanson (1984; 1986) (Sanukitoids), respectively. Lithium concentrations in the TTGs from Scourie vary from as low as 3.0 up to 12.5 μg/g, with average [Li] = 8.1 ± 5.5 μg/g, (2σ). The TTGs from Barberton have higher average [Li] and show a larger overall variation than those of the other two localities, with [Li] = 10 to 96 μg/g (average [Li] = 35 ± 47 μg/g, 2σ, Figs. 7-1 and 7-2a). The [Li] of younger Barberton TTGs (3.24 Ga) are generally lower than those of the older TTGs (3.45 and 3.55Ga), with [Li] of 3.24 Ga TTG = 13 to 33 μg/g (average [Li] = 24 ± 16 μg/g, 2σ) and [Li] of 3.45 and 3.55 Ga TTG = 10 to 96 μg/g (average [Li] = 42 ± 54 μg/g, 2σ). The [Li] in Sanukitoids is similar to that of the younger Barberton TTGs, varying from 16 to 36 μg/g, with average [Li] = 27± 20 μg/g (Fig. 7-2a).

The Li isotopic compositions of the sanukitoids and younger Barberton TTGs (3.24 Ga) are relatively constant and average values are nearly identical to each other: δ^7Li = 4.6 ± 0.8 (2σ) and 4.4 ± 0.8 (2σ), respectively (Fig. 7-2b). By contrast, the δ^7Li values are heterogeneous in Scourian TTGs and older Barberton TTGs (Figs. 7-1 and 7-2b). The Sourian TTGs have δ^7Li spanning a large range from +0.2 to +11.7, with an average δ^7Li = +5.8 ± 6.5 (2σ), and the δ^7Li in older Barberton TTGs (3.45 Ga and 3.55 Ga) vary from +0.8 to +7.0 with an average δ^7Li = +4.5 ± 3.6 (2σ).

5. Discussion

5.1. Factors controlling [Li] and δ^7Li in Barberton TTGs

Clemens et al. (2006) suggested that the older and younger Barberton TTGs are both derived from melting of thickened crust, but the magmas of older TTGs are likely

generated at shallower depth; thus, the large variation of [Li] in older Barberton TTGs might be related to the depths of the magma source region. Heavy Rare Earth Elements (HREE) and Eu abundances in the Barberton TTGs have been used to indicate the relative depth where partial melting took place (Clemens et al., 2006). As the depth of partial melting increases, plagioclase in the residue is replaced by garnet, and HREE in the melt are depleted due to the affinity of HREE with garnet (e.g., Martin and Moyen, 2002). Furthermore, the general lack of Eu anomalies in Barberton TTGs also indicates that plagioclase was not a major phase in the residue, and the Eu concentration, like HREE, also responds to the abundance of garnets in the residue (e.g., Clemens et al., 2006). Clemens et al. (2006), based on the REE and Eu patterns in the TTGs, indicated that the magma of older Barberton TTGs are equilibrated with a residue having a small amount of plagioclase, and the magma of younger TTGs (3.24 Ga) are derived from a plagioclase-free garnet bearing residue. The [Li] in the Barberton TTGs positively correlates with the HREE and Eu abundance, particularly for the older TTGs (Figs. 7-3 and 7-4), indicating that [Li] may also be a function of the depth of partial melting. However, [Li] in the magmas is unlikely to be controlled by residual garnet or plagioclase because of the low partition coefficients of Li between these two minerals and fluids or other slilicates (e.g., $D^{garnet/fluid} = 4.8\times10^{-3}$, $D^{plagioclase/fluid} = 2.9\times10^{-5}$, Brenan et al., 1998), and correlations observed for HREE and Eu and [Li] reflect overall degree of enrichment of the crust rather than control by a particular phase. The magmas generated at shallower depth may have more opportunities to be mixed with more evolved crust than the magmas generated at greater depth, and, thus, [Li] in the magmas could be affected by the amount of evolved crust incorporated into the magma. The [Li]

in evolved crust is higher than that of the relatively juvenile crust; for example, [Li] in the average upper, middle and lower continental crust is ~35, ~12 and ~8 μg/g, respectively (Teng et al., 2004; 2008). Therefore, the higher average [Li] in the older Barberton TTGs, which are derived from shallower depths, may reflect mixing primitive magmas sources with more evolved crustal components. By contrast, [Li] in the younger TTGs (3.24 Ga) is relatively low and does not show a clear correlation with the abundance of HREE or Eu (Figs. 7-3 and 7-4), probably further indicating their magma sources were generated at greater depths, where garnet is the dominant Al-bearing mineral in the residue, and the [Li] in the magma is not influenced by assimilation of evolved crust.

Like [Li], the δ^7Li in the older TTGs (3.55 and 3.45 Ga) is more variable (+0.8 to +7.0) than that of the younger TTGs (+3.8 to +5.0) (Fig. 7-2b), likely reflecting more diverse sources of the older TTGs, which include pre-existing continental crust. The average δ^7Li in the present-day upper continental crust is 0 (Teng et al., 2008), which, if also representative of Archean upper continental crust, may may contribute to the heterogeneous δ^7Li in the older Barberton TTGs, particularly for the lower end of their δ^7Li range; however, it is not clear what component contributed to the higher end of their δ^7Li range (up to +7.5) so far. Furthermore, the range of δ^7Li in older Barberton TTGs is close to that seen in TTG composites from North China Craton (+2.7 to +7.5, Teng et al., 2008, Fig. 7-2b), which are also suggested to derive from shallow depth of thickened crust (e.g., Liu et al., 2004). Therefore, both the older Barberton and China TTGs indicate that magmas derived from shallower depths of thickened crust have variable δ^7Li, likely due to incorporation of more evolved crustal components in the source. In contrast to the older Barberton TTGs and Chinese TTGs, the younger Barberton TTGs (3.24 Ga) have

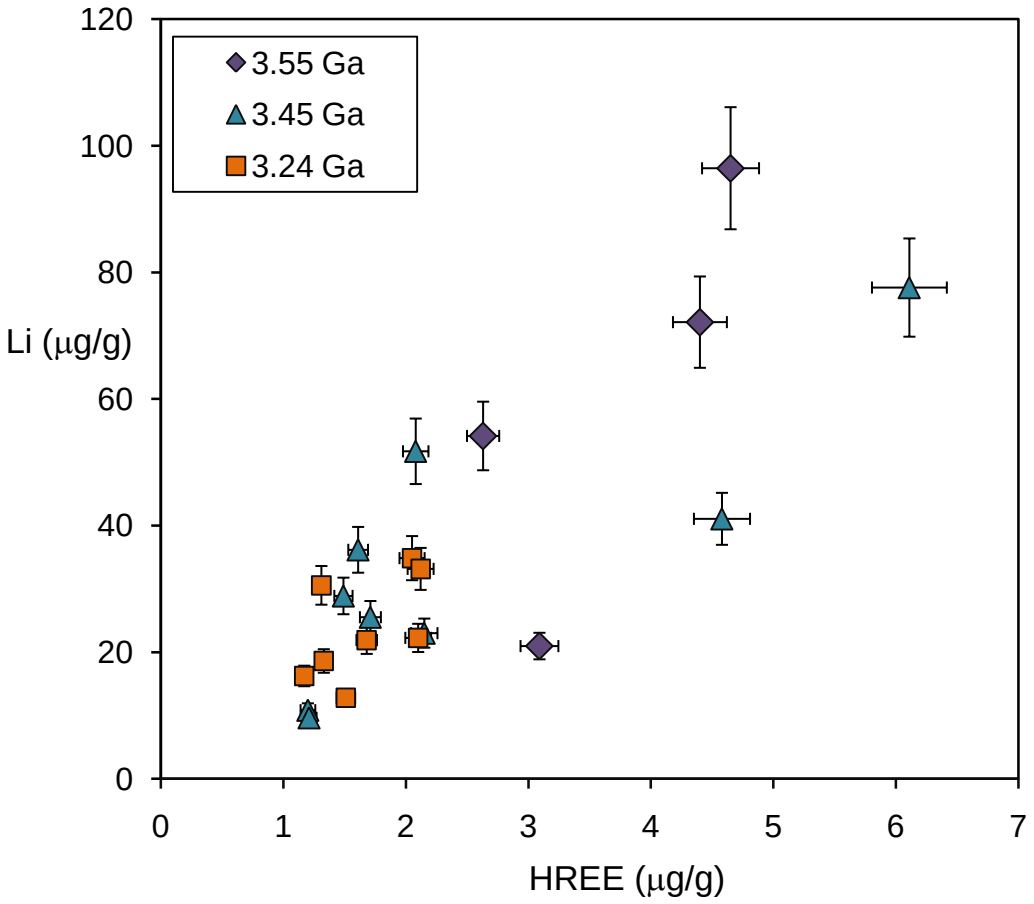

Figure 7-3. Plot of Li concentrations versus the abundance of Heavy Rare Earth Elements (HREE = Gd + Tb + Yb + Lu) in the Barberton TTGs. Error bars indicate 2σ uncertain of Li concentrations (±10%) and HREE ((±5 %).

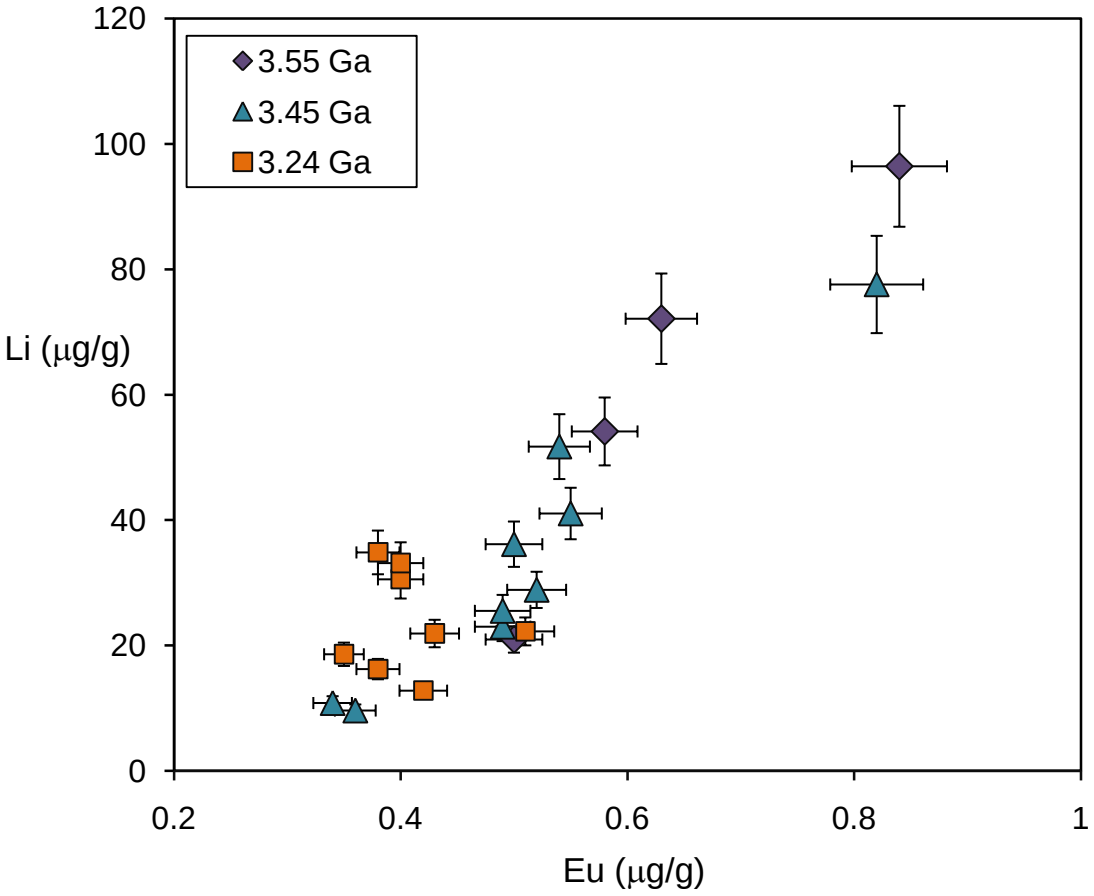

Figure 7-4. Plot of Li concentrations versus Eu concentrations in the Barberton TTGs. Error bars indicate 2σ uncertain of Li concentrations (±10%) and Eu ((±5 %).

relatively constant δ^7Li (+3.8 to +5.0, average δ^7Li = 4.4 ± 0.8, 2σ), which is similar to the δ^7Li of the mantle and mid ocean ridge basalts (~+4, e.g., Tomasack et al., 2004; 2008), further indicating that these younger TTGs are derived from partial melting of primitive basaltic sources.

5.2. Factors controlling the [Li] and δ^7Li in Scourian TTGs

The average [Li] of granulite facies Scourian TTGs (8.2 ± 6.0 μg/g, 2σ) is significantly lower than that of other TTGs and sanukitoids in this study, and also lower than that of the TTGs from the North China Craton (average = 14.1 ± 9.4, 2σ, Teng et al., 2008). However, [Li] of Scourian TTGs is similar to that of granulite facies metapelites from the Ivrea Zone, Italy (8 ± 6 μg/g, 2σ, Qiu 2011b) and [Li] of the lower continental crust (8 μg/g), as defined by the study of Teng et al. (2008). Although [Li] in the mafic source of Scourian TTGs could be depleted during the early stages of dehydration prior to partial melting, along with the depletion of K, Th and U (e.g., Rollinson, 1996). However, studies of Li depletion in metamorphic rocks, coupled with modeling of Li depletion suggest that such large degrees of depletion are unlikely to result from dehydration alone. For example, study on a metamorphic sequence in Qiu et al. (2011b) indicates that the partil melting of Mg-bearing phyllosilicates at granulite facies is the cause for significant Li depletion in metapelites. Likewise, the modeling results of Marschall et al. (2007) suggested that metamorphic dehydration of a hydrated subducting-slab from 50 to 670 °C causes Li depletion of less than 40%. By contrast, significant Li depletion has been shown to accompany the granulite facies metamorphic dehydration and partial melting of metapelites, where most of the Li escaped with the released fluids and melts (Qiu et al., 2011b). The similarity of [Li] in the Scourian TTGs,

metapelites and lower continental crust, which are all granulite facies rocks, indicates that the granulite facies metamorphism and accompanying partial melt depletion may have a great control on [Li] in the high-grade rocks and terranes, and the [Li] in the granulite facies lower continental crust is around ~8 μg/g.

In contrast to [Li], the Li isotopic compositions in Scourian TTGs spans the largest range (+0.2 to +11.7, with average δ^7Li = +5.8 ± 6.5 (2σ), among all the TTGs and sanukitoids in this study (Figs 7-1 and 7-2). The source of Scourian TTGs are suggested to be derived from partial melting of a subducting slab (e.g., Rollinson and Fowler, 1987; Rollinson and Windley, 1980; Rollinson, 1996; Weaver and Tarney, 1980; Wheeler et al., 2010). If Archean hydrous oceanic crust had the same Li signature as present-day oceanic crust, it would have high δ^7Li (up to +20, e.g., Chan et al., 2002; Magna et al., 2006a), and the overlying marine sediments could have low δ^7Li (down to -4.3) if they are derived from weathered continental crust (Chan et al., 2006; Qiu et al., 2009) or may have high δ^7Li if they derive from highly-weathered continental sources (Chapter six). Thus, the highly variable δ^7Li in Scourian TTGs may indicate that, during slab-melting, the magma source included contributions from different proportions of hydrous oceanic crust, detrital sediments, and mantle peridotite.

5.3. Factors controlling the [Li] and δ^7Li in the Rainy Lake Sanukitoids

The [Li] and δ^7Li in the sanukitoids (Fig. 7-2) vary within a limited range, with average [Li] = 27 ± 20 μg/g (2σ) and δ^7Li = 4.6 ± 0.8 (2σ), which are similar to the Li signature of younger Barberton TTGs ([Li] = 24 ± 16 μg/g, 2σ, δ^7Li = 4.6 ± 0.9, 2σ). The δ^7Li in the Sanukitoids is consistent with their derivation from the mantle source (δ^7Li of mantle = +4 ± 1, 2σ, e.g., Magna et al., 2006b). Furthermore, if this mantle source has

been enriched by slab melts as suggested by Shirey and Hanson (1984), the invariability of the δ^7Li in suanukitoids may indicate the slab melts that hybridized the manle have mantle-like δ^7Li.

5.4. Li signature of Archean juvenile flux and post Archean granitoids

The [Li] of Barberton TTGs and sanukitoid samples in this study are not likely depleted during greenschist to amphibolite facies metamorphism, as discussed earlier, and may provide information about [Li] in juvenile magmas during the Archean. However, the older Barberton TTGs (3.55 and 3.42 Ga) are suggested to be derived from partial melting of thickened crust at shallow depth and their source included more evolved crust component; thus, the older Barberton TTGs might not be a typical component of Archean juvenile flux. The younger Barberton TTGs and sanukitoids, which are mainly derived from primitive source, more likely represent the juvenile magmas during the Archean; Li signatures in these rocks indicate magmas entering the continental crust during the Archean had average [Li] of 25 ± 17 μg/g (2σ) and δ^7Li of 4.5 ± 0.8 (2σ).

In order to compare the Li signature in Archean juvenile magmas to their post Archean equivalents, the published [Li] in post Archean I-type granites are selected for comparison. Although the petrogenesis of I-type granites is still under debate and the role of the mantle in their source is uncertain (e.g., Chappell and White, 2001; Kemp et al., 2007), the I-type granites may represent the equivalent of Archean granitoids (e.g., Condie, 1993 and references therein). The compilation of published Li data in I-type granites (Teng et al., 2004; Bryant et al., 2004; Marks et al., 2007) shows the post-Archean juvenile granitoids have [Li] = 22 ± 24 μg/g (2σ) and δ^7Li = 2.6 ± 5.2, 2σ (Figs.

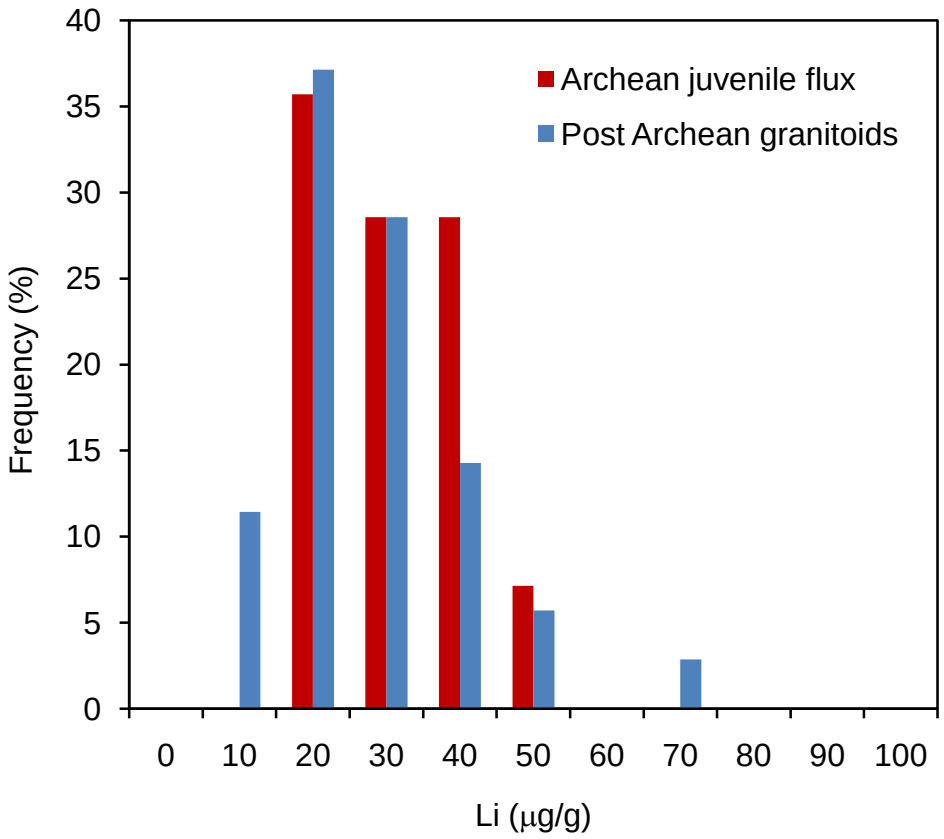

Figure 7-5. Histogram of Li concentrations in Archean juvenile flux and post Archean I-type granites. Li concentrations in I-type granites are from Teng et al. (2004), Bryant et al. (2004) and Marks et al. (2007). See text for details.

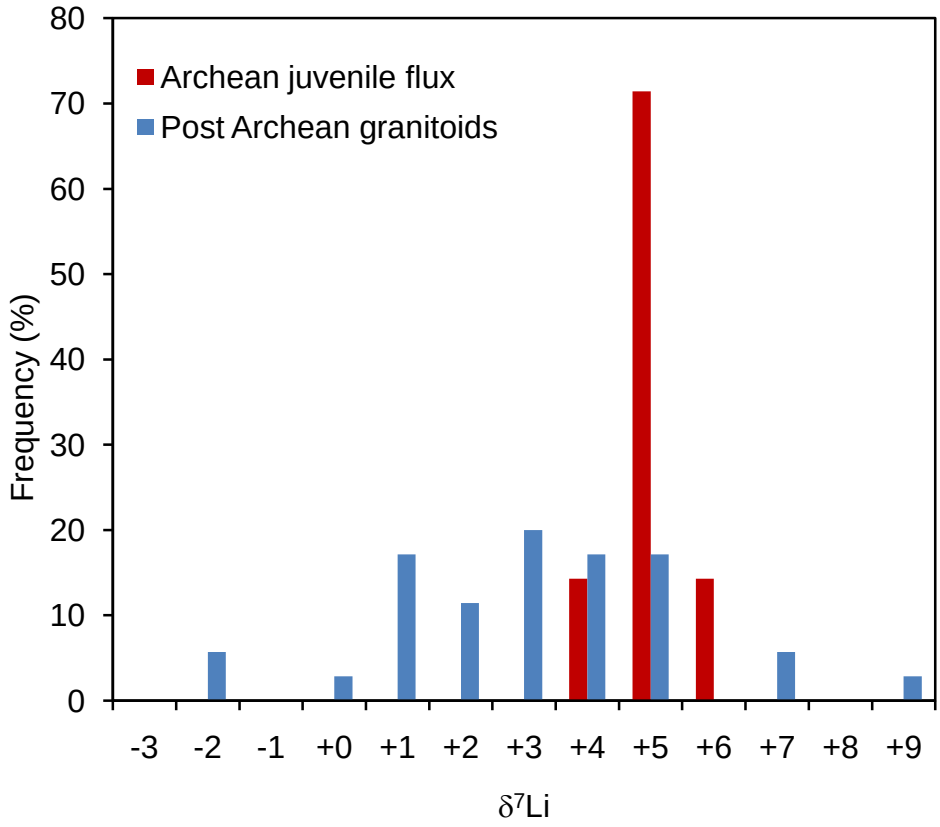

Figure 7-6. Histogram of Li isotopic compositions in Archean juvenile flux and post Archean I-type granites. Li isotopic compositions of I-type granite are from Teng et al. (2004), Bryant et al. (2004) and Marks et al. (2007). See text for details.

7-5 and 7-6). The Archean granitoids have average [Li] similar to that of post Archean I-type granites, but significantly higher than that of modern arc basalts (~6.9 μg/g), which represent juvenille additions to the modern continental crust. Moreover, the δ^7Li of the post Archean granitoids is statistically different from that of Archean granitoids and modern arc basalts (~+4) (t-test, 99% confidence level for difference). The difference of δ^7Li in post Arcehan I-type granites and modern arc balsalts suggests that magmas of I-type granites might have experienced crustal assimilation process, such as recycling weathered continental crust into their magma sources. Furthermore, the comparision of Li signatures in Archean TTGs with that of modern arc basalts indicate that [Li] in mantle-related juvenile additions to the continental crust may have decreased from the Archean to the post Archean, but the δ^7Li may have not changed significantly.

5.5. Refining crustal mass loss through chemical weathering

As discussed in the introduction, Liu and Rudnick (2010) introduced a mass balance model using [Li] and δ^7Li to quantify the crustal mass loss through chemical weathering. They indicate that, of all the parameters used in the model, [Li] in the juvenile continental crust is the most sensitive one for determining the amount of continental crust that has been lost to chemical weathering. Due to the lack of [Li] data in TTGs at that time, Liu and Rudnick (2010) assumed the juvenile continental crust (JCC) has [Li] similar to modern arc basalts (6.9 ± 1.6 μg/g, 1σ), and suggested that 50% of the crustal mass has been lost due to chemical weathering;, Liu and Rudnick (2010) suggest that their results could be impacted if [Li] in Archean TTGs are significantly different from those of arc basalts. Based on [Li] data in the Archean TTGs from this study, we may have an opportunity to reevaluate the JCC parameter and the final results of the model of Liu and

Rudnick (2010). Liu and Rudnick (2010) assume 38% of the JCC is composed of the TTG, and 62% of the JCC is composed of arc basalts. Assuming all the parameters (except JCC) in their model are constant and the average [Li] in Archean TTGs and sanukitoids from this study is ~25μg/g, the [Li] in the present day juvenile continental crust is 14 μg/g, and, consequently, ~30% crustal mass has been lost due to chemical weathering.

6. Conclusions

The [Li] and δ^7Li of the Archean TTGs and sanukitoids from three localities show a heterogeneous signature, which span a range of [Li] from 3.0 to 96 μg/g and δ^7Li from +0.2 to +11.7. The [Li] of Scourian TTGs is likely depleted by granulite facies metamorphic dehydration or partial melting, and the average [Li] of these TTGs (8.1 ± 5.5 μg/g, 2σ) is consistent with the [Li] of the lower continental crust estimated in previous studies. The highly heterogeneous δ^7Li in Scourian TTGs may reflect the various Li isotopic compositions in their source components, including hydrous oceanic crusts, detrital sediment and mantle. The older Archean Barberton TTGs have higher average [Li] and more variable δ^7Li than the younger TTGs, which likely reflect the contributions of evolved crust in the source of the former. The [Li] and δ^7Li in the younger Barberton TTGs and Canadian sanukitoids vary within a limited range and are nearly identical to each other, consistent with both of them being derived from a juvenile source. The Li signature in the younger Barberton TTGs and sanukitoids more likely represent the mantle-related Archean juvenile flux, and Archean juvenile flux has average [Li] = 25 ± 17 μg/g (2σ) and δ^7Li = 4.5 ± 0.8 (2σ). Post Archean I-type granites have similar average [Li] (22 ± 24 μg/g, 2σ) but lower δ^7Li (+2.6 ± 5.2, 2σ) relative to the

Archean TTGs; the lower δ^7Li in post Archean granitoids might reflect incorporation of weathered continental crust into their source. The Li signatures in Archean TTGs and modern arc basalts indicate that [Li] in mantle-related juvenile additions to the continental crust may have decreased from the Archean to the post Archean, but the δ^7Li may have not changed significantly. In addition, assuming the average [Li] in juvenile magmas added to the crust during the Archean is ~25μg/g, [Li] in present-day juvenile continental crust will be ~14μg/g and around 30% crustal mass may have been lost due to chemical weathering.

Chapter 8: Synthesis and future work[1]

[1] The text of this chapter was written by L. Qiu.

The traditional stable isotopes (e.g., H, C, N, O, and S) have been studied for over fifty years with measurements and interpretations of mass-dependent enrichments or depletions; most of the measurements are carried out using gas source mass spectrometers and other analytical techniques. Following the advent of MC-ICP-MS, a large amount of measurements and studies of non-traditional stable isotopes (e.g., Li, Mg, Cl, Ca, Cr, Fe, Cu, Zn, Se, and Mo) have been started in geological science. Li isotopes have been used as a tracer of a wide range of geological processes, generally because the two stable isotopes of Li have significant relative mass difference and have large elemental dispersion in Earth. With the improvement of analytical techniques in the past decades, a better than 1‰ precision of Li isotope measurements have been made and some basic consensuses about Li isotopes have been reached, such as the Li concentration and isotopic compositions in the major reservoirs of Earth, the partitioning of ^{6}Li and ^{7}Li between fluid and rock during continental weathering, and the behavior of Li isotopes during metamorphic dehydration. My study has primarily focused on Li behavior during fluid transport in subduction zones, fluid-rock exchange during sub-greenschist to granulite facies metamorphism and partial melting, the influence of weathering on the composition of continental crust, and the evolution of the juvenile flux to the continental crust through time. The basic conclusions drawn from this dissertation are:

1. Sub-greenschist facies metamorphism has negligible effect on Li in sediments; metamorphic dehydration from greenschist to granulite facies metamorphism may cause significant Li depletion but has had little influence on δ^7Li in sedimentary rocks. A key factor controlling the [Li] of metapelites in metamorphic rocks is the stability of Mg-bearing phyllosilicates. The Li released during granulite facies partial melting of metapelites can contribute to S-type granites, with excess Li being partitioned into Li-pegmatites.

2. Provenance exerts the greatest control on Li in fine grained sediments, and Li concentrations generally increase and δ^7Li values decrease with CIA (Chemical Index of Alteration) in post-Archean shales. Some Archean shales have low [Li] and significantly high δ^7Li and CIA relative to post-Archean shales, and may have been produced by severe weathering in their source region during the Archean. The Li signatures in Archean and post Archean shales indicate that Li isotopes reflect Archean weathering conditions and paleo-climate.

3. If the [Li] of slab-derived fluids is less than a few μg/g, the δ^7Li of the overlying sediments is not significantly influenced by the passage of these fluids. Indeed the slab-derived fluids will take on a high δ^7Li of > +10 after reacting with the prism sediments during their ascent; results from the fluid-fluxed Otago schists suggest that [Li] in the slab-derived fluids is likely in the range of $0 < [Li] \leq 41$(μg/g).

4. Based on the [Li] in the granulite facies metapelites from Ivrea Zone, Italy and granulite facies TTGs from Scourie, Scotland, the [Li] of lower continental crust is close to 8 μg/g or less, and the concentration weighted δ^7Li of the lower continental crust is +1.0, both of which are close to the estimates from previous studies (e.g., [Li] = 8 μg/g, δ^7Li = +2.5, Teng et al., 2008).

5. Archean TTGs derived from slab melting have variable δ^7Li likely because of the presence of seawater-altered crust and detrital sediments into their magma source; By contrast, TTGs derived directly from mantle or partial melting of thickened crust at greater depth has mantle-like δ^7Li. Archean juvenile granitoids have similar average [Li] and higher average δ^7Li relative to post Archean granitoids. Moreover, the comparision of Li signatures in mantle-derived Archean TTGs with that of modern arc basalts indicate that [Li] in mantle-related juvenile additions to the continental crust may have decreased from the Archean to the post Archean, but the δ^7Li may have not changed significantly.

Future Work:

1. Compared with other stable isotope systems, (e.g., O, S), experimental studies of Li isotopes is still in its infancy, and a robust explanation of Li results requires better quantification of Li's partition coefficients, diffusion coefficients and isotopic fractionation factors. Therefore, more experimental studies on the behavior of Li during fluid-rock and fluid-mineral interactions are sorely needed.

2. Although the analytical methods of measuring Li isotopes have improved dramatically in recent decades and some studies have reported precisions <0.5‰, a better precision is still needed to provide more information about Li behavior during geochemical processes; therefore, the improvement of analytical technique is also a major goal.

3. The initial findings of low [Li], high δ^7Li and high CIA in several Archean shales appears to be recording different weathering conditions in the Archean. However, due to the limited number of samples, it is difficult to conclude that the Li signature of Archean sediments is globally different from Post Archean sediments. In order to investigate the possible link between the Li signature and Archean weathering conditions further, shales from a number of other Archean cratons, spanning ages from Early Archean to Late Archean, should be investigated. The results will further test the hypothesis that Li can be used as an indicator of Archean weathering conditions and paleo-climate, and improve our knowledge of the Li concentration and isotopic composition of Archean upper continental crust.

In addition to fine-grained sedimentary rocks, the evolution of the Li isotopic composition in seawater will also provide robust information about how weathering processes influence the composition of continental crust throughout Earth history. Studies using planktic foraminifera as a proxy to trace the change of δ^7Li in paleo-ocean water for short-term geological time scale (<Ma) indicate significant changes in the δ^7Li of Phanerozoic seawater (e.g., Hall et al., 2005; Misra and Froelich, 2010). Thus, finding a proxy for determining the Li isotopes in paleo-ocean for a long-term geological time

scale, and constructing the evolution of Li signature in seawater from Archean to post Archean is another important task.

4. A preliminary study of Li in Archean TTGs sheds light on the Li signature in the Archean juvenile magma flux to the Archean continental crust, the variation of which is related to the petrogenesis of magma source; however, only a few studies have been carried out to date on Li isotopes in adakites (intermediate or felsic volcanic and plutonic rocks), which have debated, but probably have similar origins to slab-derived Archean TTGs (e.g., Tomascak et al., 2002). In order to understand better the relationship between the Archean and post Archean juvenile magma petrogenesis, the Li concentration and isotopic compositions in modern adakites also needs to be constrained well.

5. Several chapters in this dissertation show that the Li in some minerals, such as smectite, illite and biotite, may exert some influence on the Li signatures in their whole rocks. Therefore, developing a technique for in-situ measurement of Li isotopic compositions in these minerals would help us to understand better the factors that control the Li isotopic fractionation during geological processes.

6. Other non-traditional stable isotope systems, such as Mg, are similar to Li isotopes in terms of fluid mobility, mass difference between its isotopes, and its behavior during fluid-rock interactions (e.g., Teng et al., 2010; Li et al., 2010). Therefore, the investigation of the correlation between Li isotopes and Mg isotopes in natural samples,

such as sediments and metapelites, may become a powerful tool to trace a large variety of geological processes.

References

Ague, J.J., 1994. Mass-Transfer during Barrovian Metamorphism of Pelites, South-Central Connecticut.1: Evidence for Changes in Composition and Volume. *Am. J. Sci.* 294, 989-1057.

Albarede, F., 1998. The growth of continental crust. *Tectonophysics* 296, 1-14.

Armstrong, R.A., Compston, W., Dewit, M.J., Williams, I.S., 1990. The Stratigraphy of the 3.5-3.2-Ga Barberton Greenstone-Belt Revisited - a Single Zircon Ion Microprobe Study. *Earth Planet. Sci. Lett.* 101, 90-106.

Armstrong, R.A., Compston, W., Retief, E.A., Williams, I.S., Welke, H.J., 1991. Zircon Ion Microprobe Studies Bearing on the Age and Evolution of the Witwatersrand Triad. *Precamb. Res.* 53, 243-266.

Arth, J.G., Hanson, G.N., 1975. Geochemistry and Origin of Early Precambrian Crust of Northeastern Minnesota. *Geochim. Cosmochim. Acta* 39, 325-362.

Asiedu, D.K., Suzuki, S., Nogami, K., Shibata, T., 2000. Geochemistry of Lower Cretaceous sediments, Inner Zone of Southwest Japan: Constraints on provenance and tectonic environment. *Geochem J* 34, 155-173.

Aulbach, S., Rudnick, R.L., McDonough, W.F., 2008. Li-Sr-Nd isotope signatures of the plume and cratonic lithospheric mantle beneath the margin of the rifted Tanzanian Craton (Labait) *Contrib. Mineral. Petrol.* 155, 79-92.

Aulbach, S., Rudnick, R.L., 2009. Origins of non-equilibrium lithium isotopic fractionation in xenolithic peridotite minerals: Examples from Tanzania. *Chem. Geol.* 258, 17-27.

Barboza, S.A., Bergantz, G.W., 2000. Metamorphism and anatexis in the mafic complex contact aureole, Ivrea zone, northern Italy. *J. Petrol.* 41, 1307-1327.

Barker, F., Arth, J.G., Peterman, Z.E., Friedman, I., 1976. 1.7-by-Old to 1.8-by-Old Trondhjemites of Southwestern Colorado and Northern New-Mexico - Geochemistry and Depths of Genesis. *Geological Society of America Bulletin* 87, 189-198.

Barton, E.S., Altermann, W., Williams, I.S., Smith, C.B., 1994. U-Pb Zircon Age for a Tuff in the Campbell Group, Griqualand West Sequence, South-Africa - Implications for Early Proterozoic Rock Accumulation Rates. *Geology* 22, 343-346.

Basu, A., 1981. Weathering before the Advent of Land Plants - Evidence from Unaltered Detrital K-Feldspars in Cambrian-Ordovician Arenites. *Geology* 9, 132-133.

Batt, G.E., Brandon, M.T., Farley, K.A., Roden-Tice, M., 2001. Tectonic synthesis of the Olympic Mountains segment of the Cascadia wedge, using two-dimensional thermal and kinematic modeling of thermochronological ages. *J Geophys Res-Sol Ea* 106, 26731-26746.

Bea, F., Montero, P., 1999. Behavior of accessory phases and redistribution of Zr, REE, Y, Th, and U during metamorphism and partial melting of metapelites in the lower crust: An example from the Kinzigite Formation of Ivrea-Verbano, NW Italy. *Geochim. Cosmochim. Acta* 63, 1133-1153.

Beck, P., Chaussidon, M., Barrat, J.A., Gillet, P., Bohn, M., 2005. An ion-microprobe study of lithium isotopes behavior in nakhlites *Meteorit. Planet. Sci.* 40, A18

Beinlich, A., Klemd, R., John, T., Gao, J., 2010. Trace-element mobilization during Ca-metasomatism along a major fluid conduit: Eclogitization of blueschist as a consequence of fluid-rock interaction. *Geochim. Cosmochim. Acta* 74, 1892-1922.

Berckhem, H., 1969. Direct Evidence for Composition of Lower Crust and Moho. *Tectonophysics* 8, 97-105.

Berger, M., Rollinson, H., 1997. Isotopic and geochemical evidence for crust-mantle interaction during late Archaean crustal growth. *Geochim. Cosmochim. Acta* 61, 4809-4829.

Bertolani, M., Garuti, G., 1970. Aspetti petrografici della formatione basica Ivrea-Verbano in Val Sessera (Vercelli). *Rendiconti Societa Italiana di Mineralogia e Petrologia* 26, 433-474.

Bishop, D.G., 1972. Progressive Metamorphism from Prehnite-Pumpellyite to Greenschist Facies in Dansey Pass Area, Otago, New-Zealand. *Geological Society of America Bulletin* 83, 3177-3198.

Bock, B., McLennan, S.M., Hanson, G.N., 1998. Geochemistry and provenance of the Middle Ordovician Austin Glen Member (Normanskill Formation) and the Taconian Orogeny in New England. *Sedimentology* 45, 635-655.

Bouman, C., Vroon, P.Z., Elliott, T., 2004. Lithium inputs to subduction zones *Chem. Geol.* 212, 59-79

Breeding, C.M., Ague, J.J., 2002. Slab-derived fluids and quartz-vein formation in an accretionary prism, Otago Schist, New Zealand. *Geology* 30, 499-502.

Breeding, C.M., 2004. Fluid flow and mass transfer in subduction zones: A multi-scale view. Ph.D thesis. Yale University (AAT 3125163).

Brenan, J.M., Neroda, E., Lundstrom, C.C., Shaw, H.F., Ryerson, F.J., Phinney, D.L., 1998. Behaviour of boron, beryllium, and lithium during melting and crystallization: Constraints from mineral-melt partitioning experiments. *Geochim. Cosmochim. Acta* 62, 2129-2141.

Bryant, C.J., Chappell, B.W., Bennett, V.C., McCulloch, M.T., 2004. Lithium isotopic compositions of the New England Batholith; correlations with inferred source rock compositions. *Trans. R. Soc. Edinburgh: Earth Sci.* 95, 199-214.

Burton, K.W., Capmas, F., Birck, J.L., Allegre, C.J., Cohen, A.S., 2000. Resolving crystallisation ages of Archean mafic-ultramafic rocks using the Re-Os isotope system. *Earth Planet. Sci. Lett.* 179, 453-467.

Button, A., 1981. The cratonic enviroment, the Ventersdorp Supergroup In Precambrian of the Southern Hemisphere (ed. D. R. Hunter), pp. 520-536. Elsevier, Amsterdam.

Cameron, E.M., Garrels, R.M., 1980. Geochemical Compositions of Some Precambrian Shales from the Canadian Shield. *Chem. Geol.* 28, 181-197.

Cerny, P., Meintzer, R.E., Anderson, A.J., 1985. Extreme Fractionation in Rare-Element Granitic Pegmatites - Selected Examples of Data and Mechanisms. *Can. Mineral.* 23, 381-421.

Chan, L.H., 1987. Lithium Isotope Analysis by Thermal Ionization Mass-Spectrometry of Lithium Tetraborate. *Anal. Chem.* 59, 2662-2665.

Chan, L.H., Edmond, J.M., 1988. Variation of lithium isotope composition in the marine-environment—a preliminary-report. *Geochim. Cosmochim. Acta* 52, 1711 – 1717.

Chan, L.H., Edmond, J.M., Thompson, G., Gillis, K., 1992. Lithium isotopic composition of submarine basalts - implications for the lithium cycle in the oceans. *Earth Planet. Sci. Lett.* 108, 151-160.

Chan, L.H., Edmond, J.M., Thompson, G., 1993. A Lithium Isotope Study of Hot-Springs and Metabasalts from Midocean Ridge Hydrothermal Systems. *J Geophys Res-Sol Ea* 98, 9653-9659.

Chan, L.H., Gieskes, J.M., You, C.F., Edmond, J.M., 1994. Lithium Isotope Geochemistry of Sediments and Hydrothermal Fluids of the Guaymas Basin, Gulf of California. *Geochim. Cosmochim. Acta* 58, 4443-4454.

Chan, L.H., Kastner, M., 2000. Lithium isotopic compositions of pore fluids and sediments in the Costa Rica subduction zone: Implications for fluid processes and sediment contribution to the arc volcanoes. *Earth Planet. Sci. Lett.* 183, 275-290.

Chan, L.H., Leeman, W.P., You, C.F., 2002. Lithium isotopic composition of Central American volcanic arc lavas: implications for modification of subarc mantle by slab-derived fluids: correction. *Chem. Geol.* 182, 293-300.

Chan, L.H., Leeman, W.P., Plank, T., 2006. Lithium isotopic composition of marine sediments *Geochem. Geophys. Geosyst* 7, doi:10.1029/2005GC001202.

Chapman, H.J., Moorbath, S., 1977. Lead Isotope Measurements from Oldest Recognized Lewisian Gneisses of Northwest Scotland. *Nature* 268, 41-42.

Chappell, B.W., White, A.J.R., 2001. Two contrasting granite types: 25 years later. *Aust J Earth Sci* 48, 489-499.

Clemens, J.D., Yearron, L.M., Stevens, G., 2006. Barberton (South Africa) TTG magmas: Geochemical and experimental constraints on source-rock petrology, pressure of formation and tectonic setting. *Precamb. Res.* 151, 53-78.

Condie, K.C., 1993. Chemical-Composition and Evolution of the Upper Continental-Crust - Contrasting Results from Surface Samples and Shales. *Chem. Geol.* 104, 1-37.

Cooper, A.H., Fortey, N.J., Hughes, R.A., Molyneux, S.G., Moore, R.M., Rushton, A.W.A., Stone, P., 2004. The Skiddaw Group of the English Lake District. *Memoir of the British Geological Survey*, British Geological Survey, Keyworth, Nottingham, 110-120.

Crow, C., Condie, K.C., 1988. Geochemistry and Origin of Late Archean Volcanics from the Ventersdorp Supergroup, South-Africa. *Precamb. Res.* 42, 19-37.

Davey, F.J., Eberhart-Phillips, D., Kohler, M.D., Bannister, S., Caldwell, G., Henrys, S., Scherwath, M., Stern, T., Avendonk, H.v., 2007. Geophysical Structure of the Southern Alps Orogen, South Island, New Zealand, in A Continental Boundary: Tectonics at South Island, New Zealand (eds Okaya, D., Stern, T. & Davey, F.). *Geophysical Monograph Series* 175, AGU, 47-73.

De Ronde, C.E.J., Faure, K., Bray, C.J., Whitford, D.J., 2000. Round hill shear zone-hosted gold deposit, Macraes Flat, Otago, New Zealand: Evidence of a magmatic ore fluid. *Econ. Geol.* 95, 1025-1048.

De Wit, M.J., Roering, C., Hart, R.J., Armstrong, R.A., Deronde, C.E.J., Green, R.W.E., Tredoux, M., Peberdy, E., Hart, R.A., 1992. Formation of an Archean Continent. *Nature* 357, 553-562.

DePaolo, D.J., Linn, A.M., Schubert, G., 1991. The continental crustal age distribution: Methods of deteriming mantle separation ages from Sm-Nd isotopic data and application to the Southeastern United States. *J. Geophys. Res.* 96, 2071-2088.

Dipple, G.M., Ferry, J.M., 1992. Fluid-Flow and Stable Isotopic Alteration in Rocks at Elevated-Temperatures with Applications to Metamorphism. *Geochim. Cosmochim. Acta* 56, 3539-3550.

Dohmen, R., Kasemann, S.A., Coogan, L., Chakraborty, S., 2010. Diffusion of Li in olivine. Part I: Experimental observations and a multi species diffusion model. *Geochim. Cosmochim. Acta* 74, 274-292.

Drummond, M.S., Defant, M.J., Kepezhinskas, P.K., 1996. Petrogenesis of slab-derived trondhjemite-tonalite-dacite/adakite magmas. *Transactions of the Royal Society of Edinburgh-Earth Sciences* 87, 205-215.

Dutta, P.K., Suttner, L.J., 1986. Alluvial Sandstone Composition and Paleoclimate .2. Authigenic Mineralogy. *J Sediment Petrol* 56, 346-358.

Eberl, D.D., 1984. Clay Mineral Formation and Transformation in Rocks and Soils. *Philos T Roy Soc A* 311, 241-257.

Elliott, T., Jeffcoate, A., Bouman, C., 2004. The terrestrial Li isotope cycle: light-weight constraints on mantle convection. *Earth Planet. Sci. Lett.* 220, 231-245.

Elliott, T., Thomas, A., Jeffcoate, A.B., Niu, Y., 2006. Lithium isotope evidence for subduction-enriched mantle in the source of mid-ocean-ridge basalts *Nature (London)* 443, 565-568

Flesch, G.D., Anderson, A.R., Svec, H.J., 1973. A secondary isotopic standard for 6Li/7Li determinations *International Journal or Mass Spectrometry and Ion Physics* 12, 265-272.

Fortey, N.J., 1989. Low grade metamorphism in the Lower Ordovician Skiddaw Group of the Lake District, England. *Proc. Yorks. Geol. Soc.* 47, 325-337.

Fountain, D.M., 1976. Ivrea-Verbano and Strona-Ceneri Zones, Northern Italy - Cross-Section of Continental Crust - New Evidence from Seismic Velocities of Rock Samples. *Tectonophysics* 33, 145-165.

Frey, M., Robinson, D., 1999. Low-Grade Metamorphism. Blackwell Sciences Ltd., Oxford. 313-320.

Gibbs, A.K., Montgomery, C.W., Oday, P.A., Erslev, E.A., 1986. The Archean-Proterozoic Transition - Evidence from the Geochemistry of Meta-Sedimentary Rocks of Guyana and Montana. *Geochim. Cosmochim. Acta* 50, 2125-2141.

Gibson, R.L., Jones, M.Q.W., 2002. Late Archaean to Palaeoproterozoic geotherms in the Kaapvaal craton, South Africa: constraints on the thermal evolution of the Witwatersrand Basin. *Basin Res* 14, 169-181.

Goldich, S.S., Fischer, L.B., 1986. Air-Abrasion Experiments in U-Pb Dating of Zircon. *Chem. Geol.* 58, 195-215.

Halama, R., McDonough, W.F., Rudnick, R.L., Keller, J., Klaudius, J., 2007. The Li isotopic composition of Oldoinyo Lengai: Nature of the mantle sources and lack of isotopic fractionation during carbonatite petrogenesis. *Earth Planet. Sci. Lett.* 254, 77-89.

Halama, R., John, T., Herms, P., Hauff, F., Schenk, V., 2011. A stable (Li, O) and radiogenic (Sr, Nd) isotope perspective on metasomatic processes in a subducting slab. *Chem. Geol.*, doi:10.1016/j.chemgeo.2010.12.001.

Hall, J.M., Chan, L.H., McDonough, W.F., Turekian, K.K., 2005. Determination of the lithium isotopic composition of planktic foraminifera and its application as a paleo-seawater proxy. *Mar Geol* 217, 255-265.

Hessler, A.M., Lowe, D.R., 2006. Weathering and sediment generation in the Archean: An integrated study of the evolution of siliciclastic sedimentary rocks of the 3.2 Ga Moodies Group, Barberton greenstone belt, South Africa. *Precamb. Res.* 151, 185-210.

Hower, J., 1976. The determination of diagenetic and metamorphic temperatures using clay mineral assemblages *Geological Society of America* 8, 201-215.

Huh, Y., Chan, L.H., Chadwick, O.A., 2004. Behavior of lithium and its isotopes during weathering of Hawaiian basalt. *Geochem. Geophys. Geosyst* 5, doi:10.1029/2004GC000729.

Jahn, B., Bertrandsarfati, J., Morin, N., Mace, J., 1990. Direct Dating of Stromatolitic Carbonates from the Schmidtsdrif Formation (Transvaal Dolomite), South-Africa, with Implications on the Age of the Ventersdorp Supergroup. *Geology* 18, 1211-1214.

Jahn, B.M., Condie, K.C., 1995. Evolution of the Kaapvaal-Craton as Viewed from Geochemical and Sm-Nd Isotopic Analyses of Intracratonic Pelites. *Geochim. Cosmochim. Acta* 59, 2239-2258.

James, R.H., Rudnicki, M.D., Palmer, M.R., 1999. The alkali element and boron geochemistry of the Escanaba Trough sediment-hosted hydrothermal system. *Earth Planet. Sci. Lett.* 171, 157-169.

James, R.H., Allen, D.E., Seyfried, W.E., 2003. An experimental study of alteration of oceanic crust and terrigenous sediments at moderate temperatures (51 to 350 degrees C): Insights as to chemical processes in near-shore ridge-flank hydrothermal systems. *Geochim. Cosmochim. Acta* 67, 681-691.

James, W.C., Mack, G.H., Suttner, L.J., 1981. Relative Alteration of Microcline and Sodic Plagioclase in Semi-Arid and Humid Climates. *J Sediment Petrol* 51, 151-164.

Jeffcoate, A.B., Elliott, T., Kasemann, S.A., Ionov, D., Cooper, K., Brooker, R., 2007. Li isotope fractionation in peridotites and mafic melts. *Geochim. Cosmochim. Acta* 71, 202-218.

Jochum, K.P., Nohl, U., 2008. Reference materials in geochemistry and environmental research and the GeoReM database. *Chem. Geol.* 253, 50-53.

Kamo, S.L., Davis, D.W., 1994. Reassessment of Archean Crustal Development in the Barberton Mountain Land, South-Africa, Based on U-Pb Dating. *Tectonics* 13, 167-192.

Kamo, S.L., Key, R.M., Daniels, L.R.M., 1995. New Evidence for Neoarchaean, Hydrothermally Altered Granites in South-Central Botswana. *Journal of the Geological Society* 152, 747-750.

Kasting, J.F., Ackerman, T.P., 1986. Climatic Consequences of Very High-Carbon Dioxide Levels in the Earths Early Atmosphere. *Science* 234, 1383-1385.

Kasting, J.F., 1987. Theoretical Constraints on Oxygen and Carbon-Dioxide Concentrations in the Precambrian Atmosphere. *Precamb. Res.* 34, 205-229.

Kasting, J.F., 1993. Earths Early Atmosphere. *Science* 259, 920-926.

Kelemen, P.B., Hanghøj, K., Greene, A.R., 2003. One view of the geochemistry of subduction-related magmatic arcs, with an emphasis on primitive andesite and lower crust. One view of the geochemistry of subduction-related magmatic arcs with an emphasis on primitive andesite and lower crust, in The Crust, (ed. R.L. Rudnick). In Treatise on Geochemistry, (eds. H.D. Holland and K.K. Turekian). Elsevier-Pergamon, Oxford, pp. 593-659.

Kemp, A.I.S., Hawkesworth, C.J., Foster, G.L., Paterson, B.A., Woodhead, J.D., Hergt, J.M., Gray, C.M., Whitehouse, M.J., 2007. Magmatic and crustal differentiation history of granitic rocks from Hf-O isotopes in zircon. *Science* 315, 980-983.

Kerrich, R., 1999. Geochemistry - Nature's gold factory. *Science* 284, 2101-2102.

Kisakurek, B., Widdowson, M., James, R.H., 2004. Behaviour of Li isotopes during continental weathering: the Bidar laterite profile, India. *Chem. Geol.* 212, 27-44.

Kisch, H.J., 1983. Mineralogy and petrology of burial diagenesis (burial metamorphism) and incipient metamorphism in clastic rocks. In Diagenesis in Sediments and Sedimentary Rocks (G. Larsen and G.V. Chilingar eds). Elsevier, New York. 213-289.

Klemd, R., 1999. A comparison of fluids causing post-depositional hydrothermal alteration in Archaean basement granitoids and the Witwatersrand Basin. *Miner Petrol* 66, 111-122.

Knauth, L.P., Lowe, D.R., 2003. High Archean climatic temperature inferred from oxygen isotope geochemistry of cherts in the 3.5 Ga Swaziland Supergroup, South Africa. *Geological Society of America Bulletin* 115, 566-580.

Kneller, B.C., 1991. A foreland basin on the southern margin of Iapetus *J. Geol. Soc. London* 148, 207-210.

Kroner, A., Hegner, E., Wendt, J.I., Byerly, G.R., 1996. The oldest part of the Barberton granitoid-greenstone terrain, South Africa: Evidence for crust formation between 3.5 and 3.7 Ga. *Precamb. Res.* 78, 105-124.

Lahtinen, R., 2000. Archaean-Proterozoic transition: geochemistry, provenance and tectonic setting of metasedimentary rocks in central Fennoscandian Shield, Finland. *Precamb. Res.* 104, 147-174.

Lee, C.T.A., Morton, D.M., Little, M.G., Kistler, R., Horodyskyj, U.N., Leeman, W.P., Agranier, A., 2008. Regulating continent growth and composition by chemical weathering. *Proc. Natl. Acad. Sci. U. S. A.* 105, 4981-4986.

Leggett, J.K., Mckerrow, W.S., Eales, M.H., 1979. Southern Uplands of Scotland - Lower Paleozoic Accretionary Prism. *J. Geol. Soc. London* 136, 755-770.

Li, W.-Y., Teng, F.-Z., Ke, S., Rudnick, R.L., Gao, S., Wug, F.-Y., Chappell, B.W., 2010. Heterogeneous magnesium isotopic composition of the upper continental crust. *Geochim. Cosmochim. Acta* 74, 6867-6884.

Liu, S.W., Pan, Y.M., Xie, Q.L., Zhang, J., Li, Q.G., 2004. Archean geodynamics in the Central Zone, North China Craton: constraints from geochemistry of two contrasting series of granitoids in the Fuping and Wutai complexes. *Precamb. Res.* 130, 229-249.

Liu, X.-M., Rudnick, R.L., 2010. Quantifying Continental Crustal Mass Loss through Chemical Weathering Using Lithium and its Isotopes. *Geology*, in review.

Liu, X.-M., Rudnick, R.L., Hier-Majumder, S., Sirbescu, M.-L.C., 2010. Processes controlling lithium isotopic distribution in contact aureoles: A case study of the Florence County pegmatites, Wisconsin. *Geochem. Geophys. Geosyst* 11, doi:10.1029/2010GC003063.

Lowe, D.R., Tice, M.M., 2004. Geologic evidence for Archean atmospheric and climatic evolution: Fluctuating levels of CO2, CH4, and O-2, with an overriding tectonic control. *Geology* 32, 493-496.

Lundstrom, C.C., Chaussidon, M., Hsui, A.T., Kelemen, P., Zimmerman, M., 2005. Observations of Li isotopic variations in the Trinity Ophiolite: Evidence for isotopic fractionation by diffusion during mantle melting. *Geochim. Cosmochim. Acta* 69, 735-751.

Magna, T., Wiechert, U.H., Halliday, A.N., 2004. Low-blank isotope ratio measurement of small samples of lithium using multiple-collector ICPMS. *Int J Mass Spectrom* 239, 67-76.

Magna, T., Wiechert, U., Grove, T.L., Halliday, A.N., 2006a. Lithium isotope fractionation in the southern Cascadia subduction zone. *Earth Planet. Sci. Lett.* 250, 428-443.

Magna, T., Wiechert, U., Halliday, A.N., 2006b. New constraints on the lithium isotope compositions of the Moon and terrestrial planets. *Earth Planet. Sci. Lett.* 243, 336-353.

Magna, T., Ionov, D.A., Oberli, F., Wiechert, U., 2008. Links between mantle metasomatism and lithium isotopes: Evidence from glass-bearing and cryptically metasomatized xenoliths from Mongolia. *Earth Planet. Sci. Lett.* 276, 214-222.

Magna, T., Janousek, V., Kohut, M., Oberli, F., Wiechert, U., 2010. Fingerprinting sources of orogenic plutonic rocks from Variscan belt with lithium isotopes and possible link to subduction-related origin of some A-type granites. *Chem. Geol.* 274, 94-107.

Manikyamba, C., Kerrich, R., 2006. Geochemistry of black shales from the Neoarchaean Sandur Superterrane, India: First cycle volcanogenic sedimentary rocks in an intraoceanic arc-trench complex. *Geochim. Cosmochim. Acta* 70, 4663-4679.

Marks, M.A.W., Rudnick, R.L., McCammon, C., Vennemann, T., Markl, G., 2007. Arrested kinetic Li isotope fractionation at the margin of the llimaussaq complex, South Greenland: Evidence for open-system processes during final cooling of peralkaline igneous rocks. *Chem. Geol.* 246, 207-230.

Marschall, H.R., Pogge von Strandmann, P.A.E., Seitz, H.M., Elliott, T., Niu, Y.L., 2007. The lithium isotopic composition of orogenic eclogites and deep subducted slabs. *Earth Planet. Sci. Lett.* 262, 563-580.

Martin, H., Moyen, J.F., 2002. Secular changes in tonalite-trondhjemite-granodiorite composition as markers of the progressive cooling of Earth. *Geology* 30, 319-322.

Mazzucchelli, M., Siena, F., 1986. Geotectonic Significance of the Metabasites of the Kinzigitic Series, Ivrea-Verbano Zone (Western Italian Alps). *Tscher Miner Petrog* 35, 99-116.

McCulloch, M.T., Wasserburg, G.J., 1978. Sm-Nd and Rb-Sr Chronology of Continental Crust Formation. *Science* 200, 1003-1011.

McCulloch, M.T., Bradshaw, J.Y., Taylor, S.R., 1987. Sm-Nd and Rb-Sr isotopic and geochemical systematics in Phanerozoic granulites from Fjordland, Southwest New Zealand *Contrib. Mineral. Petrol.* 97, 183-195

McLennan, S.M., Taylor, S.R., 1991. Sedimentary-Rocks and Crustal Evolution - Tectonic Setting and Secular Trends. *J Geol* 99, 1-21.

McLennan, S.M., Hemming, S., McDaniel, D.K., Hanson, G.N., 1993a. Geochemical approaches to sedimentation, provenance, and tectonics. In Processes Controlling the Composition of Clastic Sediments (eds. M. J. Johnsson and A. Basu). *Geol. Soc. Am., Boulder, Colorado.* 284, 21–40.

McLennan, S.M., Hemming, S.R., Taylor, S.R., Eriksson, K.A., 1993b. Early Proterozoic crustal evolution: Geochemical and Nd-Pb isotopic evidence from metasedimentary rocks, southwestern North America *Geochim. Cosmochim. Acta* 59, 1153-1177.

Merriman, R.J., Frey, M., 1999. Patterns of very low-grade metamorphism in metapelitic rocks. *In: Low-Grade Metamorphism (eds Frey, M., Robinson, D.),* Blackwell Sciences Ltd., Oxford. 61-77.

Merriman, R.J., Peacor, D.R., 1999. Very low-grade metapelites; mineralogy, microfabrics and measuring reaction progress. *In Low-Grade metamorphism (eds Frey, M., Robinson, D.),* Blackwell Sciences Ltd., Oxford. 10-60.

Merriman, R.J., Roberts, B., 2001. Low-grade metamorphism in the Scottish Southern Uplands terrane: deciphering the patterns of accretionary burial, shearing and cryptic aureoles. *Trans. R. Soc. Edinburgh: Earth Sci.* 91, 521-537.

Merriman, R.J., 2006. Clay minerals assemblages in British Lower Palaeozoic mudrocks. *Clay Miner.* 41, 473-512.

Merriman, R.J., Breward, N., Stone, P., Green, K., 2009. Element mobility and low-grade metamorphism of mudrocks in British Caledonian Basins. *British Geological Survey Open Report, OR/09/017.*

Millot, R., Scaillet, B., Sanjuan, B., 2010. Lithium isotopes in island arc geothermal systems: Guadeloupe, Martinique (French West Indies) and experimental approach. *Geochim. Cosmochim. Acta* 74, 1852-1871.

Misra, S., Froelich, P.N., 2010. Seawater Lithium isotope evolution during the Cenozoic. *Goldschmidt Conference Abstracts, A713.*

Moriguti, T., Nakamura, E., 1998. Across-arc variation of Li isotopes in lavas and implications for crust/mantle recycling at subduction zones. *Earth Planet. Sci. Lett.* 163, 167-174.

Moriguti, T., Shibata, T., Nakamura, E., 2004. Lithium, boron and lead isotope and trace element systematics of Quaternary basaltic volcanic rocks in northeastern Japan: mineralogical controls on slab-derived fluid composition. *Chem. Geol.* 212, 81-100.

Mortensen, J.K., Craw, D., MacKenzie, D.J., Gabites, J.E., Ullrich, T., 2010. Age and Origin of Orogenic Gold Mineralization in the Otago Schist Belt, South Island,

New Zealand: Constraints from Lead Isotope and Ar-40/Ar-39 Dating Studies. *Economic Geology* 105, 777-793.

Mortimer, N., 1993. Jurassic Tectonic History of the Otago Schist, New-Zealand. *Tectonics* 12, 237-244.

Mortimer, N., 2000. Metamorphic discontinuities in orogenic belts: example of the garnet-biotite-albite zone in the Otago Schist, New Zealand. *International Journal of Earth Sciences* 89, 295-306.

Mortimer, N., 2003. A provisional structural thickness map of the Otago Schist, New Zealand. *Am. J. Sci.* 303, 603-621.

Moyen, J.F., Martin, H., Jayananda, M., 2001. Multi-element geochemical modelling of crust-mantle interactions during late-Archaean crustal growth: the Closepet granite (South India). *Precamb. Res.* 112, 87-105.

Nesbitt, H.W., Young, G.M., 1982. Early Proterozoic Climates and Plate Motions Inferred from Major Element Chemistry of Lutites. *Nature* 299, 715-717.

Nesbitt, H.W., Young, G.M., 1984. Prediction of some weathering trends of plutonic and volcanic-rocks based on thermodynamic and kinetic considerations. *Geochim. Cosmochim. Acta* 48, 1523-1534.

Nishio, Y., Nakai, S., Ishii, T., Sano, Y., 2007. Isotope systematics of Li, Sr, Nd, and volatiles in Indian Ocean MORBs of the Rodrigues Triple Junction: Constraints on the origin of the DUPAL anomaly. *Geochim. Cosmochim. Acta* 71, 745-759.

Parkinson, I.J., Hammond, S.J., James, R.H., Rogers, N.W., 2007. High-temperature lithium isotope fractionation: Insights from lithium isotope diffusion in magmatic systems. *Earth Planet. Sci. Lett.* 257, 609-621.

Paul, D., White, W.M., Turcotte, D.L., 2003. Constraints on the $^{232}Th/^{238}U$ ratio (κ) of the continental crust. *Geochem. Geophys. Geosyst* 4, doi:10.1029/2002GC000497.

Peacor, D.R., 1992. Diagenesis and Low-Grade Metamorphism of Shales and Slates. *Rev. Mineral.* 27, 335-380.

Penniston-Dorland, S.C., Sorensen, S.S., Ash, R.D., Khadke, S.V., 2010. Lithium isotopes as a tracer of fluids in a subduction zone mélange: Franciscan Complex, CA. *Earth Planet. Sci. Lett.* 292, 181-190.

Philpotts, A.R., Ague, J.J., 2009. Principles of Igneous and Metamorphic Petrology (2nd ed.). *Cambridge, Cambridge University Press*, 551-556.

Pistiner, J.S., Henderson, G.M., 2003. Lithium-isotope fractionation during continental weathering processes. *Earth Planet. Sci. Lett.* 214, 327-339.

Plank, T., 2005. Constraints from thorium/lanthanum on sediment recycling at subduction zones and the evolution of the continents. *J. Petrol.* 46, 921-944.

Pogge von Strandmann, P.A.E., Burton, K.W., James, R.H., van Calsteren, P., Gislason, S.R., Mokadem, F., 2006. Riverine behaviour of uranium and lithium isotopes in an actively glaciated basaltic terrain. *Earth Planet. Sci. Lett.* 251, 134-147.

Press, W.H., Teukolsky, S.A., Vetterling, W.T., Flannery, B.P., 1992. Numerical recipes in Fortran 77: The art of scientific computing (2nd ed.). *New York, Cambridge University Press, 963 p.*

Pretorius, D.A., 1976. The nature of the Witwatersrand gold-uranium deposits. *In Handbook of stratibound Stratiform Ore Deposits*, (ed. K. H. Wolf), pp. 29-88. Elsevier.

Pretorius, D.A., 1981. Gold and uranium in quartz-pebble conglomerates. *Econ. Geol.*, (75th Anniv. Vol; ed. B. J. Skinner), 117-138.

Qiu, L., Rudnick, R.L., McDonough, W.F., Merriman, R.J., 2009. Li and δ^7Li in mudrocks from the British Caledonides: Metamorphism and source influences. *Geochim. Cosmochim. Acta* 73, 7325-7340.

Qiu, L., Rudnick, R.L., Ague, J.J., McDonough, W.F., 2011a. A lithium isotopic study of sub-greenschist to greenschist facies metamorphism in an accretionary prism, New Zealand. *Earth Planet. Sci. Lett.* 301, 213-221.

Qiu, L., Rudnick, R.L., McDonough, W.F., Bea, F., 2011b. The behavior of lithium in amphibolite- to granulite-facies rocks of the Ivrea-Verbano Zone, NW Italy. *Chem. Geol.*, in review.

Quick, J.E., Sinigoi, S., Peressini, G., Demarchi, G., Wooden, J.L., Sbisa, A., 2009. Magmatic plumbing of a large Permian caldera exposed to a depth of 25 km. *Geology* 37, 603-606.

Rapp, R.P., 1997. Heterogeneous source regions for Archaean granitoids: experimental and geochemical evidence. In: M.J. de Wit and L.D. Ashwal, Editors, Greenstone Belts, Oxford University Press, Oxford (1997), pp. 267–279.

Rapp, R.P., Shimizu, N., Norman, M.D., 2003. Growth of early continental crust by partial melting of eclogite. *Nature* 425, 605-609.

Rasmussen, B., Buick, R., 1999. Redox state of the Archean atmosphere: Evidence from detrital heavy minerals in ca. 3250-2750 Ma sandstones from the Pilbara Craton, Australia. *Geology* 27, 115-118.

Richter, F.M., Davis, A.M., DePaolo, D.J., Watson, E.B., 2003. Isotope fractionation by chemical diffusion between molten basalt and rhyolite. *Geochim. Cosmochim. Acta* 67, 3905-3923.

Richter, F.M., Mendybaev, R.A., Christensen, J.N., Hutcheon, I.D., Williams, R.W., Sturchio, N.C., Beloso, A.D., 2006. Kinetic isotopic fractionation during diffusion of ionic species in water. *Geochim. Cosmochim. Acta* 70, 277-289.

Robb, L.J., Meyer, F.M., 1990. The nature of the Witwatersrand hinterland; conjectures on the source area problem. *Econ. Geol.* 85, 511-536.

Rollinson, H., 1994. Origin of Felsic Sheets in the Scourian Granulites - New Evidence from Rare-Earth Elements. *Scottish Journal of Geology* 30, 121-129.

Rollinson, H., 2008. Secular evolution of the continental crust: Implications for crust evolution models. *Geochem. Geophys. Geosyst* 9, doi:10.1029/2008GC002262.

Rollinson, H.R., Windley, B.F., 1980. An Archean Granulite-Grade Tonalite-Trondhjemite-Granite Suite from Scourie, Nw Scotland - Geochemistry and Origin. *Contrib. Mineral. Petrol.* 72, 265-281.

Rollinson, H.R., 1987. Early Basic Magmatism in the Evolution of Archean High-Grade Gneiss Terrains - an Example from the Lewisian of Nw Scotland. *Mineralogical Magazine* 51, 345-355.

Rollinson, H.R., Fowler, M.B., 1987. The magmatic evolution of the Scourian Complex at Gruinard Bay In: Park, R. G. & Tarney, J. (eds) The evolution of the Lewisan and Comparable Precambrian High Grade Terrains. *Geological Society of London, Special Publication* 27, 265-281.

Rollinson, H.R., 1996. Tonalite-trondhjemite-granodiorite magmatism and the genesis of Lewisian crust during the Archean. *Geological society of London, Special Publications* 112, 25-42.

Rudnick, R.L., Presper, T., 1990. Geochemistry of intermediate- to high-pressure granulites. In (Vielzeuf, D. and Vidal, Ph., eds.) Granulites and Crustal Differentiation, NATO ASI ser., Kluwer, Dordrecht. 523-550.

Rudnick, R.L., 1995. Making Continental-Crust. *Nature* 378, 571-578.

Rudnick, R.L., Fountain, D.M., 1995. Nature and Composition of the Continental-Crust - a Lower Crustal Perspective. *Rev Geophys* 33, 267-309.

Rudnick, R.L., Gao, S., 2003. Composition of the continental crust. In The Crust (ed. R.L. Rudnick). In Treatise on Geochemistry (eds. H.D. Holland and K.K. Turekian). Elsevier-Pergamon, Oxford. 3, 1-64.

Rudnick, R.L., Tomascak, P.B., Njo, H.B., Gardner, R.L., 2004. Extreme isotopic fractionation during continental weathering revealed in saprolites from South Carolina. *Chem. Geol.* 212, 45-57.

Sartbaeva, A., Wells, S.A., Redfern, S.A.T., 2004. Li^+ ion motion in quartz and beta-eucryptite studied by dielectric spectroscopy and atomistic simulations. *J. Phys.: Condens. Matter* 16, 949-960.

Schnetger, B., 1994. Partial Melting during the Evolution of the Amphibolite-Facies to Granulite-Facies Gneisses of the Ivrea Zone, Northern Italy. *Chem. Geol.* 113, 71-101.

Seyfried, W.E., Chen, X., Chan, L.H., 1998. Trace element mobility and lithium isotope exchange during hydrothermal alteration of seafloor weathered basalt: An

experimental study at 350 degrees C, 500 bars. *Geochim. Cosmochim. Acta* 62, 949-960.

Shaw, D.M., Dickin, A.P., Li, H., Mcnutt, R.H., Schwarcz, H.P., Truscott, M.G., 1994. Crustal Geochemistry in the Wawa-Foleyet Region, Ontario. *Can. J. Earth Sci.* 31, 1104-1121.

Shirey, S.B., Hanson, G.N., 1984. Mantle-Derived Archean Monozodiorites and Trachyandesites. *Nature* 310, 222-224.

Shirey, S.B., Hanson, G.N., 1986. Mantle Heterogeneity and Crustal Recycling in Archean Granite-Greenstone Belts - Evidence from Nd Isotopes and Trace-Elements in the Rainy Lake Area, Superior-Province, Ontario, Canada. *Geochim. Cosmochim. Acta* 50, 2631-2651.

Sighinolfi, G.P., Gorgoni, C., 1978. Chemical Evolution of High-Grade Metamorphic Rocks - Anatexis and Remotion of Material from Granulite Terrains. *Chem. Geol.* 22, 157-176.

Simons, K.K., Harlow, G.E., Brueckner, H.K., Goldstein, S.L., Sorensen, S.S., Hemming, N.G., Langmuir, C.H., 2010. Lithium isotopes in Guatemalan and Franciscan HP–LT rocks: Insights into the role of sediment-derived fluids during subduction. *Geochim. Cosmochim. Acta* 74, 3621–3641.

Smith, M.P., Yardley, B.W.D., 1999. Fluid evolution during metamorphism of the Otago Schist, New Zealand: (I) Evidence from fluid inclusions. *J. Metamorph. Geol.* 17, 173-186.

Soper, N., Woodcock, N., 2003. The lost Lower Old Red Sandstone of England and Wales: a record of post-Iapetan flexure or Early Devonian transtension. *Geol. Mag.* 140, 627-647

Spear, F.S., Cheney, J.T., 1989. A Petrogenetic Grid for Pelitic Schists in the System SiO_2-Al_2O_3-FeO-MgO-K_2O-H_2O. *Contrib. Mineral. Petrol.* 101, 149-164.

Stern, T., Okaya, D., Kleffmann, S., Scherwath, M., Henrys, S., Davey, F., 2007. Geophysical Exploration and Dynamics of the Alpine Fault Zone, in A Continental Boundary: Tectonics at South Island, New Zealand (eds Okaya, D., Stern, T. and Davey, F.). *Geophysical Monograph Series* 175, AGU, 207-233.

Stockwell, C.H., 1982. Proposals for time classification and correlation of Precambrian rocks and events in Canada and adjacent areas of the Canadian shield. Part I: A time classification of Precambrian rocks and events. *Geological Survey of Canada Paper*, 80-19.

Stoffynegli, P., Mackenzie, F.T., 1984. Mass Balance of Dissolved Lithium in the Oceans. *Geochim. Cosmochim. Acta* 48, 859-872.

Stone, P., Floyd, J.D., Barnes, R.P., Lintern, B.C., 1987. A Sequential Back-Arc and Foreland Basin Thrust Duplex Model for the Southern Uplands of Scotland. *J. Geol. Soc. London* 144, 753-764.

Stone, P., Merriman, R.J., 2004. Basin thermal history favaours an accretionary origin for the Southern Uplands terrane, Scottish Caledonides. *J. Geol. Soc. London* 161, 829-836.

Sun, S.S., McDonough, W.F., 1989. Chemical and isotopic systematics of oceanic basalts; implications for mantle composition and processes. In: A.D. Saunders and

M.J. Norry, Editors, Magmatism in the Ocean Basins. *Spec. Pub. Geol. Soc. Lond.* 42, 313-345.

Tankard, A.J., Jackson, M.P.A., Eriksson, K.A., Hobday, D.K., Hunter, D.R., Minter, W.E.L., 1982. . *Crustal Evolution of Southern Africa: 3.8 billion Years of Earth History*, Springer.

Taylor, S.R., McLennan, S.M., 1985. The Continental crust: Its Composition and Evolution. Blackwell, Oxford.

Teng, F.Z., McDonough, W.F., Rudnick, R.L., Dalpe, C., Tomascak, P.B., Chappell, B.W., Gao, S., 2004. Lithium isotopic composition and concentration of the upper continental crust. *Geochim. Cosmochim. Acta* 68, 4167-4178.

Teng, F.Z., McDonough, W.F., Rudnick, R.L., Walker, R.J., 2006a. Diffusion-driven extreme lithium isotopic fractionation in country rocks of the Tin Mountain pegmatite. *Earth Planet. Sci. Lett.* 243, 701-710.

Teng, F.Z., McDonough, W.F., Rudnick, R.L., Walker, R.J., Sirbescu, M.L.C., 2006b. Lithium isotopic systematics of granites and pegmatites from the Black Hills, South Dakota. *Am. Mineral.* 91, 1488-1498.

Teng, F.Z., McDonough, W.F., Rudnick, R.L., Wing, B.A., 2007. Limited lithium isotopic fractionation during progressive metamorphic dehydration in metapelites: A case study from the Onawa contact aureole, Maine. *Chem. Geol.* 239, 1-12.

Teng, F.Z., Rudnick, R.L., McDonough, W.F., Gao, S., Tomascak, P.B., Liu, Y.S., 2008. Lithium isotopic composition and concentration of the deep continental crust. *Chem. Geol.* 255, 47-59.

Teng, F.Z., Li, W.-Y., Rudnick, R.L., Gardner, L.R., 2010. Contrasting lithium and magnesium isotope fractionation during continental weathering. *Earth Planet. Sci. Lett.* 300, 63-71.

Tomascak, P.B., Carlson, R.W., Shirey, S.B., 1999. Accurate and precise determination of Li isotopic compositions by multi-collector sector ICP-MS. *Chem. Geol.* 158, 145-154.

Tomascak, P.B., Widom, E., Benton, L.D., Goldstein, S.L., Ryan, J.G., 2002. The control of lithium budgets in island arcs. *Earth Planet. Sci. Lett.* 196, 227-238.

Tomascak, P.B., 2004. Developments in the understanding and application of lithium isotopes in the earth and planetary sciences. In Geochemistry of Non-traditional Stable Isotopes (Editors, C. M. Johnson, B.A. Beard and F. Albarede). *Reviews in Mineralogy and Geochemistry* 55, 153-195.

Tomascak, P.B., Langmuir, C.H., le Roux, P.J., Shirey, S.B., 2008. Lithium isotopes in global mid-ocean ridge basalts. *Geochim. Cosmochim. Acta* 72, 1626-1637.

Tosca, N.J., Johnston, D.T., Mushegian, A., Rothman, D.H., Summons, R.E., Knoll, A.H., 2010. Clay mineralogy, organic carbon burial, and redox evolution in Proterozoic oceans. *Geochim. Cosmochim. Acta* 74, 1579-1592.

Vigier, N., Decarreau, A., Millot, R., Carignan, J., Petit, S., France-Lanord, C., 2008. Quantifying Li isotope fractionation during smectite formation and implications for the Li cycle. *Geochim. Cosmochim. Acta* 72, 780-792.

Voshage, H., Hofmann, A.W., Mazzucchelli, M., Rivalenti, G., Sinigoi, S., Raczek, I., Demarchi, G., 1990. Isotopic Evidence from the Ivrea Zone for a Hybrid Lower Crust Formed by Magmatic Underplating. *Nature* 347, 731-736.

Walker, J.C.G., 1986. Carbon dioxide on the early Earth. *Origins Life* 16, 117-127.

Walraven, F., Martini, J., 1995. Zircon Pb-evaporation age determinations for the Oak Tree Formation, Chuniespoort Group, Transvaal Sequence; implications for Transvaal-Griqualand West basin correlations *S. Afr. J. Geol.* 98, 58-67.

Walraven, F., 1997. Geochronology of the Rooiberg Group, Transvaal Supergroup, South Africa. *In: Information Circular vol.316,* Economic Geology Research Unit, University of the Witwatersrand, Johannesburg, South Africa.

Weaver, B.L., Tarney, J., 1980. Rare-Earth Geochemistry of Lewisian Granulite-Facies Gneisses, Northwest Scotland - Implications for the Petrogenesis of the Archean Lower Continental-Crust. *Earth Planet. Sci. Lett.* 51, 279-296.

Weaver, C.E., 1989. *Clays, Muds, and Shales*. Elsevier, New York.

Wedepohl, K.H., 1995. The Composition of the Continental-Crust. *Geochim. Cosmochim. Acta* 59, 1217-1232.

Wheeler, J., Park, R.G., Rollinson, H.R., Beach, A., 2010. The Lewisian Complex: insights into deep crustal evolution. *The Geological Society of London* 335, 51-79.

White, A.F., Blum, A.E., 1995. Effects of Climate on Chemical-Weathering in Watersheds. *Geochim. Cosmochim. Acta* 59, 1729-1747.

Widmer, T., Thompson, A.B., 2001. Local origin of high pressure vein material in eclogite facies rocks of the Zermatt-Saas Zone, Switzerland. *Am. J. Sci.* 301, 627-656.

Williams, L.B., Hervig, R.L., 2005. Lithium and boron isotopes in illite-smectite: The importance of crystal size. *Geochim. Cosmochim. Acta* 69, 5705-5716.

Wimpenny, J., Gislason, S.R., James, R.H., Gannoun, A., Pogge Von Strandmann, P.A.E., Burton, K.W., 2010a. The behaviour of Li and Mg isotopes during primary phase dissolution and secondary mineral formation in basalt. *Geochim. Cosmochim. Acta* 74, 5259-5279.

Wimpenny, J., James, R.H., Burton, K.W., Gannoun, A., Mokadem, F., Gislason, S.R., 2010b. Glacial effects on weathering processes: New insights from the elemental and lithium isotopic composition of West Greenland rivers. *Earth Planet. Sci. Lett.* 290, 427-437.

Winter, J.D., 2010. Principles of Igneous and Metamorphic Petrology, second edition. Prentice Hall.

Wollast, R., Chou, L., 1992. Surface-Reactions during the Early Stages of Weathering of Albite. *Geochim. Cosmochim. Acta* 56, 3113-3121.

Wronkiewicz, D.J., Condie, K.C., 1987. Geochemistry of Archean Shales from the Witwatersrand Supergroup, South-Africa - Source-Area Weathering and Provenance. *Geochim. Cosmochim. Acta* 51, 2401-2416.

Wronkiewicz, D.J., Condie, K.C., 1989. Geochemistry and Provenance of Sediments from the Pongola Supergroup, South-Africa - Evidence for a 3.0-Ga-Old Continental Craton. *Geochim. Cosmochim. Acta* 53, 1537-1549.

Wronkiewicz, D.J., Condie, K.C., 1990. Geochemistry and Mineralogy of Sediments from the Ventersdorp and Transvaal Supergroups, South-Africa - Cratonic Evolution during the Early Proterozoic. *Geochim. Cosmochim. Acta* 54, 343-354.

Wunder, B., Meixner, A., Romer, R.L., Heinrich, W., 2006. Temperature-dependent isotopic fractionation of lithium between clinopyroxene and high-pressure hydrous fluids. *Contrib. Mineral. Petrol.* 151, 112-120.

Wunder, B., Meixner, A., Romer, R.L., Feenstra, A., Schettler, G., Heinrich, W., 2007. Lithium isotope fractionation between Li-bearing staurolite, Li-mica and aqueous fluids: An experimental study. *Chem. Geol.* 238, 277-290.

You, C.F., Chan, L.H., 1996. Precise determination of lithium isotopic composition in low concentration natural samples. *Geochim. Cosmochim. Acta* 60, 909-915.

Zack, T., Tomascak, P.B., Rudnick, R.L., Dalpe, C., McDonough, W.F., 2003. Extremely light Li in orogenic eclogites: The role of isotope fractionation during dehydration in subducted oceanic crust. *Earth Planet. Sci. Lett.* 208, 279-290.

Zingg, A., 1984. Development Stages of Ivrea Paragneiss (Southern Alps, Northern Italy). *Fortschritte Der Mineralogie* 62, 266-268.